To the Graduate Council:

I am submitting herewith a thesis written by John H. Weitz, Jr., entitled "A Mesoscopic Fabric Analysis of the Tellico-Sevier Shale Belt at Northeastern Douglas Lake, Tennessee." I have examined the final copy of this thesis for form and content and recommend that it be accepted in partial fulfillment of the requirements for the degree of Master of Science, with a major in Geology.

N. B. Woodward, Major Professor

We have read this thesis and recommend its acceptance:

Accepted for the Council:

Vice Chancellor
Graduate Studies and Research

A MESOSCOPIC FABRIC ANALYSIS OF THE TELLICO-SEVIER SHALE BELT AT NORTHEASTERN DOUGLAS LAKE, TENNESSEE

A Thesis

Presented for the

Master of Science

Degree

The University of Tennessee, Knoxville

John H. Weitz, Jr.

March 1983

3067119

ACKNOWLEDGMENTS

I wish to extend thanks to my advisor, Nick Woodward, for his incisive comments and encouragement during the fieldwork, analysis, and writing portions of the thesis. I also want to thank committee members Kula Misra and Don Byerly for reading two drafts of the thesis and providing constructive criticisms. Discussions with Charles Conway concerning many areas of structural geology were invaluable. I offer my sincerest appreciation to my parents, who made this possible.

ABSTRACT

Mesoscopic fabric analysis in a portion of the Middle Ordovician Tellico-Sevier belt indicates that relative deformation intensity increases southeastward toward the overlying Great Smoky thrust. Bed-parallel shortening (early), mesoscopic folding, spaced cleavage and contraction faulting developed during a single, partially noncoaxial deformation during thrust sheet emplacement. Buckle folding and associated contraction faulting were the predominant means of lateral shortening. Irregular, modified concentric, precleavage folds developed above a major décollement dominantly by flexural slip, modified by strain at the hinges, flattening, and pressure solution cleavage. Cleavage often transects folds, in which case it is subvertical while the axial plane is inclined in the direction of transport on the associated dominant set of contraction faults. Cleavage transection angle ranges from 0 degrees (axial planar) to more than 45 degrees. Cleavage development was related to second order and small-scale contraction faulting, which occurred in late stages of folding. Mechanisms for producing folds transected by cleavage included: (a) overprinting of irregular folds by cleavage, (b) a fault-controlled local reorientation of strain axes prior to cleavage development,

and (c) fault drag-induced rotation of a fold core prior to cleavage development.

The shortening axis varied from southeast dipping in the northwest (above a postulated ramp in the Saltville fault), through horizontal to northwest dipping in the central and southeastern portions of the shale belt. A minimum of 23 percent buckle shortening was calculated for the northwestern half of the Tellico-Sevier belt.

The Douglas décollement underlies the deformed Middle Ordovician shales and is exposed at the northwest boundary of the shale belt. It is localized at a zone of major ductility contrast at the contact between Blockhouse shale and underlying carbonates. Location of the fault coincides with a previously hypothesized décollement having 20 kilometers of slip. Aside from early bed-parallel shortening, most deformation within the shale belt occurred during emplacement of the Douglas décollement. A high angle fault, possible representing a splay from this décollement, causes repetition of the lower mudstones and siltstones at the surface. An unmapped low angle thrust may underlie a large, second order, nearly recumbent anticline.

TABLE OF CONTENTS

CHAPTER		PAGE
1.	INTRODUCTION	1
	A. Purpose	1
	B. Location and General Geology	2
	C. Previous Investigations	10
	D. Methods Used in Present Investigation	13
	1. Geometric and Scale Descriptions	13
	2. Photomosaics	17
	3. Graphical Analysis of Fabric Data	17
	4. Fold Mechanism Analyses	18
	5. Stratigraphic Analysis and Correlations	18
	6. Construction of Cross-Section	18
	E. Stratigraphy	19
	1. General	19
	2. Upper Knox Group	19
	3. Lenoir Formation	20
	4. Whitesburg Formation	21
	5. Blockhouse Formation	22
	6. Sevier Formation	23
	a. Tellico unit (within Sevier)	25
2.	DESCRIPTIONS AND INTERPRETATIONS OF PROFILE SECTIONS	26
	A. Introduction	26
	B. Section A	27
	1. Introduction	27
	2. Stratigraphy	30
	a. Blockhouse formation	30
	b. Sevier formation	34
	3. Structure	37
	C. Section B	50
	1. Introduction	50
	2. Stratigraphy	52
	3. Structure	56
	D. Section C	67
	1. Introduction	67
	2. Stratigraphy	70
	3. Structure	71
	E. Section D	76
	1. Introduction	76
	2. Stratigraphy	80
	3. Structure	83

CHAPTER PAGE

3. MESOSCOPIC FABRIC ANALYSIS: MECHANISMS OF FOLDING AND CLEAVAGE DEVELOPMENT 92

A. Introduction 92
B. Theoretical Models and Their Significance 94
1. Introduction 94
2. Fold Profiles 106
3. Fold Classes 109
a. Class 1 109
b. Class 2 109
c. Class 3 110
4. Fold Symmetry 111
5. Kink Folds 111
6. Fold Flattening 112
7. Origin of Cleavage by Pressure Solution 115
8. Rigid-Body Deformation with Selective Removal of Material . . . 116
a. Model A 117
b. Model B 117
c. Model C 117
9. Folds Transected by Cleavage 117
10. Buckle Shortening Strain 118
C. Data Presentation and Analysis 119
1. Controls on Fold Geometry: Chevron versus Concentric 119
2. Evidence for Flexural-Slip Buckle Folding 126
3. Kink Folds 126
4. Fold Shape Modification 128
5. Fold Flattening Strain Analysis . . 133
6. Cleavage and Cleavage-Fold Relations 135
a. Introduction 135
b. Cleavage refraction 147
c. Cleavage fan angle versus dip transection (d) 147
d. Refraction of cleavage strike . 149
e. Bedding-cleavage angle relative abundances versus lithology . . 151
f. Cleavage fan angle versus fold flattening strain 151
g. Cleavage fan angle versus fold interlimb angle 153
h. Cleavage intensity versus angularity parameter, cleavage fan angle, and fold interlimb angle 154

CHAPTER		PAGE
	i. Transecting cleavage	154
	j. Δ versus d transection parameters	158
	k. Δ, d transection parameters versus fold interlimb angle . .	161
	l. Comparison of axial plane trace, cleavage plane trace, and flattening extension direction	161
	m. Development of transecting cleavage	165
	7. Comparison of Computer Simulated Strain Patterns with Natural Folds	168
	8. Rigid-Body Deformation with Selective Removal of Material by Pressure Solution	170
	9. Buckle Shortening Strain Calculations	170
	D. Conclusions	171
4.	FAULTING, FAULT-CONTROLLED CLEAVAGE AND MEGASCOPIC FABRIC ANALYSIS	174
	A. Introduction	174
	B. Theoretical Models of Fault Analysis . .	175
	1. Arthaud's Method for Determining Brittle Deformation Axes	175
	2. Discfold Analysis of Planar Shear Zone	176
	C. Fault Data and Analysis	176
	1. Determination of Principal Axes of the Deformation Ellipsoid	176
	2. Discfold Analysis at Douglas Fault Zone, Section A	184
	3. Cleavage-Contraction Fault Relationship in Transected Folds	184
	4. Analysis of Bed-Parallel Contraction	188
	5. Analysis of Superimposed Strain . .	188
	D. Megascopic Structure	193
	E. Conclusions	197
5.	SUMMARY AND CONCLUSIONS	201
LIST OF REFERENCES		206

PAGE

APPENDICES 213

A. GLOSSARY OF TERMINOLOGY USED 214
B. FOLD PARAMETER TABLES 216
C. GRAPHIC METHOD OF DETERMINATION OF BRITTLE DEFORMATION AXES FROM FAULT ATTITUDES (AFTER ARTHAUD, 1969) 219
D. ACCURACY OF PHOTOMOSAICS 222
E. MAP OF PREVIOUS WORK LOCATIONS 223
F. ADJACENT STRATIGRAPHIC SECTION (SHANMUGAM, 1978) 225
G. INDEPENDENT FOLD PARAMETERS 229

VITA 239

LIST OF FIGURES

FIGURE		PAGE
1.	Tellico-Sevier Belt on Saltville Thrust Sheet of East Tennessee, Showing Location of Study Area and Important Tectonic and Physiographic Features	3
2.	Portion of the Tellico-Sevier Belt, Showing Locations of the Four Detailed Profile Sections at Douglas Lake (Portion of Geologic Map of Tennessee, Hardeman, 1966) . .	4
3.	Stratigraphic Cross-Section (Palinspastically Restored) of the Ordovician of East Tennessee (after Walker, 1980)	6
4.	Generalized Stratigraphic Column at Study Area	7
5.	Fundamental Fault Nomenclature	15
6.	Stratigraphic Column for Section A	29
7.	Douglas Décollement Zone at Base of Blockhouse (A00-A00.2)	32
8.	Regional Cross-Section through Western Blue Ridge and Eastern Valley and Ridge (Witherspoon, 1981)	39
9.	Cleavage Superimposed on Irregular Folds with Variable Axial Plane Dips (A14-20)	42
10.	Faulted Anticline with Transecting Cleavage (A19)	44
11.	Pattern of Observed Cleavage Transection with Respect to the Fold Axial Plane and the Associated Dominant Contraction Fault . . .	47
12.	Stratigraphic Column at Section B	51
13.	Profile Axial Plane Dips Across Strike for the Four Sections	53
14.	Concentric Anticline Displaying Strong Interlayer Competence Contrast (B65)	58

FIGURE		PAGE
15.	Recumbent Anticline in Tellico Sandstone of Sevier (B203)	66
16.	Stratigraphic Column at Section C	68
17.	Profile of an Intensely Deformed Portion of Section C	74
18.	Extensional Fractures Superimposed on Sheared Discfolds (C36-38)	77
19.	Stratigraphic Column at Section D	78
20.	Asymmetrical Anticline (D109b) with Cleaved, Crenulated Southeast Limb	86
21.	Close-Up Views of Portions of the Crenulated and Cleaved Southeast Limb of Anticline in Figure 20	87
22.	Thickness Plots for Second Order Chevron-Kink Fold (B30) with Class 2 Hinges	95
23.	Thickness Plots for Second Order Concentric Fold (C29, Class 1b)	96
24.	Ideal Concentric (Class 1b) and Similar (Class 2) Folds with Thickness Parameters t and T (after Ramsay, 1967)	97
25.	Representative Dip Isogon Patterns for Folds of Different Geometries	98
26.	Illustration and Definition of Hinge Angularity Parameter A	99
27.	Terms Used to Describe the Tightness of a Fold (after Fleuty, 1964), Based on the Interlimb Angle (β)	100
28.	Nomograms for Estimating Amount of Flattening Strain from Thickness Ratios and Limb Dips for a Given Fold or Folded Layer	101
29.	Orthogonal Thickness Ratio Curves for Flattening Analysis of 9 Folds in the Sevier Formation	103

FIGURE PAGE

30. Models of Deformation Caused by Removal of Material from Folds in Which Cleavage Is Symmetrical about the Axial Plane 104

31. Comparison of Fold Bedding-Cleavage Angles with Groshong's (1975) Models a, b, and c, Which Plot as Dashed Lines 105

32. Illustrations of Fold Transection Types (after Borradaile, 1978) 118

33. Buckle Shortening Formula and Illustration . . 120

34. Hinge Angularity (A) versus Location in Strike Belt 121

35. Hinge Angularity (A) versus Lithology 123

36. Bed Thickness Classification Terms (after Ingram, 1954) 124

37. Hinge Angularity (A) versus Bed Thickness . . . 125

38. Buckle and Kink Fold Axial Orientations 127

39. Disharmonic Folds in Thin-Bedded Sandy Siltstone 129

40. Bed-Parallel Faults Which Die Out into Folds . 131

41. Axial Planar Cleaved Folds in Sevier 136

42. Mesofabric Data from Symmetrically Cleaved A33 Syncline 140

43. Mesofabric Data from Symmetrically Cleaved B76 Anticline 141

44. Mesofabric Data from Symmetrically Cleaved C36 Syncline 142

45. Mesofabric Data from Symmetrically Cleaved, Faulted C29 Anticline 143

46. Mesofabric Data from Axial Planar Cleaved D109 Anticline 144

FIGURE		PAGE
47.	Frequency Percent of Cleavage Intensities versus Lithology	145
48.	Cleavage Fan Angle (γ) versus Dip Transection (d)	148
49.	Lithologic Control on the Refraction of Cleavage Strike at Dandridge Municipal Park	150
50.	Frequency Percent of Cleavage/Bedding Angles ($S_0 \wedge S_1$) versus Lithology	152
51.	Cleavage Intensity versus Fold Interlimb Angle (β)	155
52.	Mesofabric Data Contrasting Axial Planar Cleaved Fold (A15) with Adjacent Noncoaxial Cleaved fold (A19)	156
53.	Graphical Representations of Typical Fold Transections	157
54.	(Δ, d) Transection Parameter Graph	159
55.	Mesofabric Data for All Localities	160
56.	Fold Flattening Strain (Rf) versus Cleavage/ Flattening Scatter (ϕ_S)	163
57.	Fold Flattening Strain (Rf) versus Axial Plane/Flattening Scatter (ϕ_A)	164
58.	Mechanisms for Development of Transecting Cleavage (d Transection)	166
59.	Computer Simulation Models of Cleavage Patterns (after Dieterich, 1970), with Percent Total Shortening	169
60.	Discfold Analysis of Douglas Décollement Zone	177
61.	Deformation Axes at C36-38 Shear Zone	178
62.	Flattening of Dihedral Angle between Conjugate Shear Surfaces by Pure Shear Plane Strain	180
63.	Reversal of X and Y Axes between Stages of Thrusting and Wrench Faulting	182

FIGURE		PAGE
64.	Deformation Axes for Thrust and Wrench Faults in Hanging Wall of Douglas Décollement	183
65.	Mesoscopic Deformation Chronology	186
66.	Mesofabric Data from Transected Fold Core (A64)	187
67.	Bed-Parallel Extension Superimposed on Bed-Parallel Contraction	189
68.	Telescoping in Sevier (A73.2, A06.4)	191
69.	Megascopic Deformation Chronology	196
C-1.	Arthaud Method of Determination of Brittle Deformation Axes	221
E-1.	Map of Previous Work Locations	224
G-1.	Angularity Parameter A versus Fold Interlimb Angle β	230
G-2.	Fold Flattening Strain Ratio R_f versus Fold Interlimb Angle β	231
G-3.	Fold Flattening Strain R_f versus Cleavage Fan Angle γ	232
G-4.	Cleavage Fan Angle γ versus Fold Interlimb Angle β	233
G-5.	Angularity Parameter A versus Cleavage Intensity	234
G-6.	Cleavage Intensity versus Cleavage Fan Angle γ	235
G-7.	Interlimb Angle β versus Transection Parameter Δ	236
G-8.	Interlimb Angle β versus Transection Parameter d	237
G-9.	Fold Half-Wavelength $\lambda/2$ versus Bed Thickness .	238

LIST OF PLATES

PLATE

1. Section A Profile . . . . . In Pocket
2. Section B Profile . . . . . In Pocket
3. Section C Profile . . . . . In Pocket
4. Section D Profile . . . . . In Pocket
5. Geologic Map of Northeastern Douglas Lake . . . . . In Pocket
6. Structure Section . . . . . In Pocket

CHAPTER 1

INTRODUCTION

A. Purpose

The objective of this study was to examine representative tectonic fabric data from the Douglas Lake area (Figures 1, 2) within the Tennessee Valley and Ridge Province in order to describe the deformational sequences and mechanisms. This involved geometric, geographic, and strain (relative) analyses of mesoscopic structures (fabric elements ranging in size from hand specimens to extensive continuous outcrops) such as folds, cleavage and faults; the relationships among them and their relationships to large-scale structures. The large-scale structural features (e.g., major faults) were the primary controls of deformation. The mesoscopic data formed the basis for an interpretation of the megascopic structural style of the research area. The fabric data were used to calculate positions for kinematic strain axes. In the case of fold flattening, estimates were made of the axial proportions of the finite strain ellipsoid. The relative sequences among mesoscopic and megascopic fabric elements (i.e., the order of structural events) determined the mesoscopic and megascopic deformation chronologies. Contrasting hypotheses of monophase and polyphase deformation

for the Valley and Ridge were investigated for the study area.

B. Location and General Geology

Geographically, the study area is located about 60 kilometers east of downtown Knoxville, Tennessee (Figure 1). It includes much of the northeastern half of Douglas Lake in southeastern Jefferson County (Figure 2), and the southern half of the White Pine (153-SE) 7.5 minute quadrangle as well as the northern portion of the Chestnut Hill (164-NE) quadrangle.

The Valley and Ridge Province consists of folded and faulted Paleozoic sedimentary rocks (Figure 1). The regional structure is basically homoclinal bedding with southeast dips and faults either parallel to or slightly steeper than bedding. The area lies southeast of the Dumplin Valley fault, and on a larger scale, on the Saltville thrust sheet (Figures 1; also see the regional cross-section shown on p. 39). The Dumplin Valley thrust fault is mapped extending from Morristown to Etowah, Tennessee (Hardeman, 1966). The northwestern boundary of the Tellico-Sevier belt may coincide with a recently hypothesized (Figure 1 and p. 39), but unmapped, bedding plane thrust (fault a, described in this thesis; Plates 1, 5, 6) within the Dumplin Valley sheet (Witherspoon, 1981). The Fair Garden anticline, consisting

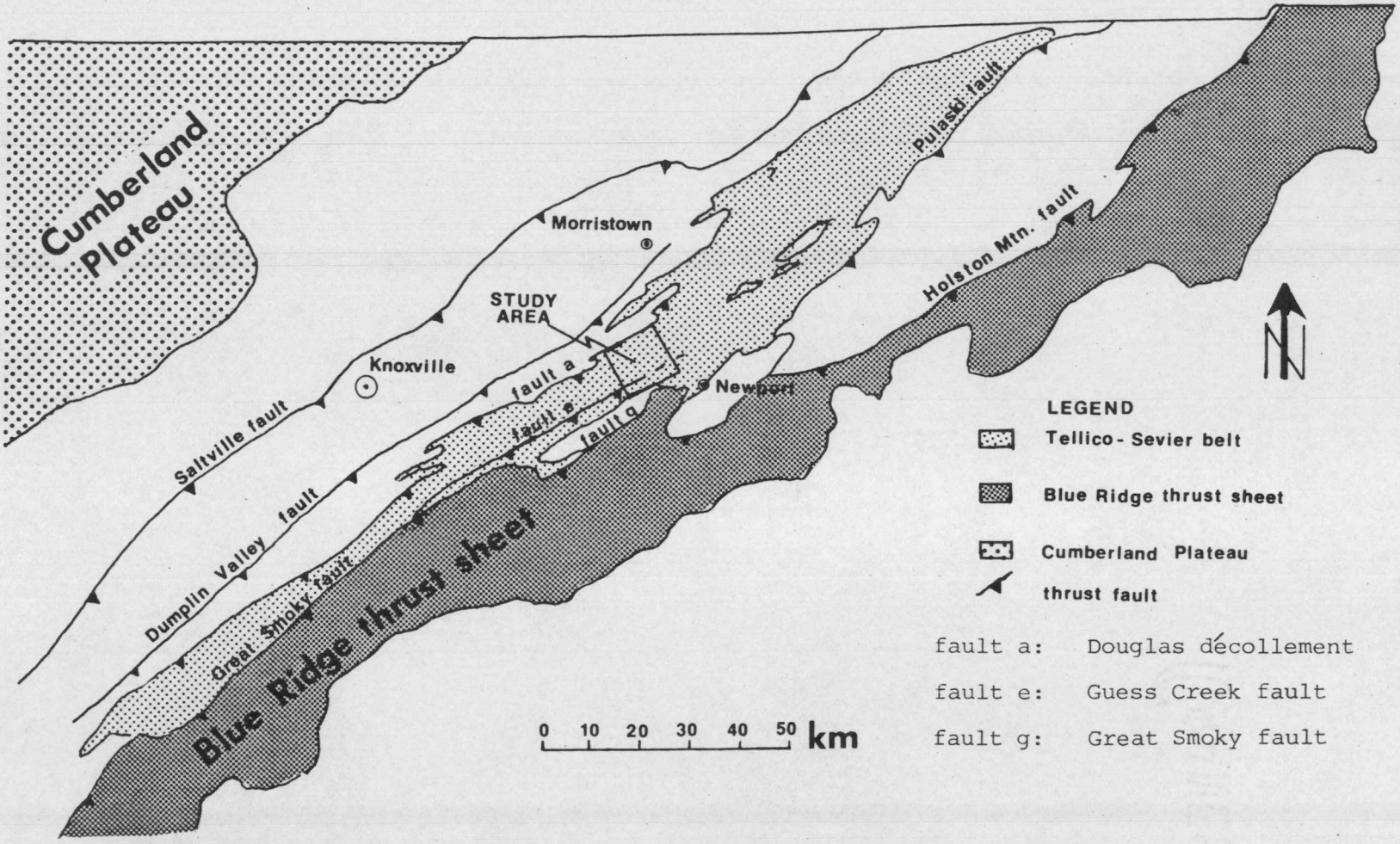

Figure 1. Tellico-Sevier belt on Saltville thrust sheet of east Tennessee, showing location of study area and important tectonic and physiographic features.

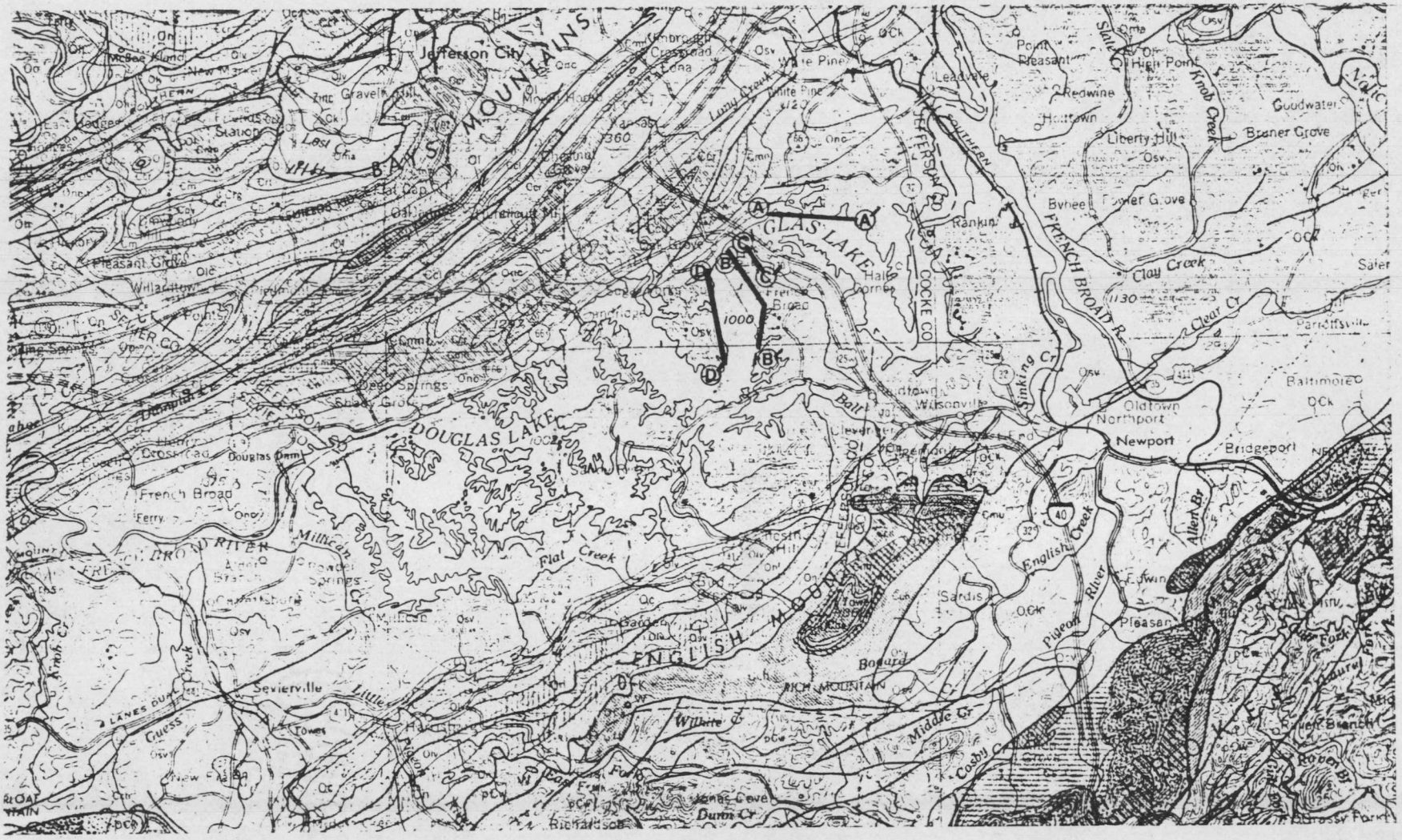

Figure 2. Portion of the Tellico-Sevier belt, showing locations of the four detailed profile sections at Douglas Lake (portion of Geologic Map of Tennessee, Hardeman, 1966).

of Knox carbonates in its core, bounds the shale belt to the southeast. The Fair Garden anticline is faulted near the hinge by a thrust (Hardeman, 1966). The Great Smoky fault system to the southeast thrusts Cambrian and Precambrian rocks of the Blue Ridge out onto the Tellico-Sevier belt as well as onto the east flank of the Fair Garden anticline, west of the English Mountain salient (Figure 2). A branch of the Pulaski fault trends toward the southeast part of the area from the east (Figure 1). Numerous imbricate faults north of English Mountain thrust Lower Ordovician Knox on top of Middle Ordovician Sevier (Rodgers, 1953). The study area is situated along strike southwest of the terminus of the Bays Mountain synclinorium.

The study area within the Tellico-Sevier belt at Douglas Lake is dissected by multiple imbricate faults, most of which are approximately parallel to bedding and usually associated with folding. Some of these may sole out at the zone of major ductility contrast near the base of the Blockhouse-Sevier shales. One of these imbricate faults, the Guess Creek fault, truncates the northwest limb of the Fair Garden anticline (Witherspoon, 1981). It is situated southeast of Douglas Lake within the Tellico-Sevier belt.

A disconformity (Figures 3, 4) separates carbonate rocks of Early Ordovician age (Knox) from a thin sequence of carbonate rocks of earliest Middle Ordovician age (Lenoir and

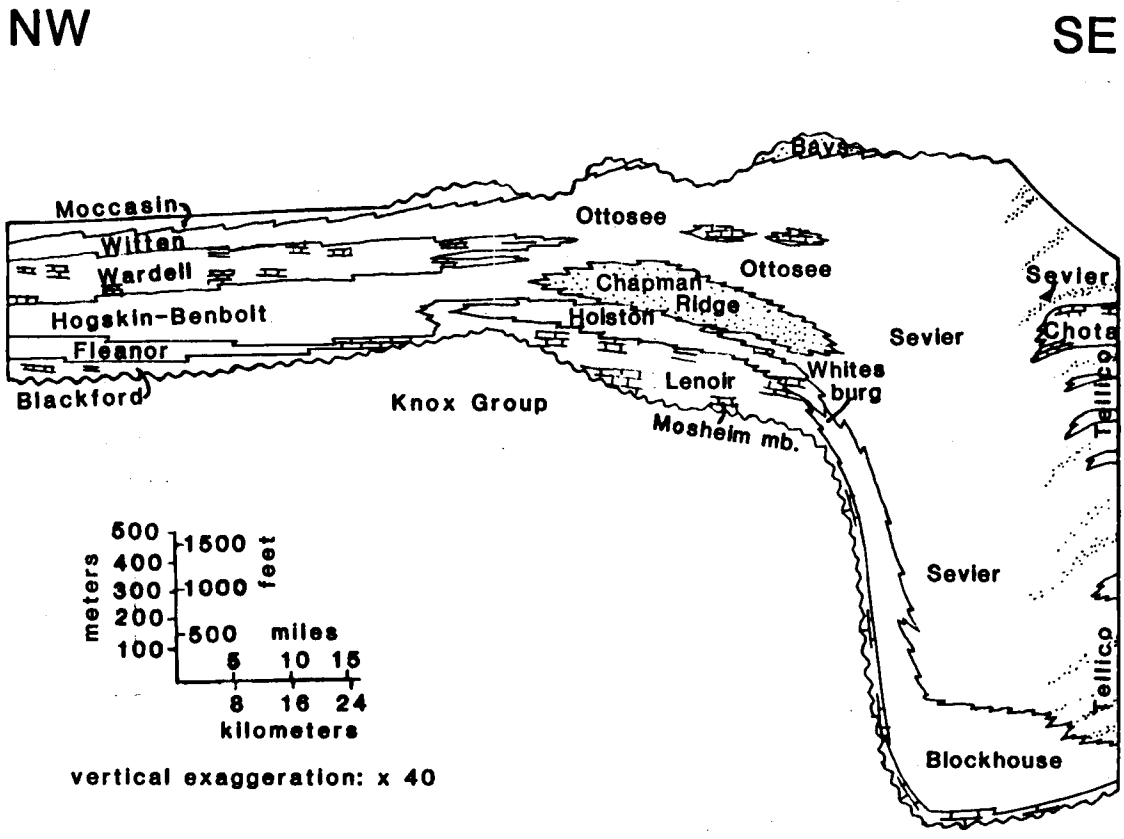

Figure 3. Stratigraphic cross-section (palinspastically restored) of the Ordovician of east Tennessee (after Walker, 1980). Lower wavy line is the Knox Unconformity. Upper wavy line is present erosion surface.

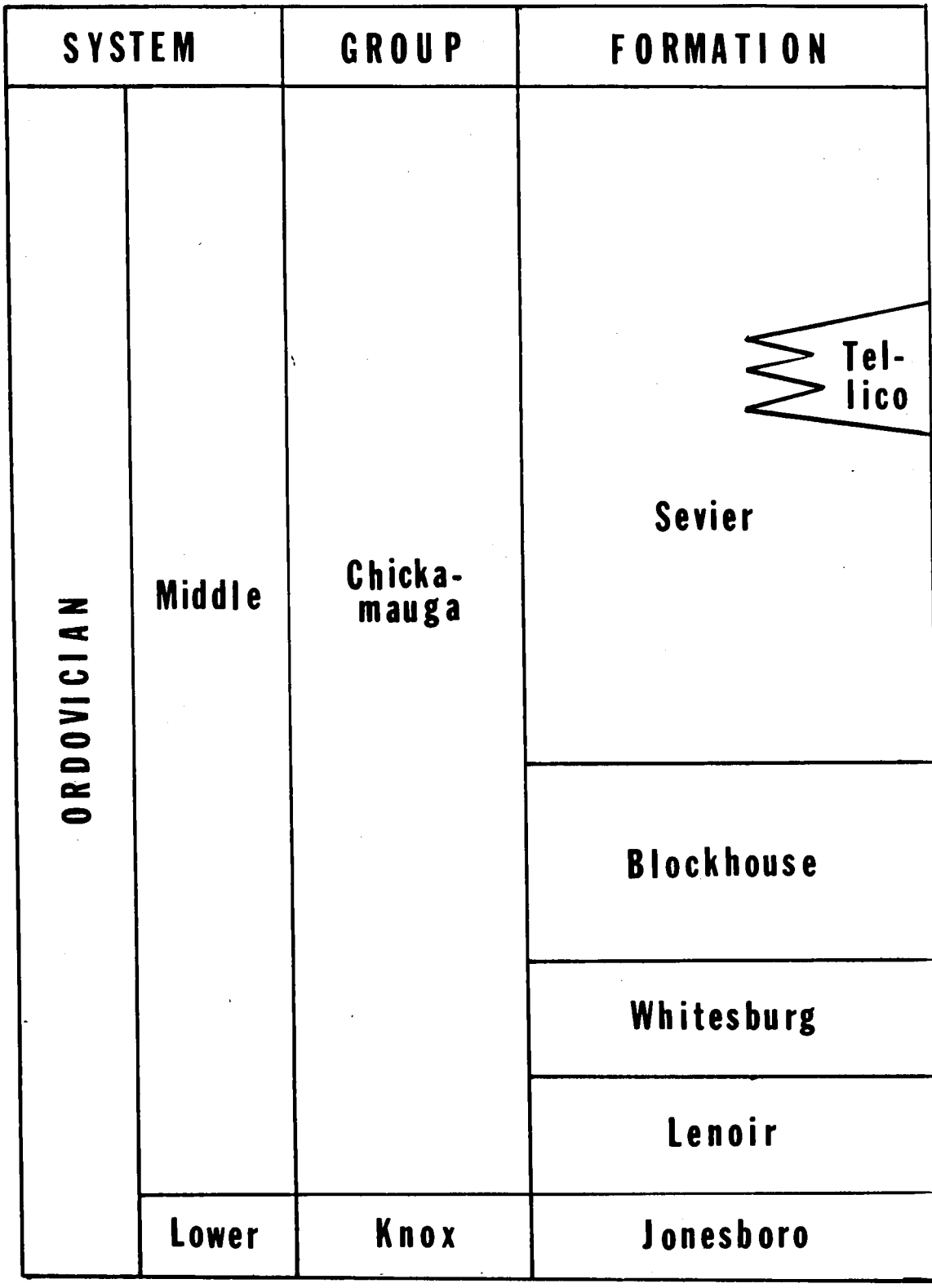

Figure 4. Generalized stratigraphic column at study area. The column is a combination of the 4 sections and adjacent exposures.

Whitesburg), although the distribution was unmappable on the scale of the state geologic map of Tennessee (Hardeman, 1966). The overlying thick section of shales, siltstones, and sandstones comprises the main body of the Middle Ordovician system in the Tellico-Sevier belt. Upper Middle Ordovician Bays formation is not exposed in the area.

Estimates of thickness for the combined Blockhouse, Sevier, and Tellico units at Douglas Lake vary considerably due to structural complexities (particularly fault imbrications causing thickening of the section) and a lack of stratigraphic markers. These estimates range from a minimum of 550 meters (Wedow, 1943) to a maximum of greater than 2,500 meters (Shanmugam and Walker, 1978).

Vertical and lateral facies variations in lower Middle Ordovician rocks suggest evolution of a deep basin from a stable continental platform (Rodgers, 1953; Neuman, 1955). Above this transition, vertically rhythmic units of various scales suggest active tectonism contemporaneous with sedimentation (Shanmugam, (1978). Basin plain sedimentation has been proposed for the lower noncyclic clayey shale sequence (Blockhouse), and a lower deep sea fan is indicated by fine-grained cyclic turbidites (Sevier) on top of the noncyclic clayey shales (Shanmugam, 1980). Proximal fan turbidites have been proposed for deposition of Tellico sandstones and conglomerates (Kellberg and Grant, 1956),

which occur as lenses within the Sevier. The thin conglomerates and sandstones, found in the extreme southeastern portion of the study area, are derived from erosion of carbonate rocks and more distant crystalline and metamorphic source rocks to the southeast.

Maximum temperatures of thermal metamorphism have been inferred from the conodont color alteration index (Epstein et al., 1976). The index for the Dumplin Valley thrust sheet (Harris et al., 1981), indicates an approximate temperature range of 180-230 degrees C (Gray, 1981). This suggests a 6 kilometer maximum depth of burial with a temperature gradient for the Middle Ordovician sediments of 30 degrees/km. The relationship between the thermal peak and tectonism is unclear.

Tectonic fabric elements in Middle Ordovician sediments have been attributed to the late Paleozoic Alleghanian orogeny. Evidence for such a late deformation event is provided by Ordovician and even Precambrian rocks thrust on top of Mississippian rocks to the southwest on the same strike belt and thrust sheet as the study area (Hardemen, 1966). Studies in other areas of east Tennessee suggest an earlier stage of deformation (Roeder, Yust, and Little, 1978), possibly contemporaneous with basinal sedimentation.

The locations of the four detailed profile sections, measured and investigated for mesoscopic structural data are

specified, according to Tennessee Rectangular Coordinates (Figure 2, Plate 5):

Section A: 613,800; 2,791,400 -- 613,100; 2,797,700

Section B: 607,300; 2,786,000 -- 605,900; 2,786,300

Section C: 609,100; 2,787,800 -- 606,800; 2,788,850

Section D: 605,760; 2,782,080 -- 594,700; 2,786,300

C. Previous Investigations

Safford (1869) published the first reconnaissance stratigraphic work in the region and applied the term Gray belt for the strike belt of shale. He grouped the Middle Ordovician rocks regionally into the Trenton and Nashville Series. Keith (1895) subdivided lithologies in the Gray belt into the Athens Shale, Tellico Sandstone and Sevier Shale. Reconnaissance mapping by TVA geologists (Wedow and Laurence, 1943) at Douglas Lake used the same formation names, except that the Tellico (or, "Sandy Ridge") was mapped separately in the vicinity of Indian Creek interfingering laterally with Sevier. Rodgers (1953) divided the shale belt into Athens, Holston, and Ottosee formations southwest of the western edge of Sevier County, but he used "Sevier" for the entire shale belt to the northeast (including the Douglas Lake area), because of the structural complexity. Neuman (1955) described the Tellico-Sevier belt in Blount and Sevier Counties in detail, using the names: Blockhouse, Tellico, Chota (does

not occur in the present study area) and Sevier. Twenty-five kilometers southwest of the present study area, Marie (1963) described units correlating with the Blockhouse and the Tellico of Neuman (1955). On the revised state geologic map, Hardemen (1966) retained the regional use of the term Sevier for the entire shale belt. Shanmugam (1978) measured sections of Blockhouse and the lower Sevier along an embayment of Douglas Lake (adjacent to the north end of the area of the present report). His nomenclature is followed in the present report. Shanmugam's stratigraphic section (Appendix G) was continued in the present report, with minor thickening due to third order faulting, until it is no longer exposed. Sevier interfingers and intergrades both laterally and vertically with Tellico sandstone to the southeast. Feder (1963) mapped the underlying Knox group to the northwest of the Tellico-Sevier belt near the study area. Greene (1959) mapped Cambrian Chilhowee group rocks to the southeast in the hanging wall of the Great Smoky thrust.

Previous structural investigations in the area were mainly restricted to large-scale mapping. Wedow and Laurence (1943) prepared structural cross-sections at Douglas Lake, based on their reconnaissance mapping. The subsequent flooding of the lake removed soil and regolith from the shorelines, and the resulting outcrops display more structural complexity than was recognized by Wedow and Laurence.

Adjacent to the present study area, Troensegaard (1965) described cleavage which he believed to have been formed by shear late in fold development. He noted a dominant axial planar orientation for cleavage, and strongest cleavage development near fold hinges in weak layers interbedded with rigid ones (a high ductility contrast). Yust (1976) did a mesoscopic fabric study in an adjacent area. He concluded that brittle deformation such as faulting was related to buckle folding suggesting monophase deformation. An interpretation of solution cleavage and cleavage-fold relationships in argillaceous limestone (Lenoir formation) in another portion of the Saltville thrust sheet was made by Wise (1980).

As an example of a regional structural synthesis, Roeder, Yust, and Little (1978) propose four sequential stages of deformation in the East Tennessee Valley and Ridge Province: (1) north/south striking conjugate kinks, (2) major, low-angle, bed-parallel transport (including bed-parallel telescopes), (3) tight folding (hard to distinguish from stage two folds) accompanied by thrusting, and (4) low-angle, fold discordant thrusts. Harris and Milici (1977) studied large-scale structures and the characteristics of décollement zones and thin-skinned deformational styles in the western Valley and Ridge Province. Epstein et al. (1977) determined that thrust

faults disrupt conodont color alteration index (CAI) isograds, indicating that thermal maturity in the southern Appalachians developed before the thrusting. Witherspoon (1981) used a combination of available seismic lines, field work and previous mapping to reexamine the structure of the western Blue Ridge and the eastern Valley and Ridge and to characterize the Blue Ridge thrust front in east Tennessee. He postulated that about 20 kilometers of net slip occurred on the unmapped bedding plane thrust near the base of the shales in the Tellico-Sevier belt, or that the 20 kilometers of shortening occurred on several faults within the belt.

D. Methods Used in Present Investigation

1. Geometric and Scale Descriptions

The first step in describing structural style and analyzing deformational fabric elements was a detailed field study of the outcrops. Multiple measurements were taken of mesoscopic structural fabric elements, including: cleavage planes, bedding planes, axial planes of folds, fault planes, and joint planes. Measurements were also made of the following kinds of lineations contained in planes: cleavage-bedding intersections, fold axes, and slip linears. Field relationships between fabric elements were determined, using cross-cutting relationships, sense of vergence and down

plunge asymmetry of folds, and offset and direction of movement on fault surfaces.

The sense and direction of fault movement was determined by examination of the frictional striations (which may indicate only the last increment of motion). The terms "contractional" and "extensional" faulting are terms which describe the shortening and lengthening, respectively, of bedding, regardless of spatial orientation of the fault surface Figure 5b. "Reverse" and "normal" faults Figure 5a are distinguishable, based only on present orientation with respect to horizontal. All four of these fault types (the latter two of which are not mutually exclusive of the former two) were probably produced by compression applied by the Blue Ridge part of the thrust belt in the southeast (Roeder et al., 1978b).

Faults are classified as major (first order), second order (outcrop-scale) or small-scale (third order), based on the magnitude of slip which could be measured or estimated. Major faults have at least several kilometers of displacement. They offset formation contacts. In shales, they may occur in a thick shear zone (10 meters or more), or they may be split into several discrete surfaces. Second order faults have displacements exceeding outcrop-scale (20 meters or so) and ranging up to hundreds of meters or a few kilometers (beds cannot be matched in a single exposure). Small-scale faults

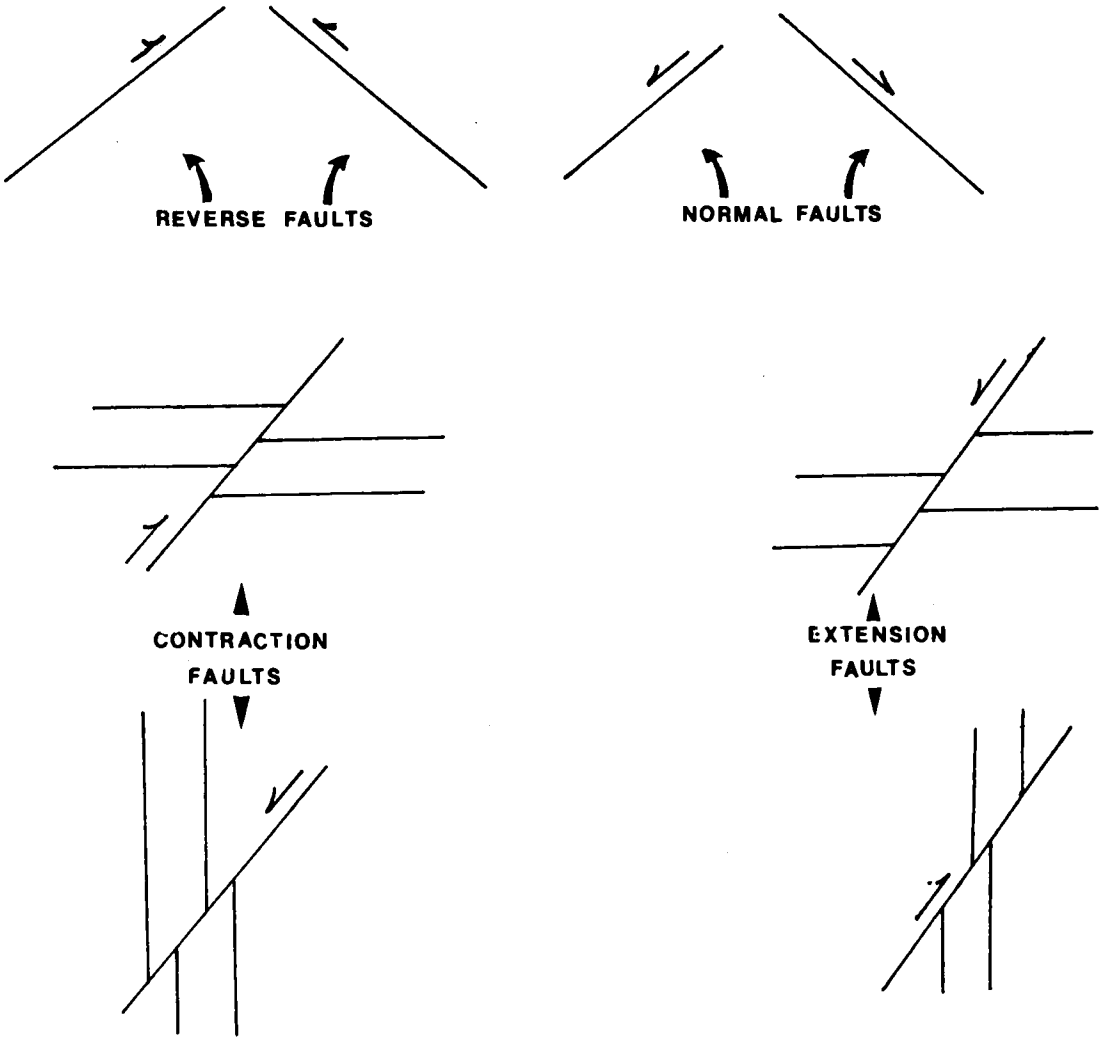

Figure 5. Fundamental fault nomenclature. (a) "Reverse" and "normal" faults depend only on present orientation with respect to horizontal. (b) "Contraction" and "extension" faults depend only on augmenting or diminishing length parallel to bedding.

show displacement not exceeding the size of the outcrop, and they include quite small offsets.

Major first order folds within the Blockhouse-Sevier shales are too large to be observed in outcrop, ranging from hundreds of meters to several kilometers in wavelength. These folds might be more aptly described as broad (gentle, open, or close) warps with second and third order folds on the limbs. Second order folds are outcrop-scale folds and they normally exceed three meters in half wavelength. These frequently form as paired folds (anticline-syncline pairs), with the sense of asymmetry giving the vergence. Small-scale third order folds include parasitic folds on the limbs of second order folds and most kink folds, as well as other small-scale folds (half wavelengths less than three meters) that do not fit into either of these classes.

Cleavage is descriptively classified, on the basis of spacing between cleavage traces in profile, as one of three types: weak (spacing: 3-10 cm), moderate (spacing: 1-3 cm) or strong (spacing: less than 2 cm and frequently less than 0.5 cm) after Simon (1981).

The fabric elements are shown on outcrop sketches in their relative positions in profile view. The sketches are referenced to 20 meter intervals measured horizontally across strike at the outcrop.

2. Photomosaics

The second step in the investigation consisted of photographing level profile sections and constructing panoramic photomosaics. Acetate tracings (outcrop drawings of fair accuracy) were prepared from these photographs and outcrop sketches. The photomosaics and drawings are also referenced to the 20 meter intervals (Plates 1-4). Beds of medium thickness or greater and relatively large faults and folds are depicted to scale in the drawings, while cleavage planes and senses of offset on faults are shown schematically.

3. Graphical Analysis of Fabric Data

Fabric elements, zone axes (Arthaud, 1969), and estimates of shear zone orientation (Hansen, 1971; Wheeler, 1978) were compared on Schmidt net projections. In order to describe the geometries and orientations of deformational fabric elements in rocks, three principal axes of deformation are defined, after Arthaud's (1969) method of determining principal strain axes for brittle deformation. Arthaud's method uses the sense of fault movement indicated by frictional striations. This includes:

X-axis: direction of principal elongation

Z-axis: direction of principal shortening (normal to X)

Y-axis: intermediate principal direction; length will remain the same, given plane strain (normal to both X and Z).

4. Fold Mechanism Analyses

The fold geometries were described (Appendix B) and compared with theoretical models (Flinn, 1962; Curie et al., 1962; Ramsay, 1967; Chapple, 1969; Dieterich and Carter, 1969; Dieterich, 1970; Gray, 1981), to suggest mechanisms that may have produced the folds.

5. Stratigraphic Analysis and Correlations

Stratigraphic correlations were made between recognizable units along strike (between sections across the lake) and across strike for the four sections. Sections were offset along strike to compensate for covered intervals. Stratigraphic facing directions were determined when necessary by making polished slabs. In siltstones, sandy siltstones, and sandstones in the Sevier formation, they were determined from truncated cross laminae. Graded bedding and ripple marks were also used.

6. Construction of Cross-Section

Depth to the Knox "basement" for a cross-section across the shale belt was derived from "approximately balanced" regional cross-sections (Roeder et al., 1978; Witherspoon,

1981). The nearest available interpreted seismic section is located 30 kilometers to the northeast (Tegland, 1978), but it was very helpful.

E. Stratigraphy

1. General

The stratigraphic units in the study area (Figure 4, p. 7) include the upper Knox group (Lower Ordovician) and the following Middle Ordovician formations: Lenoir, Whitesburg, Blockhouse, and Sevier (including a thick lens of Tellico). The Middle Ordovician units are parts of the lower Chickamauga group (Hardeman, 1966), and lie atop the post-Knox unconformity. Neither the upper contact of the Sevier formation, nor the middle or upper parts of the Chickamauga group (Bays and Martinsburg formations) are exposed in the area.

Environmental interpretations covering upper Knox through Blockhouse deposition were made from field observations and thin section study of a section at Dandridge Municipal Park. This work was performed by the Carbonate Sedimentalogy class (in which the author participated) at The University of Tennessee, Knoxville, in the spring of 1981.

2. Upper Knox Group

The upper exposed part of the upper Knox group consists of ribboned limestone and dolostone, dolomitic wackestone,

dolomitic packstone and dolomitic boundstone. Diagenetic chert nodules are present. The thickness of upper Knox is about 600 meters (Hardeman, 1966), beneath an upper erosional contact.

The upper part of the unit shows characteristics of deposition in various platform carbonate subenvironments, such as: lime mud-tidal flat on a restricted platform, normal marine open platform (Benedict and Walker, 1978), evaporite platform, and a position near the shelf edge at the top of upper Knox.

Following deposition of the upper Knox group, subaerial exposure, implied by a rubble breccia consisting of Knox clasts on top of the post-Knox unconformity, caused weathering and erosion. The unconformity marks the hiatus between Lower and Middle Ordovician rocks (Bridge, 1955).

3. Lenoir Formation

The basal member of the Lenoir formation, the Douglas Lake member, contains angular clasts of dolostone and chert which are similar in lithology to upper Knox group carbonates, and these are probably derived from the Knox. Interbedded thick dolostones and limestones comprise much of the Douglas Lake member. Thickness of the unit does not exceed 10 meters on the north shore of Douglas Lake.

The Douglas Lake member represents a Middle Ordovician marine transgression following the post-Knox depositional

hiatus, resulting in deposition in either fluvial or nearshore marine channels in topographic low areas on the erosional surface.

The Mosheim member of the Lenoir consists of thick to massive-bedded, nearly pure, medium-gray lime mudstone. It characteristically has a "fluted" weathering surface on the northwest shore of Douglas Lake, unlike surrounding carbonate units. The Mosheim ranges from 10 to 22 meters in thickness on the north shore of the lake. Mosheim lithology suggests deposition on a carbonate mud-tidal flat.

The main body of Lenoir consists of nodular-bedded, fossiliferous, argillaceous limestone. Cross-bedded, fossiliferous grainstone is sometimes present near the top of the unit. Thickness of this unit does not exceed 12 meters on the north shore of the lake.

The main body of Lenoir represents further transgression and a water depth of more than 10 meters. Organic reef masses developed on a shallow carbonate shelf. Varying thickness relationships between the Mosheim and the main body of Lenoir suggest that these may be partly time-equivalent facies.

4. Whitesburg Formation

The very thin, lower part of the Whitesburg overlies the main body of Lenoir. It consists of pelmatozoan limestone

with thin shale interbeds. Overlying this lower limestone member, an upper member consisting of interbedded thin lime mudstone and clayey shale represents a transition between Whitesburg and Blockhouse formations. This transitional member is often faulted and poorly exposed because of its position at the interface of units with a major ductility contrast (thick underlying carbonates and thick overlying shales). The Whitesburg is between 2 and 14 meters thick.

The lower Whitesburg member is a deep water, manganese-rich packstone, suggesting a rapid increase in water depth to the toe of slope facies (Benedict and Walker, 1978). The upper Whitesburg transitional member was probably deposited in a deep marginal basin below oxygenation level.

5. Blockhouse Formation

The Blockhouse on the northwest shore of Douglas Lake consists predominantly of highly deformed shales, particularly near the basal fault contact with Whitesburg. Above the basal sheared zone, the main lithology in Blockhouss is dark-gray calcareous clayey shales. Thin chert lenses are present at about the middle (as measured in its deformed state). Rare, thin, sandy siltstones and thin silt laminae within clayey shales also occur near the middle, and the silt laminae increase in thickness towards the top of the Blockhouse. Clayey shales become subordinate to siltstones

at a transitional upper contact. Measurements of the deformed thickness of the Blockhouse on the north shore of Douglas Lake range from 36 meters (Shanmugam, 1978) to 49 meters (author's section).

The depositional environment for the Blockhouse was probably a basin plain, below oxygenation level, on which pelagic sedimentation took place.

6. Sevier Formation

The Sevier formation in the study area consists predominantly of calcareous siltstone, mudstone, and shale with smaller amounts of sandstone and limestone. Silty mudstones predominate over clayey shales at the transitional basal contact with the Blockhouse. A thick section (179 meters thick in Section A) of calcareous silty mudstone occurs in the lower Sevier. Above this unit, a thinner sequence (39 meters thick in Section A) of interbedded light-gray, calcareous siltstones and silty shale is present, and it thins along strike toward the northeast. The next unit consists of 172 meters (Section A) of calcareous siltstones interbedded with silty shales in generally thinning upward cycles. Thinner units within the overlying upper Sevier include: calcareous siltstone, interbedded nodular limestone and silty shale, interbedded calcareous sandy siltstone and silty clayey shale, fossiliferous

limestone, calcareous silty mudstone, interbedded clayey shale and silty clayey shale, clayey shale, and calcareous sandstone. The measured stratigraphic sections (see the figures on pp. 29, 51, 68, 78) end to the southeast where faulting causes repetition of the section (see p. 51) or where exposure becomes poor (see p. 29). An unknown thickness of Sevier remains above the highest measured unit. Abundant imbricate faulting duplicates strata and brings more southeastern facies northwestward. Toward the southeast, the Sevier probably grades laterally and vertically into the Tellico sandstone unit, with increasing thicknesses of sandstone interbedded with the Sevier. The measured thickness of the Sevier (up to the point at which a second order fault indicates significant duplication of the section; Section B) is 1,154 meters. The total thickness of the Sevier in the shale belt may be considerably greater.

Deposition during Sevier time probably involved the westward progradation of a deep-sea fan system, probably analogous to deltaic progradation cycles (Shanmugam, 1980). The boundary between basin plain and lower fan is suggested by the first appearance of minor thickening upward, progradational cycles. More rapid deposition of Sevier distal turbidites than of Blockhouse pelagic sediments is suggested by sedimentary features such as flame-structures and load casts (Walker et al., 1980). Deposition by contour currents occurs well up in the Sevier at Douglas Lake.

a. Tellico unit (within Sevier). The Tellico unit of Sevier is exposed in the study area at the mouth of the Indian Creek embayment on the southeast shore of Douglas Lake, 5 kilometers southeast of the base of the Middle Ordovician in this strike belt. The basal contact of the Tellico is gradational with siltstone and shale of the Sevier. The Tellico consists of an undetermined thickness of quartz sandstone (with calcareous cement) interbedded with siltstone and shale. Granule or small pebble conglomerates are present in some of the sandstone beds. They are composed of well-rounded limestone clasts and a small amount of more angular quartz or chert clasts (Kellberg and Grant, 1956). Some of the finer sandstone beds that are gradational with Sevier preserve graptolites, as do the interbedded shales.

The sequences of interbedded sandstones, conglomerates and shales in the Tellico unit are characteristic of turbidity current deposits. The shallow water fauna in the sandstone contrasts with graptolites in the shale interbeds and suggests transport by turbidity currents into a deeper water environment (Keller, 1980). Keller concludes that the Tellico sandstones at the Indian Creek embayment were deposited by turbidity currents in the midregion of a submarine fan.

CHAPTER 2

DESCRIPTIONS AND INTERPRETATIONS OF PROFILE SECTIONS

A. Introduction

This chapter describes the structural geometries and styles in the four measured shoreline profile sections (A-D; Plates 1-4). The text supplements the four plates illustrating the mesoscopic structures displayed in the sections. In both the text and plates, letters (A, B, C, or D) followed by two-digit numbers refer to locations on the profile sections based on intervals of 20 meters measured in horizontal, perpendicular to strike, and from northwest to southeast. The sections are standardized (A00, B00, etc.) so that the numbering begins at the observed or projected basal contact of the Blockhouse formation. This contact is well exposed in Section A, less well exposed in Section D, and lacks exposure in Sections B and C (requiring interpolations to be made between A00 and D00 to obtain approximate locations of B00 and C00). Continuous stratigraphic sections are compiled for the lower units in Section A (762 meters of combined Blockhouse and Sevier; see p. 29) and the lower units (but not the lowest) in Section B (1,204 meters of Blockhouse and Sevier; see p. 51). The text for each of the

four sections begins with an overview summarizing gross aspects of the structure and stratigraphy. Following this is a description of the stratigraphy either until it can no longer be traced upsection (Section A), or until duplication by faulting occurs (Section B). Then, a description of mesoscopic structure is given for each section (A-D), accompanied by an analysis of significant fabric elements.

Mirror images of the outcrops representing Sections C and D are presented in Plates 3 and 4, in order that each of the four sections is observed from northwest to southeast (from left to right). Consequently, outcrop photographs from Sections C and D included in the text are also mirror images of the corresponding portions of Plates 3 and 4.

B. Section A

1. Introduction

Section A (Plate 1) extends 1,540 meters perpendicular to strike on the north shore of Douglas Lake (between Tennessee Rectangular Coordinates: 613,800; 2,791,400 and 613,100; 2,797,700). It begins at a fault contact between the lower Middle Ordovician carbonates and the Middle Ordovician Blockhouse shale.

Above a major décollement fault (fault a, Plates 5, 6) of uncertain magnitude at the base of the section (in the lower Blockhouse), more than 700 meters of exposed strata

(Figure 6) in the Sevier are deformed mainly by folding on a mesoscopic scale with related minor faulting. Fold axial surfaces rotate from northwest dipping at the northwest end of the section through vertical to southeast dipping at the southeast end of the section. Cleavage development is strongest (displaying minimum spacing between traces) in calcareous mudstone, the predominant lithology in the lower Sevier. Cleavage is also controlled by structure, being most closely spaced in the vicinity of fold hinges and contraction faults. Cleavage that transects fold axial surfaces is usually associated with faulting of the folds. In the downplunge direction (to the southwest), toward a higher structural position, axial surfaces rotate to vertical and more northwest dipping. This trend indicates that axial surfaces at depth probably dip more shallowly to the southeast. In the up-plunge direction (lower structural position), folds are more likely to be faulted and to show transection of the axial plane by cleavage.

Section A is considerably less faulted than the sections which extend further upsection, i.e., D and the southeastern part of B. A second order fault zone occurs in the extreme southeastern portion of the section, where it is associated with second order folding. Small-scale contraction faults are more numerous, including both antithetic and synthetic sense with respect to regional northwestward transport.

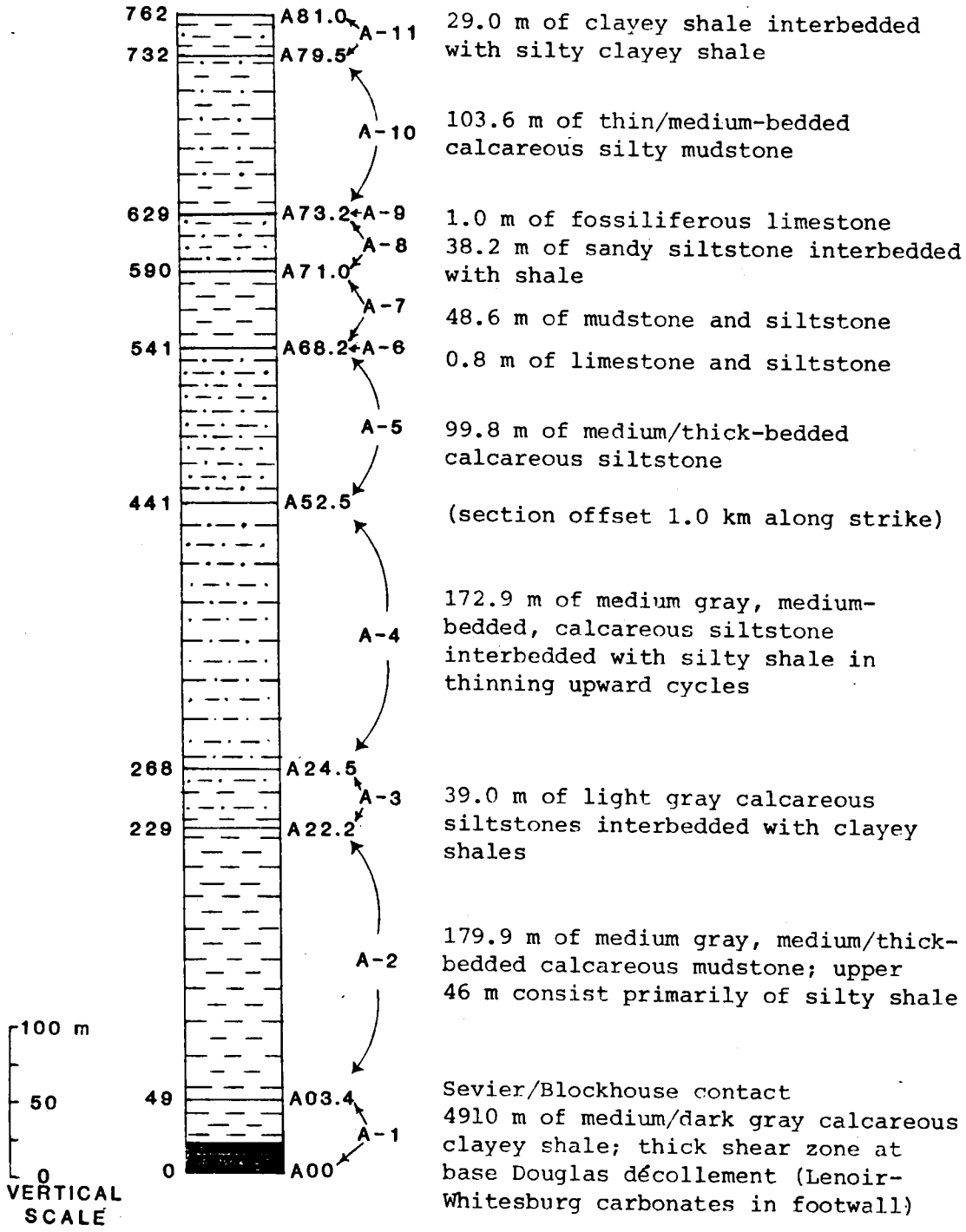

Figure 6. Stratigraphic column for Section A (see Figure 2, p. 3; Plate 1). The letter A followed by a number refers to a location in Section A based on the number of 20 meter intervals measured in horizontal, perpendicular to strike, beginning at the northwest end of the section (A00). A-1, A-2, A-3, etc., represent stratigraphic units within the Sevier at Section A.

Cumulative buckle shortening calculated for the 1,554-meter-long section is 14 percent.

2. Stratigraphy

The best exposure of the contact between lower Middle Ordovician carbonates (Lenoir and Whitesburg) and Middle Ordovician shales (Blockhouse) in the vicinity of Douglas Lake occurs at the northwest end of Section A. Slip linears and intense shearing at this locality indicate that the contact is a faulted contact (Douglas fault) rather than a stratigraphically conformable one, despite the lack of stratigraphic duplication (Figure 6). There are no preserved primary sedimentary laminations in the lower five meters of the sheared zone.

The significance of the Douglas fault (fault a, Plates 5, 6), aside from its structural importance, involves the fact that its presence must alter any paleoenvironmental interpretations of stratigraphic units because the strata which are now juxtaposed across the fault were not deposited in the same part of the basin; they may have been widely separated facies.

a. Blockhouse formation. The undeformed thickness of Blockhouse cannot be determined accurately, since no undeformed exposures of Blockhouse were observed in the area. Thickening of the Blockhouse has undoubtedly occurred due to

folding and faulting. It is speculated, due to discordant bedding attitudes adjacent to the fault, that some of the lower Blockhouse may have been faulted out at depth. The deformed thickness of Blockhouse (unit A-1) above the faulted basal contact (Figure 7) was estimated at 49 meters (Figure 6), measured normal to the attitude of uninvolved Whitesburg in the footwall. The only indicators of bedding in the 5-meter-thick shear zone (which thickens southwestward) above the basal contact are broken, telescoped pods of dark gray crystalline limestone occurring within clayey shales. These shredded limestones may be derived from upper Whitesburg, which is transitional upwards with Blockhouse (Shanmugam, 1978). This transitional unit was deformed along with the Blockhouse because of its large proportion of ductile shale.

The predominant lithology in the Blockhouse is medium to dark gray calcareous clayey shale (Figure 6). Rare, thin chert lenses are found in the middle of the unit. Rare, thin sandy siltstones also occur near the middle of the unit within clayey shales. From 23.8 meters up, thin silt laminae increase in thickness within the clayey shales. At A02.9, exposure is missing to the southeast due to an embayment on the north shore of Douglas Lake. The section is, therefore, offset across the embayment along strike to the northeast, where shale in the northeastern part of the embayment was

Figure 7. Douglas décollement zone at base of Blockhouse (A00-A00.2). View is to northeast. Clockwise from bottom: (a) Incompetent sheared Blockhouse, lying atop competent Whitesburg carbonates (vertical stick at water level represents 2 meters). (b) Tight discfold (penny for scale) in fissile shale in shear zone; part of a. (c) Limestone fragments in shale in lower part of sheared zone; part of a (knife for scale).

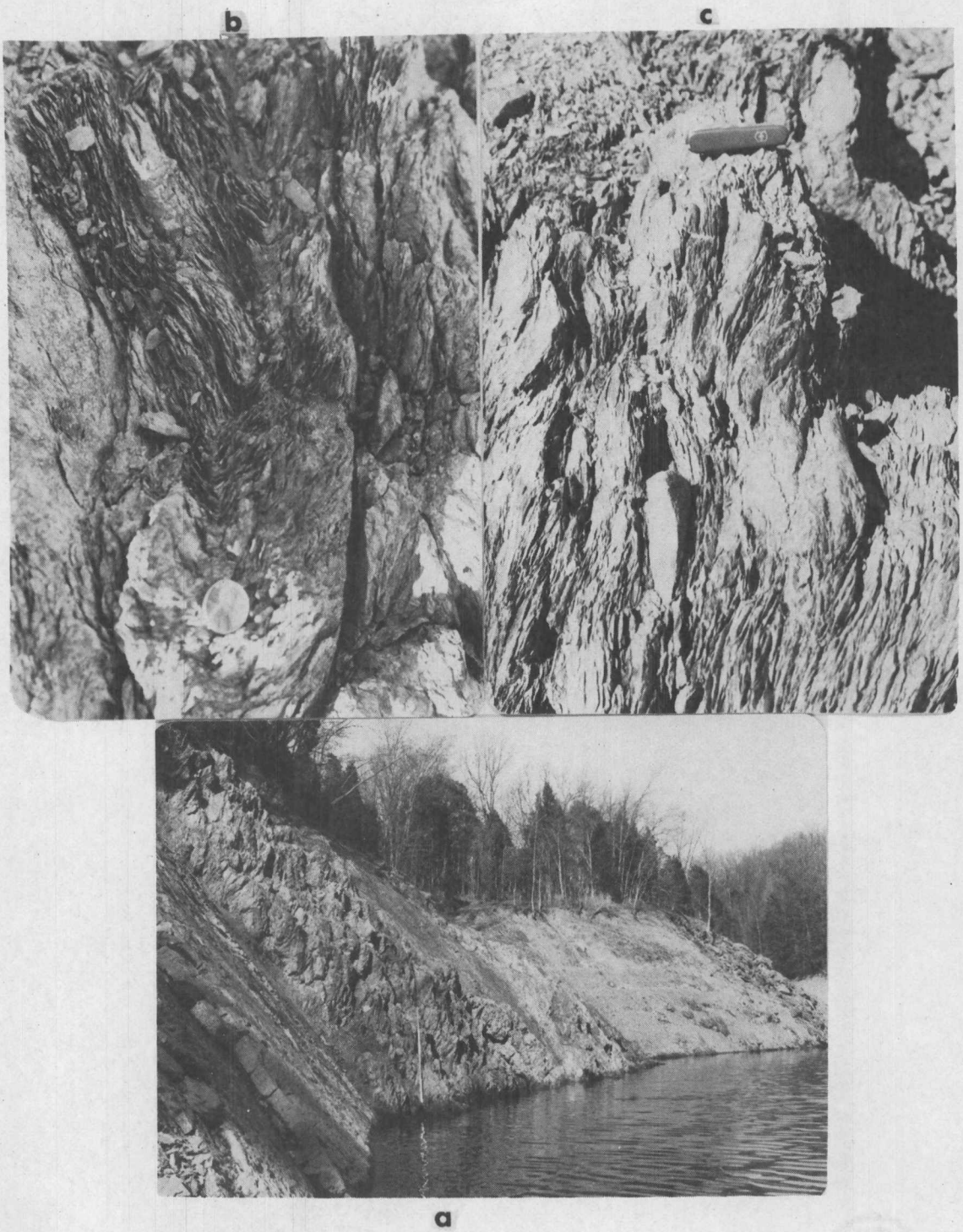

Figure 7

measured to fill the gap on the main profile (A02.9-03.6). The upper contact of Blockhouse clayey shale with the silty mudstone of the Sevier is exposed on the east side of this embayment. The contact is moderately sharp, although rare silt beds are present below the contact, interbedded with the Blockhouse. Criteria for recognizing the contact are from Shanmugam (1978) at his Nina sections (Appendix F) located 0.4 to 0.9 kilometers to the northeast in an adjacent embayment.

b. Sevier formation. At Section A 712.8+ meters of the Sevier formation were measured (Figure 6, p. 28). Poor exposure occurs further to the southeast from A81 (Plate 1). The lower 179 meters (unit A-2) of the Sevier (A03.4-22.2) consist of slightly silty calcareous mudstone (in mostly medium/thick parting units), with the upper 46 meters consisting primarily of silty shale. It is correlated with Shanmugam's (1978) unit no. 7, measured 0.75 kilometers to the northeast along strike (Appendix F).

The next stratigraphic unit (A-3) within Sevier consists of 39.0 meters (A22.2-24.5) of interbedded (5 to 15 cm thick) calcareous siltstones and clayey shales, resembling a shaly flysch. It is correlated with Shanmugam's (1978) unit no. 8 (Appendix F), measured 0.6 kilometers to the northeast.

The overlying unit (A-4) in Sevier is 172.9 meters (A24.5-52.5) of medium-bedded, calcareous siltstones with

silty shales in generally thinning upward cycles. The lower and middle parts of it are correlated with Shanmugam's (1978) unit no. 9 (Appendix F). The lower contact of unit A-4 is located 0.5 kilometers to the southwest along strike from the base of Shanmugam's unit no. 9. The two sections converge southeastward, merging just before Shanmugam's measured section (Appendix F) terminates. Section A is offset along strike 100 meters across an embayment of the lake at A33. Section A was also offset 80 meters along strike (at A36) across another embayment. Section A is covered for 10 meters from A39-39.5, followed by continuous exposure from A39.5-52.5. A covered interval southeast of A52.5 extends 182 meters perpendicular to strike necessitating another offset of the section 1.0 kilometer to the northeast along strike. A52.5 is regarded as the top of unit A-4, since the offset along strike encounters consistently thicker-bedded siltstones.

A unit of medium/thick-bedded calcareous siltstone (99.8 meters in thickness) comprises unit A-5 (A52.5-68.2) in the offset section.

A thin unit (0.8 meters thick) of interbedded cobbly limestone and thin-bedded siltstone and shale (A-6) outcrops from A68.20-68.25.

Above the limestone unit, lies 48.6 meters of predominantly thin-bedded calcareous mudstone and siltstone

(A-7), with 1 meter of interbedded shale at A68.8. Calcareous mudstone occurs within unit A-7 as thin/medium beds in a zone from A69-71.2. The upper contact of the thin-bedded mudstone and siltstone unit is placed where light-gray, thin, calcareous, sandy siltstone beds first appear.

In unit A-8 (similar to unit A-3), sandy calcareous siltstones (5 to 15 cm thick) are interbedded with silty clayey shale. Unit A-8 is 38.2 meters thick, and the siltstones are thickest (10 to 15 cm) near the middle of the unit.

One meter of fossiliferous limestone (unit A-9) at A73.2-73.25 overlies the interbedded siltstone and shale sequence at a sharp contact. Pelmatozoans, gastropods, and other fossil debris are present. As a paleobathymetric indicator, pelmatazoans usually indicate a water depth less than 100 meters and nearly always less than 300 meters (Benedict and Walker, 1978); however, a paleodepth of 1,000 meters is proposed for this part of the Sevier by Walker et al. (1980). Possibly the fossil fragments underwent considerable transport prior to deposition.

The overlying unit (A-10) from A73.25-79.5 consists of 103.6 meters of calcareous silty mudstone. The base of the unit dominantly consists of clayey shale, although it becomes siltier within the first 5 meters. The upper 27 meters (A78.1-79.5) of A-10 consists of silty mudstone displaying

bipolar current indicators (contourites). A sharp upper contact for unit A-10 occurs at the top of the contourites.

Above the silty mudstone contourites, a section of interbedded fissle clayey shale and silty clayey shale (unit A-11, 29+ meters thick) continues to the end of the exposed section (A81).

3. Structure

A few meters below the base of Section A (in the relatively undeformed carbonates comprising the footwall of the Douglas fault), strong cleavage was observed in the more argillaceous beds of the Lenoir formation. The cleavage is hackly (rough, irregular) to anastomosing in form, and it cuts bedding at a high angle.

The first order Douglas décollement fault (fault a, Plates 5, 6) involves a thick shear zone (Figure 7) at the base of section A. A 23-meter-thick zone of strongly deformed Blockhouse (measured normal to the uninvolved footwall carbonates), overlain by another 21 meters of less intensely deformed, yet faulted, Blockhouse, occurs above the basal fault contact. The contrast in behavior between the footwall carbonates and hanging wall shales is due to a competence contrast between the rigid underlying carbonates and the weaker Blockhouse shales above. Much of the estimated 49 meters of Blockhouse is at least moderately deformed.

Other outcrops of basal Blockhouse at Douglas Lake are poorly exposed, such as exposures 7.5 kilometers to the southwest (Dandridge Municipal Park) and 14 kilometers to the southwest (Island View). These localities, however, show discordance of Blockhouse and underlying carbonate bedding attitudes. At an exposure 17 kilometers to the southwest (Douglas Dam), Laurence (1943) noted that: "Many veins of calcite are present in the black shale (Blockhouse), especially in the crumpled and sheared zones." These outcrops suggest a continuity of faulting at the contact along strike.

Displacement on this fault is not calculable from available exposures, because there is no stratigraphic duplication. Prior to this description of the Douglas fault, Witherspoon (1981) proposed a hypothetical fault near the northwest boundary of the shale strike belt in order to balance his regional cross-sections and explain a structural high to the southeast (Newport anticline) using a duplex folded-fault structure (Figure 8). Witherspoon suggested that a position for the fault close to the base of Middle Ordovician clastics seemed to be a favorable gliding horizon at this and other locations. He noted that poor exposure in most areas caused the fault zone to be missed previously. Witherspoon's regional southern Appalachian cross-sections, based on the COCORP seismic data (Cook et al., 1979) require

NW SE

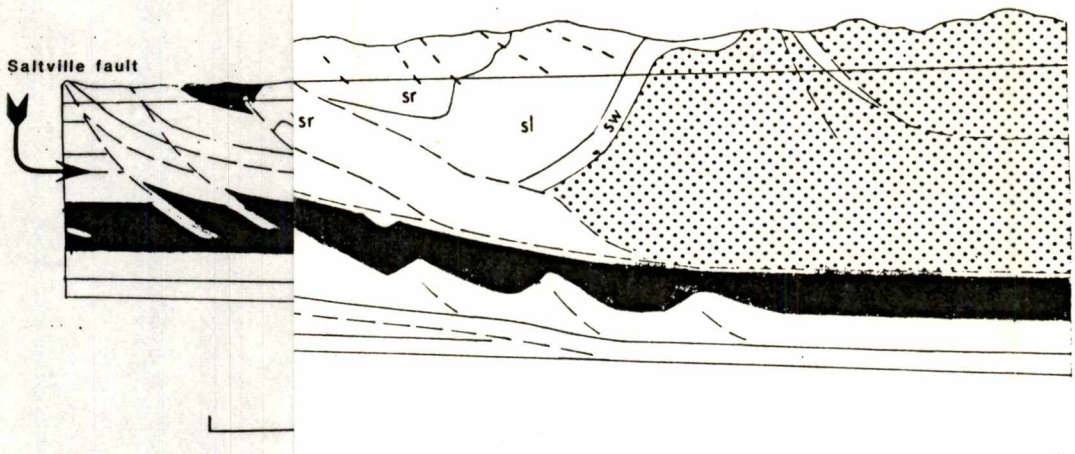

Ridge (Witherspoon,
198s Creek fault (e).

a large (approximately 20 kilometer) displacement on a single fault or a combination of faults in this area. He shows the hypothetical fault as having a surface strike trace of about 160 kilometers. The lower Blockhouse/upper Knox stratigraphic level is also observed as a décollement horizon (in a more eastward facies) in the footwall of the Great Smoky fault in the Cove Windows toward the southeast (formed by erosion through the Great Smoky fault; Witherspoon, 1981).

Faulting above the Douglas fault zone and within the measured portion of Section A is generally either bed-parallel (and marked by slickenlines), in which case net slip cannot be determined, or else it is related to folding. Faults observed above the basal shear zone which are other than bed-parallel are almost exclusively small-scale. The exceptions are two second order faults in the southeastern part of the section, one of which is associated with a second order paired fold displaying axial planar cleavage (Plate 1, A74).

The lower Sevier unit (A-2) is the most intensely cleaved lithology in the vicinity of Douglas Lake. This portion of the Sevier in Section A is cut by abundant wrench faults, some of which are observed to offset cleavage surfaces. Rare telescoping (cut by cleavage) occurs, and the low ductility contrast between beds throughout most of the unit is the likely reason why telescoping is only rarely

present. Fold wavelength is large (exclusively second order), and this may be an effect of the bed thickness (Hudleston, 1973). The folds closely approach similar geometry, and this is again an effect of low ductility contrast between layers (Ramsay, 1962), as is the presence of slip surfaces other than bedding observed near the hinge of the A15 syncline (Plate 1).

Fold axial surfaces (within unit A-2) have variable dips with a range of nearly 50 degrees, from 55 degrees northwest to 76 degrees southeast. The author believes that these irregular folds were due to transport of the shales on the underlying décollement.

Cleavage maintains more consistent dip orientations, being nearly axial planar to the upright syncline at A15 and retaining a steep southeast to vertical dip orientation as it strongly transects the northwest-dipping axial surface of the anticline at A19 (Figure 9). Where cleavage is subparallel to bedding from A19 to A22.2, a fissility is imparted to bedding in contrast with the thick-bedded/massive northwest limb from A15 to A19, in which cleavage is nearly perpendicular to bedding. The greater fissility caused by the close parallelism of cleavage and bedding southeast of the A19 anticline is the main reason that the upper 46 meters of the unit are described as silty "shale," rather than silty "mudstone." Northwest dipping contraction faults (back-



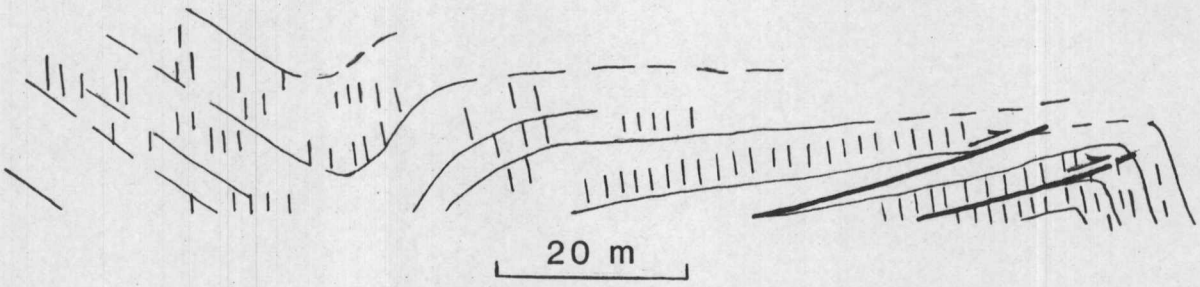

Figure 9. Cleavage superimposed on irregular folds with variable axial plane dips (A14-20).

thrusts) are localized on the middle limb between adjacent second order fold hinges at A15 and A19. These backthrusts are small-scale faults (based on visible displacement of the anticlinal hinge at A19; Plate 1), and they are late syn- to postfolding. The cleavage is superimposed on the strongly transected fold at A19 and it may be related to movement on the backthrusts (Plate 1; Figure 10). The orientation of cleavage is refracted slightly across fault surfaces, indicating that some fault movement occurred after cleavage formation. Rare telescopes and second order buckle folds indicate initially bed-parallel contraction.

In unit A-3, steep, homoclinally southeast-dipping strata occur with weakly developed cleavage either parallel to or slightly steeper than bedding. Small-scale kink-band folds (Plate 1) are observed in this otherwise homoclinal section. They are open folds, the middle limbs having been rotated less than 45 degrees relative to the outer limbs, and consequently, they have neither reached a locking position nor ruptured. Conjugate senses of vergence occur on the kink-band folds: a sense synthetic to regional northwestward transport and another sense antithetic to the first. The shortening axis determined for the two conjugate sets is nearly parallel to bedding, implying that these folds were formed relatively early in larger scale folding when layer-parallel contraction was predominant. An antithetic

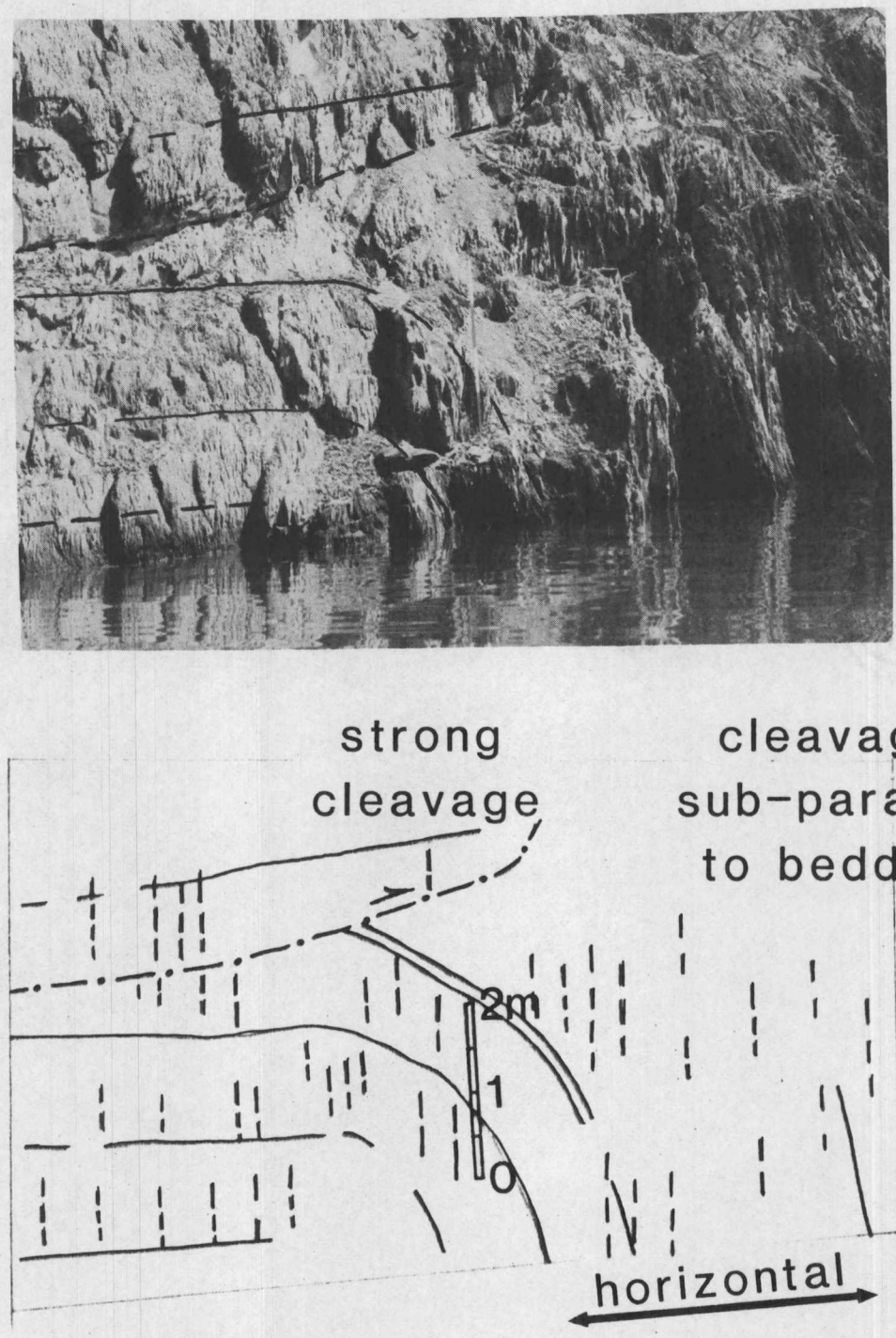

Figure 10. Faulted anticline with transecting cleavage (A19). Southeast is at right. Heavy solid lines represent bedding. Dashed lines represent cleavage. Dotted and dashed line is fault (with arrow for sense of displacement). Two meter stick for scale.

kink-band of this type (A23) is refolded by a larger scale kink fold which is synthetic to the flexural slip sense of major folding.

Folds in unit A-4 are mostly upright. The syncline at A33 has a modified concentric geometry (Ramsay, 1967). It is closer to the ideal concentric fold than the folds in A-2, possibly because of the presence of the coarser lithology (Ramsay, 1962) and a higher ductility contrast with surrounding rocks. Cleavage is more significantly fanned in this fold, probably due to refraction of cleavage by more competent beds. Right-side-up homoclinal limbs with divergent dips on either side of a covered interval (A39-39.5) suggest the presence of an unexposed anticlinal hinge, possessing a vertical axial surface. The nearly upright chevron syncline at A48 is uncleaved, but a flexural slip induced kink (A48.1) on the southeast limb of the syncline displays anastomosing cleavage which strongly transects the axial surface of the syncline. Two asymmetrical, small-scale fold pairs (A38.65-46.25) occur on homoclinal limbs in unit A-4, and both plunge more than 20 degrees to the southwest, which is considerably greater than the plunges of the major folds. The vergence of each is consistent with flexural slip. The paired folds at A38.65 display moderate axial planar cleavage, in contrast with the folds at A46.25 which are uncleaved. Small-scale conjugate kink folds,

related to bed-parallel contraction (like the folds in unit A-3) are also present in unit A-4 on homoclinal limbs. Axial planes of the parasitic folds at A38.65 and A46.25 are very nearly parallel to the axial planes of the corresponding second order folds. Faults in unit A-4 are small-scale contractional thrusts, generally having the backthrust (antithetic) sense of displacement on northwest dipping beds and having the synthetic thrust sense on southeast dipping beds, implying a homotactic relationship to folding.

Cleavage is restricted to fold hinges in three of the four areas in which it was observed in unit A-4; in the fourth area, the cleaved rocks are adjacent to a covered interval at the upper exposed part of the unit (A52.5). It is speculated that an anticlinal fold hinge exists in the covered interval, based on the presence of the cleavage. The dip of the missing axial surface is constrained by probable cleavage fanning on either side of the fold. The possibility that the cleavage may significantly transect the axial plane is small because no faulting is observed in the cleaved rocks. At most localities where strongly transected folds are observed, the folds are faulted and the cleavage is geometrically related to the faulting (Figure 11). The minimum shortening strain due to buckling alone for the interval from A00-52.5 (northwest of the covered interval) was calculated to be 14.1 percent.

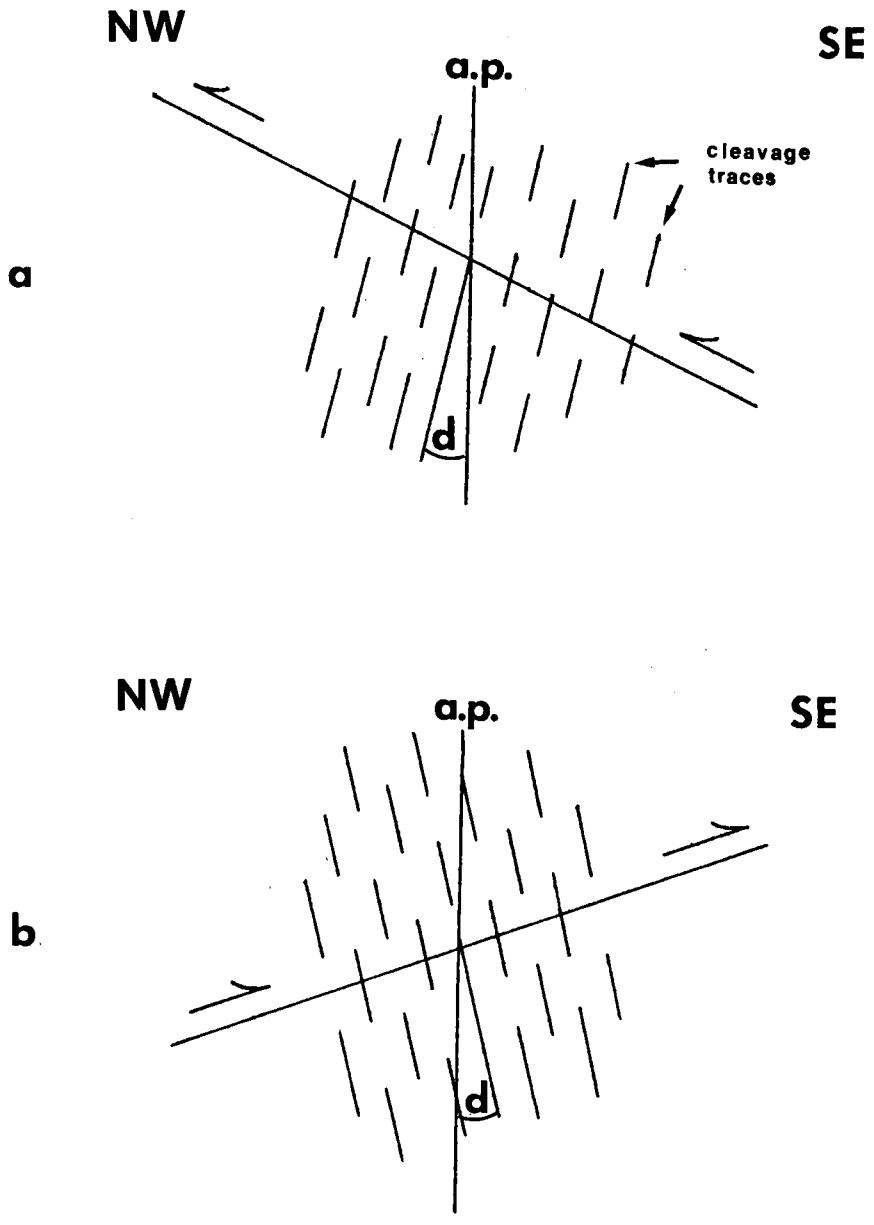

Figure 11. Pattern of observed cleavage transection with respect to the fold axial plane and the associated dominant contraction fault. In each case (a and b), the transecting cleavage is more nearly normal to the fault surface than the axial plane trace is to the fault. Localities: A19 (case b; d = 50°), A48 (case b; d = 16°), A64 (case a; d = 36°), B65 (case a; d = 13°), B96.1 (case a, d = 5.5°), D131.5 (case b; d = -35°).

Upright, modified concentric anticlines at A50e and A51e, exposed in an embayment, exhibit backlimb thrusts that are parallel to bedding in the southeast limb and displace the hinges to the northwest. These folded rocks also display strong transecting cleavage (consistent with Figure 11) in the hanging walls of the thrusts.

The syncline at A58.9 is poorly exposed and apparently uncleaved; its proposed hinge location is based on discordant adjacent facing direction indicators, in a 1 to 2 meter covered interval. Hackly cleavage is present in homoclinal beds from A60.6-62 and again at A66.5-66.7. A faulted anticline (A64), in which a small-scale southeast dipping thrust fault displaces the hinge northwestward, displays strongly transecting cleavage (nearly vertical) across a southeast dipping axial surface. The cleavage has different orientations on opposite sides of the fault (Plate 1), indicating that the faulting postdated cleavage and displaced the cleaved rocks. The bearing of this anticline projects southwest in the downplunge direction (0.67 kilometers) to the main channel where the corresponding fold exposure is unfaulted. Either the fold is faulted at a lower structural level (encountered in the up-plunge direction), or the fault dies out along strike. Numerous kink folds in unit A-5 display antithetic vergence with respect to second order folding, suggesting that they are early effects of

bed-parallel contraction. An approximately bed-parallel fault at A66 (Plate 1) displaces such a kink.

Bed-parallel faults at A68.75 and A68.8 bound a 1-meter-thick zone of deformed shales. At A68.95, a southeast dipping second order thrust fault cuts upsection in both the hanging wall and the footwall at a low angle to bedding.

Steep, northwest dipping cleavage is present in silty mudstone (unit A-7) from A69-71.0. Bedding in this interval is homoclinal and the cleavage intensity is moderate to weak.

Conjugate extension faults are observed at A72.3 and A72.6 in the homoclinal sequence. Minor kink folds occur at the base of the unit at A71 and minor drag folds adjacent to reverse contraction fault surfaces occur in the upper part of the unit at A72-73.

Brittle deformation, involving telescoping and intense veining of the limestone at A73.2 (unit A-9) contrasts with deformation of the more ductile units above and below. The lower contact of the clayey shales (unit A-10) is a nearly bed-parallel fault contact, as shown by slip linears on the contact with the limestone. Approximately bed-parallel fault surfaces were observed at A73.54 and A73.6, and a second order vertical fault at A73.68 cuts a syncline which exhibits axial planar cleavage (Plate 1). A complex, faulted second order anticline at A73.9 has slightly convergent fanning of cleavage around the axial surface. High-angle faults which

extend bedding (A74.0-74.2) are clearly later than both the formation of cleavage and folding. A bed-parallel shear zone at A74.5 indicates slip towards the north (Plate 1). Other approximately bed-parallel shear zones occur at A75.6, A76.0, and A76.25. A small, antithetic kink fold is cut by a related small-scale backthrust at A78.7.

The minimum shortening strain due to buckling alone for the interval A63.5-77.7 (southeast of the covered interval) was calculated to be 14.1 percent. This coincides with the cumulative buckle shortening value for the entire length of Section A of 14.1 percent.

C. Section B

1. Introduction

Section B (Tennessee Rectangular Coordinates: 607,300; 2,786,000-605,900; 2,686,300) begins on the southeast shore of the lake and a considerable distance above the base of the Sevier. It extends continuously 680 meters perpendicular to strike toward the southeast (Plate 2), and then sporadically for another 1,910+ meters (not shown on Plate 2). Including an offset projection of the missing lower Middle Ordovician shales (from Section D, 1 kilometer to the southwest along strike), 1,203 meters of Blockhouse and Sevier strata (Figure 12) occur from the base of the section to a large second order fault (fault b: Plates 2, 5, 6). The fault is located 1.3 kilometers from the northwest boundary of the

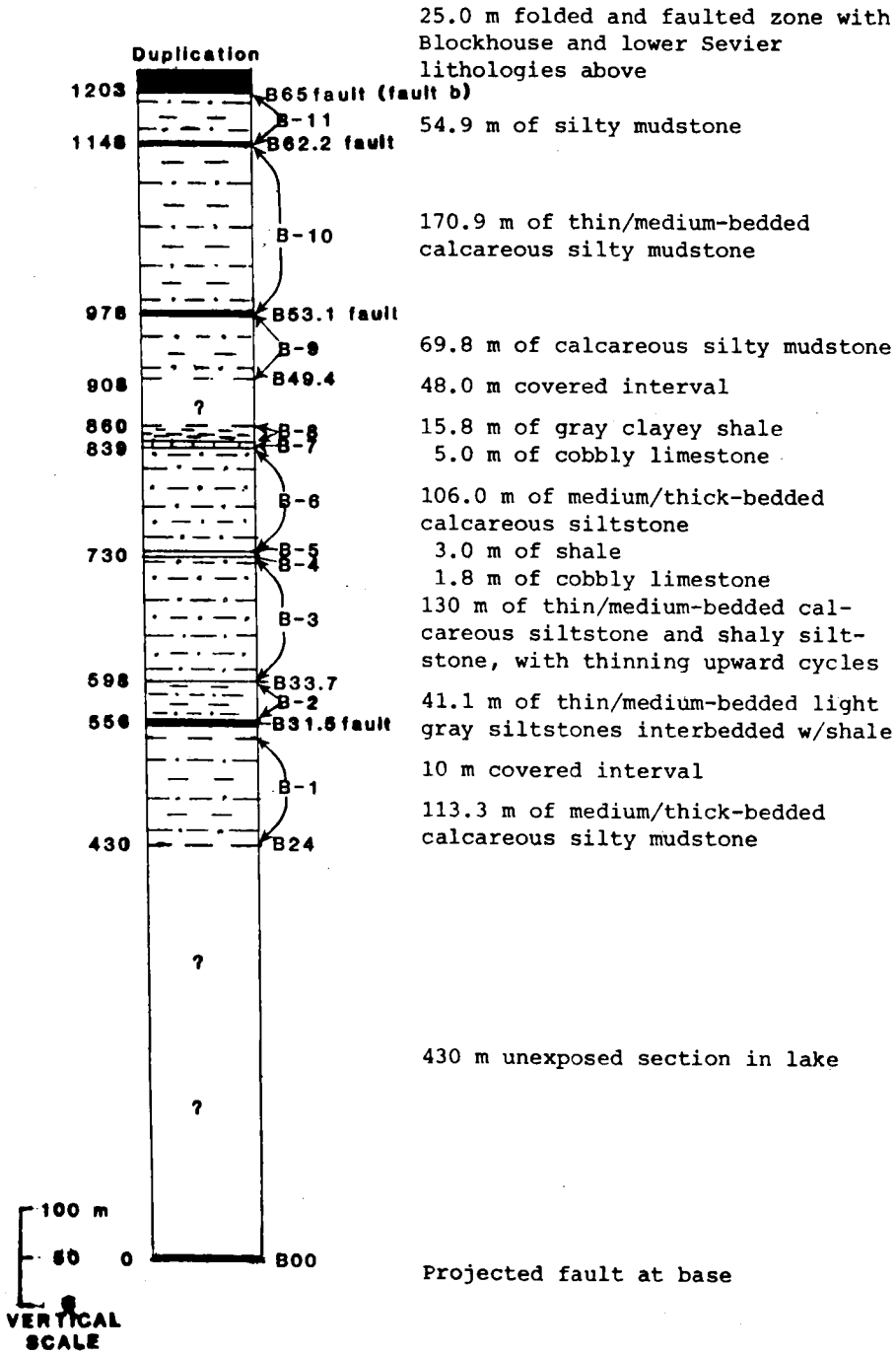

Figure 12. Stratigraphic column at Section B (see Figure 2, p. 3; Plate 2). The letter B followed by a number refers to a location in Section B based on the number of 20 meter intervals measured in horizontal, perpendicular to strike, beginning at the northwest end of the section (B00). B-1, B-2, B-3, etc., represent stratigraphic units within the Sevier at Section B.

shales. The lower shales (Blockhouse) and mudstones (lower Sevier) are duplicated above this second order fault in its hanging wall.

Axial surfaces of folds vary systematically (Figure 13) from northwest dipping low in the section (in the northwest), to vertical in the middle of the section and southeast dipping to recumbent in the extreme southeast. Cleavage is predominantly axial planar, but it shows negative d (Borradaile, 1978) transection (anticlockwise when viewed toward the northeast; see Chapter 3) values in the transected folds. Cleavage is either localized by structures or it occurs in predominantly fine-grained, calcareous mudstone. The large-scale changing trend of cleavage surfaces, fold axial surfaces, and other planar fabrics in Section B implies the existence of a major syncline, which is broken by second and third order contraction faults. A large second order contraction fault system causes considerable stratigraphic duplication. This fault may be an imbricate fault that merges with the major Douglas décollement at depth. Cumulative buckle shortening strain for the 1,680-meter-long section was calculated to be 16 percent, with a general southeastward increase.

2. Stratigraphy

The Blockhouse-Sevier contact and lower units are buried beneath alluvium below the normal low water (winter) level of

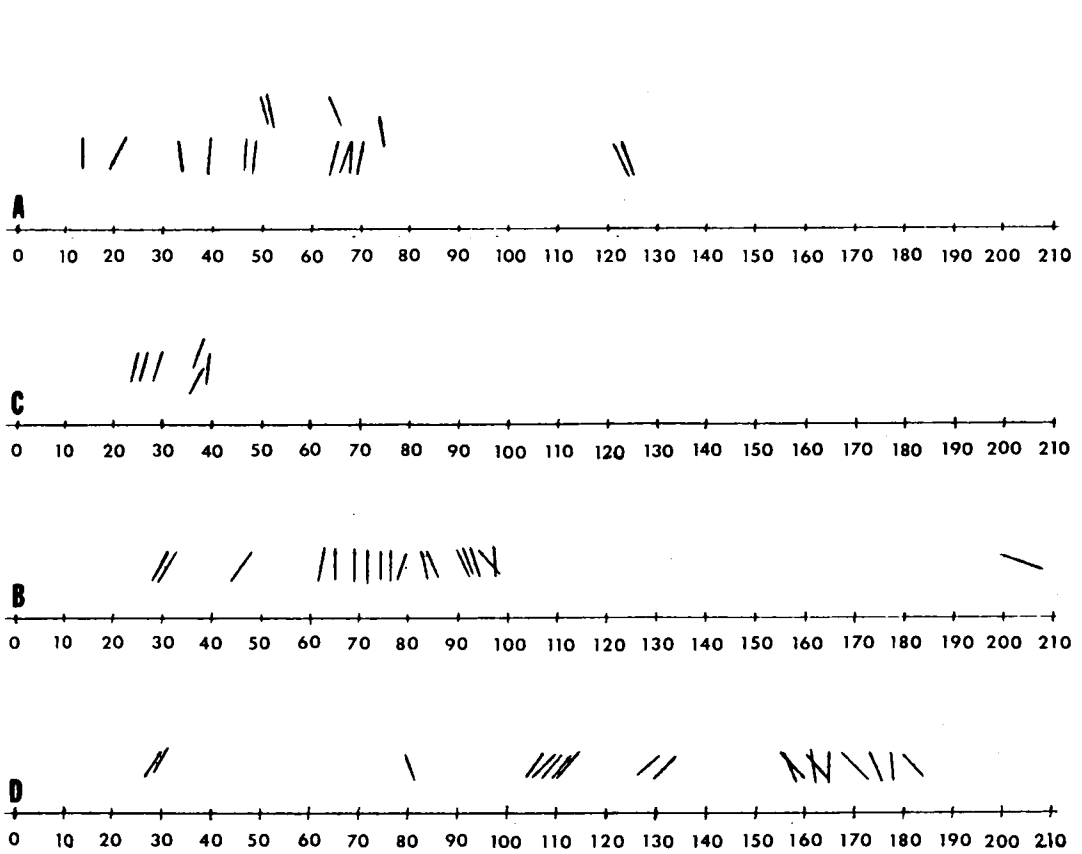

Figure 13. Profile axial plane dips across strike for the four sections. Numbering refers to Plates 1-4. The shortening axis is presumed to be normal to these buckle fold axial plane dips.

Douglas Lake. The thickness of the missing section is estimated by projecting the Blockhouse and lower Sevier of Section D 0.8 kilometers along strike from the southwest. The measured part of the section begins at a southward bend on the left bank of the French Broad River. The estimated missing interval is 480 meters (horizontally) across strike. Assuming that the Blockhouse and the lower unexposed portion of Sevier dip homoclinally at 63 degrees to the southeast (the same as the exposed section at D), the estimated thickness for the missing lower portion of Section B would be 430 meters (Figure 12). If the presumed regional dip is reasonable, then the estimated missing thickness must be a maximum value, since either folding, thickening by faulting or both probably occurred.

The first measured unit in Section B (B24-30.9, Plate 2; Figure 12) consists of 113.3 meters of calcareous silty mudstone (unit B-1), similar in lithology to unit A-2 (Plate 1). The upper contact of unit B-1 is indistinct because it becomes shaly for 3 meters at the top beneath a 10-meter-thick covered interval. Above this gap, shaly siltstone is exposed in a bed-parallel fault zone (probably second order) at least 4 meters thick (B31.4-31.6).

Above the sheared shaly siltstone, a homoclinal southeast dipping sequence of light gray siltstones interbedded with shale (unit B-2) has a thickness of 41.1 meters

(B31.5-33.7). This unit is roughly comparable to unit A-3 in Section A, although the siltstones are neither as regular nor as thick.

Above this unit lies 129.6 meters of calcareous siltstone and shaly siltstone (unit B-3), sometimes in thinning upward cycles (B33.7-40.33). This sequence is analogous to unit A-4 in Section A. Thin units consisting of 1.8 meters of argillaceous cobbly limestone (unit B-4) and 3.0 meters of well cleaved mudstone (unit B-5) overlie the somewhat cyclic unit.

Another thick unit (106.0 meters) of calcareous siltstone (unit B-6) in generally thinning upward cycles (B40.57-45.95) overlies the thin limestone and mudstone. A thin (5.0 meter) unit above consists of argillaceous cobbly limestone (unit B-7). At least 15.8 meters of clayey shale (unit B-8) overlie the limestone (unit B-7), before the exposure is terminated at an embayment on the east shore of Douglas Lake (B47.0).

After a covered interval which extends 48.0 meters perpendicular to strike, exposure resumes with a 69.8 meter thick unit (B-9) of calcareous silty mudstone (B49.4-52.9). Above a second order fault zone extending from B52.9-53.3, a thick section (170.9 meters of poorly exposed, calcareous silty mudstones (unit B-10) was measured. Most of this unit was projected onto the section from the back of an embayment

of the lake. Unit B-10 is bounded at the top by a fault contact (B62.2). More calcareous silty mudstone occurs above the fault and continues with homoclinal dip up to the beginning of a major deformed zone and duplication of strata at B65 (fault b: Plates 5, 6, Figure 12); 54.4 meters of this lithology (unit B-11) dip steeply southeast in a homocline beneath the folded and faulted zone. The monotonous lithology is disrupted only by coarser grained, calcareous siltstone beds at B63.8 and B64.0.

3. Structure

Unit B-1 is homoclinal with steep southeast dips (Plate 2), except for a large, second order kink fold displaying chevron geometry at B30. Northwest dipping cleavage is present in zones throughout the unit. Cleavage is nearly axial planar in the kink with moderate to strong intensity in the synclinal hinge at B29.8, while it is moderate in the adjacent anticlinal hinge and weak in the intervening middle limb.

The poorly exposed shear zone separating units B-1 and B-2 involves faulting nearly parallel to bedding in adjacent rocks. Above the shear zone, unit B-2 is southeast dipping and homoclinal. Gentle kink-band folding with both antithetic and synthetic senses of vergence is present in unit B-3. A few small-scale, synthetic kinks occur in

unit B-6, including one at B45.6 that is associated with a synthetic contraction fault. The small-scale fault is parallel to bedding on the backlimb and then cuts upsection across the hinge of the fold, thickening the unit. The fold is uncleaved, suggesting a predominance of shear over compression at the kink fold zone.

The nearly vertical, predominantly homoclinal unit (B-9) from B49.4-52.9 is cut by small-scale contraction faults, nearly parallel to bedding, causing thickening of the section. The top of the measured unit is a second order fault zone, delineated by synthetic contraction fault surfaces at B52.9 and B53.3 which bound obliquely oriented east/southeast striking, calcareous silty mudstone and shale beds between.

A thrust faulted, synthetic kink fold at B62.2 disrupts an otherwise homoclinal part of the section and divides units B-9 and B-10. The displacement is probably only slightly more than the scale of the outcrop, and the fault is classified as third order. The faulting is related to, and evidently subsequent to the folding. Cleavage is absent in the fold, and this, coupled with the marked asymmetry of the fold, suggests a predominance of shear during fold development. Disharmony occurs near the hinge of the syncline.

A poorly exposed fault at B65 (Plate 2) bounds an upright, concentric anticline (Figure 14) with hackly, weakly

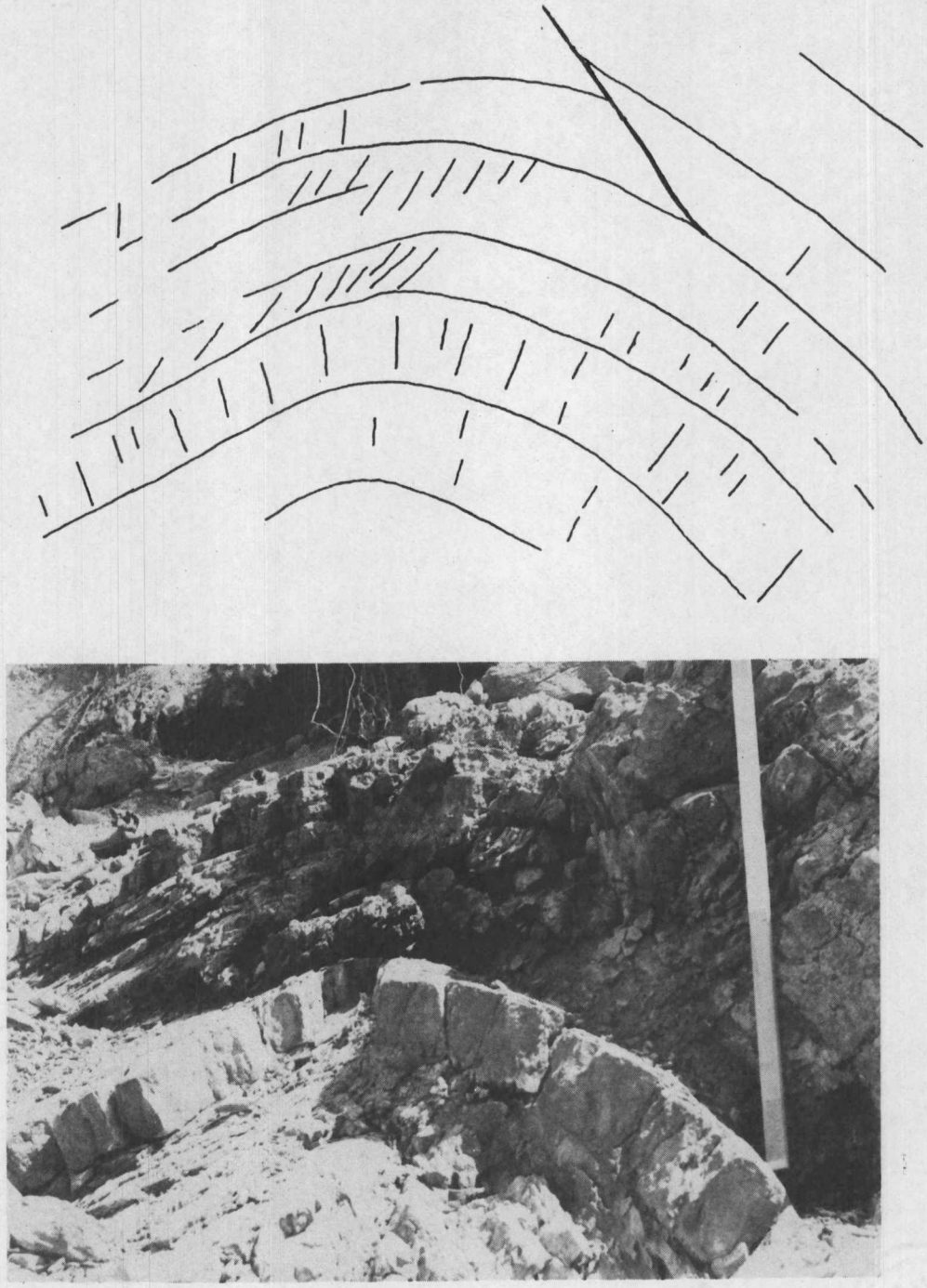

Figure 14. Concentric anticline displaying strong interlayer competence contrast (B65). Medium-thick, calcareous siltstone beds are interbedded with mudstone. Note interlayer change in cleavage intensity (weak in siltstone, moderate to strong in mudstone) and orientation (due to refraction). Scale is 1.0 meter.

transecting cleavage. The most competent siltstone bed maintains uniform thickness around the fold (despite parallax which causes apparent thickening on the southeast limb in Figure 14). The lithology is calcareous siltstone with shale interbeds. The siltstones display weak cleavage and the shales show moderate to strong cleavage. One or two thick, competent calcareous siltstone beds appear to be the dominant layers constraining the fold geometry (concentric) as the overlying, less thickly bedded siltstones assume a modified concentric or nearly similar fold geometry (Ramsay, 1967). The competent siltstone beds show considerable fanning of cleavage, which is almost perpendicular to bedding in these layers (Figure 14). Cleavage is significantly refracted between the siltstone and shale layers.

The fault at B65 (Plate 2) does not decapitate the fold hinge. Movement on the fault apparently occurred after the folding, and a synclinal hinge northwest of the anticline may have been faulted out. Multiple small-scale imbricate thrusts are present on the southeast limb of the anticline. These faults originate parallel to bedding in the down-dip direction and climb upsection toward the hinge. Considerable displacement has occurred at this faulted anticline. The offset is probably on the order of tens or hundreds of meters to as much as a few kilometers, because the deformed zone is approximately 25 meters thick and includes numerous fault

surfaces which juxtapose beds having strongly divergent dips. A large part of the offset is subparallel to bedding, but the bounding fault northwest of the anticline as well as the buckle folding and the portions of the backlimb thrusts near the hinge thicken the section considerably. Shortening and thickening in this zone are not calculable. At B66.0, a 1 to 2 meter-thick unit consists of a sequence of interbedded shale and 1.5 centimeter thick, dark gray limestone beds. The brittle limestone beds show extension fractures, boundinage, and telescoping, suggesting that both extension and contraction have occurred nearly parallel to bedding during the deformation history. The homoclinal unit overlying this interbedded limestone and shale unit consists of 39.3 meters of thick bedded, calcareous silty mudstone with steep northwest dipping cleavage. This relatively undeformed, thick-bedded, calcareous mudstone unit has approximately the same lithology, bed morphology, and cleavage type (although the lack of mesoscopic buckle folding precludes a high cleavage intensity) as unit A-2 at the base of Sevier in Section A. It also resembles the exposed portion of unit B-1 (however, the lower portion of unit B-1 is not exposed). Since this unit overlies a slice of Blockhouse-like lithology (the deformed unit of thin, interbedded limestones and shales) above the B65 fault system, I propose that the B65 fault splays from the Douglas

fault at the basal Middle Ordovician shale contact, and that a repetition of the Blockhouse and lower Sevier has occurred. No other lithology encountered up to the stratigraphic level of the footwall rocks of the B65 thrust fault similarly resembles the Blockhouse.

Another large fault zone, above the fault slice of Blockhouse and lower Sevier, begins at B68.7 (Plate 2), just 75 meters southeast of the base of the previously mentioned large second order fault zone. The base of this second order fault is approximately parallel to bedding in the footwall, and a faulted anticline again is present above the basal fault. Faulting on each limb of the anticline caused northwestward transport, implying that the displacement was secondary to the majority of the folding. Extrapolation of the fault to depth indicates that it may be parallel to bedding in the backlimb of the anticline at depth. The open concentric form of the upright anticline is probably controlled by the competent, medium/thick-bedded calcareous siltstone beds. Cleavage in the siltstones is weak, while cleavage is strong to moderate in the interbedded clayey shales.

At B69.5, above the faulted backlimb of the anticline, another second order fault (parallel to the fault at B68.7) thrusts heavily veined (with calcite) and sheared dark gray shale on top of calcareous siltstones. The thickness of this

fault zone (which is at least 12 meters and may be much more depending on its possible continuation into an adjacent covered interval beginning at B70.1), suggests that the fault at B69.5 is an important second order fault. If so, then these shales may have been brought up from a lower stratigraphic level such as the Blockhouse at the base of the shale section.

The combined thickness of the second order shear zone associated with faults at B68.7 and B69.5 is 25 meters. The section from B65-70.1 is a significant fault zone (Fault B, Plate 5) with several slices, and it is interpreted as an imbricate from the underlying Douglas décollement (Plate 6). The minimum slip on this fault needed to return the Blockhouse to its original position is discussed in the chapter on faulting and megascopic structure (Chapter 4). Structural style changes above the B65-70.1 fault zone.

The next 560 meters above the fault zone consist of tightly folded and intensely faulted fine-grained clastic sediments which show a gradual increase in quartz sand toward the southeast. Changes in structural style to the southeast of the fault zone at B70.1 (Plate 2) include:

1. A predominance of chevron (straight-limb) folds over concentric (curved-limb) folds.
2. Ubiquitous conjugate reverse faults (most of which contract bedding; Figure 5, p. 15).

3. A marked change in the orientation of the regional shortening axis as derived from orientations of fold axial surfaces (Figure 13, p. 53), fold flattening directions, cleavage and conjugate reverse fault pairs.

The shortening axis changes from southeast plunging to horizontal approaching the B65-70.1 fault zone from the northwest, and then to northwest plunging southeast of the B65-70.1 fault (Figure 13). The predominance of axial surfaces which dip to the southeast in the southeastern part of the section (southeast of the B69.5 fault) suggests either that the principal deformation axes were originally differently oriented or that they were subsequently rotated, probably by a subsurface thrust ramp.

Cleavage is generally absent in the chevron folds, kink folds and box folds in this part of the section, although it is present in a large number of the concentric folds. Cleavage intensity is strongest in folds developed in slightly silty calcareous mudstone, such as the anticline at B76.5 (Plate 2). The gently fanning cleavage in this fold is axial planar. In outcrop, the cleavage (spacing < 0.5 cm) nearly obliterates bedding in the hinge region, but is less intense on the limbs. This cleaved anticline marks the furthest southeast occurrence of such strong cleavage in Section B.

Abundant small-scale, conjugate reverse faults of unknown slip are present in the next 270 meters perpendicular to strike (Plate 2, B76.5-90). These consist generally of high angle contraction faults, with the obtuse bisector shallowly northwest plunging and parallel to the maximum shortening direction (indicated by displacement senses of the conjugate contraction faults). The southeast dipping fault set is the dominant one, and frequently offsets the steep, northwest dipping set. The less dominant set, consisting of vertical to northwest dipping fault surfaces, both contracts (more often) and extends (less often) bedding. Several of the faults cut both up and down section in decapitating small-scale folds (Plate 2; B73.6, B84.5, B89.1), suggesting a change in conditions of deformation responsible for reducing the mechanical importance of layering anisotropy after development of the folds. The faults which decapitate folds are referred to as fold-discordant, small-scale faults.

Folds between B76-89.5 occur mainly in calcareous mudstone with a modified concentric geometry (Plate 2; Appendix B, Table B-1). Folds in the interval between B89.5-94 display chevron geometry (Plate 2, Table 1) in sandy siltstone, implying the mechanical importance of bedding and easy interlayer slip. Folds occurring between B94-98 are modified concentric folds and they occur in siltstone or interbedded siltstone and shale.

Cleavage is not observed in the zone of conjugate reverse faults and fold-discordant faults between B77-89.5, nor is it observed in the zone of chevron folds between B89.5-94. Moderate intensity cleavage transects the axial surfaces of four folds (of which three are modified concentric) between B96-98. The constant orientation (neither refracted nor fanned) of cleavage across these transected folds implies that the cleavage was superimposed on the folds as will be discussed further later (Chapter 3).

A southeast dipping, homoclinal limb between B98-108 has evidence of only minor shortening strain. Minor kinking is present locally, as are sporadic occurrences of moderate intensity cleavage. An extensive gap (due primarily to poor exposure) is present between this part of the section and the interfingering Tellico sandstones to the southeast.

A recumbent chevron anticline in fine-grained sandstone beds at B203.5 (Figure 15) is one of the largest folds in the study area. It contains weak, nearly flat-lying axial planar cleavage locally in the tight hinge. It is interpreted as overlying a major, unmapped, low angle thrust fault (fault d), the trace of which may coincide with the trend of the strike-parallel Moore Branch embayment (Plates 5, 6).

Estimated shortening due to buckling was calculated to be 8.6 percent for the interval B24-65 (northwest part of the

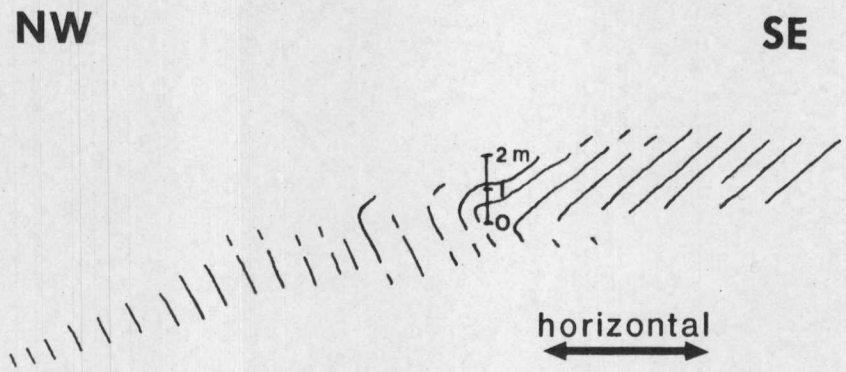

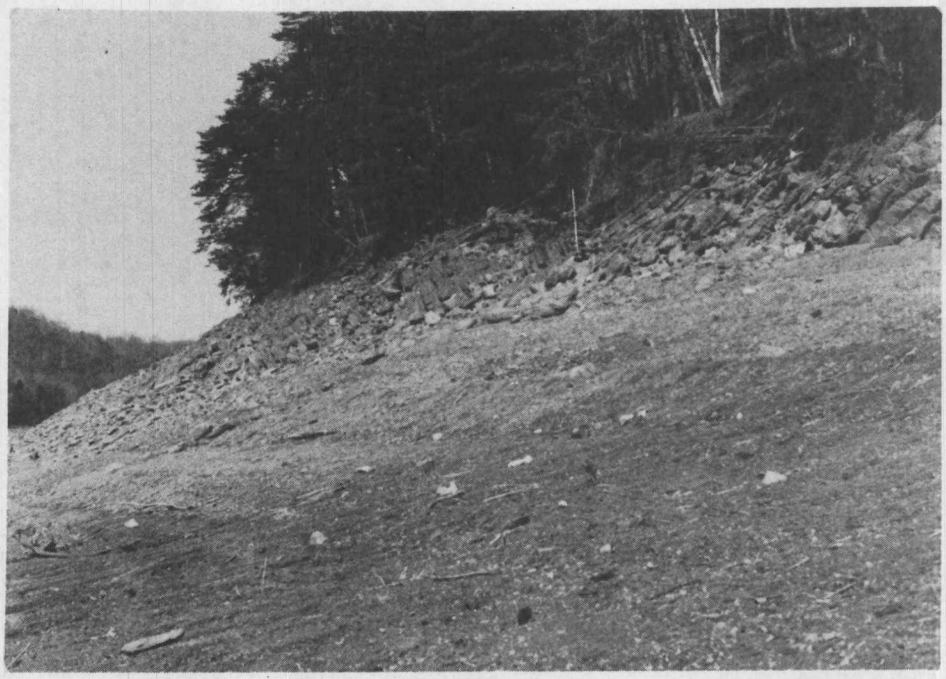

Figure 15. Recumbent anticline in Tellico sandstone of Sevier (B203). Axial surface dips at low angle to southeast (right of photograph). Vertical stick at hinge is 2.0 meters long.

exposed section). This is considerably less than the buckle strain calculated for Section C, situated less than 1 kilometer to the northeast along strike. The value is also significantly less than for the more southeastern part of Section B, in which buckle folding is prominent and homoclines are of lesser extent. On the other hand, the second order fault zone at B65-70.1 may make the overall shortening from section to section more compatible. Buckle shortening for the interval B70-98 was calculated to be 22.7 percent. Buckle shortening between B98-108 is nearly zero. Minimum cumulative buckle shortening (disregarding fault shortening) for Section B was calculated to be 16 percent, with a general southeastward increase.

D. Section C

1. Introduction

Section C (Plate 3) is exposed on the west side (left bank) of the Seahorn Creek embayment near its mouth, adjacent to the main channel of the French Broad River. It extends (using Tennessee Rectangular Coordinates) from 609,100; 2,787,800 to 606,800; 2,788,850. Only Sevier formation is exposed in the section (Figure 16), although the basal 340 meters are not exposed (similar to Section B). The dominant lithology in the section is calcareous siltstone in mostly medium to thin beds with rare thick beds. The shortest of

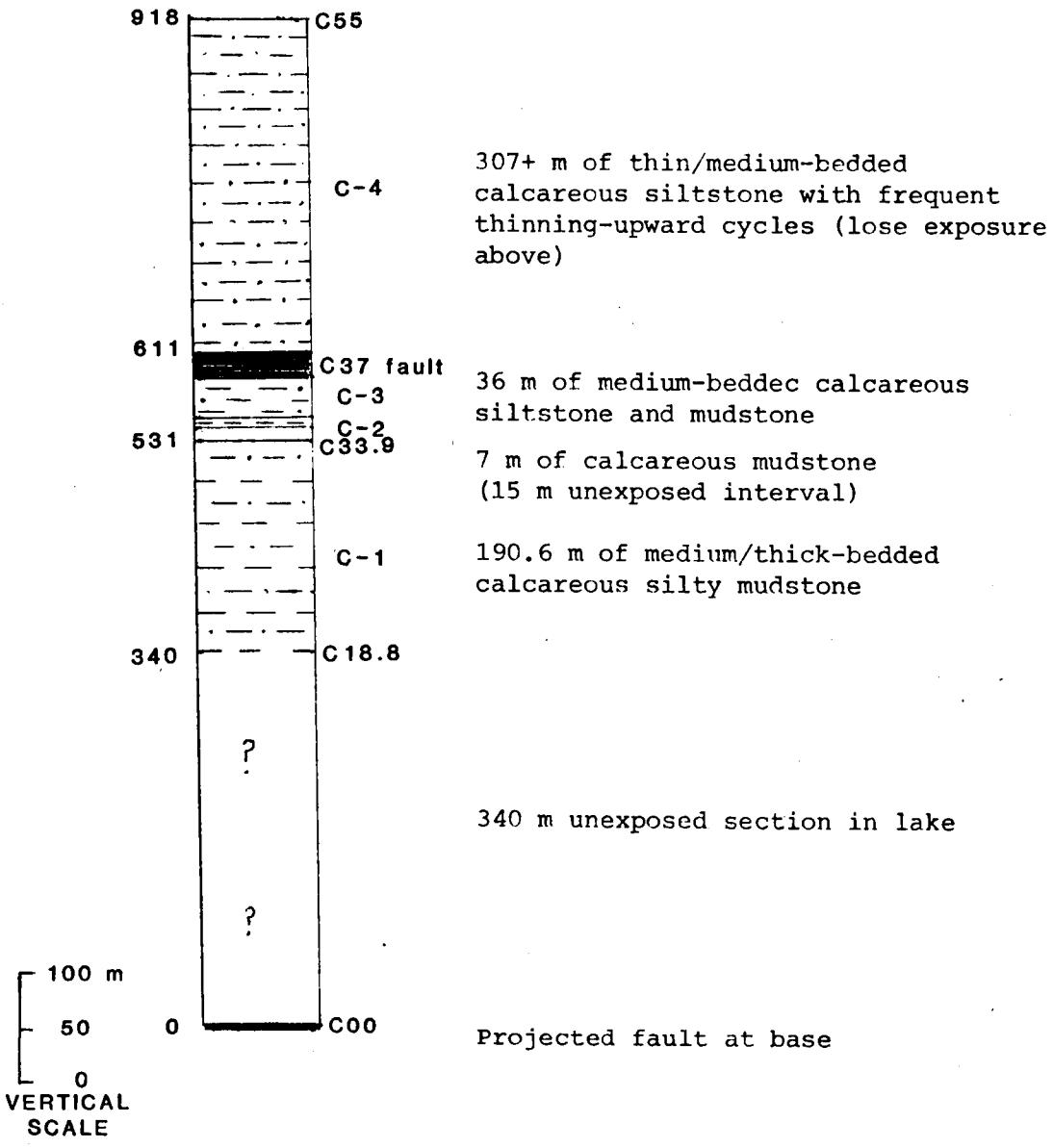

Figure 16. Stratigraphic column at Section C (see Figure 2, p. 3; Plate 3). The letter C followed by a number refers to a location in Section C based on the number of 20 meter intervals measured in horizontal, perpendicular to strike, beginning at the northwest end of the section (C00). C-1, C-2, C-3, etc., represent stratigraphic units within the Sevier at Section C.

the sections, extending 0.72 kilometers perpendicular to strike, it shows no change in orientation of deformation axes along its length (Figure 13, p. 53). Northwest vergent folds display cleavage oriented approximately (but not entirely) parallel to axial surfaces. Small-scale faulting is synfolding. A second order fault is associated with a folded zone, and it is syn- to postbuckle folding. This second order fault, which is of uncertain magnitude, is represented by a 20 meter thick shear zone of slices of Sevier siltstone. The fault, which is vertical to steeply northwest dipping at its surface exposure, masks an anticlinal hinge adjacent to an intensely flattened syncline in the hanging wall. Folding, faulting, and cleavage are homotactic subfabrics, suggesting a protracted monophase deformation. Bed-parallel extension within the shear zone had a compressional origin, since it occurred along conjugate, high angle reverse faults imposed on nearly vertical bedding. This bedding-extension fabric was superimposed on early bed-parallel contraction. An extensive, somewhat poorly exposed homoclinal section is present at the southeastern end of the section. Most of the deformational features within the homocline consist of small-scale contraction faults and small-scale conjugate kink folds for which the shortening axis is nearly parallel to bedding. The calculated cumulative buckle shortening strain is 24 percent, an anomalously high value for this far northwest.

2. Stratigraphy

The basal shale contact at the northwest end of Section C is buried beneath Douglas Lake (similar to Section B to the southwest); therefore, an interpolation between the basal contacts in Sections A and D was made along strike. An estimated 340 meters of section (C00-18.8) is missing at the base of Section C, including the Blockhouse formation and the lower part of the Sevier formation (Figure 16). Only mudstones and siltstones of the Sevier formation are exposed in the section. The southeastern half of the exposed part of the section is poorly exposed.

Above the 340 meter thick missing basal part of the section, 190.6 meters of calcareous silty mudstone (unit C-1) outcrop (C18.8-33.9). The upper part of this unit correlates with unit B-1, located just 0.9 kilometers to the southwest in Section B. The unit has similar lithology and may correlate with unit A-2, located 2.2 kilometers to the northeast in Section A, although unit C-1 is estimated to extend considerably higher in the section.

A 15 meter unexposed interval (C33.9-34.6) overlies unit C-1. This interval probably consists of the easily erodable clayey mudstone lithology. This interval may correlate with the 10 meter unexposed interval above unit B-1 in Section B. Both covered intervals (immediately overlying B-1 and C-1) are overlain by shaly calcareous mudstone. A

fault is localized in the 3-meter thick shales in Section B (B31.5), while in Section C, the 7 meters of exposed shaly mudstone is unfaulted and designated as unit C-2 (C34.5-34.9).

Unit C-3 (C34.9-36.7) consists of 36 meters of interbedded calcareous siltstone and mudstone. This unit underlies a second order fault zone (C36.7-37.8), which probably correlates with the aforementioned more poorly exposed fault at B31.5 at a slightly lower stratigraphic level.

Above the fault, a poorly exposed thick unit (C-4) of calcareous siltstone extends to the top (southeast end) of the section (C37.8-55.3). Frequent thinning upward cycles of beds occur in this unit. Extensive tectonic thickening of this unit may have gone undetected due to poor exposure along most of its extent. This unit may correlate with better exposed units of similar lithology in each of the other sections (B-3/B-6, A-4 and D-3).

3. Structure

Second order and small-scale buckle folds and second order and small-scale faults are present in the northwestern half of the section (Plate 3). The southeastern half of the section consists of poorly exposed beds, dominantly vertical, with the stratigraphic facing direction being up to the southeast.

A small-scale northwest vergent kink fold (Plate 3, C24.5), which is uncleaved but faulted at the synclinal hinge, is parasitic to a second order syncline (unexposed hinge) at about C26.2. A second order, concentric anticline is well exposed in medium-bedded calcareous silty mudstone at C29.25. The short limb between this anticline and the inferred syncline at C26.2 is cut by a small-scale, bed-parallel thrust which cuts across bedding only at the anticlinal hinge. No more than 5 meters of displacement occurred on this thrust. Hackly cleavage of moderate to strong intensity (0.5-3 cm spacing) in the footwall of the thrust is approximately axial planar to the anticlinal fold, with a minor divergent fan angle of 7 degrees. Moderate intensity, hackly cleavage in the hanging wall is noncoplanar with the axial surface of the fold there. The possibility that the thrust displaced an originally fanning cleavage is unlikely, because less than 5 meters of displacement occurred on the fault, and a reconstruction of the hanging wall and footwall blocks to a prethrust position results in too much discordance between cleavage orientations on adjacent sides of the thrust. Nor does the cleavage fan across the hinge and both limbs in the footwall. The cleavage is probably related to the thrusting and may have developed after locking of the anticline.

Small-scale thrust faults at a low angle to bedding in steeply southeast dipping beds were observed at C23.9 and C30.5 (Plate 3). Cleaved calcareous mudstone, at the edge of a 14 meter covered interval (C33.9-34.6), may suggest the presence of a fold in the covered interval; the only other occurrences of cleavage in this section occur in and adjacent to the two well exposed outcrop-scale fold hinges (C29.25 and C36.9). It is possible, however, that the presence of cleavage at C34.6 is only due to the presence of the mudstone lithology (the most favorable lithology for cleavage development). The cleavage intensity in the exposed part of this locality is strong, with an average spacing that is consistently less than 0.5 centimeters.

A second order chevron syncline in medium-bedded calcareous siltstone at C36.9 (Plate 3) displays strong axial planar cleavage. Immediately southeast of the syncline, a second order contractional fault occurs as a nearly 20-meter-wide shear zone (Figure 17). The shear zone extends from C36.7-37.8. The faulting is clearly later than the folding and probably followed fold locking. It is of uncertain magnitude, but it is at least greater than the exposed extent. The deformation may represent either a continuum of events or discrete stages. Evidence for a continuous deformation includes homotactic structures and the absence of decapitated folds. This fault is correlated with a poorly

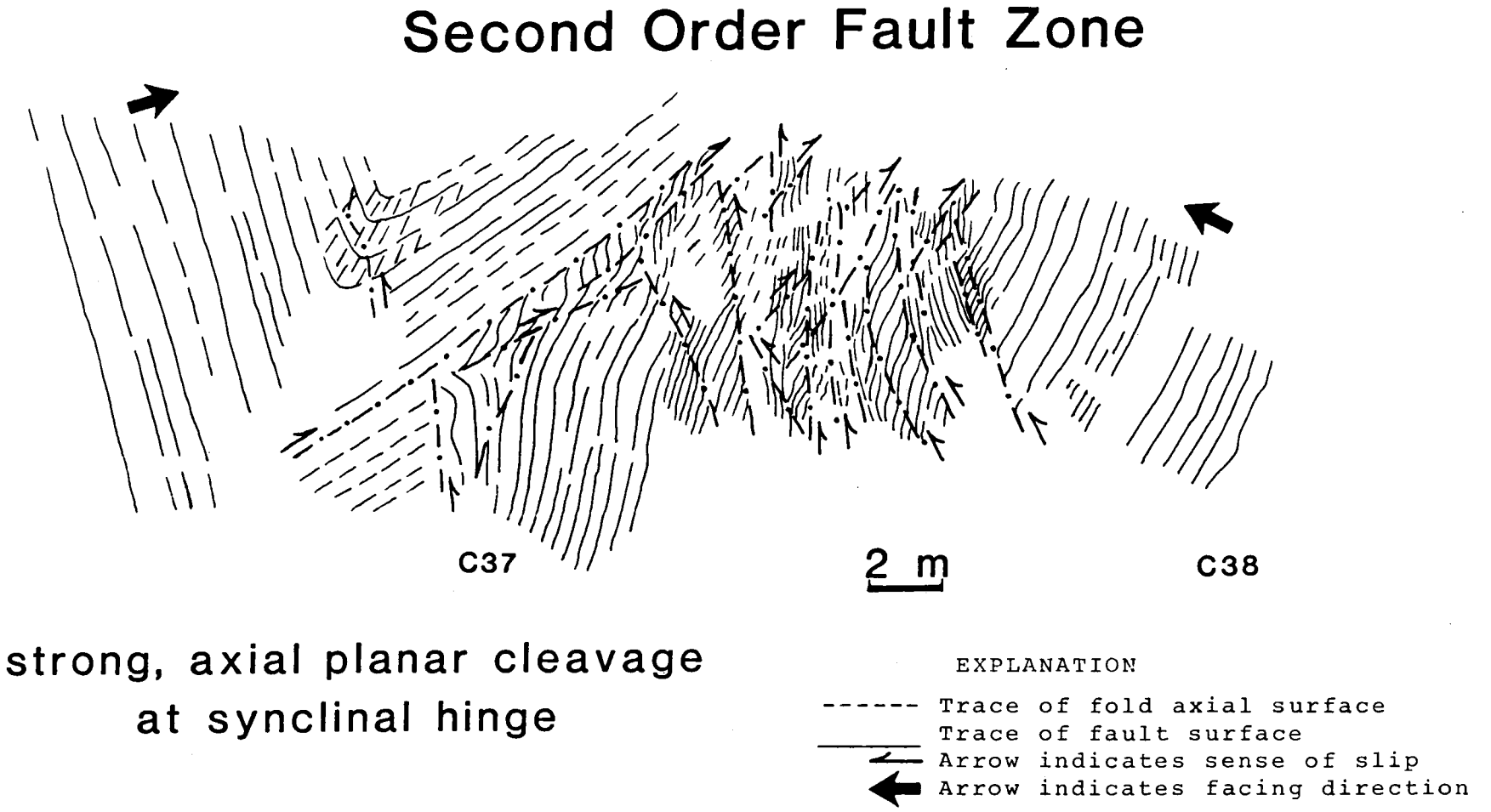

Figure 17. Profile of an intensely deformed portion of Section C.

exposed zone of faulted shales (B31.4-31.6) above an unexposed interval (B30.9-31.4) in Section B (Plate 5).

Conjugate sets of faults in the shear zone at C36.7-37.8 imply a gently plunging (20 degrees to the southeast) maximum contractional deformation axis. Neither fault set consistently offsets the other, although slip is indicated on most of the surfaces by either stepped, slickensided surfaces or dragged bedding surfaces. The two fault sets are probably of conjugate shear origin (discussed further along with presentation of fault data in Chapter 4).

Two joint sets are also seen in this shear zone. Mineralized joint surfaces consist of calcite, and many of the joints are weathered out. Set 1 is nearly vertical, and it strikes in the down-dip direction, normal to strike, at 335 degrees. This set of fracture surfaces indicates minor extension approximately parallel to fold axes and perpendicular to the XZ plane, implying a minor deviation from plane strain. Set 2 joints are nearly horizontal, dipping less than 20 degrees to the northeast and striking at 346 degrees. These surfaces are found in nearly vertical beds in the shear zone, and represent bed-parallel extension. Set 2 is an approximate bisector of the high-angle, conjugate reverse fault sets. Set 2 surfaces are oriented normal to the X deformation axis in the highly deformed shear zone.

Set 2 joints are superimposed on kink folds, discfolds, and telescoped beds (Figure 18).

The remainder of Section C (the southeastern half) contains numerous minor, low angle (to bedding) contractional faults as well as ubiquitous minor kink folds implying an early stage of bed-parallel contraction. No continuation of the B65-70.1 fault is observed in this section, which is exposed only as far southeast as C55.25.

The cumulative buckle shortening strain for the section is 24.4 percent, a large value for this far northwest in the shale belt, relative to measurements in the other sections.

E. Section D

1. Introduction

Section D begins in a small embayment of the lake immediately northwest of the Douglas Lake Campground, and extends southward along the right bank of Douglas Lake toward the Indian Creek embayment. The endpoints of the section are at Tennessee Rectangular Coordinates 605,760; 2,782,080 and 594-700; 2,786,300.

The base of the section coincides with the bottom of the Middle Ordovician Blockhouse formation (Figure 19), but the section is poorly exposed for 2 kilometers to the southeast. The next 1,572 meters (horizontally) to the southeast offer better exposure for structural analysis (Plate 4).

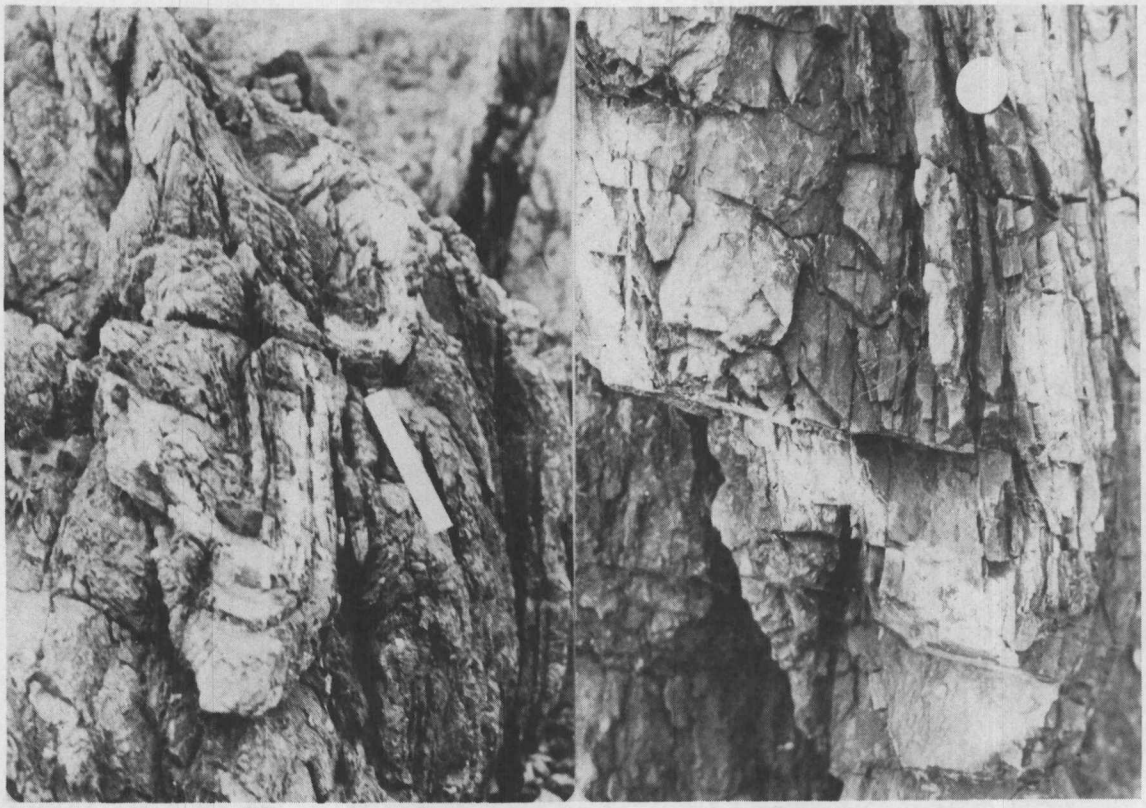

Figure 18. Extensional fractures superimposed on sheared discfolds (C36-38). Fractures cut folded beds (indicated by white paint) and extend bedding. Left to right: (a) View approximately parallel to axes of two sheared discfolds; extension fractures dip back into outcrop (6 inch ruler for scale). (b) View parallel to extension fractures which cut fold (enlargement of lower fold in a). Fold plunges toward viewer (dime for scale).

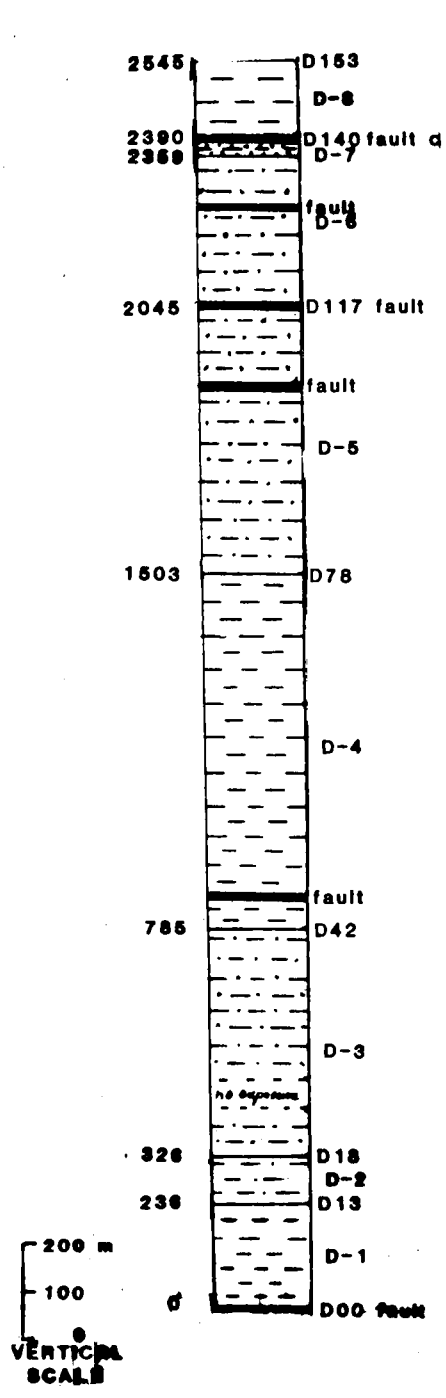

Sandstones and mudstones are duplicated by overturned folds and faults above D-8

155.3 m of calcareous mudstone

30.4 m of interbedded sandstone and mudstone

313.6 m of calcareous silty mudstone

542.3 m of thin/medium-bedded calcareous siltstone

718.0 m consisting of very poorly exposed calcareous mudstone

459.2 m of medium/thick-bedded calcareous siltstones and thin-bedded siltstones in thinning upward cycles

90.2 m of medium/thick-bedded calcareous silty mudstone

235.6 m of poorly exposed shale and mudstone

(Lenoir-Whitesburg carbonates in footwall)

Figure 19. Stratigraphic column at Section D (see Figure 2, p. 3; Plate 4). The letter D followed by a number refers to a location in Section D based on the number of 20 meter intervals measured in horizontal, perpendicular to strike, beginning at the northwest end of the section (D00). D-1, D-2, D-3, etc., represent stratigraphic units within the Sevier at Section D.

The southeasternmost of the sections shows the most complex megascopic structure, based on changes in orientations of the mesoscopic structural elements. Fold axial surfaces and generally axial planar cleavage show changes in dip across strike from northwest dips to southeast dips, back to northwest, and then finally back to southeast and shallow southeast (Figure 13, p. 53). Folded zones interrupt homoclinal sections. The southeastern part of the section is dominated by overturned folds, some of which are faulted at the hinges. The varying orientations of planar structural fabrics and implied deformation axes across strike imply a larger fold order than what is observable in outcrop, suggesting control by subsurface ramping. Buckle shortening calculations for the interval D103-132 yield a minimum estimate of 25.3 percent strain. Only 3.4 percent shortening due to buckling has been calculated for the predominantly homoclinal zone from D132-150. The largest buckle shortening estimate for the entire study area was calculated for the interval D150-183. The shortening due to buckling calculated for this interval is 37.8 percent. The cumulative minimum buckle shortening strain for the section is 32 percent. This is certainly weighted by the intense local shortening in the upper part of the section. Bearings and strikes of folds and faults in the intensely buckled and faulted southeastern

portion of the section possess easterly trends, contrasting with regional trends of about N60°E.

A system of small-scale backthrusts may represent an antithetic second order fault zone (Plate 4, D129-131.5) with displacement of at least 50 meters. These faults occur on the northwest limb of the second order anticline at D131.5. Strong transection of this fold by cleavage is probably due to the formation of cleavage during late fold tightening and the development of the third order (northwest over southeast) limbthrusts.

Magnitudes of second order thrusts were calculated using offsets of sandstone marker beds interbedded with mudstone and siltstone. Net slips of as much as several hundred meters were estimated (i.e., fault c: Plates 4, 6). Ubiquitous bed-parallel faults occur, the majority showing northwestward transport. The net slip of these bed-parallel faults is unknown. Numerous faults which extend bedding are also present, although of small scale.

2. Stratigraphy

The base of the poorly exposed Blockhouse is believed to be the top of the uppermost thin microsparrite limestone bed in the upper part of the Whitesburg formation. Blockhouse and lower Sevier are represented by 236 meters of poorly exposed shale and mudstone (unit D-1) from D00-13.0.

From the point at which good exposure begins in the Sevier at D13.0, the section (Figure 19) is nearly continuously exposed for 580 meters (horizontally) to the southeast (D13.0-42.0); 90.2 meters of calcareous silty mudstone (unit D-2) outcrop from D13.0-18.1. This unit may also include some of the underlying, poorly exposed mudstones grouped as unit D-1. It may correlate with units A-2, B-1, and C-1 in the other sections.

Overlying unit D-2 is an estimated 459.2 meters of calcareous siltstone beds in thinning-upward cycles (unit D-3). Poor exposure occurs between 105.7 and 159.6 meters above the base of this unit, which extends from D18.1-42.0. The stratigraphic facing direction for the southeast dipping upright strata was confirmed by large scale cross laminae at D20.65-20.75. These structures show bipolar sedimentary dips approximately parallel to strike, and the tops of the cross laminae are frequently truncated. These beds are classified as contourites (personal communication with Keller, 1981). Additional contourites were noted at D36.2-36.4. The lower part of the unit D-3 may correlate with units A-4, B-3 (and B-6), and C-4 in the other sections.

At D42, a conformable contact between calcareous siltstone (unit D-3) and mudstone (unit D-4) marks the end of the nearly continuous exposure and the beginning of a very poorly exposed interval (D42.0-78.2) to the southeast. An

estimated 718.0 meters of the poorly exposed D-4 was measured, and it consists mostly of calcareous mudstone. A poorly exposed faulted and deformed zone occurs at D45-47, and unknown other duplication may have occurred within this unit.

Above D-4 lies an estimated 542.3 meters of somewhat better exposed (yet including significant gaps) calcareous siltstone (unit D-5) between D78.2 and a fault contact at D117.1. Deformation in zones at D80.0-80.6 and D106-109 may cause considerable thickening of the section.

Unit D-6 (D117.1-137.0) consists of 313.6 meters of calcareous silty mudstone overlying the basal fault. An isolated sandstone bed (40 cm thick) outcrops at D124. A second order fault zone between D129-131.3 causes stratigraphic thickening of uncertain amount.

Unit D-7 (D137-140.4) consists of 30.4 meters of interbedded sandstone and mudstone. This section is duplicated on a second order contraction fault at D138.5 (fault c: Plates 2, 6, Figure 19). An estimate of the thickening caused by the fault is made by matching beds at the top of the main sandstone package on either side of the fault.

Unit D-8 (D140.4-153.3) consists of 155.3 meters of calcareous mudstone. Above (southeast of) D153.3, sandstones

and mudstones are duplicated by overturned folds and faults from D153.3-184 (Plate 4).

3. Structure

Although direct evidence of a fault in the lower part of these Middle Ordovician shales is lacking (possibly because of poor exposure), a significant change in dip angle occurs between the underlying carbonates (Knox group and Lenoir formation) and the lower shales. Southeast dips of 30-40 degrees in the carbonates contrast with 60-90 degree southeastward dips in the shales, suggesting the existence of a décollement fault in the lower part of the shales (Douglas fault). The dips in the carbonates versus those in the shales may suggest a duplex structure for the décollement (personal communication, N. Woodward, 1982). This fault is probably an extension of the major fault (Figure 1, p. 3) which was mapped in outcrop at the base of Section A, and which probably occurs at or near the same stratigraphic level along strike.

The lower exposed part of Section D (D13-42) consists predominantly of a steep southeasterly dipping homocline. Small-scale antithetic kink folds at D15.0, D15.05, D15.1, D16.05, and D16.5 display subhorizontal axial planes at a high angle to bedding. These kinks give only minor shortening. Some of the axial surfaces can be traced for up to

10 meters. Their antithetic relationship to regional northwest vergence implies a time of formation during early bed-parallel contraction.

The homocline is interrupted at D29.1 where a kink fold with a 9 meter half wavelength is exposed in saprolite near the top of the outcrop. The hinges are poorly preserved but plunge to the northeast, and the fold can be traced 1.0 kilometer across the lake along its bearing of 55 degrees to a similar second order kink fold in a quarry on Section B (Plate 2, B30). Assuming that these are the same fold, a doubly plunging structure is indicated by plunge directions on opposite sides of the lake.

Oppositely dipping beds at D45 and D47 suggest the presence of deformation, although no fold hinges or fault zones are exposed. Exposed beds dip generally steeply southeast to vertical. Poorly exposed second/third order folds and associated faults of unknown offset were observed from D75-80. The section was then projected across an embayment, to where a faulted, outcrop-scale chevron anticline (D80.4) is exposed within a continuous outcrop from D78.2-82.3. Steeply southeast dipping beds from D82.3-104.4 are poorly exposed, but the section from D104.4-183.0 was suitable for detailed analysis (Plate 4).

Between the second order anticline at D80.4 and a faulted syncline at D106.1, the gently southeast dipping

homocline changes to vertical and then slightly overturned. The orientation of mesoscopic folds reflects this macroscopic change in dip (Figure 13, p. 53), as folds with southeast dipping axial surfaces northwest of D82.4 are replaced by folds with northwest dipping axial surfaces toward the southeast, involving a 55 to 65 degree change in axial surface dips. Cleavage generally follows the same changes in orientation that the fold axial surfaces do, but transected folds display cleavage that is more nearly vertical than the axial surfaces. An asymmetrical second order anticline at D109 (Figure 20) is also inclined to the southeast. It has nonfanning axial planar cleavage and associated crenulations of bedding (Figure 21) on the southeast limb, but lacks both crenulations and cleavage on the northwest limb. The cleavage which cuts the hinges of the second order anticline at D131.5 is considerably steeper dipping than the shallowly northwest dipping fold axial surface. Small-scale (northwest over southeast) limbthrusts were observed on the northwest limb of the anticline (D129.5-131.5). Combined displacement on these numerous third order backthrusts is second order and may exceed 100 meters. The zone of folds with northwest dipping axial surfaces continues through the fold at D131.5.

Axial surfaces dip to the southeast, southeast of D132 (Figure 13, p. 53). Bed-parallel faulting occurs in a homoclinal zone from D132-150, with small-scale conjugate

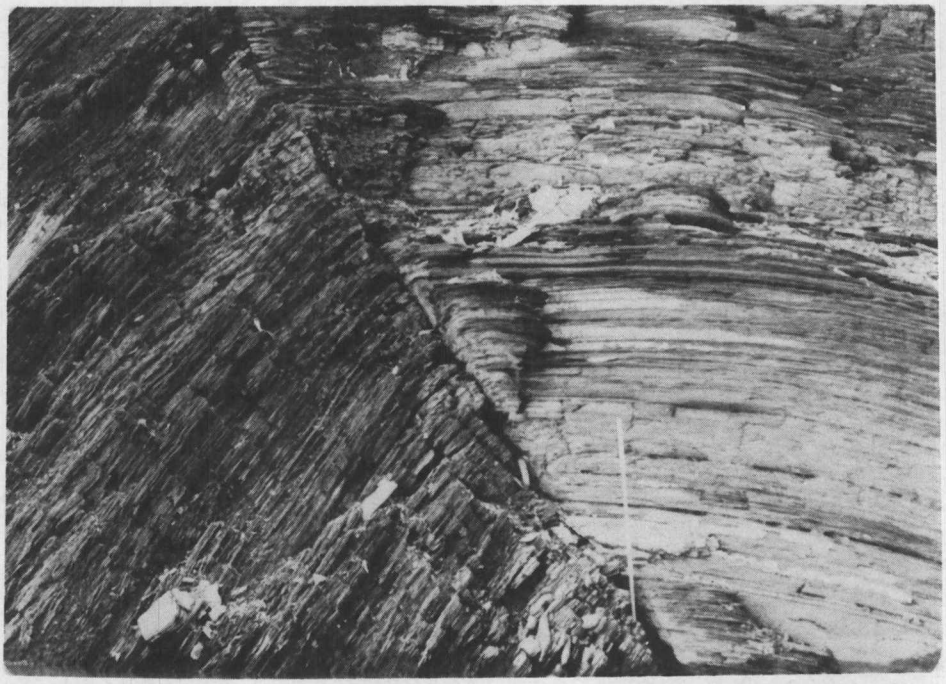

Figure 20. Asymmetrical anticline (D109b) with cleaved, crenulated southeast limb. Cleavage surfaces are axial planar and parallel to axial planes of small crenulations. Northwest is at right. Two meter stick is scale.

Figure 21. Close-up views of portions of the crenulated and cleaved southeast limb of anticline in Figure 20. Top to bottom: (a) Crenulated siltstone beds (dime scale) with widely spaced cleavage surfaces parallel to axial surfaces of crenulations. Minor shearing occurred in the lower right hand corner where the discontinuity changes orientation. (b) A 3-4 cm thick calcite seam is parallel to bedding, implying extension perpendicular to bedding.

a

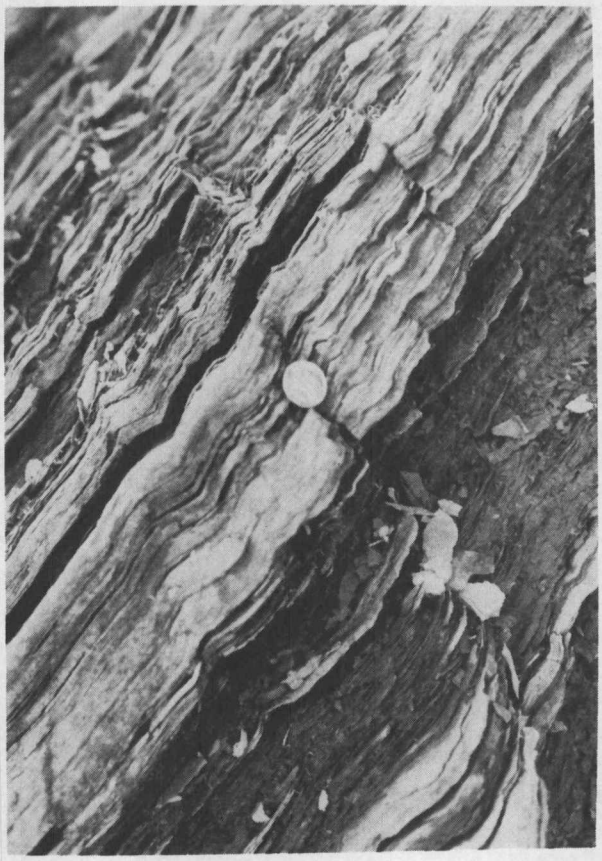

b



Figure 21

faults which extend bedding (particularly numerous between D134 and D135.5). Thick sandstone beds of the Tellico facies (within the Sevier) are present from D138-138.5. Telescoping of the sandstone beds causes small-scale kink folding in adjacent siltstones. A southeast over northwest, second order thrust at a low angle to the footwall and parallel to the hanging wall beds overlies these telescoped sandstones and folded siltstone beds (fault c, Plates 5, 6). Based on the extrapolation of the fault dip and bedding dips into the subsurface and the matching of sandstone beds in the footwall and hanging wall, a minimum displacement of 300 meters occurred on this second order thrust. At least 30 meters of stratigraphic duplication occurred on this nearly bed-parallel fault The fault does not correlate with faults in other sections, because it is considerably further southeast than the other detailed sections extend.

Isolated sandstone beds are interbedded with shales from D139-141. Thick to very thick-bedded calcareous mudstones, dipping homoclinally to the southeast, extend from D141-150.7. The unexposed hinges of a second order syncline and anticline occur near D152 and D155, respectively, on either side of a vertical remnant of the middle limb from D152-153.5.

Second order faulting at D156.6 and D157 isolates a fold pair just northwest of another second order chevron syncline

at D157.5. Bed-parallel faulting is present at D158.7. Conjugate reverse faults at D159 decapitate a small-scale paired fold. The slightly overturned northwest limb of a faulted second order anticline stretches from D157.4-159.6. Thick-bedded, telescoped Tellico sandstones occur within the Sevier in the footwall (or northwest limb) of this faulted fold (Plate 4, D159.7). The second order fault has at least a 40 meter offset (southeast over northwest), based on displaced sandstone beds. Part of a tight, faulted syncline is cut by conjugate small-scale reverse faults at D161.5. The overturned limb of another second order anticline extends from D161.8-164. The anticlinal hinge is not exposed, but is inferred from changing dips. A fault at D165.3 causes minor displacement. Telescoped sandstone beds from D166.5-167.2 are interbedded with shale and mudstone. The southeast dipping sandstone beds are heavily veined with calcite, while the interbedded shaly mudstones are poorly exposed. Bed-parallel shearing is indicated by drag and slickenlines at D168.5 and D168.7. Conjugate, small-scale reverse faults at D169.1 are homotactic with second order folding. A second order syncline at D169.8 is faulted by the antithetic member of a conjugate pair. A short, overturned limb between the faulted syncline and an intact, overturned second order anticline extends from D169.8-170.5. The close, chevron anticline is cut by strong to moderate axial planar cleavage

in medium/thick calcareous siltstone beds. Its shallow, southeast dipping limb extends from the hinge at D170.5 to a second order synclinal hinge at D174.5. The open, chevron synclinal hinge (D174.5) is cut by strong axial planar cleavage in medium-bedded calcareous siltstone. A short, vertical to overturned limb separates this synclinal hinge from the adjacent anticline, which is poorly exposed and complexly faulted near D176. The next fold is a complex, faulted, second order syncline at D178. Its vertical to overturned limb extends from D178.1-181.6, where it is interrupted by a small-scale kink synthetic to flexural slip on the limb. The limb is intermittently cleaved (D179.1, D179.6). At D182.3, an uncleaved, second order anticlinal hinge terminates the northwest dipping to overturned limb. Southeast dipping beds on the southeast flank of the anticline extend at least as far as D185, where exposures die out.

CHAPTER 3

MESOSCOPIC FABRIC ANALYSIS: MECHANISMS OF FOLDING AND CLEAVAGE DEVELOPMENT

A. Introduction

This chapter involves the analysis of more than 70 mesoscopic folds (primarily second order, i.e., half-wavelength greater than 3 meters) and their relationships with other fabric elements (namely cleavage and faults) in terms of strain, relative sequence of development, and probable mechanisms of formation. These folds (Appendix B, Table B-1) were selected as being both geographically and geometrically representative, and they include the majority of the second order folds observed along the four sections (Figure 2, p. 4).

Descriptions of fold geometries depend on the cross-sectional shape of individual layers between folded surfaces, and more specifically, on changes and rates of change in shape of the two bounding surfaces of a layer. The primary mechanism of folding in the study area is buckling with flexural slip between layers on the limbs and varying degrees of tangential longitudinal strain or ductile flow near the hinge. Flattening of previously formed buckle folds is also common. Measurements of the flattened fold

geometries were made to allow quantitative estimates of the flattening strains. Nine folds for which fold flattening analysis was performed (Appendix B, Table B-2) were selected as being both geographically and geometrically representative.

Axial surfaces are probably principal planes of finite strain in the buckling segment of this deformation. Cleavage surfaces are principal planes of the finite strain at a later time than the initiation of the buckle folds and thus may not be parallel to axial planes. Final movement on contraction faults was, at least, later than the initiation of cleavage development.

Cleavage in the Blockhouse and the Sevier is classified as spaced disjunctive cleavage. This classification is made on the basis of uneven distribution, mesoscopically observable spacing, and the lack of a preexisting, tectonically developed anisotropy (Powell, 1979, p. 21). The cleavage is controlled by both local structure and local lithology, while its relations with geographic and larger tectonic features are less clear.

Fold axial planes generally rotate in dip from northwest in the northwest part of the shale belt to vertical and then southeast in the southeast (Figure 13, p. 53). In some cases, the transition is relatively smooth (Sections A and B). In other cases, such as Section D,

rapid variations in orientations of axial surface trends complicate the megascopic structure (implying a larger scale of folding than is mappable in the field). Subsurface ramping may have caused this major (first order) folding.

A possible origin of noncoaxial folds and cleavage is thrust faulting of Blockhouse and Sevier shales over the underlying uninvolved carbonates (according to most seismic lines; Tegland, 1978). During such faulting, irregular precleavage folds may have been produced in the lower Sevier above the thin, sheared Blockhouse and basal fault zone.

B. Theoretical Models and Their Significance

1. Introduction

Types of graphical and numerical analyses which will be used in the data and analysis portion of this chapter include:

1. orthogonal thickness of folded layer (Figures 22, 23, 24)
2. thickness of layer parallel to the fold axial surface (Figure 24)
3. inclination and spacing of dip isogons (Figures 24, 25)
4. fold hinge angularity (Figure 26)
5. fold interlimb angle (Figure 27)
6. fold flattening strain (Figure 28)

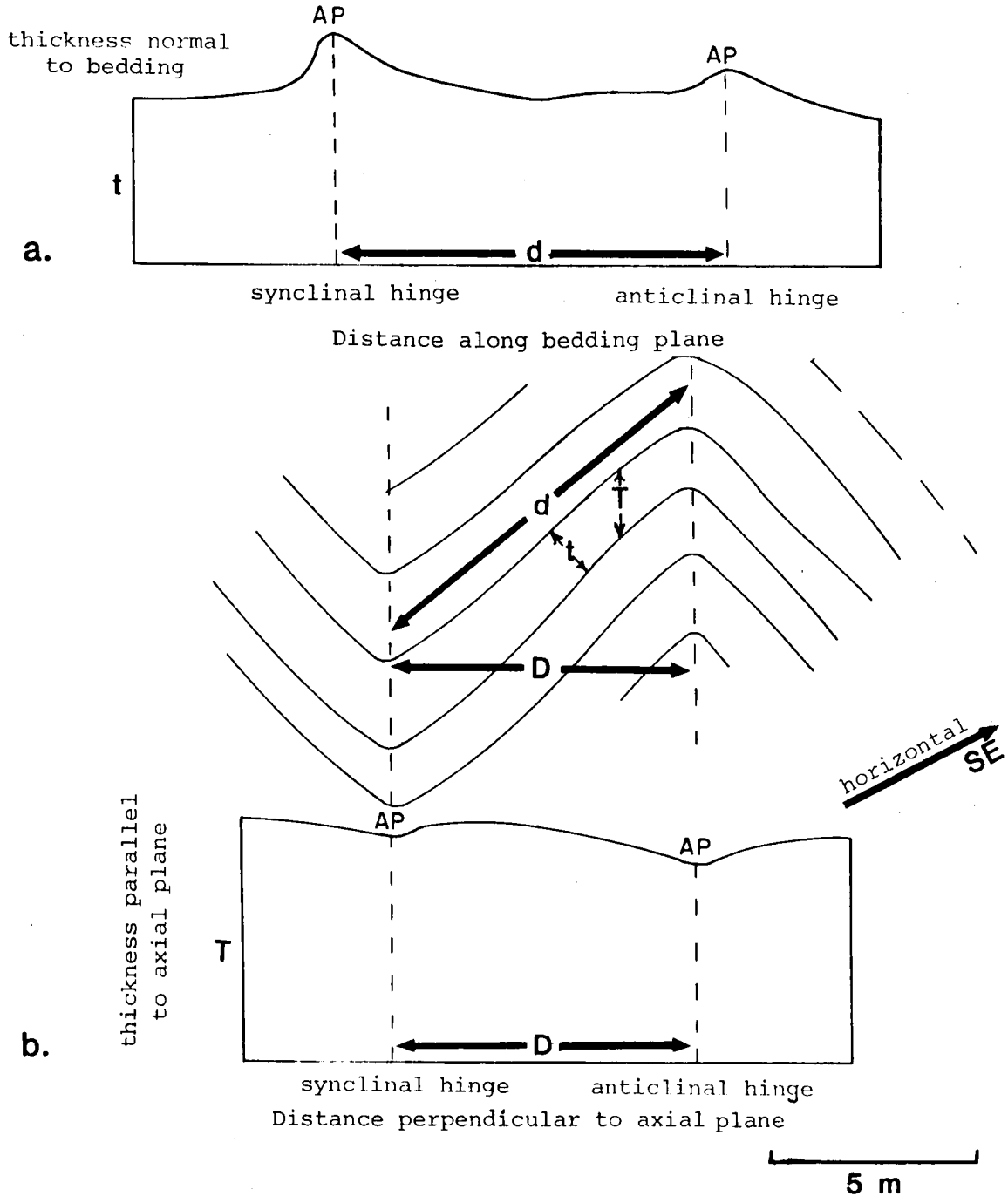

Figure 22. Thickness plots for second order chevron-kink fold (B30) with class 2 hinges. (a) Orthogonal thickness (t) versus distance along bedding plane (d). (b) Thickness parallel to axial plane (T) versus distance orthogonal to axial plane (D).

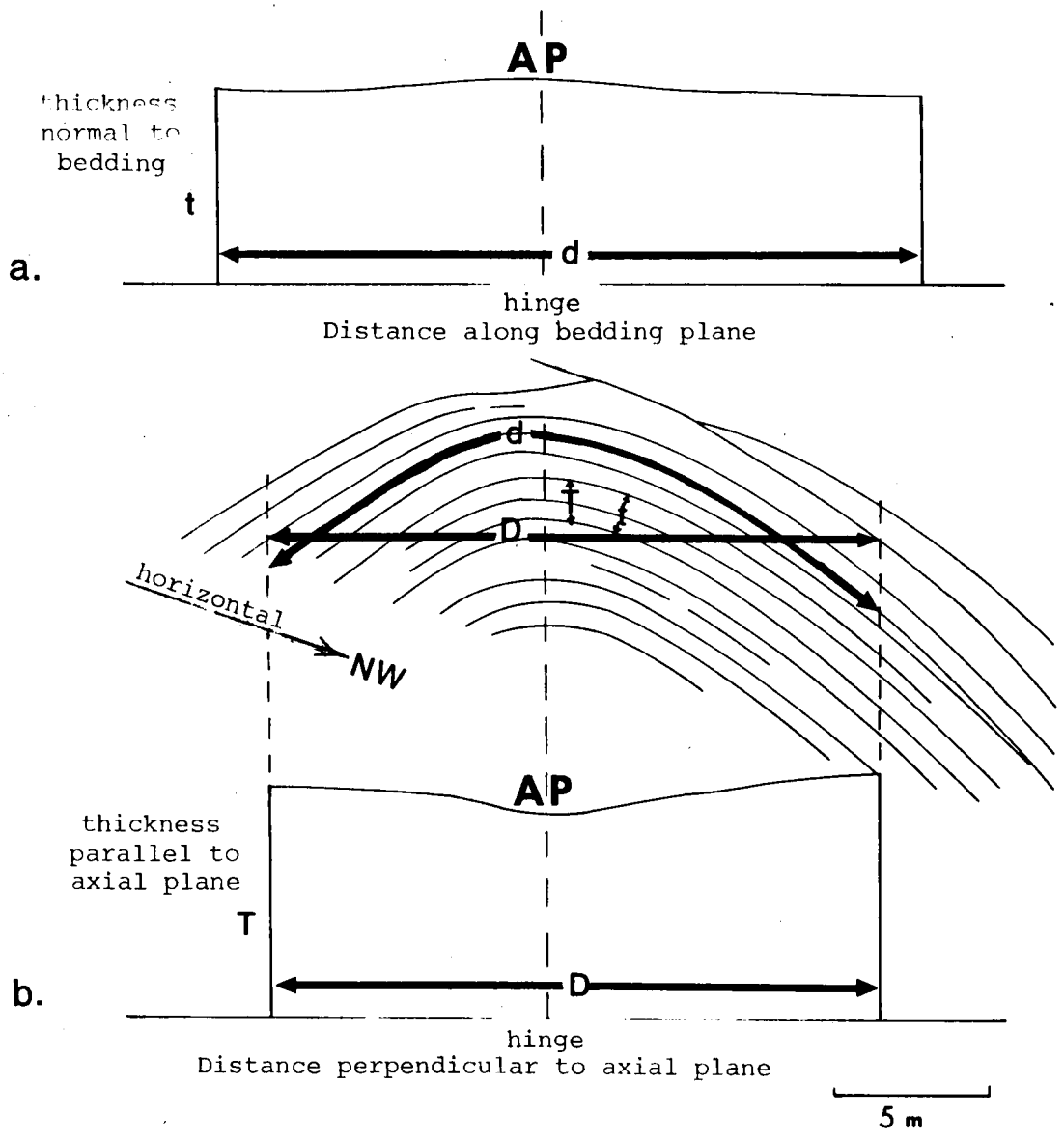

Figure 23. Thickness plots for second order concentric fold (C29, class 1b). (a) Orthogonal thickness (t) versus distance along bedding plane (d). (b) Thickness parallel to axial plane (T) versus distance normal to axial plane (D).

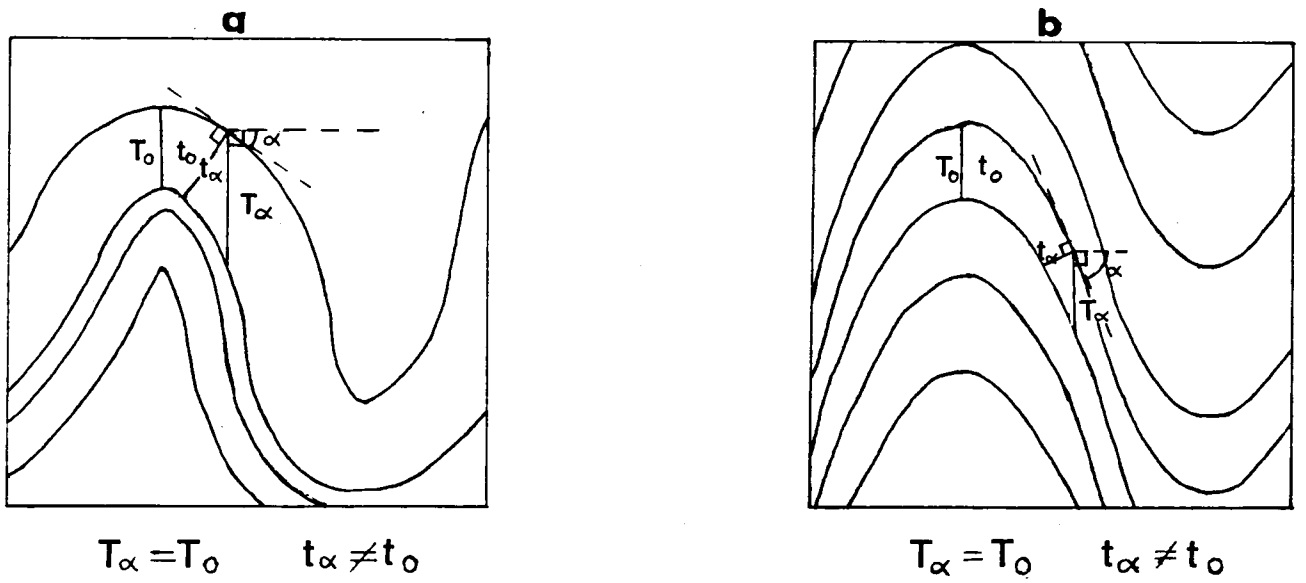

Figure 24. Ideal concentric (class 1b) and similar (class 2) folds with thickness parameters t and T (after Ramsay, 1967). (a) One wavelength of an ideal flexure fold. The dip isogons are parallel to t_α, for a given limb dip (α). (b) One wavelength of an ideal similar fold. The dip isogons are parallel to T_α.

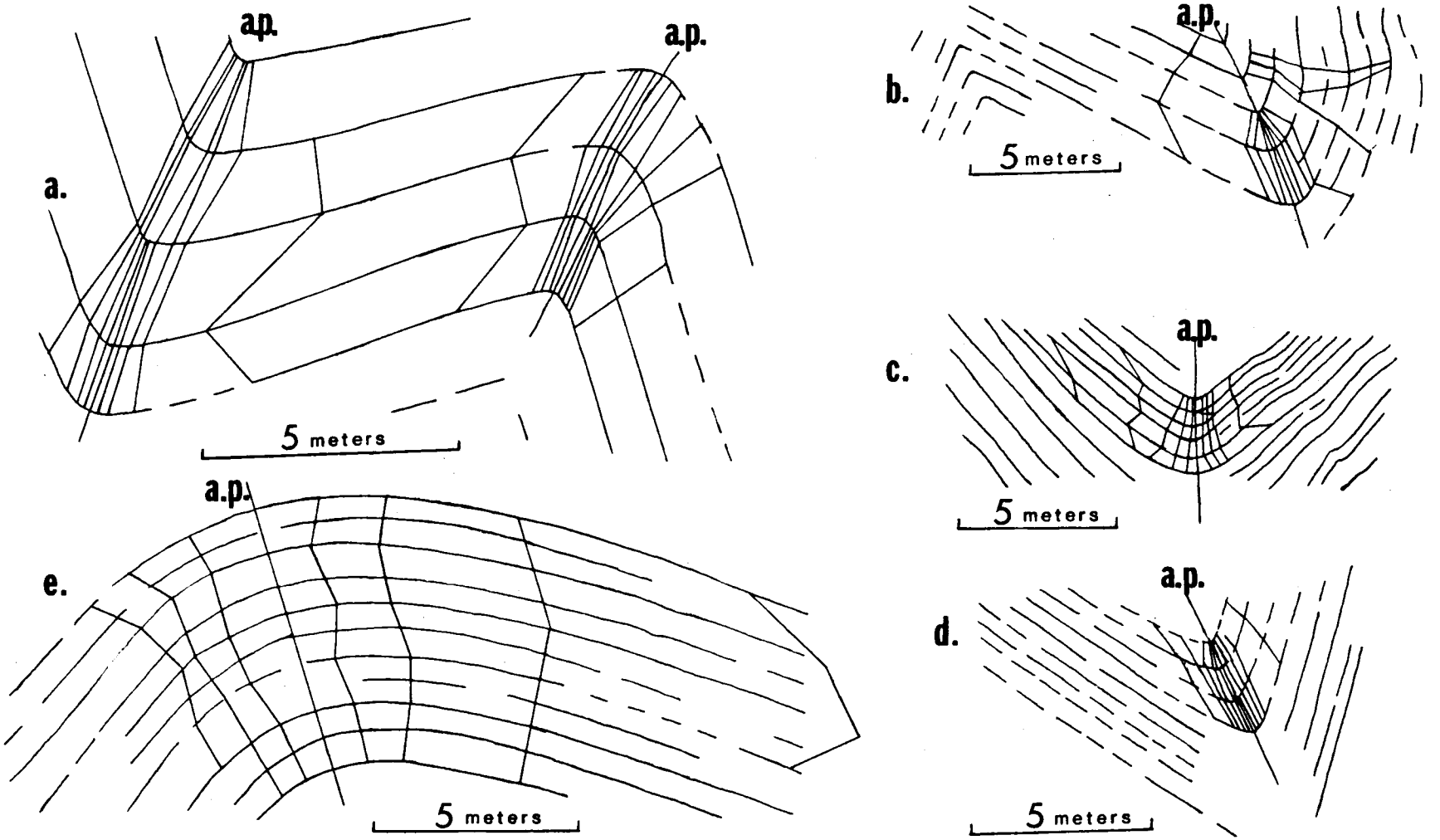

Figure 25. Representative dip isogon patterns for folds of different geometries. Based on Ramsay's (1967) classification for the folds above: (a) hinges are class 2, limbs are alternating classes 1b and 1c (B29.8-30.4), (b) hinge is alternating class 2 and 1c, limbs are alternating classes 1b and 1c (B91-91.7), (c) class 1c (A33.1), (d) alternating classes 2 and intermediate 1c/2 (C36.9), (3) class 1c (C29.3).

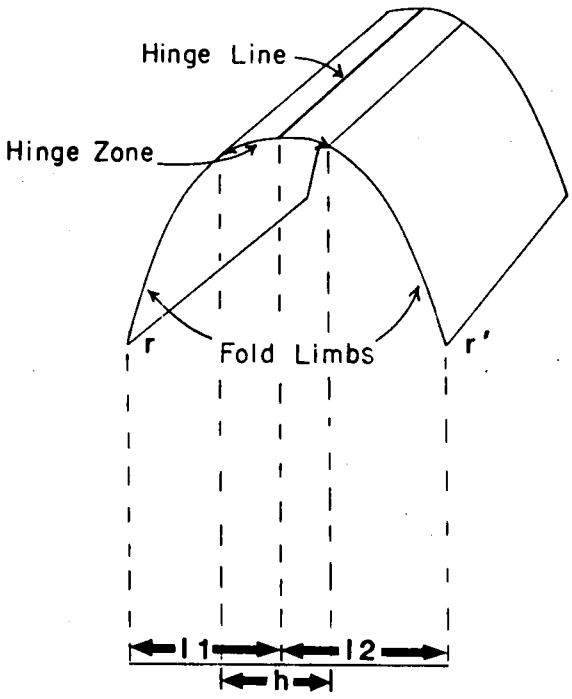

$$\text{parameter } A = \frac{\text{length of projection of limbs on rr'}}{\text{length of proj. of hinge zone on rr'}}$$

$$= \frac{l_1 + l_2}{h}$$

Figure 26. Illustration and definition of hinge angularity parameter A. r and r' are lines of inflection of the folded surface. In the hinge zone (h), the curvature of the folded surface exceeds that of a circular arc drawn with rr' as diameter. Angularity parameter A is defined (on a projection parallel to a tangent at the hinge) as the ratio of the extent of the fold limbs to that of the hinge.

Description of fold	Angle (β) between surface inclinations measured at the two inflection points, degrees
Gentle	180 - 120
Open	120 - 70
Close	70 - 30
Tight	30 - 0
Isoclinal	0
Elasticas	Negative value

Figure 27. Terms used to describe the tightness of a fold (after Fleuty, 1964), based on the interlimb angle (β).

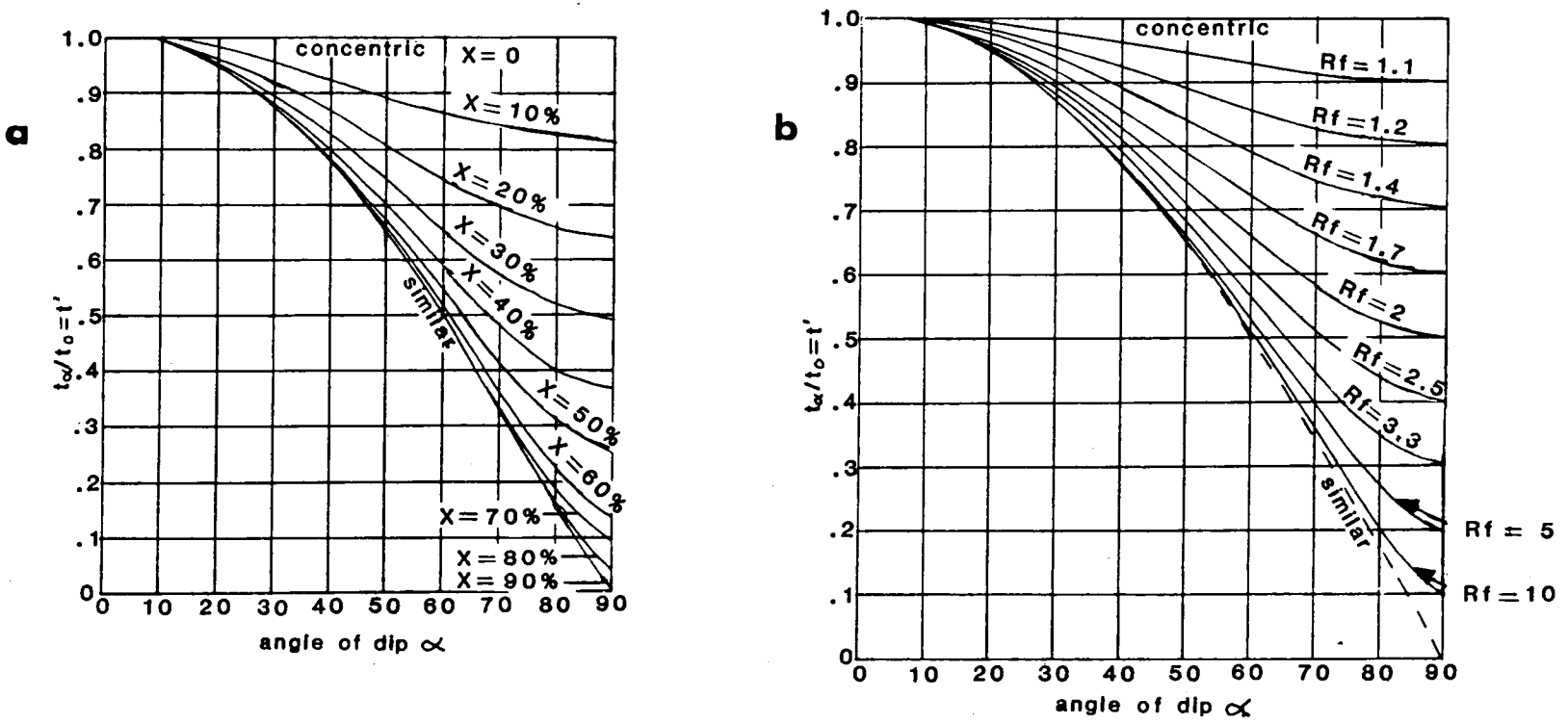

Figure 28. Nomograms for estimating amount of flattening strain from thickness ratios and limb dips for a given fold or folded layer. Each orthogonal thickness (t_α) corresponds to a limb dip (α). Thicknesses are referenced to hinge thickness (t_0) to produce thickness ratio, (t'), the ordinate on each plot. The concentric curve ($t' = 1.0$) represents an unflattened fold. The similar curve represents maximum flattening of an initially ideal concentric fold. (a) X is the amount of flattening as a percentage of that necessary to produce a similar fold (after Ramsay, 1962). (b) $Rf = (\lambda_1/\lambda_2)^{1/2}$, where λ_1 and λ_2 are the maximum and minimum strain magnitudes of the flattening strain ellipsoid (after Gray and Durney, 1979).

7. angular deviation of cleavage from fold axial surface (Figure 11, p. 47)
8. angular deviations of the fold axial surface and cleavage from the flattening extension direction (Figure 29)
9. bedding-cleavage angle versus limb dip (Figures 30, 31)

Analyzing thickness parameters (1) and (2) is a means of determining how closely natural folds approximate ideal fold geometries. They are also used in fold flattening analysis. Dip isogon analysis (3) allows classification of the fold profile and suggests how closely the folds approximate ideal fold geometries. The spacing of dip isogons implies the degree of angularity of the hinge. Angularity (4) represents the relative extent of a fold hinge zone to its limbs. The influence of the following factors on angularity are analyzed: cleavage intensity, location, lithology, and bed thickness. Interlimb angle (5) is analyzed to determine its degree of control on cleavage fan angle, cleavage intensity, and fold transection by cleavage (7). Flattening strain (6) is calculated to determine the orientation of the flattening strain ellipse (assuming plane strain) and the magnitude of its axes (the degree of fold shape modification by flattening). The timing of flattening with respect to buckle folding is

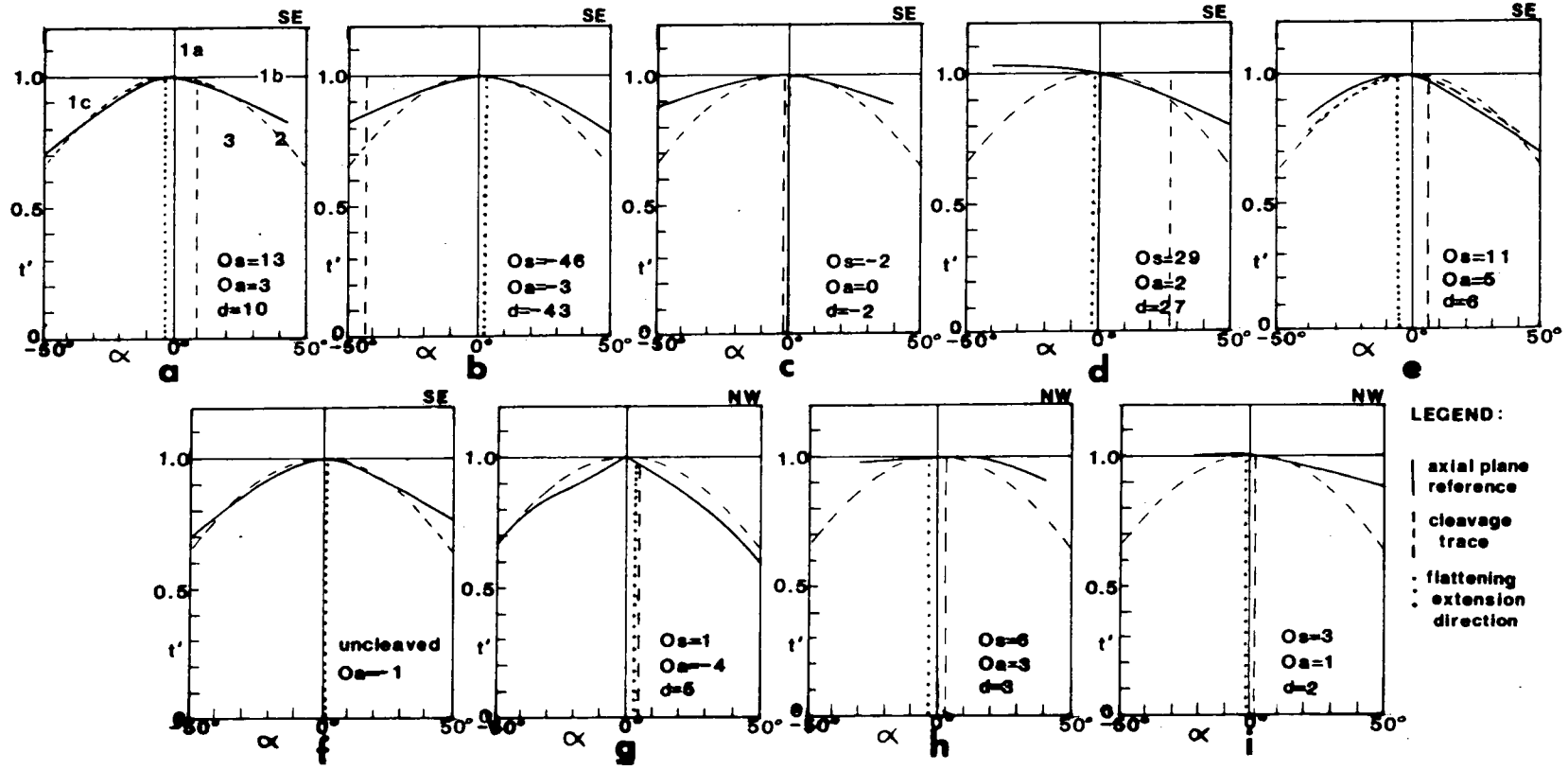

Figure 29. Orthogonal thickness ratio curves (solid curves) for flattening analysis of 9 folds in the Sevier formation. Dashed curve represents ideal class 2 folded layer (Ramsay, 1967). Based on the flattening strain nomogram (Figure 28b). The vertical axis represents orthogonal thickness ratio (t'). The horizontal axis represents both (1) limb dip (α) and (2) angular deviation of: (a) cleavage from the axial plane (d) and (b) the flattening extension direction from the axial plane (ϕ_A). The angular deviation of cleavage from the flattening extension direction is $d + \phi_A = \phi_S$. The fields of class 1a, 1b, 1c, 2 and 3 folds are shown on the plots. (a) A15 syncline. (b) A19 anticline. (c) A33 syncline. (d) A64 anticline (e) B30 kink. (f) B91.7 syncline. (g) C36 syncline. (h) C29 anticline. (i) D109 anticline.

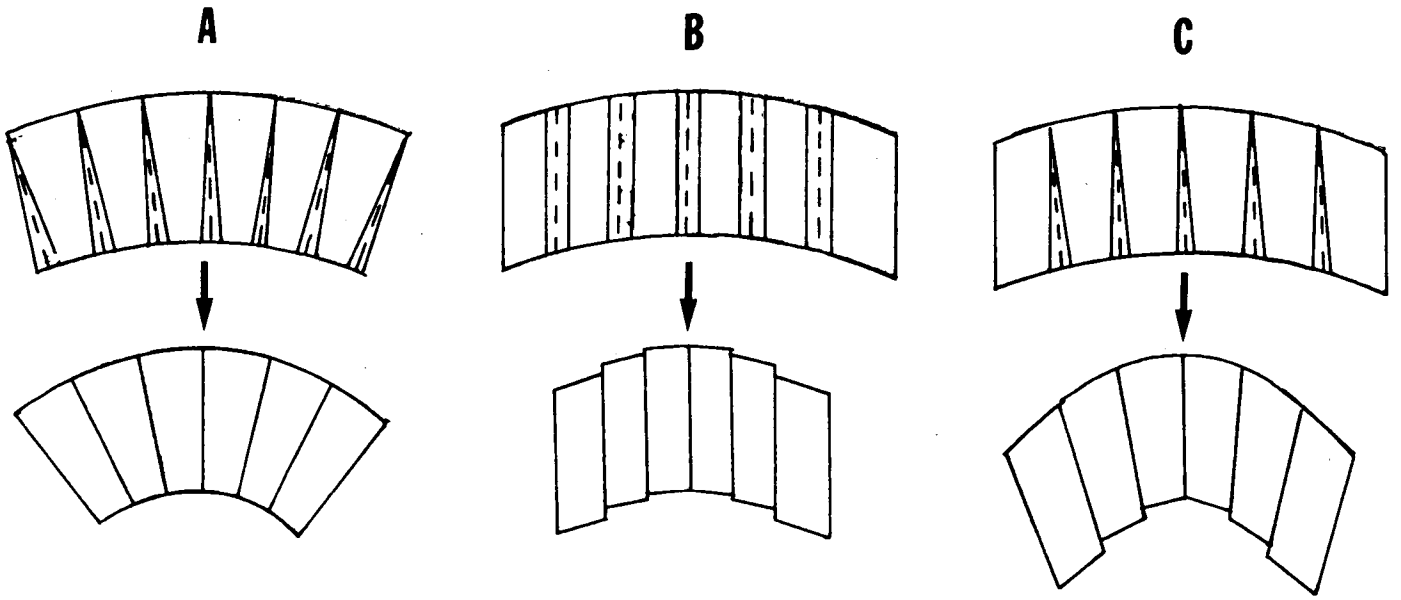

Figure 30. Models of deformation caused by removal of material from folds in which cleavage is symmetrical about the axial plane. Upper diagrams show original folds in which zones to be removed are marked. These zones are symmetrical about central lines (dashed). Lower diagrams show folds reconstructed by rotations or horizontal movements after material of zones is removed. A: removal of amount that increases into fold core from zones perpendicular to bedding. B: removal of constant amount from zones oblique to bedding and parallel to fold axial surface. C: removal of amount that increases into fold core from zones oblique to bedding and parallel to fold axial surface (after Groshong, 1975).

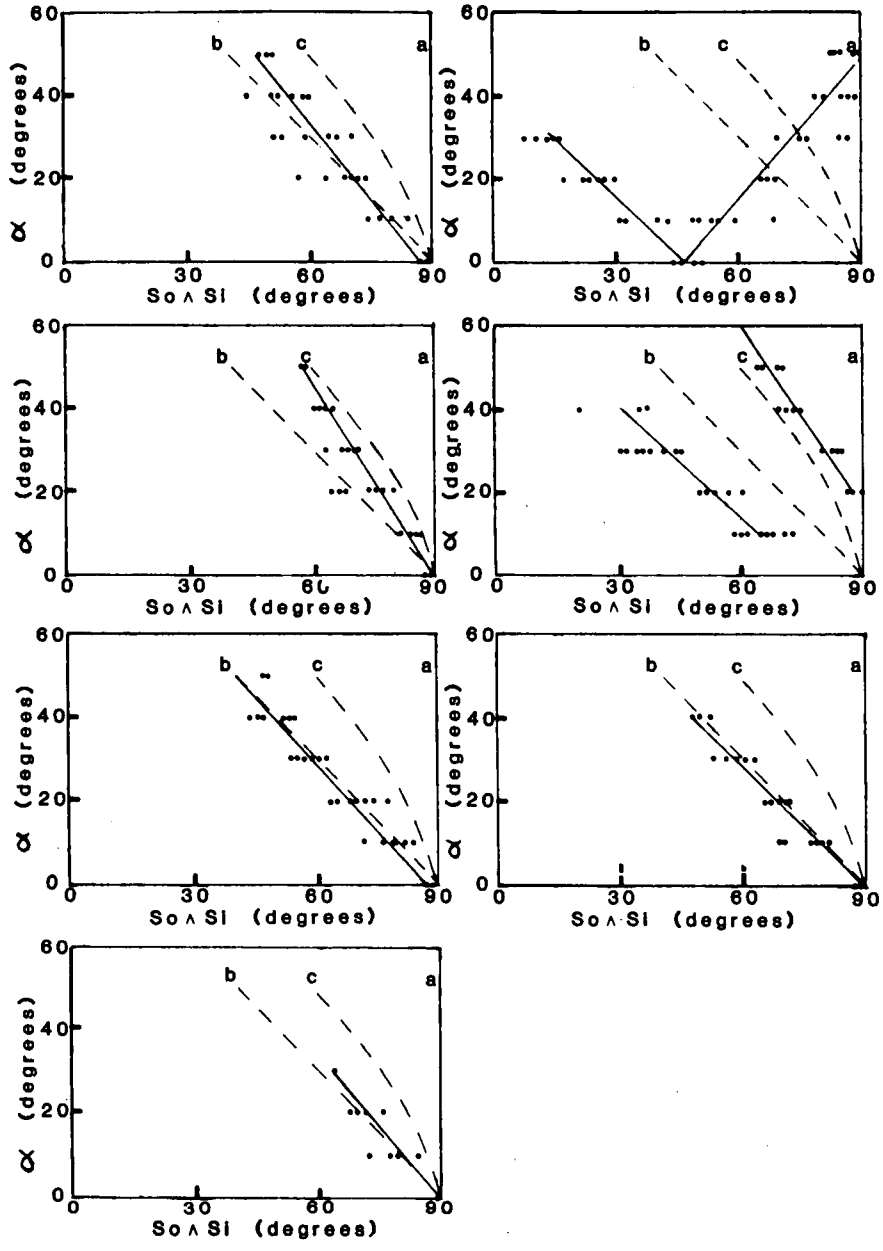

Figure 31. Comparison of fold bedding-cleavage angles with Groshong's (1975) models a, b, and c (Figure 30), which plot as dashed lines. Model a coincides with the vertical axis where $S_0 \wedge S_1 = 90°$ (cleavage is perpendicular to bedding). Solid lines represent measured fold data. Cases in which data plot as two lines are explained as significant transections of the fold axial plane by cleavage. (a) A15 syncline. (b) A19 anticline. (c) A33 syncline. (d) A64 anticline. (e) B30 kink. (f) C29 anticline. (g) D109 anticline.

investigated. The deviation between cleavage and fold axial surface orientations can provide clues to their relative timing. The deviations of axial surfaces and cleavage from flattening extension directions (8) can also be used to determine the relative timing of flattening. Analysis of bedding-cleavage angles with respect to fold limb dips (9) may aid in determining the best model for selective removal of material along cleavage planes during fold shape modification caused by pressure solution.

Qualitative analyses which will be used in this chapter include ductility contrast (based on contrasting lithologies interbedded in folds), and type and degree of symmetry. The effect of ductility contrast on fold geometry will be discussed. The presence or type of symmetry may be used to determine the initial orientation of stresses with respect to the layering. The sense of fold asymmetry may suggest timing relationships with other structures.

Buckle shortening will be used to determine a minimum shortening strain estimate. Fault shortening will be generally disregarded in this study due to the infrequent occurrence of correlatable marker beds.

2. Fold Profiles

Ramsay (1967) used three parameters to describe change in the profile shape of folded layers: (1) orthogonal

thickness t, (2) thickness parallel to the axial surface trace T, and (3) the inclination of the dip isogons.

Orthogonal thickness t (Figures 22, 23) varies with limb inclination α (Figure 24). The orthogonal thickness ratio, $t' = t_\alpha/t_0$ (t_α = t at a given α, t_0 = t at the hinge), measures changes in bed thickness going around the fold (Figure 24). Thickness parallel to the axial surface trace of the fold T (Figures 22, 23) also may vary with limb dip α, and T' (the ratio of T_α = T at a given α to T_0 = T at the hinge) is also a useful measure of changing fold shape (Figure 24). Orthogonal thickness and parallel thickness are dependent on one another as t (or t') = T (or T') cosα (Figure 24).

Dip isogons connect points having equal slope (α) on adjacent bedding surfaces. As an example, the dip isogons are parallel to t in Figure 22a, and they are parallel to T in Figure 24b. Several other naturally occurring patterns are illustrated in Figure 24. The slopes of the dip isogons relative to the axial surface trace of the fold reflect the mean curvature of adjacent folded surfaces. The isogons, and the relative spacing between them, are related to the rates of change of t' and T' with respect to the angle α.

Another useful parameter is the extent of fold hinge zones relative to limb lengths. To measure the extent of a hinge zone relative to the limbs, the limits of the hinge

zone are found by comparing the curvature of the fold surface with that of a circular arc drawn with rr' as diameter. Referring to a folded surface in general (Figure 25, p. 98), r and r' are lines of inflection. The hinge line connects points of maximum curvature on the folded surface. That part of the fold where the curvature of the fold surface exceeds that of the circular arc is defined as the hinge zone h. The limbs l_1 and l_2 connect successive hinge zones and include the inflection points.

The tightness of a fold depends on interlimb angle (β), and on the degree of change of curvature (angularity) for the fold half wavelength (between inflection points). Fleuty (1964) suggested that descriptive terms be used for the degree of tightness associated with interlimb angle measurements based on tangents to the folded layer at points of inflection in profile (Figure 27, p. 100). The ratio (A) of the extent of the fold limbs to that of the hinge zone,

$$A = \frac{\text{length of projection of limbs on rr'}}{\text{length of projection of hinge zone on rr'}} = \frac{l_1 + l_2}{h}$$

(Ramsay, 1967), is a measure of hinge zone angularity. Values of $A > 10$ correspond to straight-limbed folds with small hinge zones, approaching chevron folds. Values of $A < 10$ represent folds with larger hinge zones and smaller limbs, approaching concentric folds (class 1b; $A < 1.5$) or modified concentric folds (class 1c; $1.5 < A < 10$) which approach a similar form.

3. Fold Classes

Fold profiles are grouped into three general classes, based on dip isogons (Ramsay, 1967):

a. Class 1. Curvature of the inner fold arc always exceeds that of the outer arc and isogons converge towards each other and the axial surface trace as they are traced toward the inner arc of the fold. Three subclasses of class 1 folds can be distinguished, based on the degree of dip isogon convergence and the values of the thickness ratio parameters. A special type of class 1 fold, class 1b (illustrated in Figure 22a, p. 95), maintains constant orthogonal thickness t for a given folded layer, and the dip isogons are perpendicular to the folded surface. Class 1b folds are described as having concentric fold geometry. The other two subclasses of class 1 folds have either strong (class 1a) or weak (class 1c) convergence of the isogons.

b. Class 2. Thickness parallel to axial surface trace (T) is constant, and dip isogons are parallel to the axial surface trace; adjacent layer surfaces have equal curvature (Figure 24b, p. 97). These are similar folds. A graph of thickness parallel to the axial plane (T) plotted against distance perpendicular to the axial surface profile trace (Figures 22b and 23b, p. 96) indicates how closely a given fold coincides with similar folds. In the case of the fold

illustrated in Figure 22 (p. 95), the nearly flat axial plane-parallel thickness curve implies either extreme flattening of a preexisting concentric fold (Ramsay, 1967), ductile strain at the hinges during folding, or lamellar flow parallel to the fold axial surface (Cloos, 1947; Carey, 1954).

c. Class 3. Curvature of the outer arc always exceeds that of the inner arc, and the dip isogons diverge from each other and from the axial surface trace when traced toward the inner arc of the fold.

A graph of orthogonal thickness t plotted against distance along bedding indicates how closely a fold coincides with concentric geometry. In the case of the fold illustrated in Figure 23 (p. 96), the nearly flat orthogonal thickness curve implies a very close relationship with ideal flexural folding (Ramsay, 1962), in contrast to the fold in Figure 22. Concentric folds have a problem of room accommodation toward the cores; thus, they must die out upward and downward and can only affect a limited thickness of strata (Ramsay, 1962). This problem may be resolved by the development of complex minor folds and thrusts near the inner hinge or by changing geometry along the axial plane.

In Stephansson's (1976) experimental work dealing with the mechanics of folding in layered viscous solids, he concluded that fold geometries range from concentric for

large interlayer viscosity (and ductility) contrasts, to nearly similar for low contrasts.

4. Fold Symmetry

As defined by Turner and Weiss (1963, p. 132), symmetrical folds are those whose profiles are bilaterally symmetric across their axial surfaces, regardless of orientation. The degree of symmetry of buckle folds may indicate the initial angular relationship (θ) between bedding and the direction of compression prior to the inception of the folding (Ramsay, 1967). Thus, high fold symmetry may imply an initially small θ angle (compressive stress nearly parallel to bedding). Experimental work has shown that the axial planes of buckle folds develop approximately perpendicular to the axis of shortening (Ghosh, 1966, p. 175; Price, 1966, p. 194).

5. Kink Folds

Coupled asymmetrical chevron fold hinges form kink-bands (Figure 25a,b, p. 98). Kink-band folds are tabular fold zones in which the paired axial surfaces are usually longer (in the direction of fold amplitude) than the fold half-wavelength distance between adjacent hinges. Kink folds are most often found in relatively thin beds and with a significant anisotropy due to the layering. These folds commonly occur in conjugate sets, one of which is usually

more numerous. Kinks are generally believed to be late-formed features, because of easier interlayer slip after development of foliation (Paterson and Weiss, 1966). They are believed to be caused by compression parallel to planes of foliation. Kink fold axial surfaces develop oblique to the axis of shortening, and along a plane of shear stress (Dewey, 1965). The orientation of the shear plane depends on the internal friction of the rock (Ramsay, 1967) and the amount of subsequent flattening of the angle between the shear plane and the least compressive stress direction.

6. Fold Flattening

The term "flattening," used here after Ramsay (1967), Hudleston (1973) and Gray and Durney (1979), describes the process of deformation in which initial structures are strained, resulting specifically in shape modification of folds by finite, homogeneous, approximately plane strain. The assumption of concentric folding preceding superimposed increments of flattening strain is merely a simplification made in order to consider the buckling and flattening processes independently. The flattening results in contraction parallel to the principal compressive stress and in elongation in the direction of minimum stress (Ramsay, 1967). Flattening causes increasing limb dips (limbs rotate toward axial plane-parallel) and decreasing bed thickness away from fold hinges.

Thickness ratio plots assume that the initial thickness (t_0) of the bed is known. The plots are normalized by considering the value of t' at the fold hinges to be unity ($t = t_0$) and expressing t' for any other part of the fold as a proportion of this unit value. The ratios (t') of t_α to t_0 were plotted against limb dip for various points on the surface of a folded bed (Figure 28, p. 101, Figure 29, p. 103). Tangents were constructed (at ten degree intervals of α) to the bedding surface, then orthogonal thickness was measured and plotted as a proportion of hinge thickness against limb dip (Figure 29). Ramsay's (1962) nomogram (Figure 28a) for estimating the percentage of flattening assumes that flattening was superimposed on preexisting pure flexural folds. Gray and Durney (1979) used a similar nomogram to estimate the magnitude of flattening strain (Figure 28b). Ramsay shows that the relationships between orthogonal thickness ratio (t') and values for the maximum (λ_1) and minimum (λ_2) extensional strains is: $t' = (\cos^2\alpha + \lambda_2/\lambda_1 \sin^2\alpha)^{0/5}$. $Rf = (\lambda_1/\lambda_2)^{0/5}$ is the axial ratio of the flattening strain ellipse (Gray and Durney, 1979). The major axis of the fold flattening strain ellipse is X. The fields of class 1a, 1b, 1c, 2, and 3 folds are shown on the plots (Figure 29). The position of points on a real fold relative to these calculated curves of flattening values enables flattening strain to be determined. Plane strain is a necessary and probably reasonable assumption

which may not be strictly accurate. Plane strain implies a lack of finite strain in the intermediate stress direction. The thickness ratio versus limb dip curves (flattening strain curves, Figure 29, p. 103) yield similar results for classifying folded layer geometry as does the dip isogon method (Figure 25, p. 98).

Assuming minimum or no flattening strain to be superimposed on a concentric fold (R_f = 1.0), the thickness ratio curve will correspond to the curve for class 1b (concentric) folds. Assuming, in the opposite case, that an initially concentric fold is subjected to the maximum compressive strain modification (infinite flattening), the thickness ratio curve will correspond to the curve for class 2 (similar) folds, provided by the function $t' = \cos \alpha$.

Parameters ϕ_S and ϕ_A represent, respectively, the angular differences in degrees between: (ϕ_S) cleavage and the fold flattening (X) direction as a reference, and (ϕ_A) the axial plane trace and the fold flattening (X) direction as a reference (modified after Gray, 1979; Figure 29). The difference between ϕ_S and ϕ_A is equal to parameter d, the deviation of cleavage from the axial surface trace in the profile plane. Positive values of ϕ_S, ϕ_A, and d correspond, respectively, to clockwise rotations of: (1) cleavage with respect to the fold flattening direction, (2) the axial surface trace with respect to the fold flattening direction, and (3) cleavage with respect to the axial surface trace.

7. Origin of Cleavage by Pressure Solution

Troensegaard (1965) believed that cleavage in an adjacent area (within the Tellico-Sevier shale belt) was formed by shear acting approximately parallel to the axial surfaces of folds. This is not considered a strong argument, since no consistent evidence of shearing is observed on cleavage surfaces within the Sevier. Shearing on surfaces subparallel to axial surfaces is unlikely, since axial surfaces of buckle folds seem to represent a principal plane of strain, and shear stresses can only operate at angles oblique to principal planes.

Wise (1980) proposed that in the nearby Saltville thrust sheet, cleavage in argillaceous Lenoir limestone was developed by pressure solution. From thin sections, he determined that shortening due to pressure solution reached 50 percent in rocks with high cleavage intensities.

In Middle Ordovician mudstones (Moccasin formation in the Valley and Ridge in southwestern Virginia) at a low grade of metamorphism similar to the Sevier at Douglas Lake (comparison made on the basis of equivalent conodont color alteration; Epstein et al., 1977), Gray (1981b) believed that spaced disjunctive cleavage originated by pressure solution. He believed that the solution was delayed until after grain boundary sliding which was the initial mechanism of folding. With the aid of SEM micrography, he also

reported the presence of a more closely spaced domainal cleavage displaying a moderate to strongly preferred orientation of clay minerals, subparallel to cleavage traces. Both cleavage types occur in the same rocks, with the spaced cleavage superimposed on the domainal cleavage. Gray concluded that the increased preferred orientation and tighter packing of clays in spaced-cleavage zones indicate collapse of the primary fabric probably with rotation and grain boundary sliding accompanying removal of mobile calcite. Further evidence for the dissolution origin for the spaced disjunctive cleavage includes offsets and truncation of veins and calcite fenestrae along cleavage surfaces (Gray, 1981).

8. Rigid-Body Deformation with Selective Removal of Material

Three models of rigid-body deformation (Figure 30, p. 104) are caused by selective removal of material along pressure solution cleavage planes from preexisting buckle folds (Groshong, 1975). These models have been compared graphically with one another and with natural folds in the Sevier formation by plotting limb dip relative to the axial plane (α) versus cleavage-bedding angle ($S_0 \wedge S_1$), measured in the profile plane (Simon, 1981). This will be discussed further in subsequent sections. The models involve volume-loss deformation of three end-member geometric types.

The end-member geometries are derived as follows:

a. Model A (Figure 30a, p. 104) involves removal from zones perpendicular to bedding, with the amount increasing into the fold core, and without offset of bedding continuity.

b. Model B (Figure 30b) involves removal of constant amount from zones oblique to bedding and parallel to the axial surface, with offsets of bedding parallel to the axial surface.

c. Model C (Figure 30c) involves removal of amount increasing into the fold core from zones oblique to bedding and parallel to the axial surface, with offsets of bedding toward the fold core.

Comparison of bedding-cleavage relationships for the models with those in the Sevier formation provides a method for restricting the possible folding modes and possibly the timing of cleavage in cases of nontransected folds.

9. Folds Transected by Cleavage

A transected fold core is a fold hinge zone in which cleavage surfaces cut obliquely across the axial surface. There are two types of cleavage transection parameters (Figure 32): (1) Δ, the angle measured in the horizontal between the traces of cleavage and the fold axial plane, and (2) d, the solid angle between the axial plane and cleavage

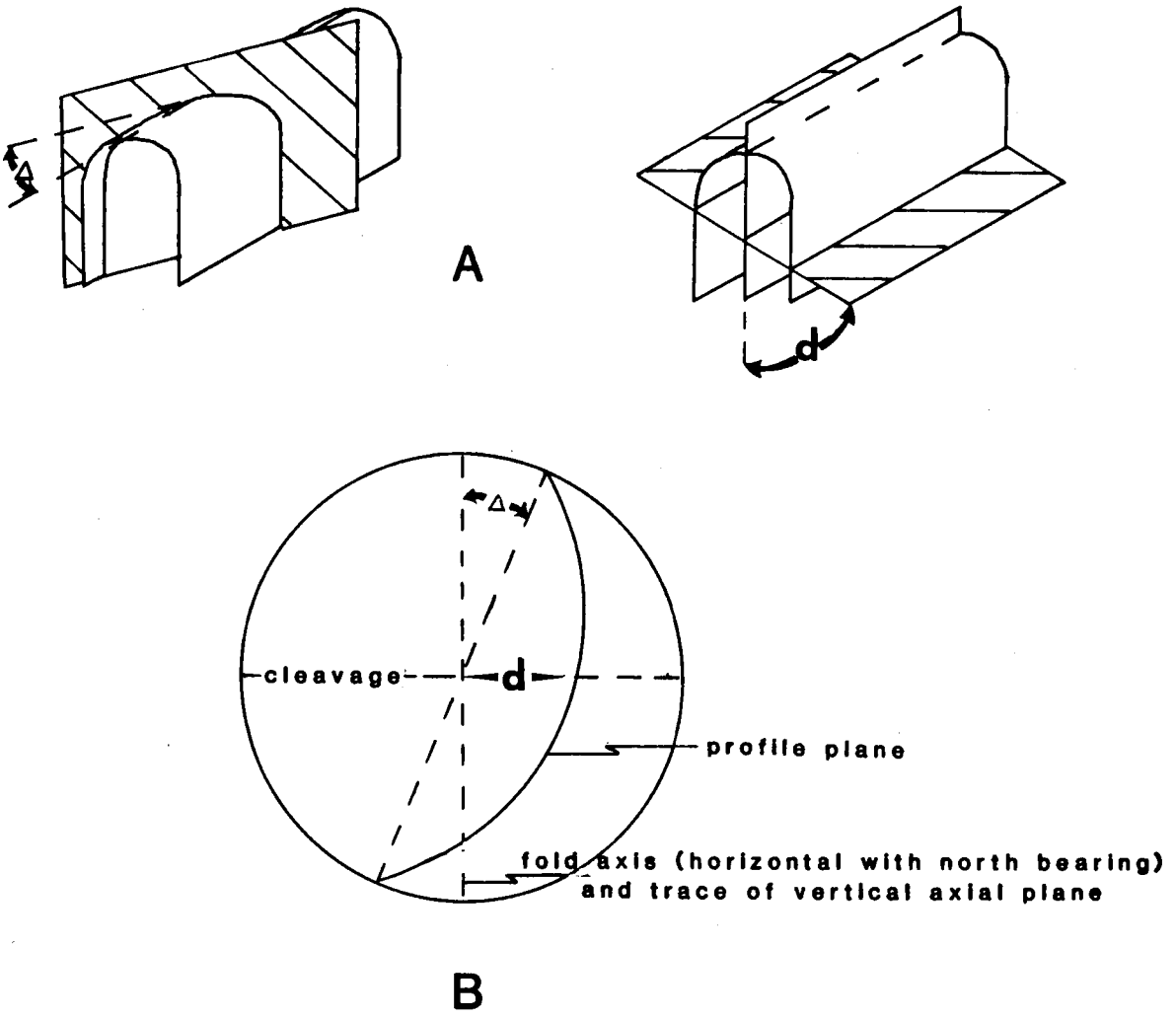

Figure 32. Illustrations of fold transection types (after Borradaile, 1978). Diagonal ruled planes are cleavage. Δ is the angle between the traces of cleavage and the fold axial surface in a horizontal plane. d is the angle between the axial plane and cleavage measured in the profile plane. For folds with cleavage symmetrical about the axial plane, Δ = d = 0. Clockwise Δ transection is considerd positive. Clockwise d transection is considered positive when viewed towards the northeast. (A) Pure Δ and d transections (respectively at left and right) are shown for two hypothetical folds. (B) A stereographic projection represents a single fold displaying both Δ and d transection components.

in the profile plane (Borradaile, 1978). The second angle, d, will be dealt with mostly in this study, as it can be roughly determined directly from the profile sections. Fold transection by cleavage is a significant problem in the study area although previously unreported in East Tennessee.

10. Buckle Shortening Strain

Calculations of shortening strain due to buckling were made by measuring fold arc lengths (original undeformed length) after removing as much of the fault displacement as possible and assuming uniform layer thickness; the original length (L_0) and resultant length modified by layer buckling (L_1) are then used in the following formula to calculate percent shortening due to buckling (Figure 33): $(L_0 - L_1)/L_0 \times 100$ = percent shortening due to layer buckling.

C. Data Presentation and Analysis

1. Controls on Fold Geometry: Chevron versus Concentric

A slightly larger proportion of chevron folds is found in the southeastern portion of the study area (Figure 34) while concentric folds occur more abundantly in the northwestern part. This relationship (indicated by dashed line, Figure 34) between geographic location and fold geometry is weak at best. Besides this comparison between location in the strike belt and fold geometry (based on

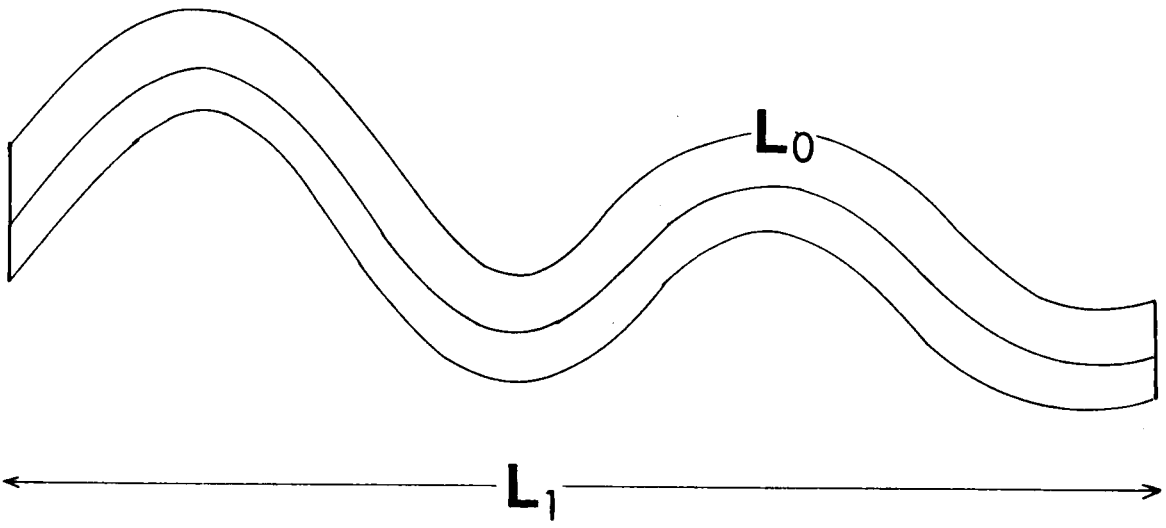

$L_0 =$ original undeformed length of layers

$L_1 =$ length modified by buckling of layers

$$\frac{L_0 - L_1}{L_0} \times 100 =$$ % shortening due to buckling of layers.

Figure 33. Buckle shortening formula and illustration.

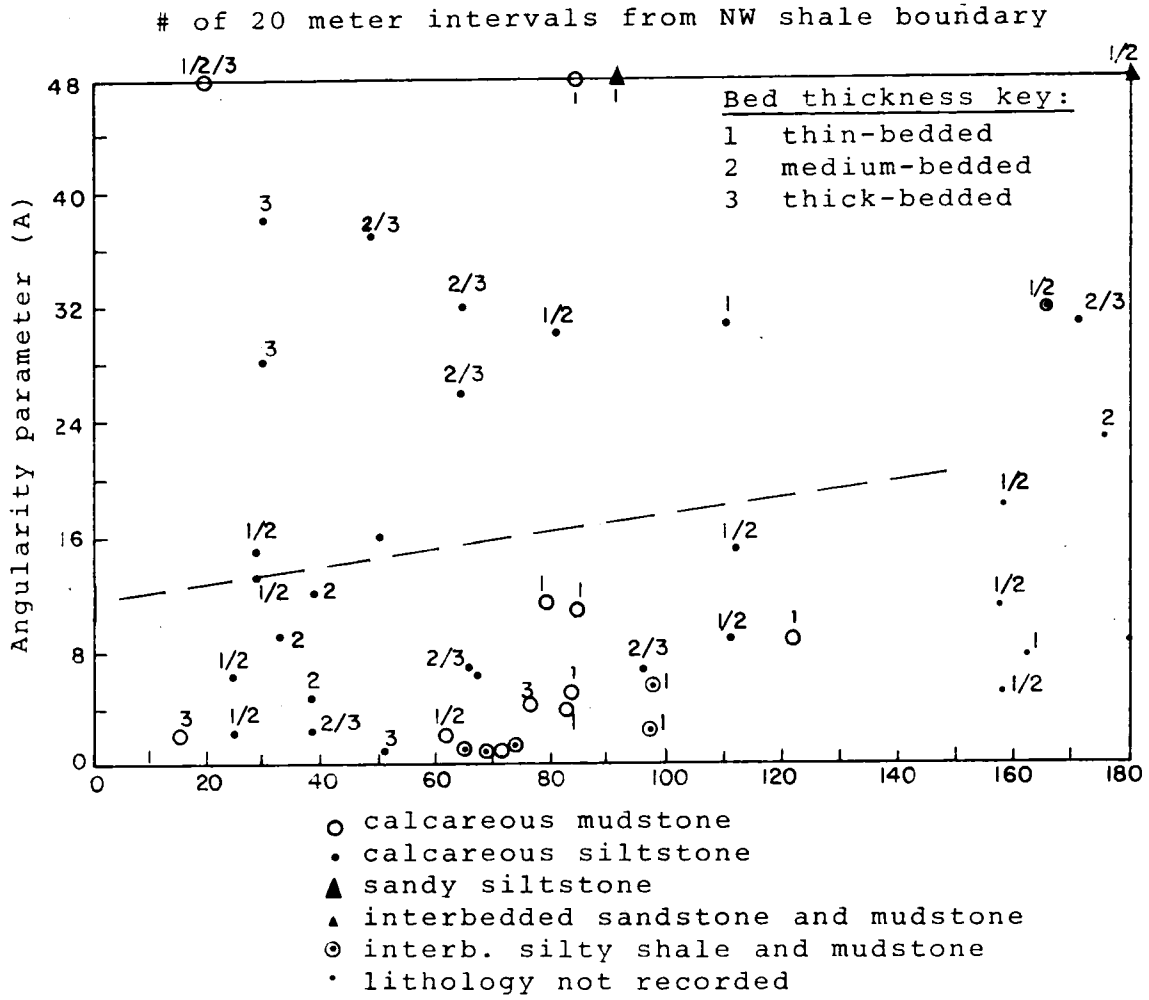

Figure 34. Hinge angularity (A) versus location in strike belt. Lithology and bed thickness are indicated for each fold. Data for 60 folds. Dashed line represents mean A across strike. Bed thickness key is based on Ingram's classification (Ingram, 1954; Figure 36).

parameter A), correlations exist between lithology and fold geometry (Figure 35), and between bed thickness (Figure 36) and fold geometry (Figure 37).

Figure 35 demonstrates a relationship between lithology (increasing grain size in particular) and increasing parameter A. For folds with lithologically homogeneous bedding, chevron folds are most abundant in sandstone and siltstone, while concentric folds are most abundant in mudstone and clayey shale. Conversely, all of the observed folds having interbedded competent and incompetent layers are concentric or modified concentric. The more competent sandstone or siltstone beds appear to constrain the fold shapes (e.g., Figure 14, p. 58), because they maintain dip isogons nearly orthogonal to the folded surface and have refracted, fanning cleavage. The incompetent shales increase their thickness at the hinge and decrease it on the limbs. This field evidence is in agreement with Stephansson's experimental work (dealing with the mechanics of folding in layered viscous solids), in which he concluded that fold geometries range from concentric, for large interlayer viscosity (and ductility) contrasts, to nearly similar, for low contrasts (Stephansson, 1976).

Figure 37 shows a weak relationship between increasing bed thickness (Figure 36) and decreasing parameter A, indicating a slightly greater mean bed thickness in

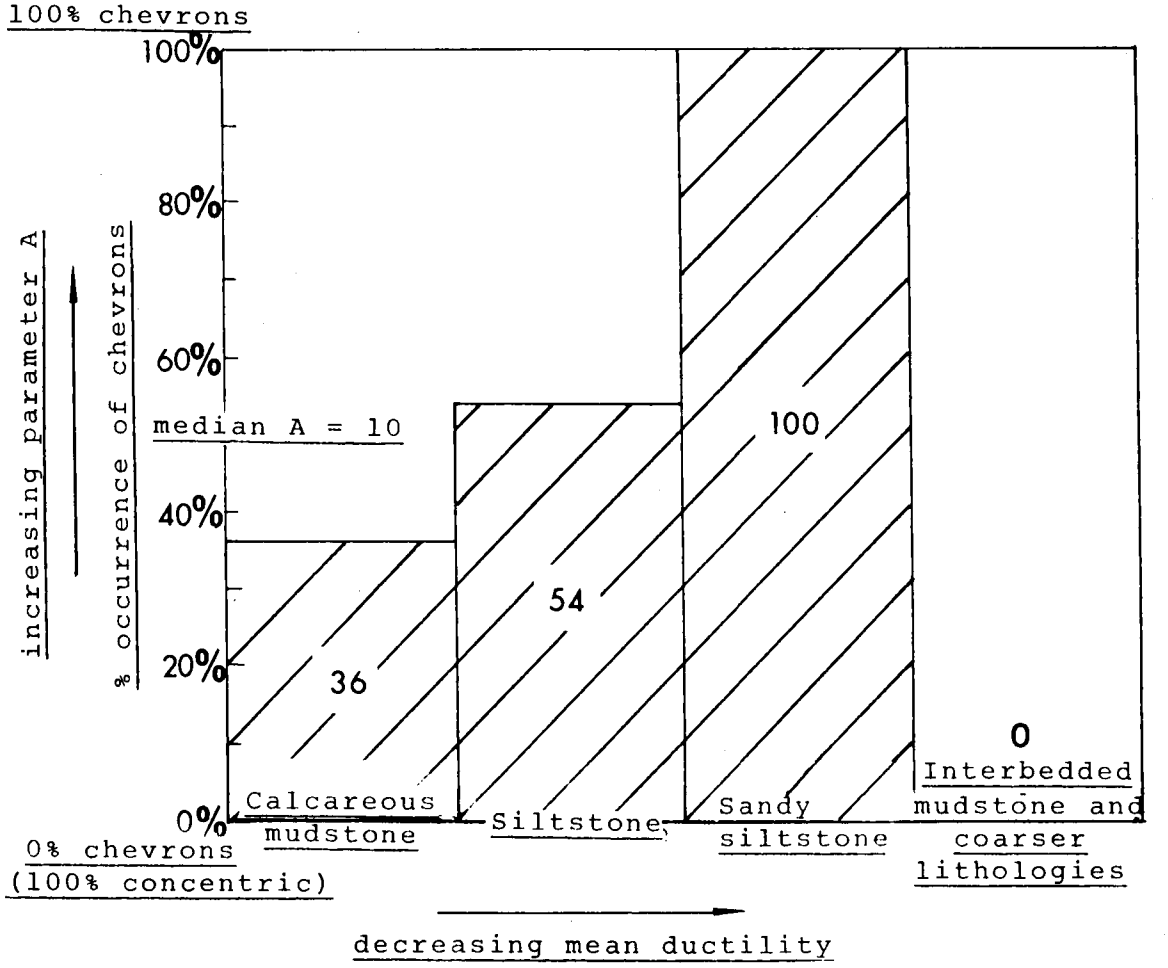

Figure 35. Hinge angularity (A) versus lithology. Percentage of chevron folds is given for each lithology. Data for 51 folds.

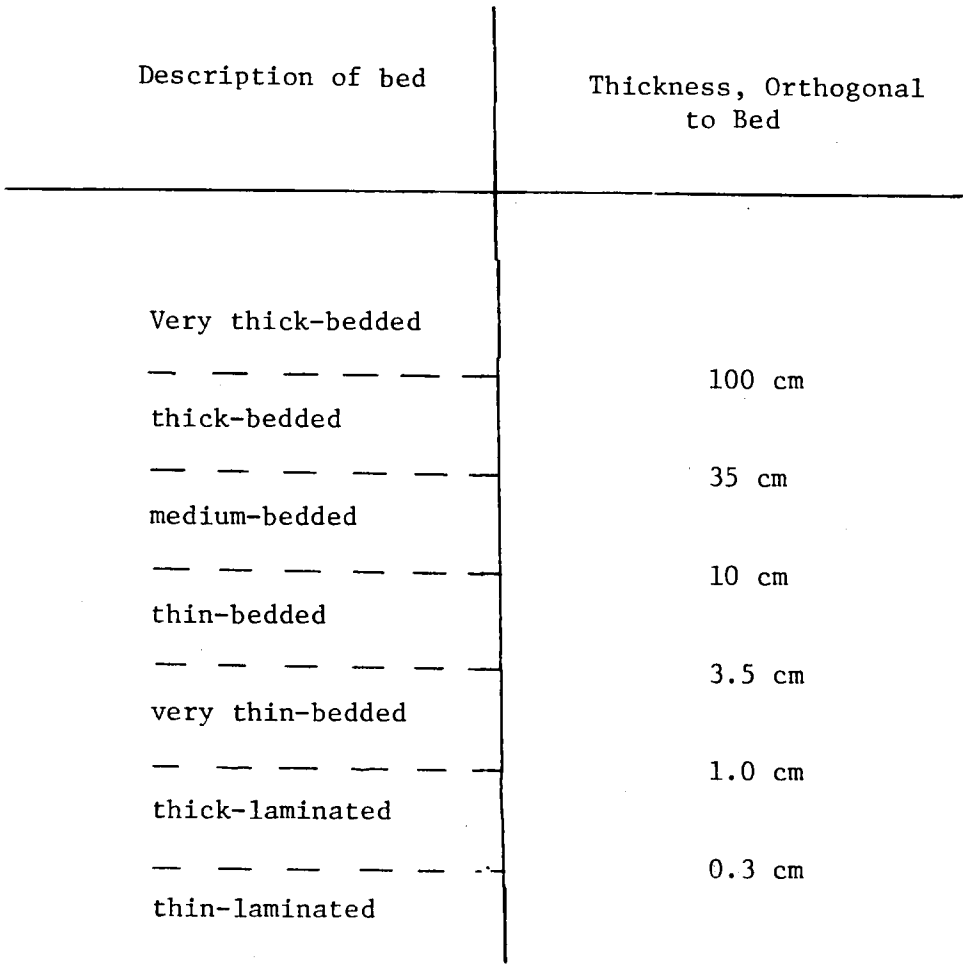

Figure 36. Bed thickness classification terms (after Ingram, 1954).

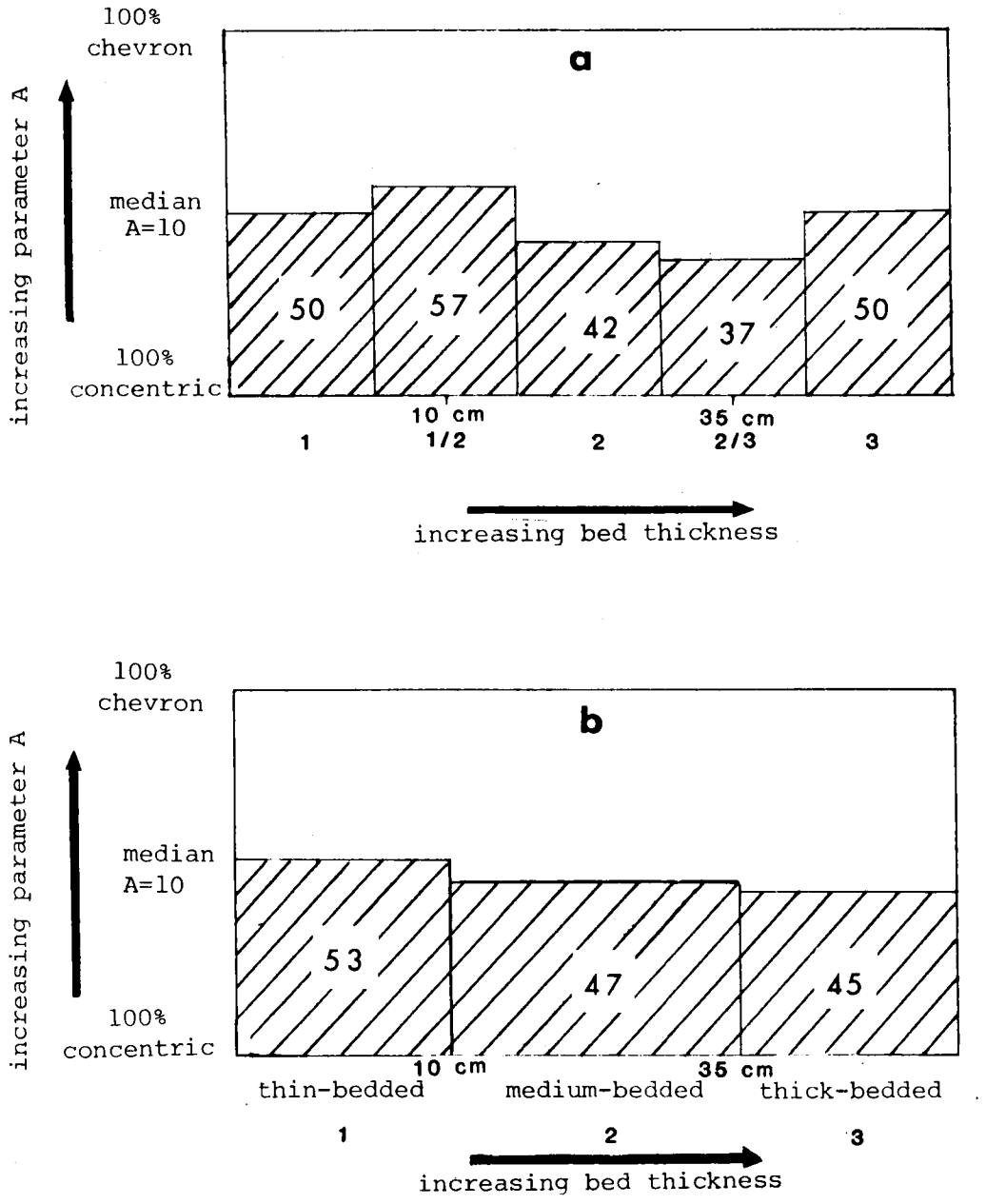

Figure 37. Hinge angularity (A) versus bed thickness. Thickness classification (Figure 36) after Ingram (1954). Data from 49 folds. "Thick-bedded" includes very thick-bedded and massive units. "Thin-bedded" includes thick and thin laminated units. (a) Histogram includes transitional thickness classes. Bed thickness key = (1) thin-bedded, (1/2) thin/medium-bedded, (2) medium-bedded, (2/3) medium/thick-bedded, (3) thick-bedded. (b) Histogram lacks transitional thickness classes.

concentric folds than in chevron folds. The typical concentric fold occurs in medium-bedded (10-35 cm thick) rocks, while the typical chevron fold occurs in thin/ medium-bedded (3.5-35 cm thick) rocks.

Bed thickness does not influence fold half wavelength ($\lambda/2$), when these parameters are compared (Appendix G). Therefore, these appear to be independent parameters in the study area, in contrast with the results of experiments and theory (Chapple, 1969). Thick, competent layers which control fold geometry possibly exist, but they are not exposed in every outcrop.

2. Evidence for Flexural-Slip Buckle Folding

Flexural-slip buckle folding (Figure 38a) in the Sevier formation at Douglas Lake is shown by slip linears on slickensided beds, with movement of the upper beds towards the hinges of upright anticlines and away from the hinges of upright synclines. Buckle folding is also indicted by the approximate symmetry of isolated fold hinges. The mean buckle fold axial orientation is 242°, 07° SW.

3. Kink Folds

Kink folds at Douglas Lake (Figure 38b) commonly occur in conjugate sets, one of which is usually more numerous. Bisectors of observed conjugate kink folds are subparallel to bedding. This orientation implies minor, approximately

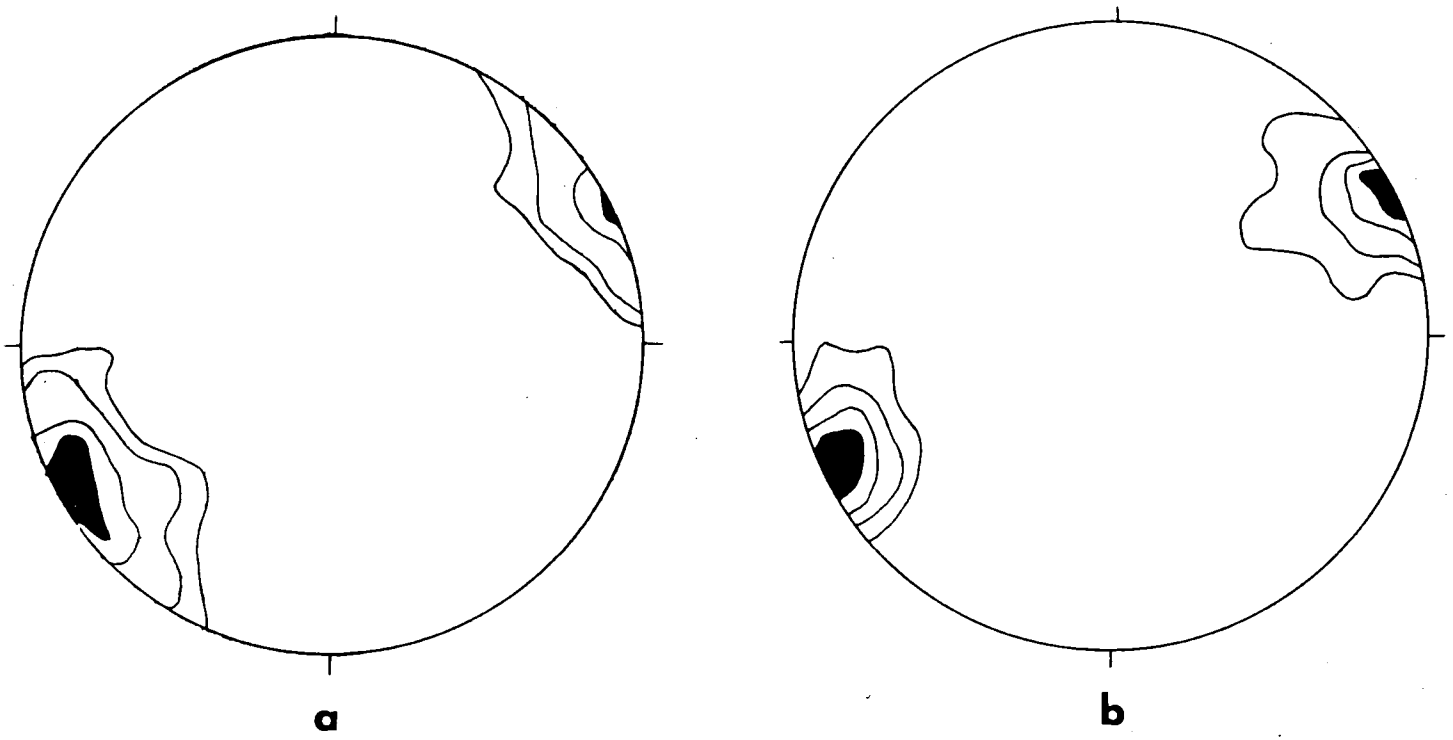

Figure 38. Buckle and kink, fold axial orientations. (a) 73 piercing points of buckle fold axes (contours at 1 percent, 3 percent, 10 percent, and 15 percent per 1 percent area). (b) 100 piercing points of kink fold axes (contours at 1 percent, 5 percent, 15 percent, and 25 percent per 1 percent area).

bed-parallel compression, indicating an early development. The mean kink fold axial orientation is 243°, 05° SW. The cozonality of kink folds and buckle folds indicates that the regional shortening axis did not change strike direction between development of the early kinks and the later folding.

4. Fold Shape Modification

Some degree of ductile flow in the hinge zone has occurred in most folds. Flexural folding sometimes leads to collapsed hinges (Figure 39b,c), with tangential longitudinal strain causing thickening at the hinge zones in more ductile, less competent layers. Flattening following buckle folding is believed to be shown by deviations from concentric (class 1b) folds. Cleavage formation causes further fold shape modification, and cleavage may show a noncoaxial relation to the folding. Minor slip during folding also occurs on surfaces other than bedding in very thick-bedded (nearly massive) mudstone. This indicates the development of a mechanical anisotropy other than bedding anisotropy. These slip surfaces provide a means of resolving the room problem in the vicinity of the hinge (Plate 1, A15). Bed-parallel contraction faults die out into sinusoidal folds of small amplitude (third order) in Figure 40. These folds may suggest possible geometric changes that occur in

Figure 39. Disharmonic folds in thin-bedded sandy siltstone. Kink folds in conjugate sets may form box folds (double-hinge folds) which may either be traceable for a distance, die out, or be disharmonic. Clockwise from top: (a) Disharmonic boxfold (B70.2); anticline passes into syncline along axial surface towards top of photo (dime for scale). (b) Uncleaved syncline (B67.7) with partially collapsed hinge (knife for scale). (c) Enlargement of b (at angle); synclinal hinge with saddle reef due to hinge collapse and hinge migration (dime for scale).

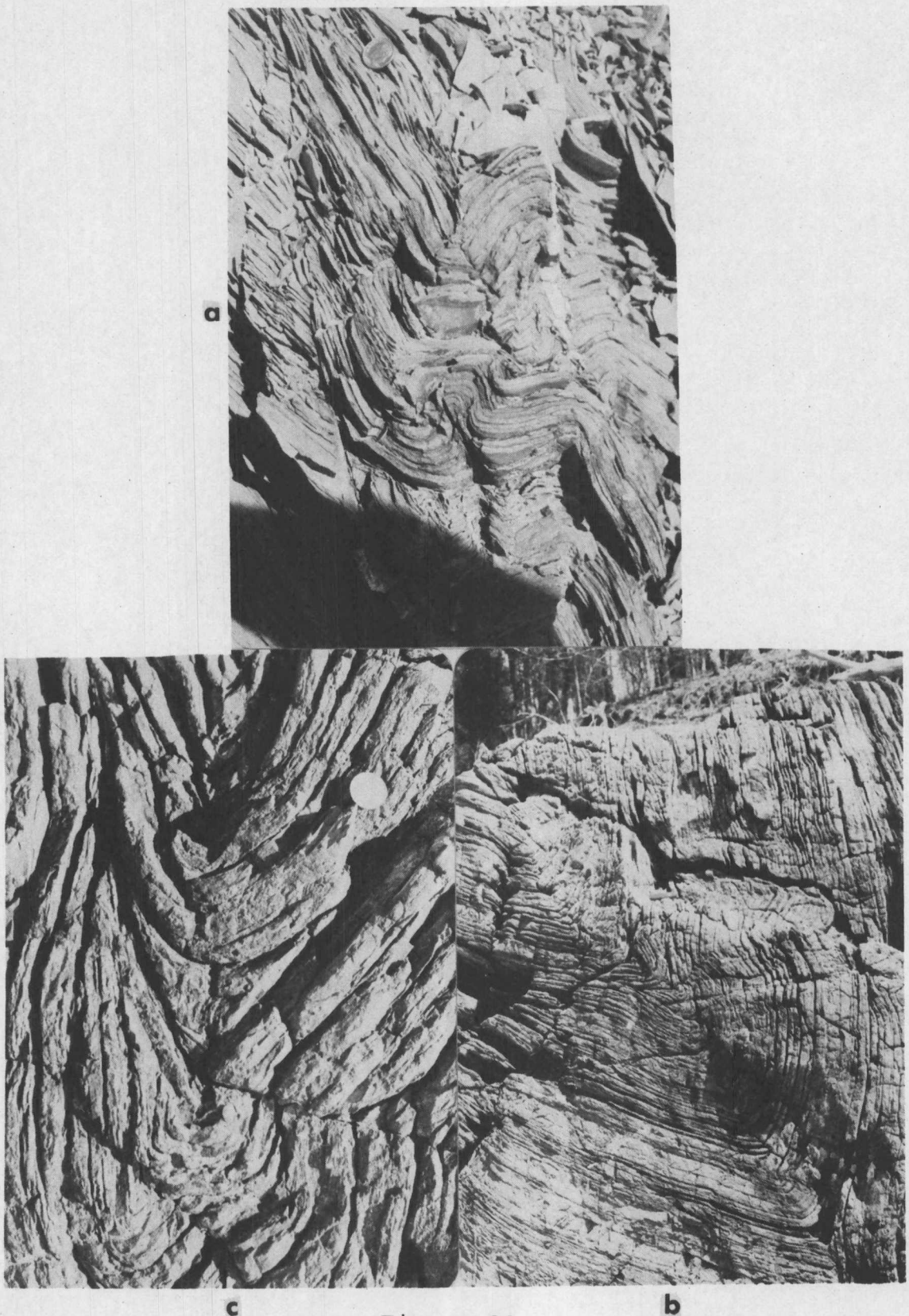

Figure 39.

Figure 40. Bed-parallel faults which die out into folds (southeast is at right). (a) Amplitude and tightness of fold (B01.5i) increase toward lower left (2 meter scale). (b) Amplitude and wavelength of fold (B21.7) increase toward lower left where bed-parallel fault (observable at lower lake level) assumes the strain (2 meter scale).

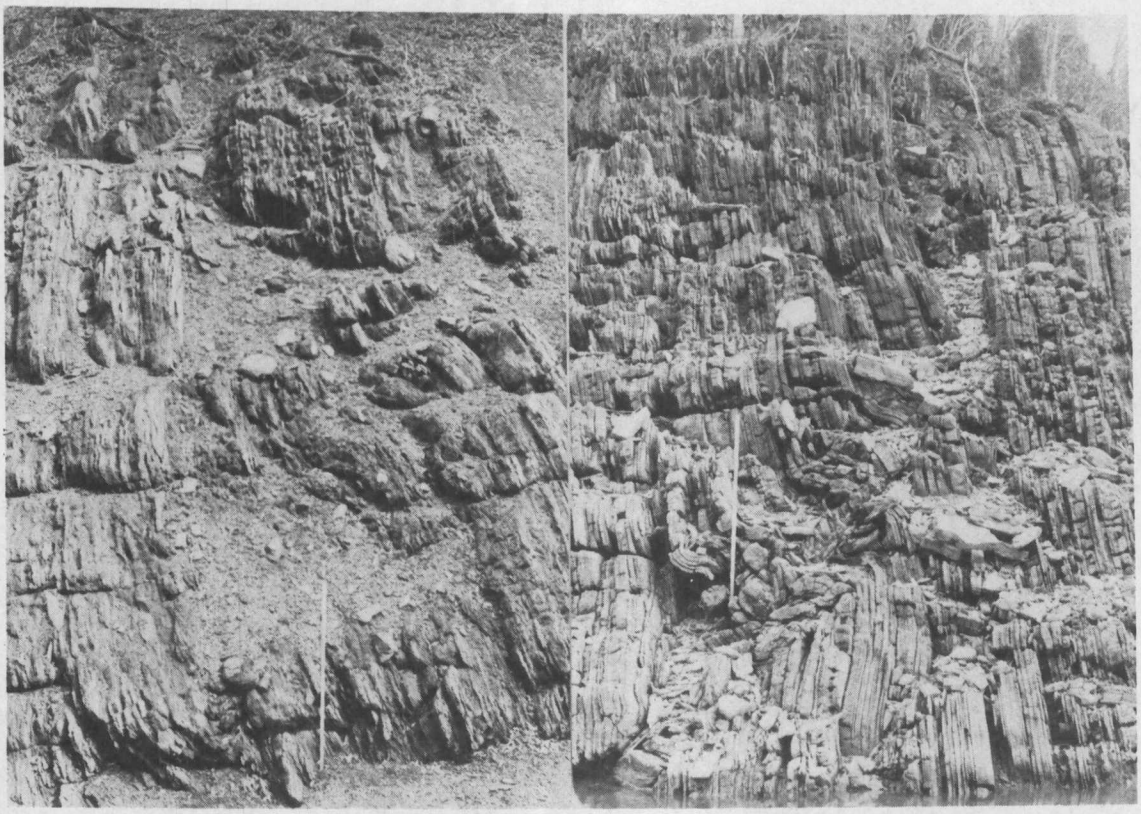

a b

Figure 40.

large second order folds at depth (and above), in order to accommodate space in the fold cores.

5. Fold Flattening Strain Analysis

Nearly concentric folds in relatively competent siltstone beds exhibit slight thickening (orthogonal to bedding) of beds toward the hinge (Figure 29, p. 103). The thickening may be caused by layer-parallel shortening within a bed simultaneous with buckling, which can mimic the effects of tangential-longitudinal strain (Ramsay, 1967).

Folds in this area display evidence of both buckling and flattening. One possibility is that the original buckle folds were modified by flattening; another is that buckling and flattening proceeded contemporaneously. Pure buckling (flexural folding) causes concentric geometry, while flattening in the form of two dimensional pure shear produces modified concentric or similar folds.

Estimated flattening strain (R_f) ranges from 1.0 (coinciding with ideal concentric folds) to infinity (Figure 28b, p. 101). An axial ratio of infinity makes no physical sense; therefore, for R_f values exceeding finite amounts, the deformation history must have been more complex than a simple two stage model of flattening superimposed on unflattened concentric folds. Shape modification may have been caused by a combination of tangential longitudinal

strain, pressure solution cleavage, and flattening or layer-parallel shortening synchronous with buckling.

The syncline represented in Figure 29a (p. 103) has extremely high calculated flattening strain ($R_f = \infty$) at the hinge (class 3); it crosses the line of similar (class 2) geometry at between 20 and 40 degrees limb dip (α), and maintains class 1c geometry on the more distal portions of the limbs. Similarly, the anticline in Figure 29b indicates that R_f equals infinity at the hinge as well as out to limb dips of 20 degrees (class 2/3). Outside 20 degrees limb dip, finite R_f values imply class 1c geometry (flattened flexural flow of Ramsay, 1967). An extreme case of high calculated R_f (infinite) occurs in Figure 29g, in which the synclinal fold maintains class 2/3 geometry throughout the extent of the exposed limbs. Folds in Figure 29h,i yield R_f values of 1.0 (class 1b) or less (class 1a) near the hinges and on the southeast limbs. Beyond 20 degrees limb dip on the northwest limbs, these folds display class 1c geometry ($1.0 < R_f < \infty$). These are inferred to be only slightly flattened, concentric buckle folds. Asymmetry is displayed by the fold in Figure 29d, as a class 1b geometry is observed on the northwest limb, but classes 2 (close to hinge) and 1c (beyond 25 degrees limb dip) occur on the southeast limb.

Based on the geometry of these folds (Figure 29, p. 103), most of them would appear to conform with class 1c, flattened flexural folds (with slightly convergent dip isogons), with shape modifications near the hinges. Fold shape near the hinge approximates similar (class 2) or class 3, probably because of high local strains. Abnormal inhomogenous thickening of the layers near fold hinges may be caused by the tangential-longitudinal-strain modification of ductile layers on the inner arc of the fold as suggested by Ramsay (1967). This would account for the plotting of hinge thickness ratios in the field of class 3 folds.

6. Cleavage and Cleavage-Fold Relations

a. Introduction. Spaced disjunctive cleavage in the Blockhouse and Sevier has the following properties:

1. Cleavage is noncontinuous (foliation is not evenly distributed throughout the rock).
2. The spacing of cleavage domains is wide enough that they can be resolved at the outcrop scale.
3. A preexisting mechanical anisotropy (other than bedding) is lacking.

Both rough and smooth cleavages (Powell, 1979) are present, with smooth (Figure 41a) being more common in mudstone. Rough cleavage (Figure 41b) is more common in siltstone and sandstone.

Figure 41. Axial planar cleaved folds in Sevier. (a) Strongly cleaved (smooth) anticline (B76.2) in mudstone. Top: approximately horizontal bedding at hinge is nearly obliterated by gently fanning cleavage (2 meter scale). Bottom: (close-up of top at hinge) strong intensity cleavage up to 5-10 selvages/cm at center; subtle bedding laminations are roughly horizontal (dime for scale). (b) Moderately cleaved anticline (B69) in siltstone. Top: portion of concentric anticline. Nonfanning cleavage is approximately parallel to scale (exposed length of scale is 1.8 meters). Bottom: (close-up of top) moderate intensity (spacing: 0.5-3.0 cm), rough cleavage (dime for scale).

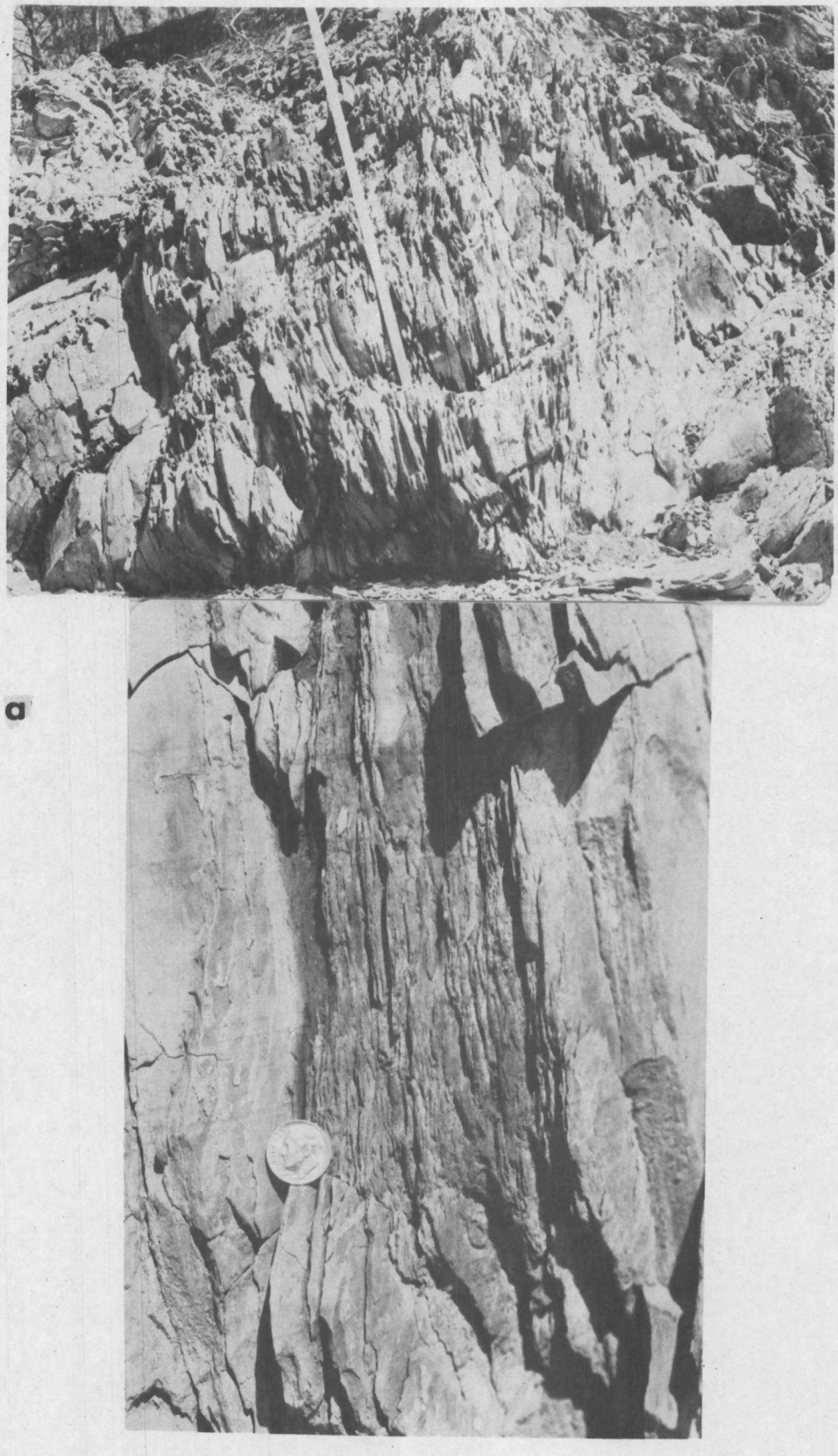

Figure 41.

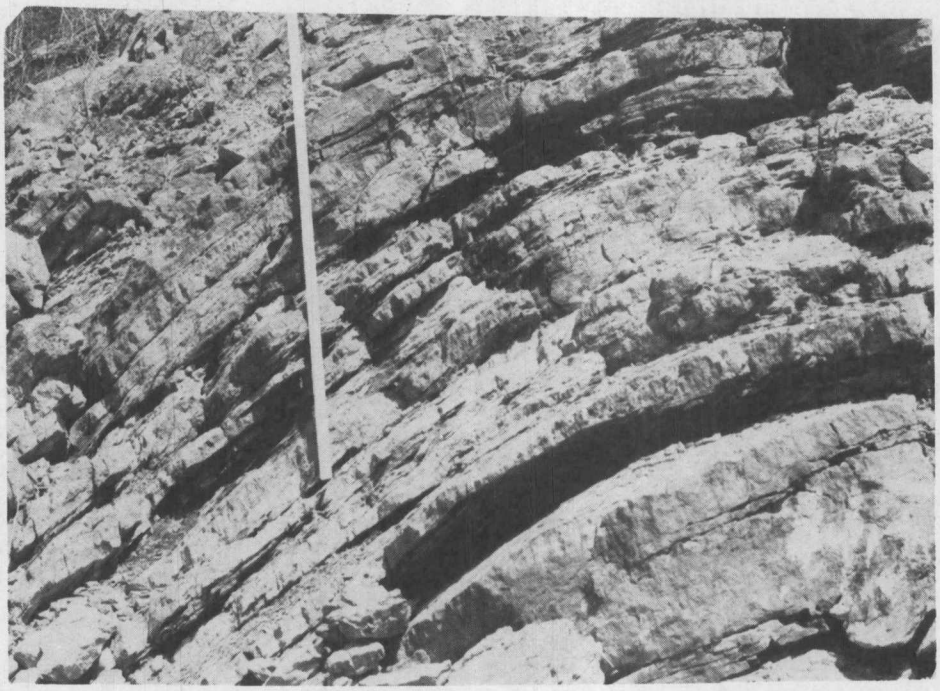

b

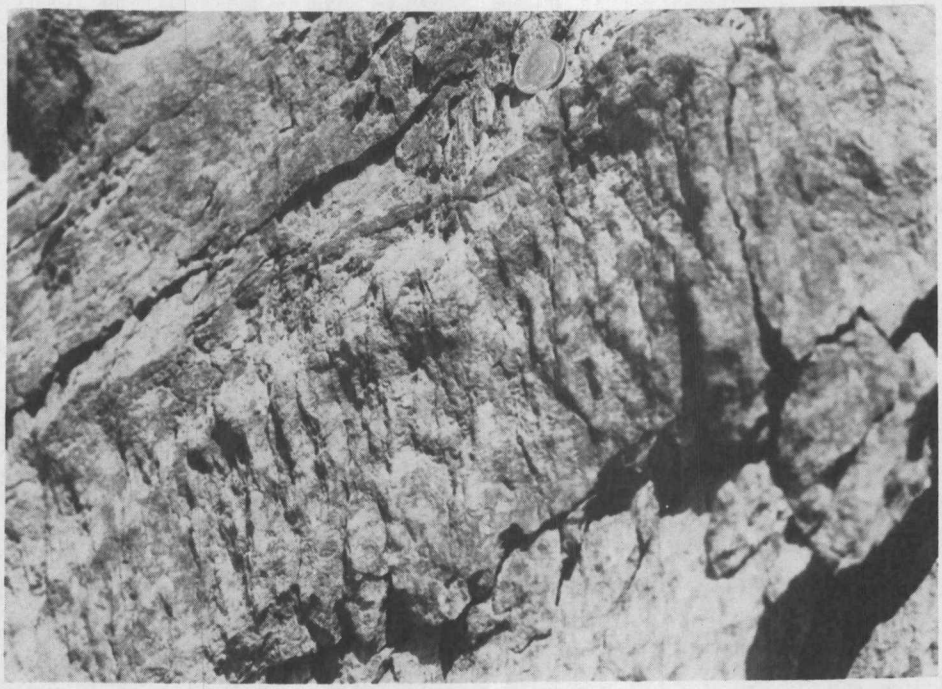

Figure 41 (continued).

The intensity and orientation of cleavage is frequently related to the presence and orientation of fold axial surfaces. Figures 42-46 are Schmidt net plots which show the symmetry and near parallelism between cleavage and fold axial surfaces for five folds. Cleavage intensity generally increases to a maximum at fold hinges from a minimum on homoclinal limbs. A variation on the general case of axial planar cleavage is the observation of numerous transected fold cores. In some cases, cleavage not only transects the fold axial surface (d transection), but it also does not decrease significantly in intensity out onto the limbs.

A second major control on cleavage development is lithology. Cleavage is best developed (more planar and more closely spaced) in fine-grained calcareous mudstone, found predominantly in the lower Sevier and Blockhouse. Unit A-2 (lower Sevier) is dominantly calcareous mudstone and is well cleaved starting at its base and continuing upsection. The cleavage becomes approximately parallel to bedding fissility at A19. Calcareous mudstone in other localities is also usually well cleaved with its intensity in nontransected folds increasing toward the hinges. Figure 47 shows the abundance of different cleavage intensities (after Simon, 1981) for the various folded lithologies. Twenty-nine folds in calcareous

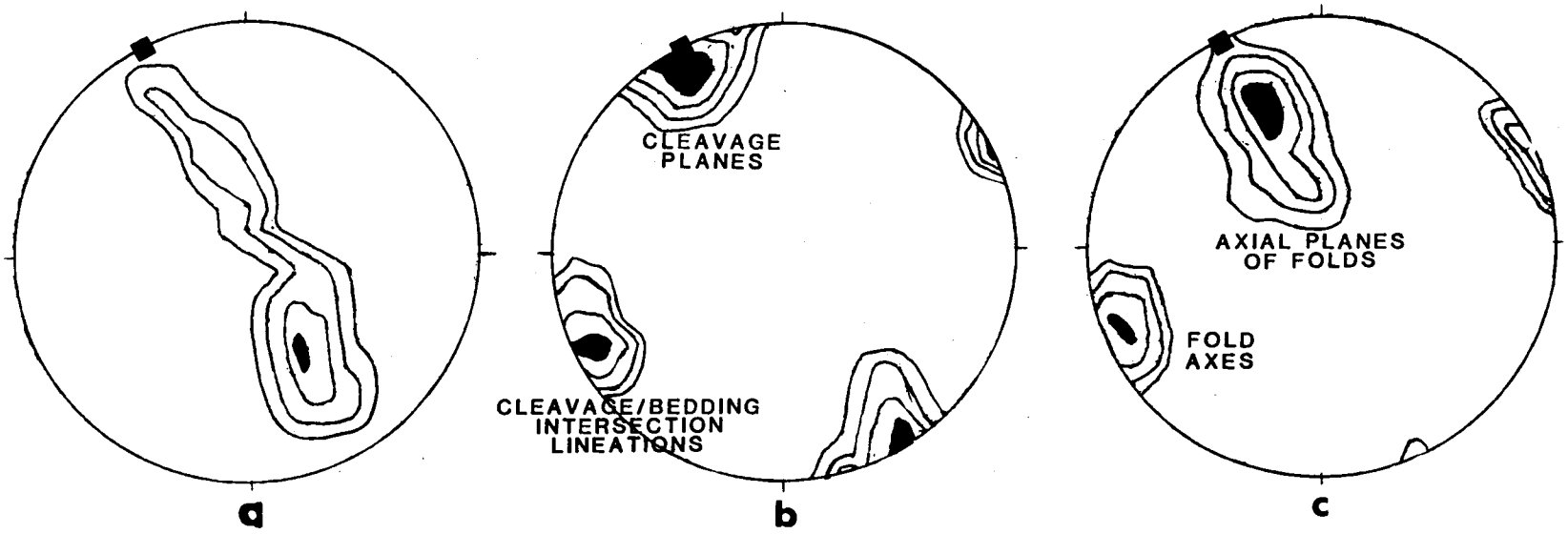

Figure 42. Mesofabric data from symmetrically cleaved A33 syncline. Square represents pole to axial plane of A33 syncline. (a) 49 poles to bedding (contours at 0.5, 1, 4, and 9 percent per 1 percent area). (b) 44 poles to cleavage (contours at 2, 5, 10, and 20 percent per 1 percent area) and 48 poles to piercing points of cleavage/bedding intersection lineations (contours at 2, 5, 20, and 50 percent per 1 percent area). (c) 49 poles to axial planes of minor folds (contours at 1, 5, 10, and 20 percent per 1 percent area) and 51 piercing points of minor fold axes (contours at 1, 5, 20, and 50 percent per 1 percent area).

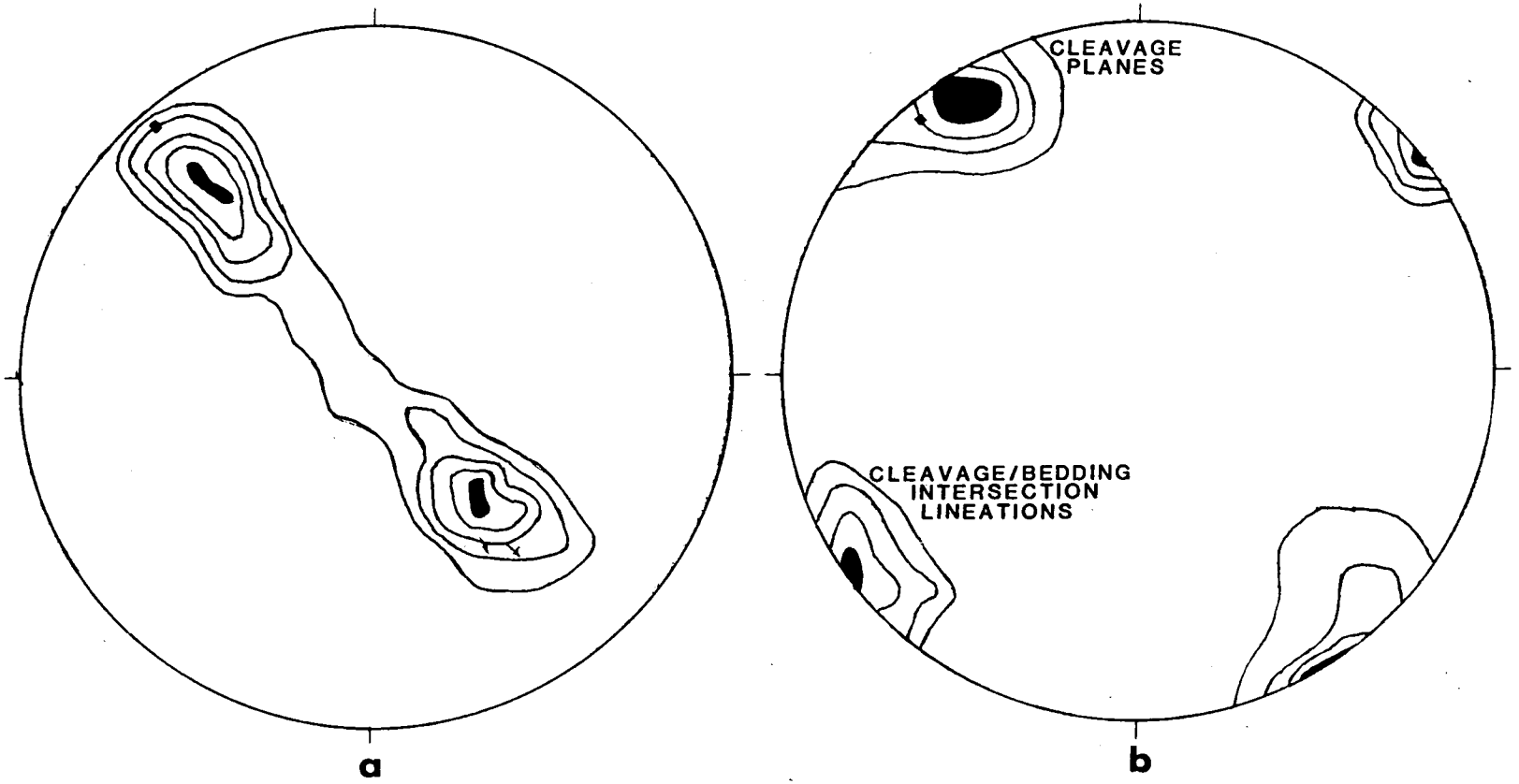

Figure 43. Mesofabric data from symmetrically cleaved B76 anticline. Square represents pole to axial plane. (a) 50 poles to bedding (contours at 2, 5, 10, 15 and 20 percent per 1 percent area). (b) 50 poles to cleavage (contours at 2, 10, 20, and 30 percent per 1 percent area) and 32 piercing points of cleavage/bedding intersection lineations (contours at 3, 10, 30, and 50 percent per 1 percent area.

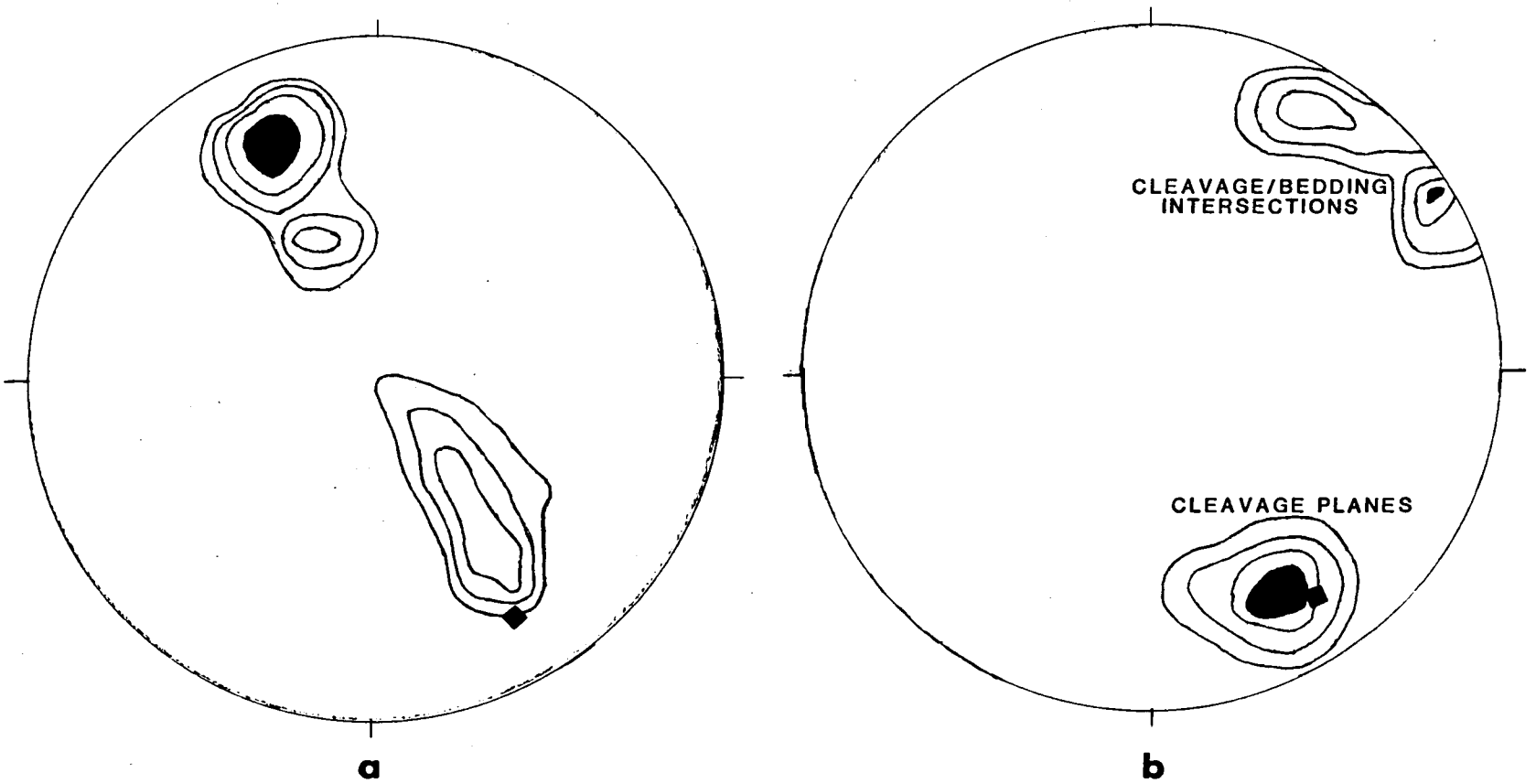

Figure 44. Mesofabric data from symmetrically cleaved C36 syncline. Square represents pole to axial plane. (a) 62 poles to bedding (contours at 2, 5, 10, and 20 percent per 1 percent area). (b) 58 poles to cleavage (contours at 5, 10, 20, and 30 percent per 1 percent area) and 12 piercing points of cleavage/bedding intersection lineations (contours at 5, 10, 25, and 30 percent per 1 percent area).

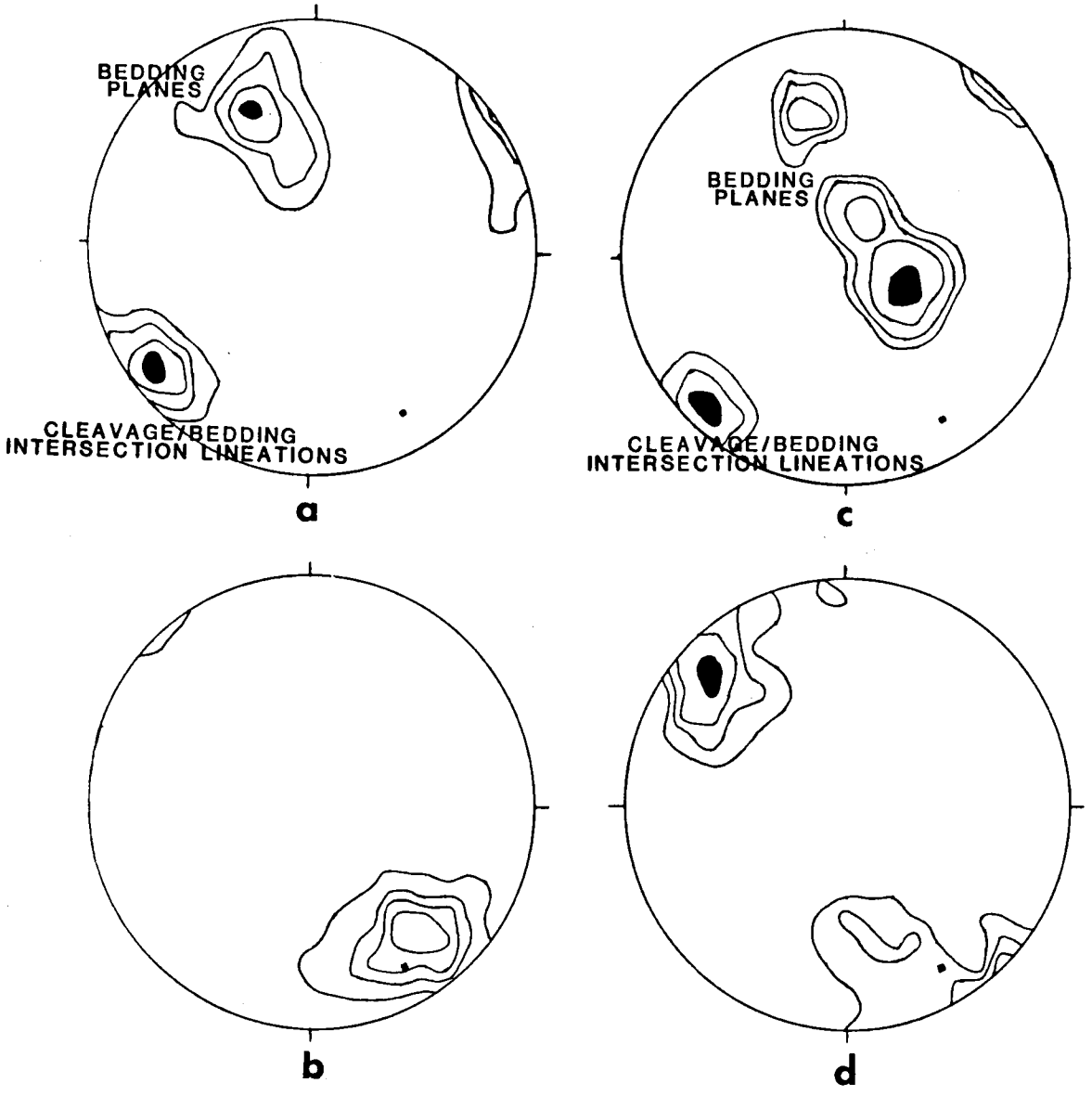

Figure 45. Mesofabric data from symmetrically cleaved, faulted C29 anticline. Square represents pole to axial plane. (a) 109 poles to bedding in footwall of backthrust (contours at 1, 5, 20, and 50 percent per 1 percent area) and 50 piercing points of cleavage/bedding intersections in footwall (contours at 2, 10, 20, and 40 percent per 1 percent area). (b) 111 poles to cleavage in footwall of backthrust (2, 5, 10, and 20 percent per 1 percent area). (c) 50 poles to bedding in hanging wall of backthrust (contours at 2, 5, 10, and 20 percent per 1 percent area) and 30 piercing points of cleavage/bedding intersection lineations in hanging wall (contours at 5, 20, and 50 percent per 1 percent area). (d) 50 poles to cleavage in hanging wall of backthrust (2, 5, 10, and 20 percent per 1 percent area).

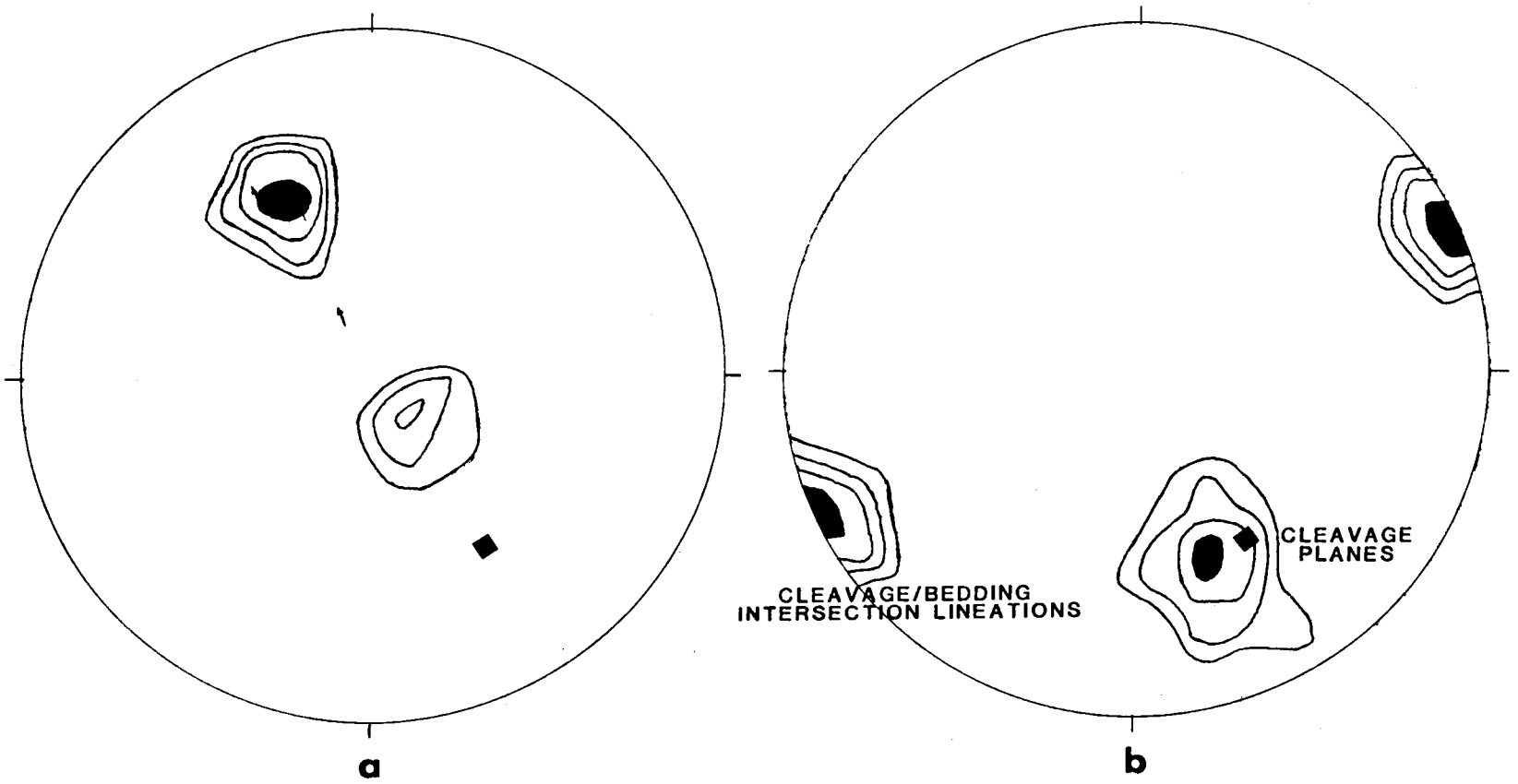

Figure 46. Mesofabric data from axial planar cleaved D109 anticline. Square represents pole to axial plane. (a) 20 poles to bedding (contours at 5, 10, 25, and 50 percent per 1 percent area). (b) 20 poles to cleavage (contours at 5, 10, 25, and 50 percent per 1 percent area) and 20 piercing points of cleavage/bedding intersection lineations (contours at 5, 10, 25, and 50 percent per 1 percent area).

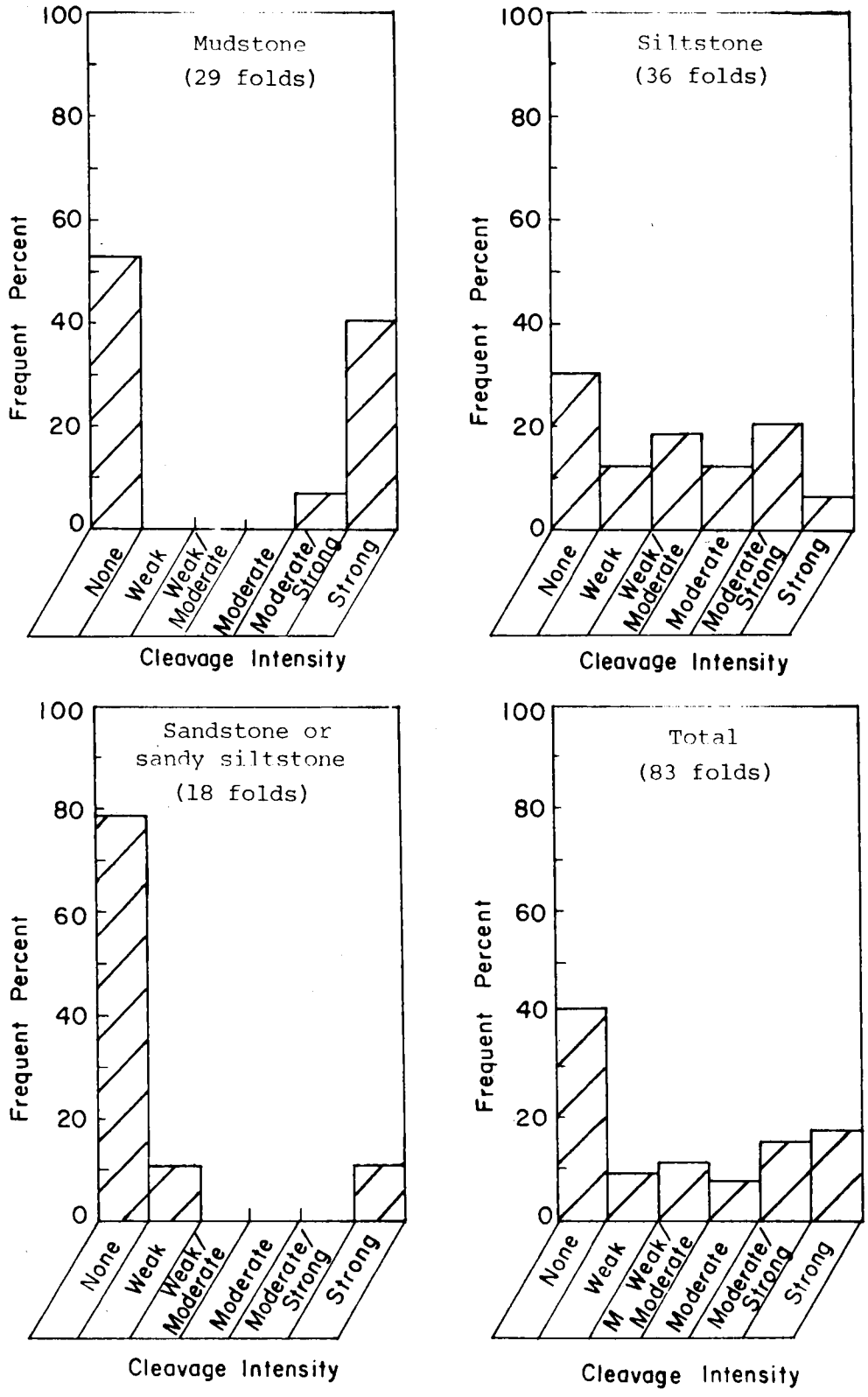

Figure 47. Frequency percent of cleavage intensities versus lithology.

mudstone show a bimodal distribution with nearly half the folds exhibiting strong cleavage and half showing none at all (Figure 47a). Seventy percent of the strongly cleaved folds occur in mudstone, while only 35 percent of all the folds occur in mudstone. The presence of a large percentage of uncleaved folds in mudstone is a problem. Explanations for this may be either: (1) that the saprolitic condition of several of these mudstone folds may obscure the cleavage, or (2) that cleavage is more related to unrecognized larger scale structural features. No weak to moderate intensity cleavage is found in the mudstone folds (except in the coarser lithologies which are sometimes interbedded with the mudstone). Usually, less intense cleavage is found for folds in siltstone (Figure 47b), although a complete range of cleavage intensities is present in these folds. A smaller number of folds are documented in sandstone and sandy siltstone (Figure 47c). Generally, little cleavage occurs in these folds in coarser lithologies.

The cleavage intensity varies between beds within individual folds (Plate 3, C29), suggesting that lithology has significant control on the degree of development of cleavage. The more intensely cleaved beds react more vigorously with hydrochloric acid than do the relatively noncleaved beds, implying that the more calcareous beds develop more intense cleavage.

b. Cleavage refraction. Cleavage is refracted across layer boundaries where competence contrasts (because of lithologic changes) occur. In Figure 14 (p. 58), cleavage refraction occurs in an interbedded sequence of siltstone (medium/thick-bedded) and shale in the Sevier formation. Cleavage is more nearly perpendicular to bedding in the more competent siltstone beds.

In folds in which cleavage is symmetrical to the axial plane, either refraction across bedding or passive rotation of cleavage accounts for convergent fan angles of up to 22 degrees between individual cleavage planes and the fold axial plane trace. Evidence that the fanning of the symmetrical cleavage may be due entirely to refraction toward bed orthogonal (rather than passive rotation) is provided by Figure 14, which shows how lithologies of contrasting ductility can significantly refract cleavage.

c. Cleavage fan angle versus dip transection (d). Figure 48 shows a nonlinear, reciprocal correlation between cleavage fan angle (γ) and dip transection parameter (d). When $d < 17$ degrees, the cleavage may fan significantly. For $d > 17$ degrees, cleavage fan angles are small (Figure 48).

The observation that folds which display significantly fanned cleavage ($\gamma > 10$ degrees) are generally not significantly transected ($d < 17$ degrees) suggests that

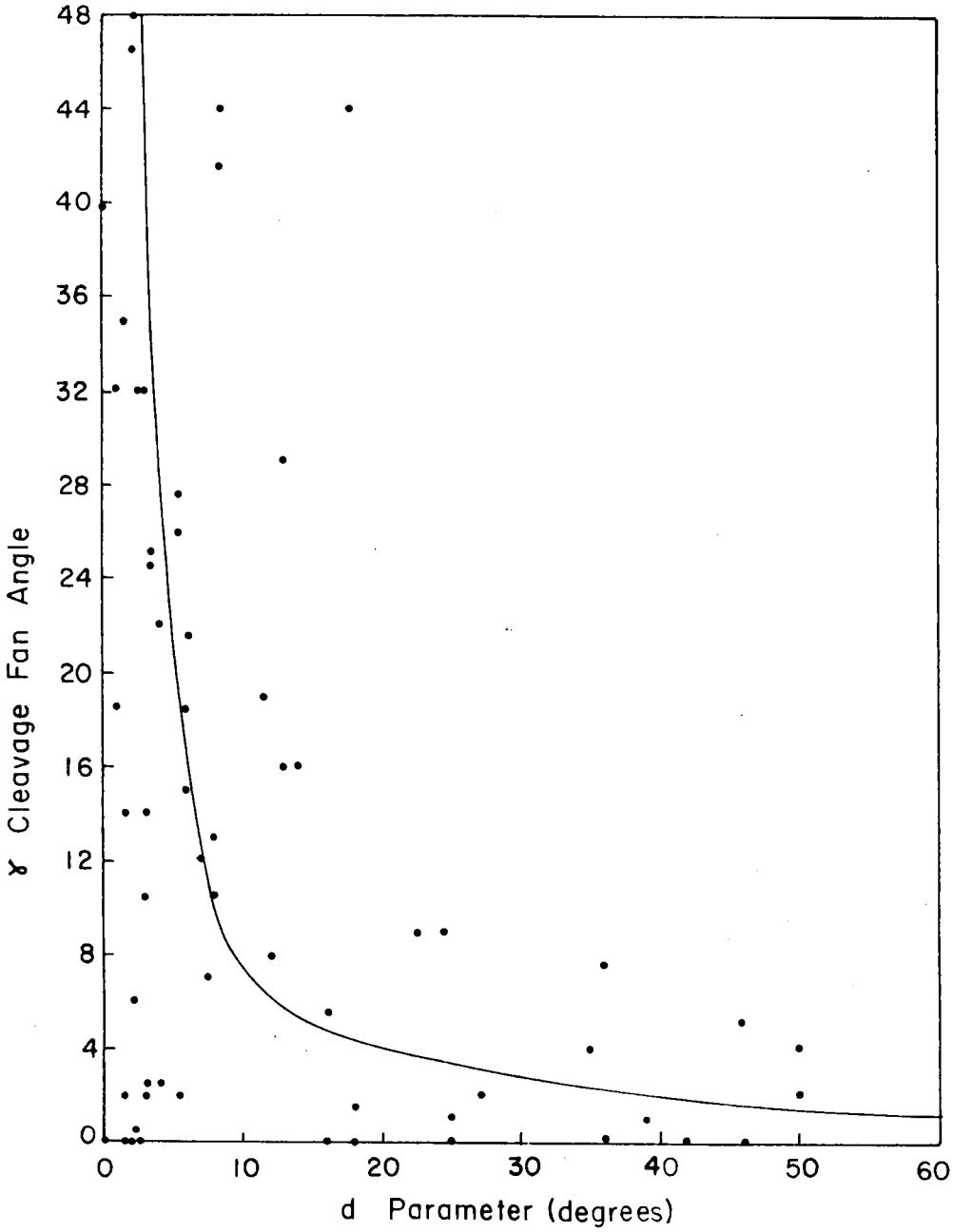

Figure 48. Cleavage fan angle (γ) versus dip transection (d).

cleavage was developed later relative to folding in the folds with high d values.

d. Refraction of cleavage strike. Considerably less data is available for cleavage refraction across strike (refraction in map patterns) than for cleavage refraction in profile view. This is because most outcrops are shoreline exposures with small map view exposure and because sketches and photographs were made predominantly in the profile plane. Dip refraction may be readily determined from the sketches and photographs, but data for refraction in map view as well as for cleavage strike transection (Δ) are scarce. However, a single exposure at Dandridge Municipal Park, where the upper Whitesburg formation is transitional with the Blockhouse formation, is available for measuring bedding-cleavage relationships on a nearly horizontal surface (Figure 49). A rough map showing bed attitudes in a relatively homoclinal sequence of interbedded limestone and shale shows strong variation in cleavage strike in the area and relatively constant bed attitudes (Figure 49a). Cleavage is refracted by as much as 45 degrees toward bed orthogonal in competent limestones, while it maintains a more nearly subparallel orientation to bedding in the interbedded shales (Figure 49b,c). The strike transection of bedding by cleavage cannot be considered strictly as Δ transection, due to the absence of folding and corresponding

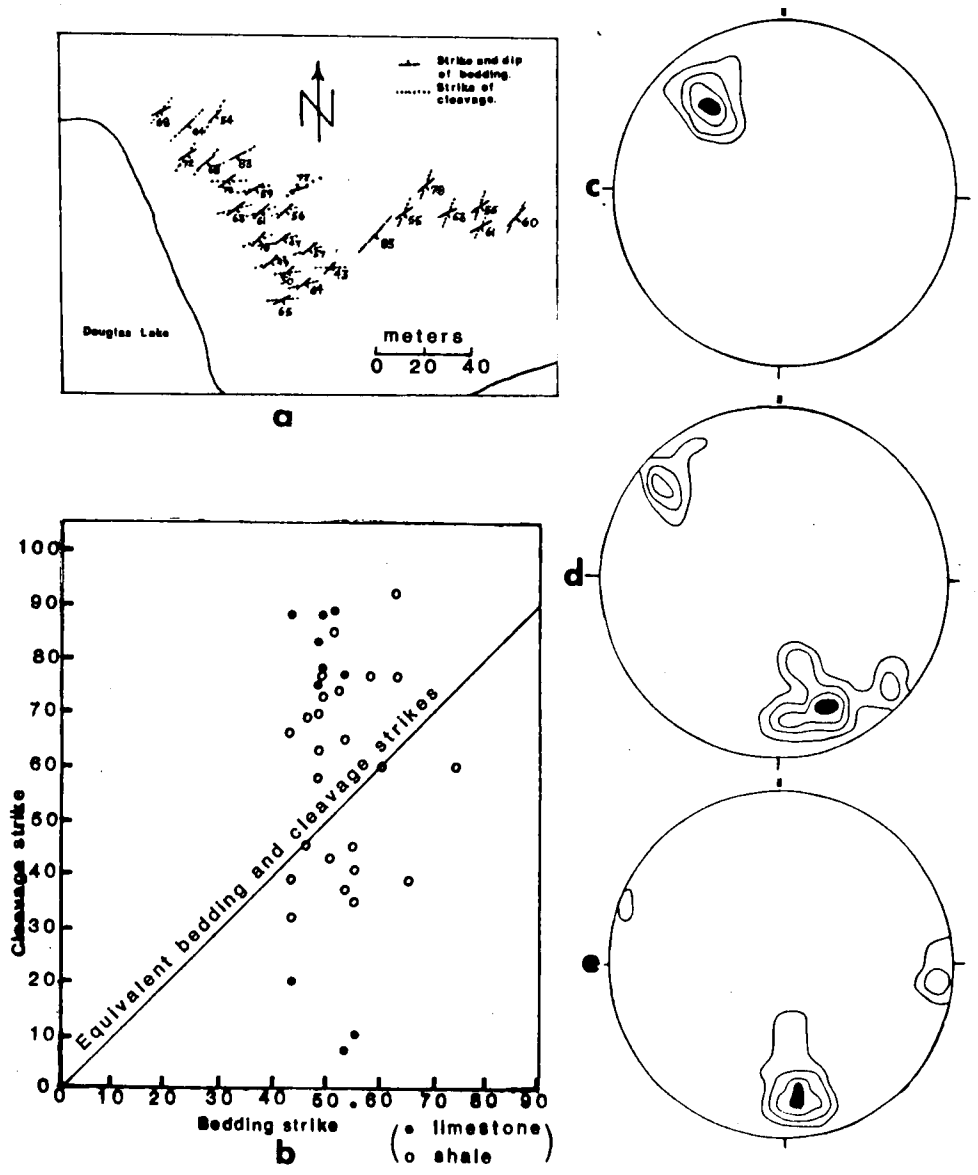

Figure 49. Lithologic control on the refraction of cleavage strike at Dandridge Municipal Park. (a) Shows divergence of cleavage and bedding strikes in map view. Thin, interbedded limestones and shales (transitional unit of upper Whitesburg) are unmappable on scale of a. (b) Shows divergence of cleavage and bedding strikes graphically. (c) 22 poles to bedding (contours at 5, 15, 30, and 45 percent per 1 percent area). (d) 24 poles to cleavage in shales (contours at 4, 8, 12, and 16 percent per 1 percent area) demonstrate weakly bimodal distribution. (e) 12 poles to cleavage in limestone (contours at 5, 10, 20, and 30 percent per 1 percent area) demonstrate strongly bimodal distribution.

axial surfaces as reference planes. The strike transection changes sense (causing the bimodal cleavage distributions in Figure 49c) both at the middle of the map and in the northwestern portion of the map (Figure 49a); therefore, it is apparently not controlled by folding. The inhomogeneity of strain may have been produced by refraction of oblique stresses in layers of strongly contrasting ductilities (Treagus, 1980).

e. Bedding-cleavage angle relative abundances versus lithology. Frequency percent histograms of bedding-cleavage angles were compiled for folds of different lithologies by measuring bedding-cleavage angles at 10 degree intervals of limb dip (α) for fold half wavelengths (Figure 50). Cleavage is more nearly orthogonal to bedding in the coarser-grained lithologies and less convergently fanning to parallel in the finer-grained lithologies.

f. Cleavage fan angle versus fold flattening strain. A plot of cleavage fan angle (γ) versus fold flattening strain (R_f) implies that these are independent factors and unrelated (Appendix G, Figure G-3). Large cleavage fan angles are rare in folds in the study area, and flattening is frequently minimal. If cleavage developed prior to fold flattening, then γ ought to decrease with increasing R_f; however, the plot of R_f versus γ implies no such relationship. Cleavage, therefore, is syn- to postflattening.

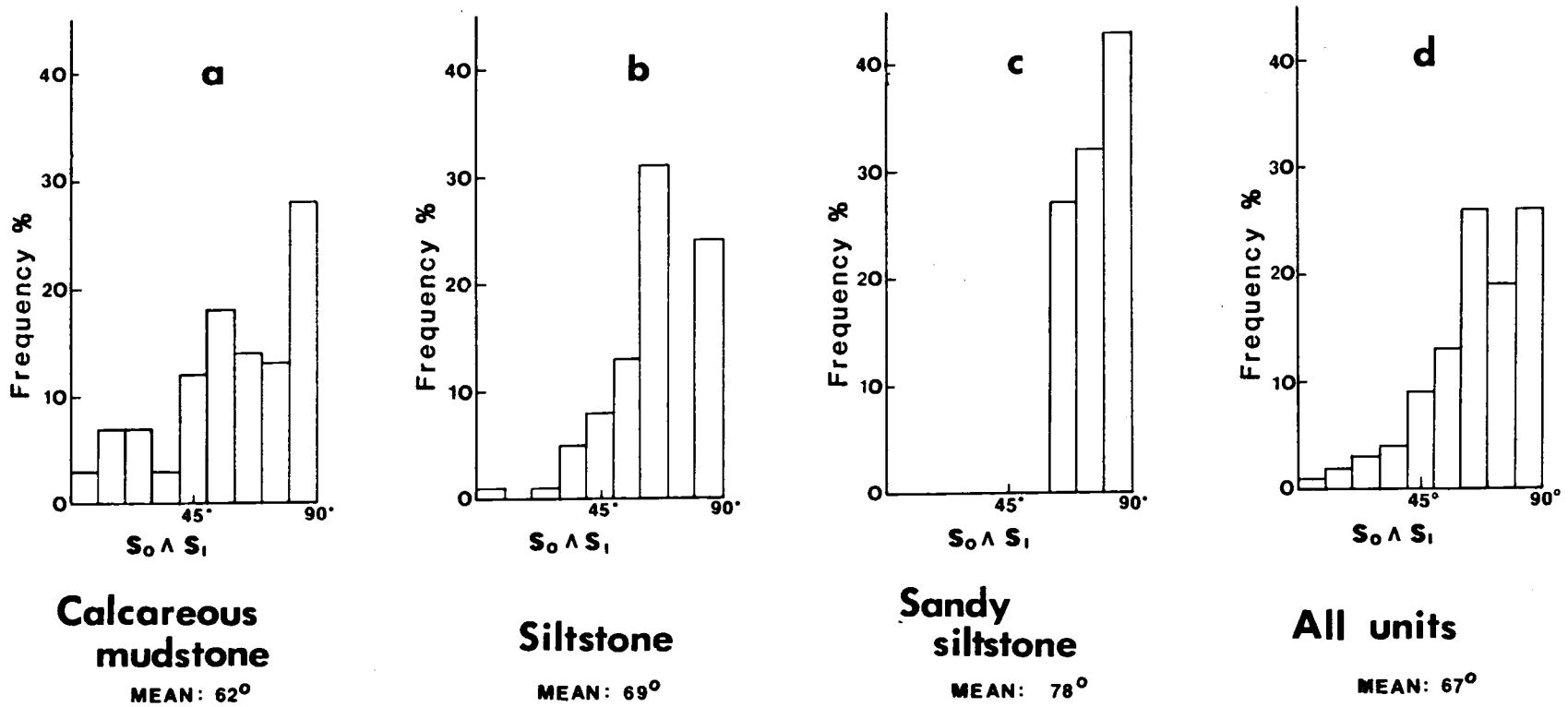

Figure 50. Frequency percent of cleavage/bedding angles ($S_0 \wedge S_1$) versus lithology. (a) Calcareous mudstone lithology (94 measurements). (b) Siltstone lithology (226 measurements). (c) Sandy siltstone lithology (19 measurements). (d) All units (339 measurements).

As an example illustrating this conclusion, the lack of fanning in the footwall block of the backthrust cutting a second order anticline at C29 (Plate 3) cannot be resolved as an effect of flattening. This is because the dip isogons for the anticline suggest that the fold approximates class 1b geometry (Ramsay, 1967), precluding the possibility of significant flattening. Thickness ratios indicate that a minimal amount of flattening has occurred on the southeast limb (1b/1c) as compared with the unflattened northwest limb (1b; Figure 27, p. 100). This structure is probably the least flattened of the outcrop-scale folds that were analyzed for flattening (after Gray and Durney, 1979) in this study, and considerably more flattened folds show more cleavage fanning (such as the second order syncline at A33, Plate 1).

g. Cleavage fan angle versus fold interlimb angle. No correlation was found between cleavage fan angle (γ) and fold interlimb angle (β), implying that these parameters are unrelated (Appendix G, Figure G-4) for folds in the study area, i.e., cleavage does not fan more or less in tighter folds. The fact that γ is not dependent on β suggests that cleavage was not consistently passively rotated by buckle folding, and thus did not predate folding. No obvious lithology-controlled difference in γ was found in the calcareous mudstone and siltstone folds. Data for both

calcareous mudstones and siltstones occupy the same area on the graph.

h. Cleavage intensity versus angularity parameter, cleavage fan angle, and fold interlimb angle. Cleavage intensity is independent of both hinge angularity (Appendix G, Figure G-5) and cleavage fan angle (Appendix G, Figure G-6). Cleavage intensity increases slightly with tighter folding (Figure 51), but the relationship is almost negligible, and so cleavage intensity and interlimb angle are also considered to be independent parameters.

i. Transecting cleavage. An example of contrast in the degree of fold control on the development of cleavage occurs between A14 and A20 (Plate 1). Slightly fanning, nearly axial planar cleavage occurs in the syncline at A15 (Plate 1; Figure 52a,b), while nonfanning cleavage of similar orientation is present in the strongly transected (meaning high d angle), faulted anticline at A19 (Figure 9, p. 42; Figure 52c,d). Aside from gentle convergent fanning in the syncline, the cleavage has a relatively constant orientation across the outcrop. The fact that cleavage is not folded indicates that it did not develop early. The large d transection angle in the fold at A19 (d = -50 degrees) and the strongly divergent axial plane orientations of the folds at A15 and A19 (Figure 53a,b)

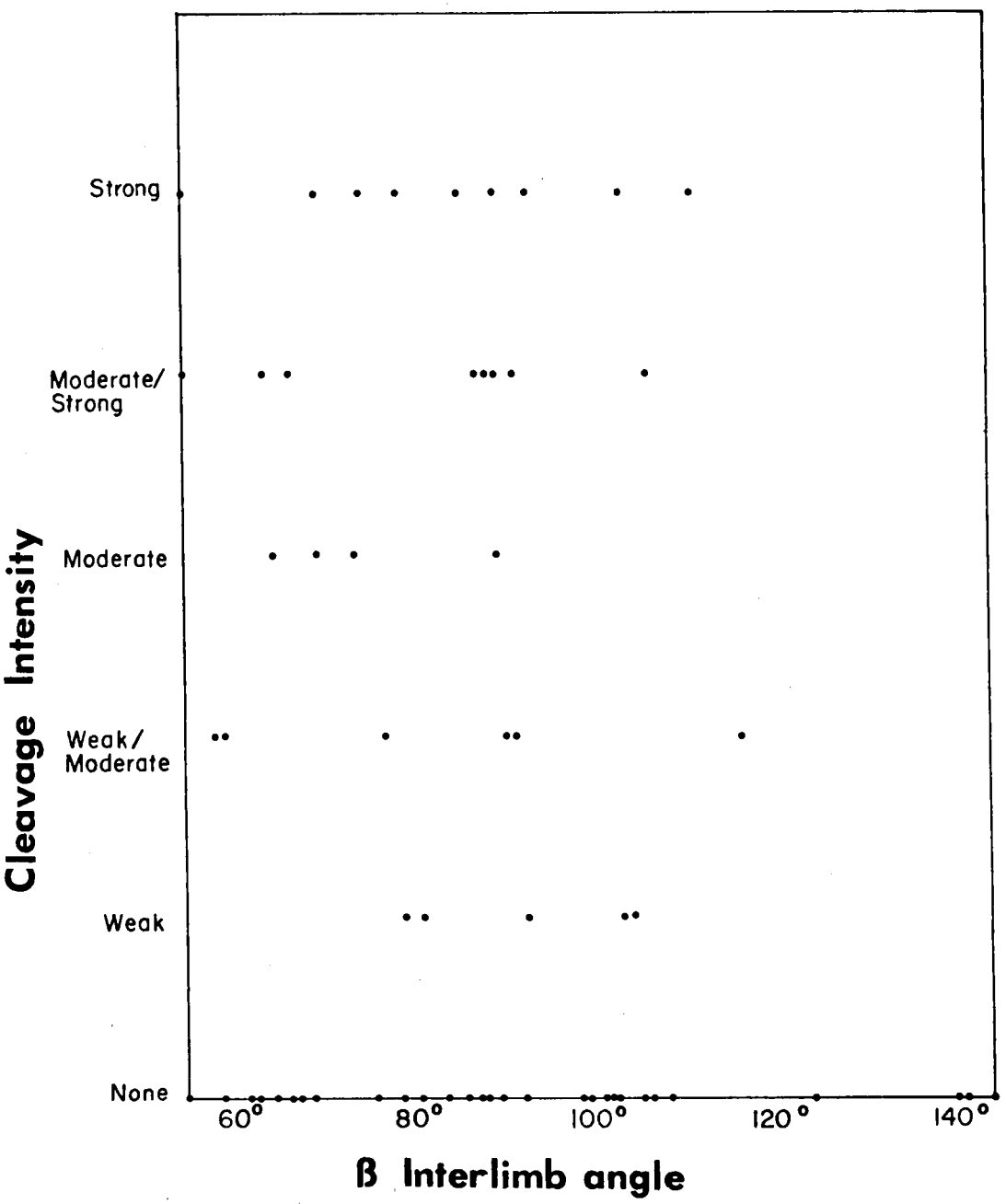

Figure 51. Cleavage intensity versus fold interlimb angle (ß). The lack of a linear relationship implies that cleavage intensity is independent of fold tightness.

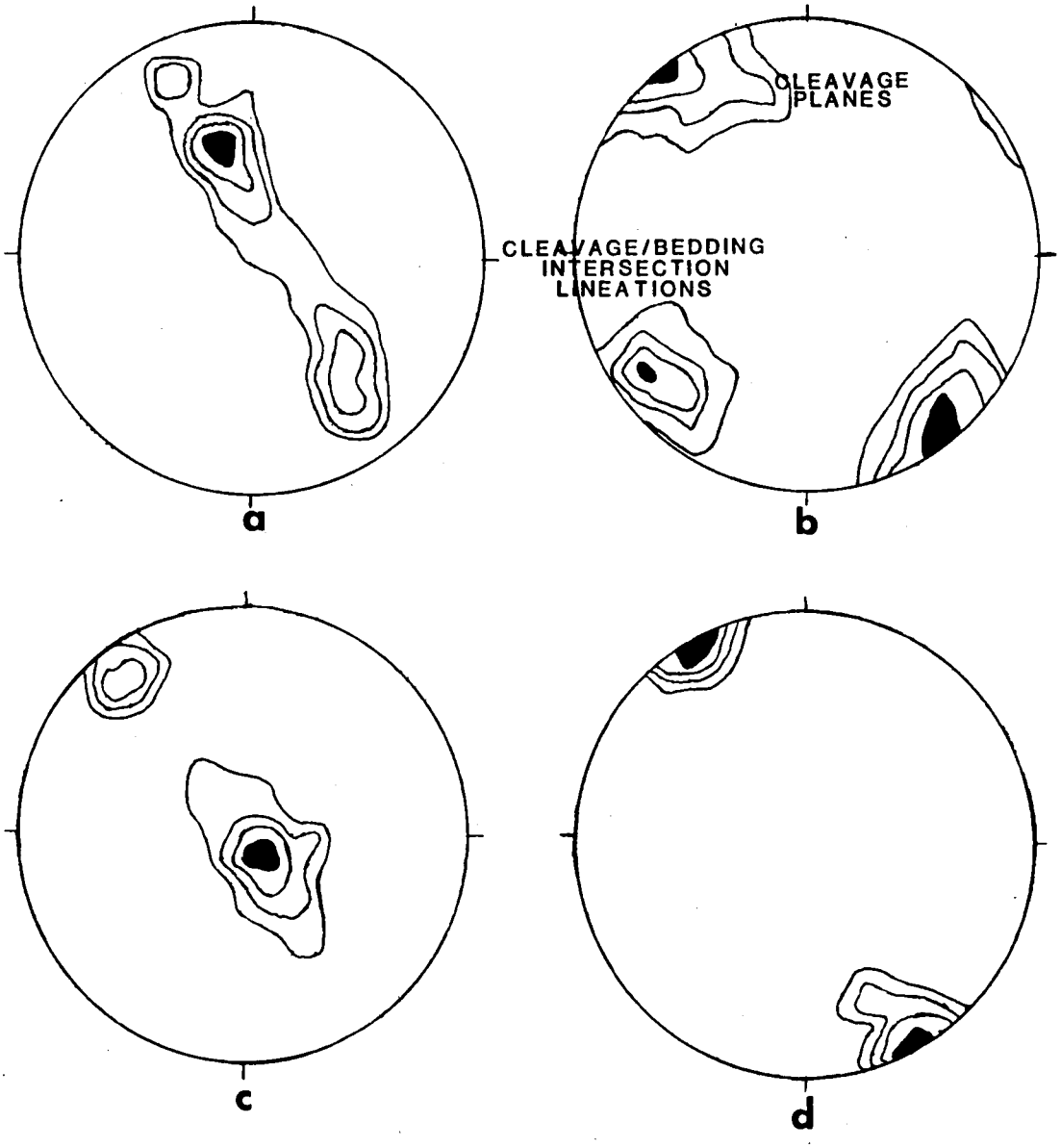

Figure 52. Mesofabric data contrasting axial planar cleaved fold (A15) with adjacent noncoaxial cleaved fold (A19). (a) 61 poles to bedding, A15 syncline (contours at 2, 5, 10, and 20 percent per 1 percent area). (b) 263 poles to cleavage, A15 syncline (contours at 1, 5, 10, and 20 percent per 1 percent area), and 49 piercing points of cleavage/bedding intersection lineations (contours at 2, 10, 20, and 40 percent per 1 percent area). (c) 30 poles to bedding, A19 anticline (contours at 3, 10, 20, and 40 percent per 1 percent area). (d) 12 poles to cleavage, A19 anticline (contours at 2, 5, 20, and 50 percent per 1 percent area).

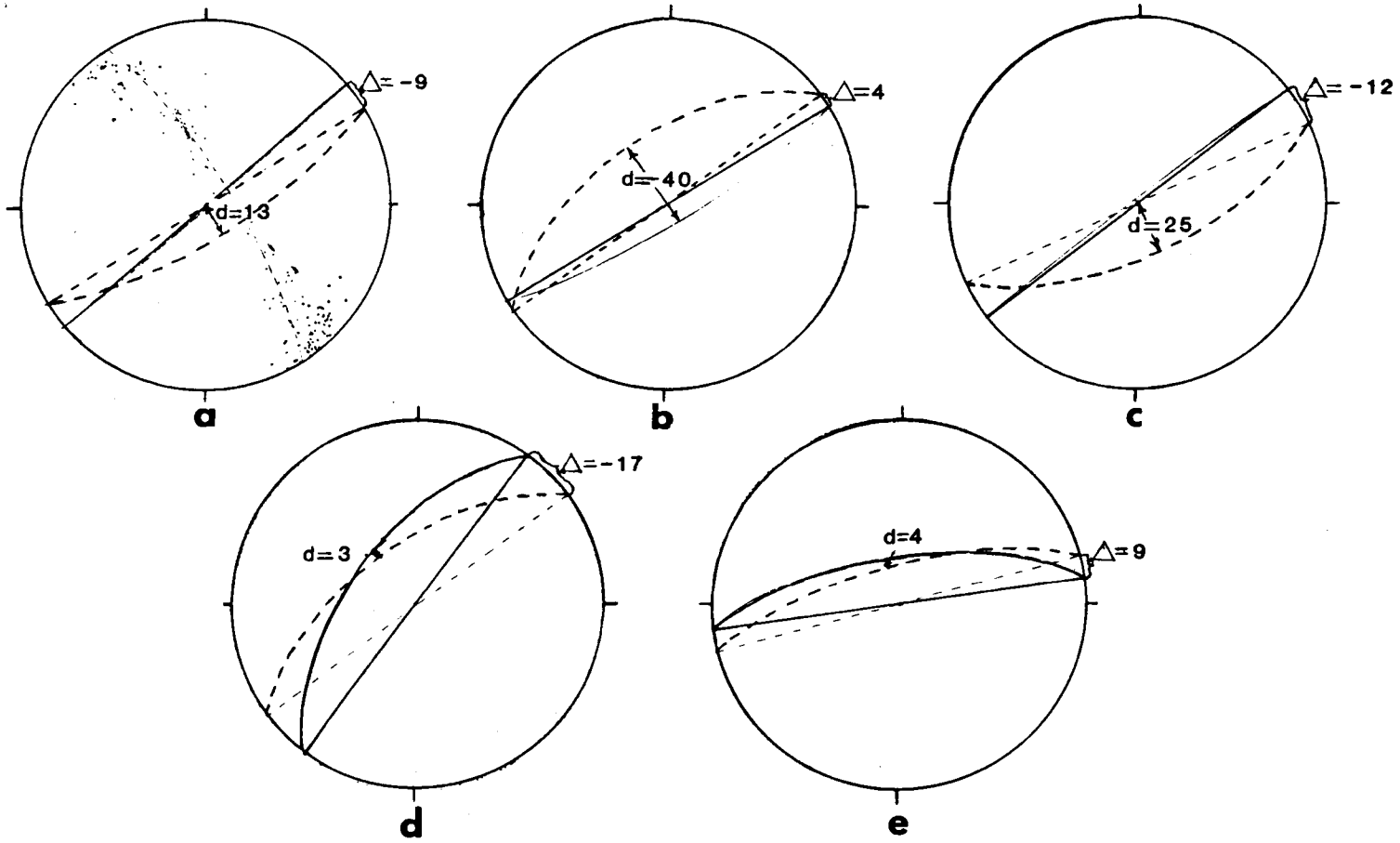

Figure 53. Graphical representations of typical fold transections. Solid lines represent traces of cleavage plane. Dashed lines represent traces of axial plane. Δ parameter measures angular deviation between cleavage strike and fold axial plane strike. d parameter measures angular deviation between cleavage dip and fold axial plane dip. (a) A15 syncline. (b) A19 anticline. (c) A64 anticline. (d) B30 kink. (e) C29 anticline.

indicate superposition of cleavage on folds. Cleavage development began either late during or after formation of the A15 fold. On the southeast limb of the A19 anticline, a strongly developed bedding plane fissility is due to the near parallelism of cleavage and bedding.

j. Δ versus d transection parameters. The Δ versus d transection parameter graph (Figure 54) indicated that Δ transection of fold axial surface traces by cleavage is usually slightly negative (averaging -9 degrees). A similar relationship occurs in Figure 55a,b between cleavage and bedding. The average measured bedding attitude strikes 58 degrees east of north, while the average measured cleavage strike is only 52 degrees east of north. An analogous relationship also occurs between fold axes and cleavage-bedding intersections (Figure 55c). These two types of linear fabric data have approximately the same plunge, but the bearing of the cleavage-bedding intersections is rotated about seven degrees counterclockwise from the bearing of the fold axes. Thus, cleavage planes usually strike slightly more northerly in the area and fold axial planes strike slightly more easterly. Examples of typical fold transections are illustrated in Figure 53a-e, in which absolute values of Δ range from 4 to 17 degrees and absolute values of d range from 3 to 40 degrees for the five folds. The graph (Figure 54) also indicates that positive d

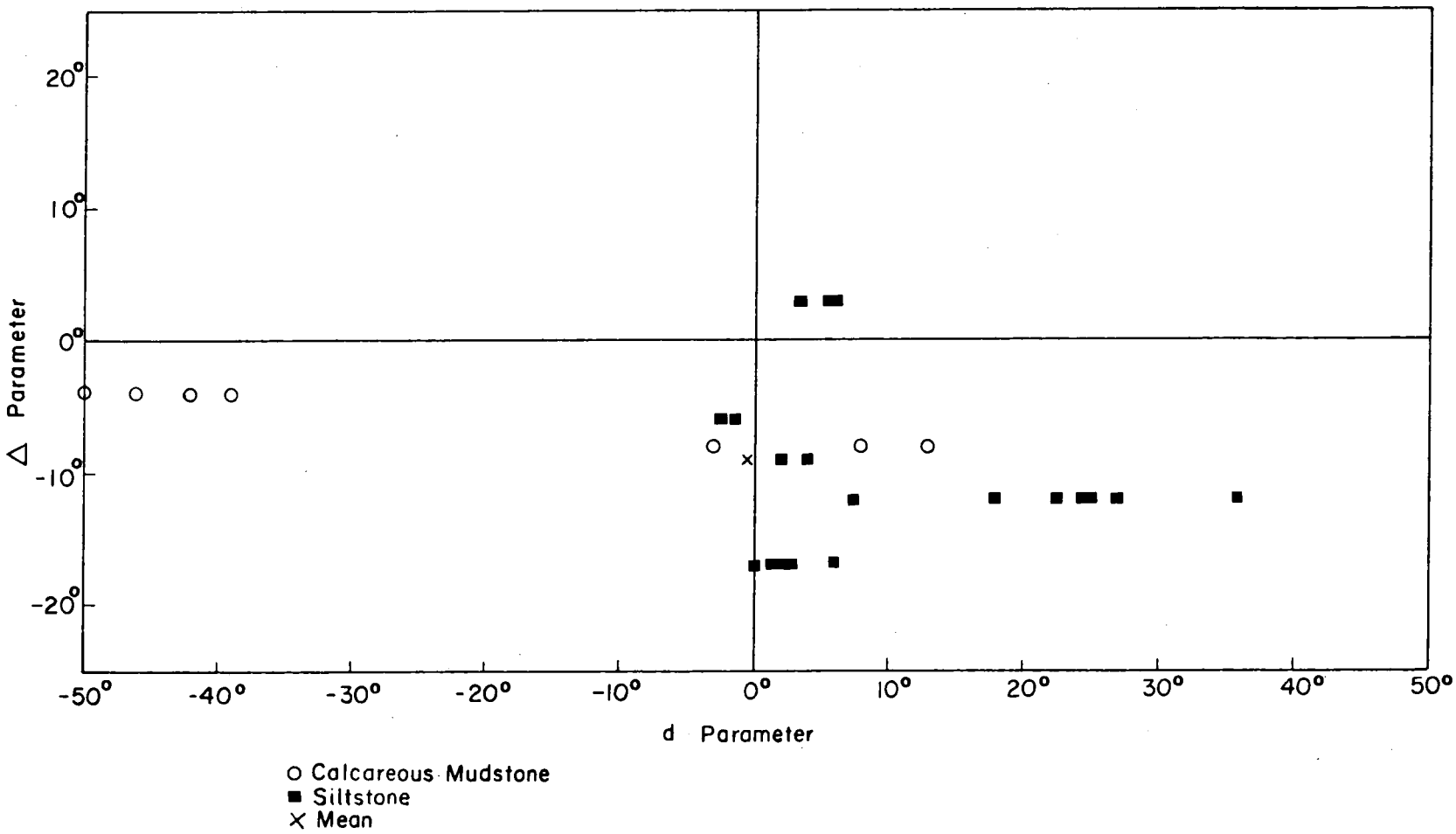

Figure 54. (Δ, d) transection parameter graph. A +Δ indicates clockwise rotation of the cleavage from the fold axis in map view. A +d indicates clockwise rotation of the cleavage from the axial plane in profile section (viewed to the northeast).

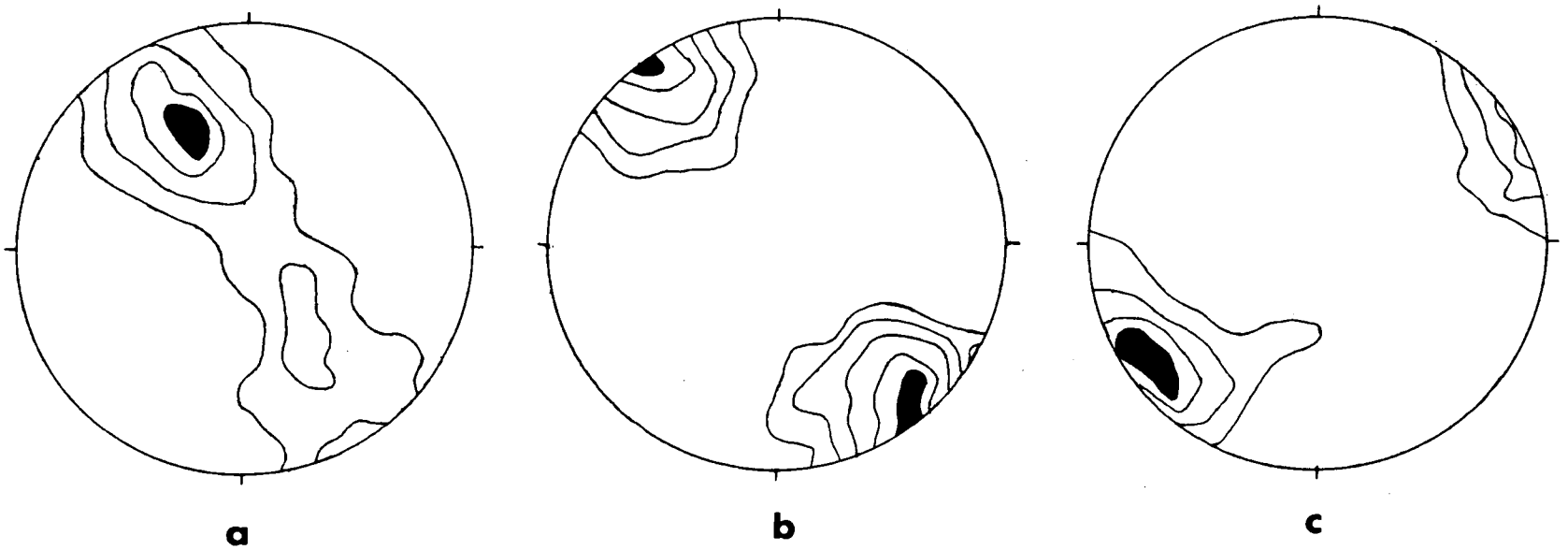

Figure 55. Mesofabric data for all localities. (a) 1,371 poles to bedding (contours at 0.5, 2, 6, and 10 percent per 1 percent area). (b) 970 poles to cleavage (contours at 1, 2, 4, 8, and 12 percent per 1 percent area). (c) 386 piercing points of cleavage/bedding intersection lineations (contours at 0.3, 2, 10, and 20 percent per 1 percent area). Square represents piercing point of mean fold axis.

transections (viewed toward the northeast) are more common. Large negative d values are also found, and the sign of the d transection is related to the orientation of faults which displace the folds. Negative values of d are associated with backthrusts cutting the folds, while positive values of d are associated with regionally synthetic (southeast dipping) thrust faults. Thus, the more frequent occurrence of southeast dipping thrust faults results in the greater abundance of positive d transection values. The relative time of faulting (late in folding) implies that related cleavage development also occurred in the latter stages of folding.

k. Δ, d transection parameters versus fold interlimb angle. Fold tightness has, at most, a weak influence on the absolute value of the Δ transections (Appendix G, Figure G-7). Any apparent relationship between lower Δ values and tighter folds (smaller β) is probably insignificant. β also has negligible influence on the absolute value of the d transection parameter values (Appendix G, Figure G-8).

l. Comparison of axial plane trace, cleavage plane trace, and flattening extension direction. Figure 29 (p. 103) shows the degree of correspondence between the axial surface dip (profile trace) and the flattening

extension direction (X), based on the maximum orthogonal thickness due to flattening. Figure 29 (p. 103) also shows the degree of correspondence between the cleavage dip and X. Of the nine folds for which fold flattening analysis was performed (Figure 29), seven showed no significant discrepancy (ϕ_A < 5 degrees) between the X direction of extension due to flattening and the axial surface trace, implying approximately coaxial buckle folding and fold flattening. Five of the seven folds with negligible ϕ_A also show low d transection values (Figure 29c,e,f,g,i). The other two show d transections of +10 (Figure 29a) and -46 (Figure 29b) degrees. Of the two folds with significant ϕ_A values (Figure 29d,h), d values are equal to +27 and +4, respectively.

Double angle graphs (Figures 56, 57) compare cleavage and axial plane orientations with varied fold flattening strain (R_f). Assuming that cleavage, axial plane and flattening extension direction (X) each indicate two dimensional finite or incremental strain, the relative scatter on the graphs can suggest the timing of folding and cleavage development with respect to fold flattening. The R_f versus ϕ_A plot shows a 20 to 30 degree relatively symmetrical distribution of X directions and corresponding R_f values (strain ratios) ranging about reference axial plane traces with deviations from -8 to +10 or +20 degrees (ϕ_A). The R_f versus ϕ_S plot shows a 97 degree asymmetric

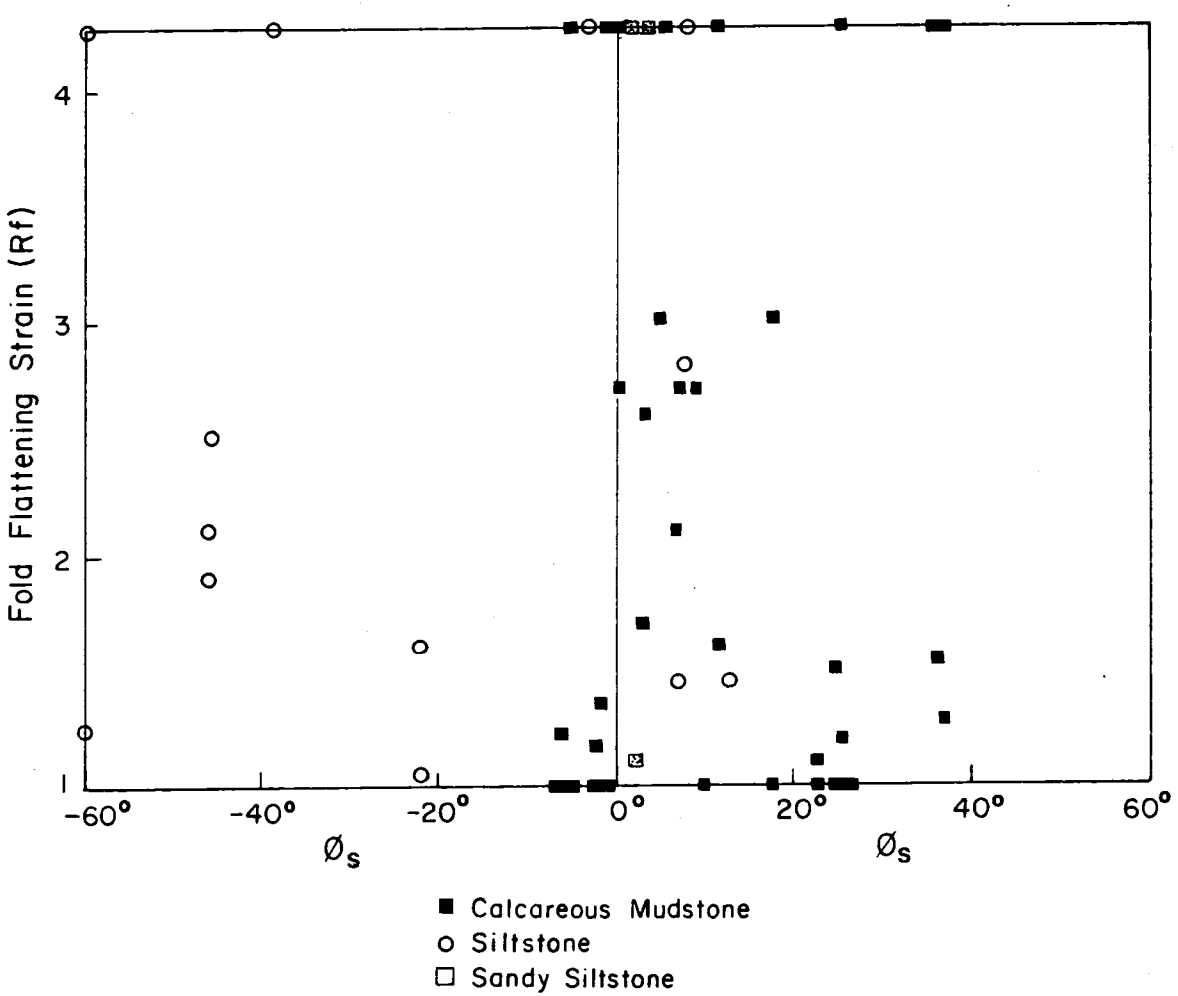

Figure 56. Fold flattening strain (Rf) versus cleavage/flattening scatter (ϕ_S). ϕ_S scatter exceeds ϕ_A scatter (Figure 57), indicating that cleavage is noncoaxial with folding and fold flattening.

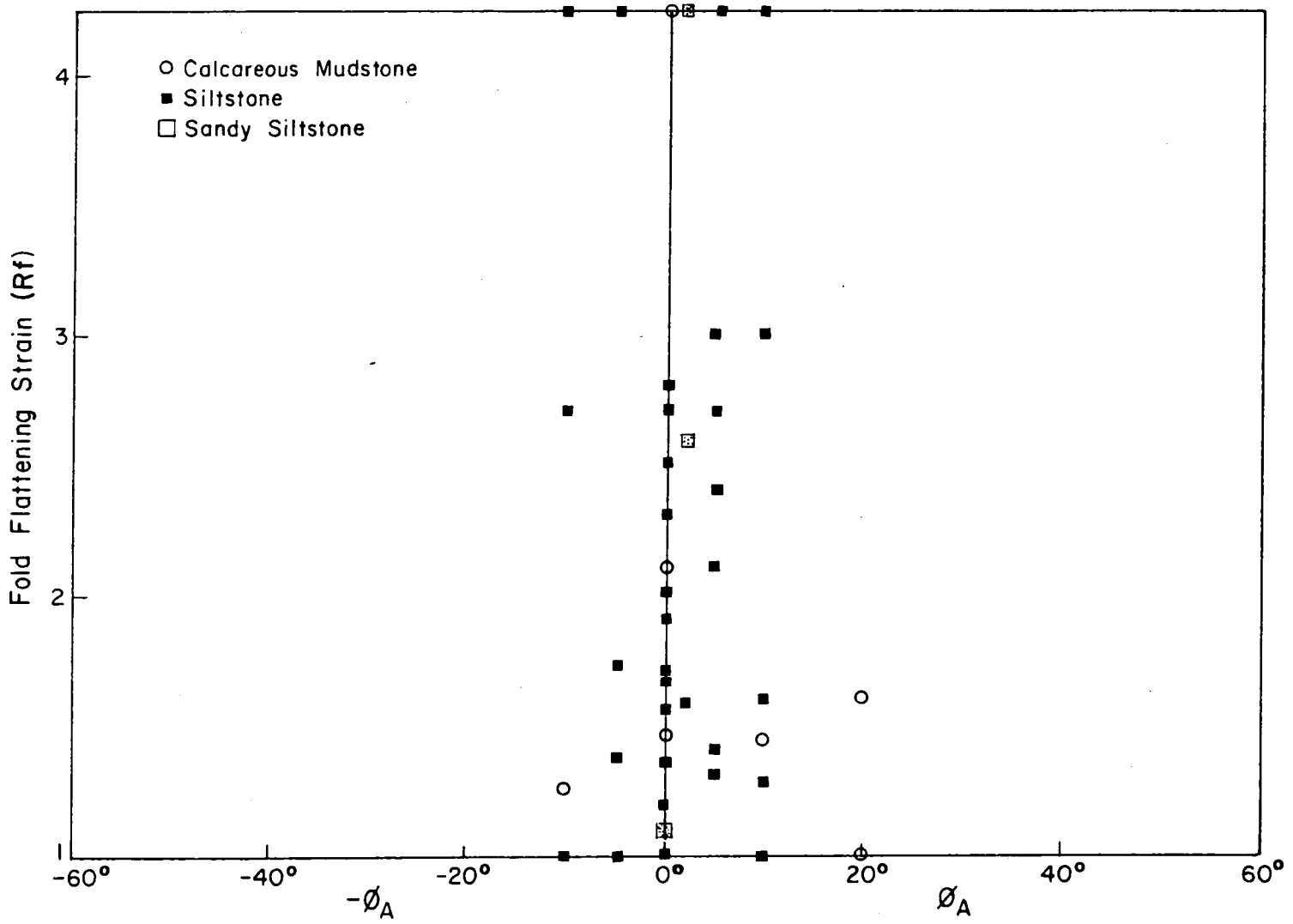

Figure 57. Fold flattening strain (Rf) versus axial plane/flattening scatter (ϕ_A).

scatter of X directions and corresponding R_f values about the reference cleavage trace with deviations ranging from -60 degrees to +37 degrees. The wide scatter of ϕ_S values indicates that cleavage does not simply form during fold flattening; if it did, the X directions ought to be more closely grouped around the cleavage reference. The X directions are fairly well clustered about the reference axial plane trace, suggesting a more synchronous relationship between buckle folding and fold flattening. Therefore, cleavage formation is not exactly synchronous with folding. If cleavage were developed prior to fold flattening strain increments, the more intensely flattened folds (with high R_f values) bearing cleavage ought to show less scatter among ϕ_S angles, due to a reduction in ϕ_S accompanying shortening in the Z direction. However, ϕ_S values do not decrease with increasing R_f. Cleavage traces scatter more than axial plane traces with respect to fold flattening directions, as is evident from comparison of ϕ_S and ϕ_A values (Figures 56, 57) and on the thickness ratio plots (Figure 29, p. 103).

m. Development of transecting cleavage. Three models are described and illustrated as possible explanations for observed cases of cleavage transection (d) in folds at Douglas Lake (Figure 58):

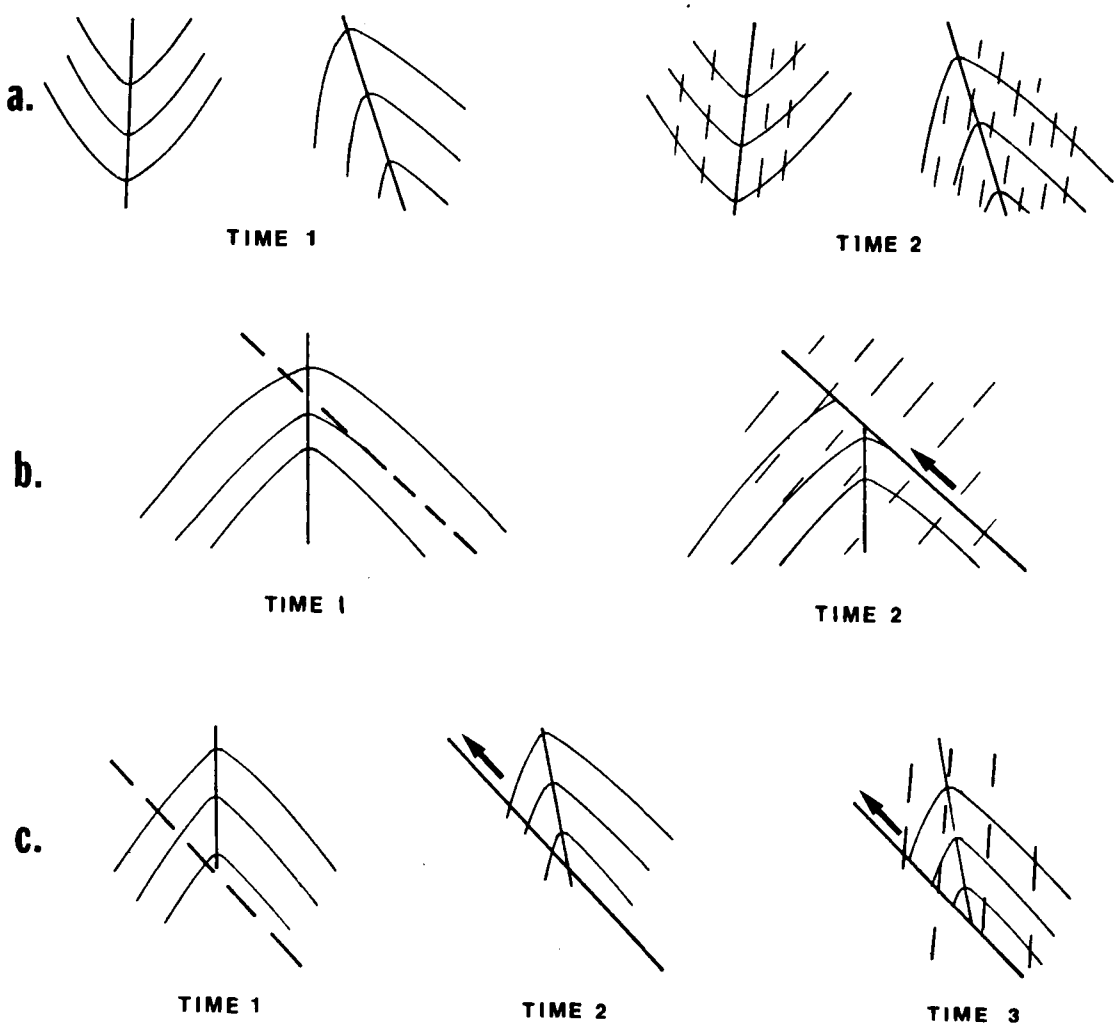

Figure 58. Mechanisms for development of transecting cleavage (d transection). (a) Cleavage is superimposed on irregular folds. (b) Faulting of fold produces secondary anisotropy which causes rotation of the local shortening axis which is then approximately orthogonal to subsequent cleavage. (c) Drag along a contraction fault may change the orientation of a fold axial surface with respect to the shortening axis prior to cleavage development.

1. Cleavage is superimposed on irregular folds (Figure 58a; Plate 1, A14-20) late in folding (similar to the northern Appalachian examples of Stringer, 1975). The irregular folds probably developed during early movement on an underlying décollement.
2. Faulting causes a reorientation of the local strain state (Wojtal, ms.). The reorientation of principal strain axes is due to a secondary anisotropy which the faulting produces (Figure 58b). Faulting of a fold may allow the shortening axis to rotate to a position compatible with noncoaxial strain represented by transecting cleavage.
3. Drag on a contraction fault may cause reorientation of an axial surface of a preexisting fold, causing a relative rotation of the strain axes with respect to the fold axial surface (Figure 58c). If cleavage is developed after faulting has been initiated, a transection of the fold by cleavage will result.

Combinations of more than one of the above models may explain certain cases of transected folds. A general rotation of the regional stress field between discrete folding and cleavage development stages would not explain

the nearly continuous range of transection (d) values (Appendix B, Table B-1).

7. Comparison of Computer Simulated Strain Patterns with Natural Folds

In Dieterich's (1970) computer fold models of the mechanics of finite amplitude folding of multilayered viscous solids (with layers of alternating viscosity), the patterns given by directions perpendicular to the principal axes of compressive strain resemble cleavage patterns in the nontransected folds. The multilayer strain models at 40 and 100 percent total shortening (Figure 59a,b) have greater ductility contrasts than those in the natural folds and as a result, greater fan angles occur in the models having layers of alternating ductilities. For this reason, the relatively thick layer model (Figure 59g) with low ductility contrast ($n/n_1 = 5.2$) most closely approximates the naturally observed patterns and accounts for minimal cleavage fan angles. The competent layers in concentrically folded, interbedded sequences of significantly contrasting ductilities display cleavage patterns similar to the more convergently fanning pattern in Figure 59a. Dieterich (1970) does not incorporate any increments of flattening strain into his computer simulation models. Consequently, his folded layers maintain equal thickness and his cleavage patterns fan slightly more than if they were flattened.

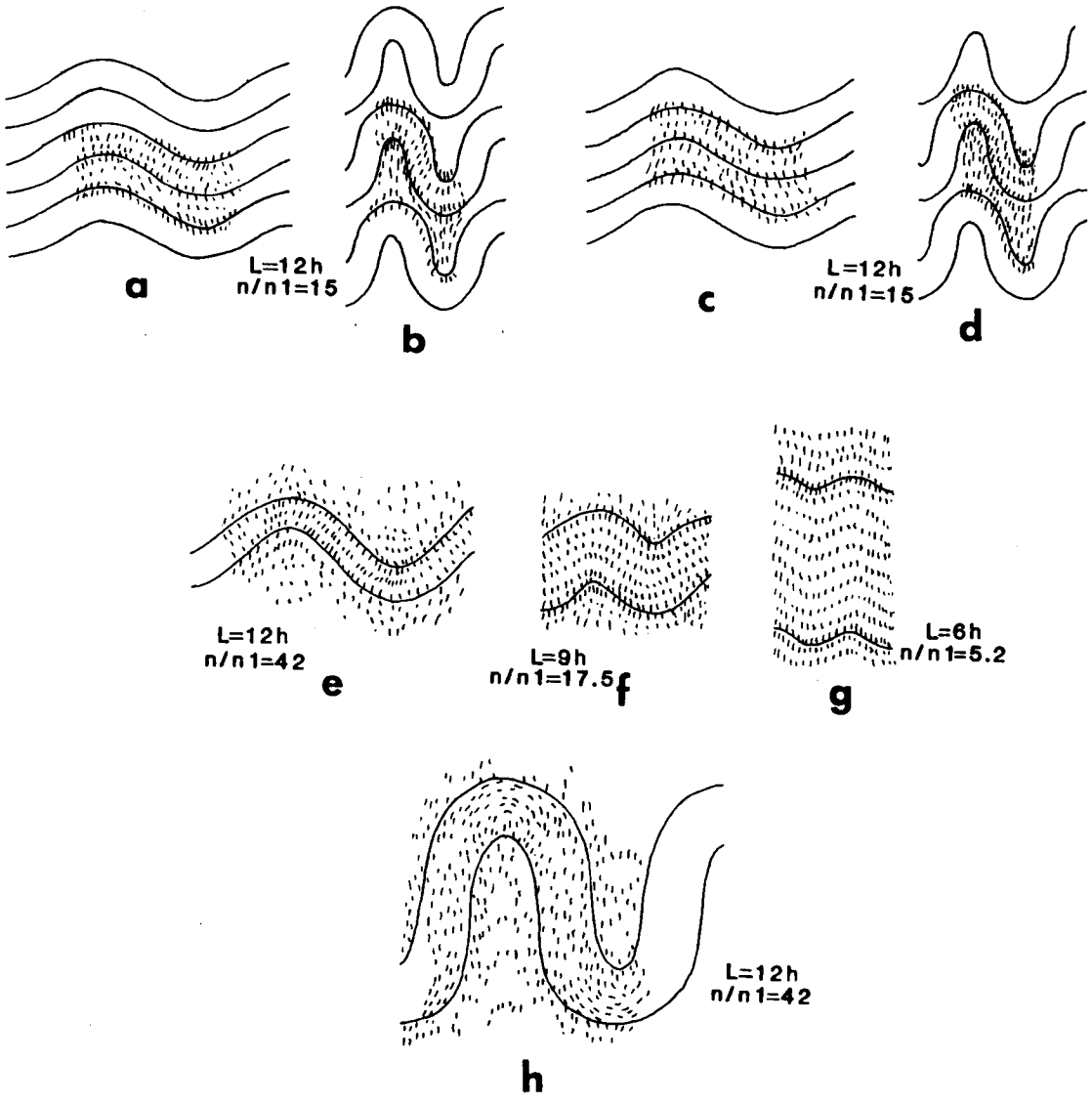

Figure 59. Computer simulation models of cleavage patterns (after Dieterich, 1970), with percent total shortening. n/n_1 is viscosity contrast. L is wavelength of initial fold. h is layer thickness. (a) (40 percent total shortening) and (b) (100 percent total shortening) represent multilayer fold strain. Short lines are drawn parallel to the direction of maximum total elongation and perpendicular to the axes of maximum total shortening. (c) (40 percent total shortening) and (d) (100 percent total shortening) represent multilayer fold stress. Short lines are drawn normal to axes of maximum compressive stress. (e) (40 percent total shortening), (f) (100 percent total shortening) and (g) (150 percent total shortening) represent single layer fold strain. Short lines are drawn normal to the axes of maximum total shortening. (h) (100 percent total shortening) represents single layer fold stress. Short lines are drawn normal to axes of maximum compressive stress.

8. Rigid-Body Deformation with Selective Removal of Material by Pressure Solution

The comparison of bedding-cleavage relationships for the rigid-body deformation models (Groshong, 1975) with observations in the Sevier formation suggests possible fold mechanisms for some observed folds. The plots of limb dip (α) versus bedding-cleavage angle (Figure 31, p. 105) show that measured data from nontransected natural folds very closely approximates the predicted relations for Groshong's model B (Figure 30, p. 104), for the majority of the folds tested in which cleavage is symmetrical about the axial surfaces. Some of the folds in coarser siltstones show transitions between models B and C (Figures 30, 31). Folds in calcareous mudstone display smooth, planar cleavage and have either parallel or weakly convergent fanning cleavage. The graphs show that the observed bedding-cleavage patterns can be related to pressure solution/fold shape modification of existing concentric folds; therefore, the pressure solution occurred predominantly during late fold modification resulting in development of spaced disjunctive cleavage.

9. Buckle Shortening Strain Calculations

Percentages of buckle shortening for the four profile sections A, B, C, and D are calculated, respectively, as 14.1, 16.4, 24.4, and 31.8. Section A is in the lowest

structural position (furthest northwest) of the sections and Section D is in the highest structural position (furthest southeast). Buckle shortening generally increases southeastward as folds become more overturned and homoclinal limbs become less extensive.

Fault shortening is neglected, because of a lack of knowledge of net slip on most of the major faults, due to the absence of distinctive marker beds. Cleavage shortening is practically negligible away from fold hinges, except in the strongly cleaved calcareous mudstone lithology.

D. Conclusions

The primary mechanism of folding determined from the observation of mesoscopic folds in the study area is buckling accompanied by flexural slip between layers on the limbs and varying degrees of strain within layers near the hinge (Figure 22a, p. 95, Figure 23a, p. 96). Fold geometries range from concentric, for interlayered materials (i.e., mudstone around sandstone) to nearly similar, for weak uniform materials. Concentric folds occur where bedding is mechanically important. Pure chevron-kink folds have very thin beds relative to the amplitude of the folds. Folding and approximately coaxial flattening probably proceeded synchronously, particularly in the hinge regions where strain is greatest and divergent (class 3) dip isogons

alternate with slightly convergent (class 1c) dip isogons, i.e., Ramsay's (1967) pseudo-similar folds. Orthogonal thickness ratios imply significantly more flattening (Figure 29, p. 103) than what is predicted by theoretical curves for flattened flexural folds (Gray and Durney, 1979). Assuming plane strain, the maximum extension direction nearly coincides with the fold axial surface dip (ϕ_A values are small), and flattening at the hinge was probably partly synchronous with flexural folding.

Cleavage in the study area is classified as a spaced disjunctive cleavage. It is controlled by both local structure and local lithology, while its relations with geographic location and large tectonic features are less clear. Bedding-cleavage patterns appear to be related to pressure solution/fold shape modification of existing concentric folds; therefore, the pressure solution occurred predominantly during late fold shape modification. Evidence that significant buckle folding and flattening did not occur in these rocks after the development of cleavage includes the following:

1. The minimum of convergent cleavage fanning.
2. The lack of significant influence of fold tightness and flattening strain on fan angle and d transection angle.

3. The nearly continuous variation over a wide range of dip transection angles.
4. The greater divergence of cleavage dip from axial plane dip than of flattening extension directions from axial plane dip.
5. The lack of folded cleavage surfaces.
6. The consistent orientation of cleavage across transected folds.

Because the cleavage probably did not begin forming until late in the deformation, it is significantly noncoaxial with the XY plane of the finite strain ellipsoid for a number of folds.

CHAPTER 4

FAULTING, FAULT-CONTROLLED CLEAVAGE AND MEGASCOPIC FABRIC ANALYSIS

A. Introduction

Fabric data for faults are analyzed using Arthaud's (1969) theory of brittle deformation to determine principal deformation axes and the orientation, if not the shape, of the deformation ellipsoid. An indirect method of determining the orientation of a fault plane from small-scale mesoscopic "discfolds" localized at a shear zone (Hansen, 1971) is performed on the Douglas décollement zone. The relationship between second order and small-scale contraction faulting and cleavage in transected mesoscopic folds is found to have significant bearing on the deciphering of a mesoscopic deformation chronology relating folding, faulting, and cleavage development. A problem involving bisection of the obtuse dihedral angle between conjugate fault pairs by the principal shortening axis (contrary to theory, Ramsay, 1967, and experimental results, Anderson, 1951) is resolved by assuming a stage of flattening after initiation of the faults. Analyses are undertaken of specific examples of deformation by bed-parallel contraction, which in certain cases has been overprinted by bed-parallel extension.

For analysis of megascopic structural fabric, a local cross-section (Plate 6) is constructed for the Tellico-Sevier shales above the local "basement" (Knox group carbonates which are relatively uninvolved in the deformation). Depth to Knox basement is derived from previous interpretations of seismic lines located to the northeast along strike (Tegland, 1978). The cross-section is fitted into a regional cross-section (Figure 8, p. 36) from a nearby transect by Witherspoon (1981). The cross-sections allow an interpretation of the chronologic deformation on a megascopic scale.

B. Theoretical Models of Fault Analysis

1. Arthaud's Method for Determining Brittle Deformation Axes

A determination of the principal axes of the deformation ellipsoid for brittle deformation fractures can be made by using the method of Arthaud (1969). This method (see Appendix C for a detailed outline of the method) uses attitudes of a large sample of fault surfaces and corresponding slip linears to graphically determine the shortening, elongation and intermediate directions of the ellipsoid. By analogy with experimental fractures (Anderson, 1951), the maximum and minimum strains are related to the bisectors of the acute (maximum contractional strain) and obtuse (maximum extensional strain) dihedral angles formed by two sets of

conjugate fault surfaces. The intermediate strain axis parallels the intersection of the conjugate fault surfaces.

2. Discfold Analysis of Planar Shear Zone

Small, asymmetrical mesoscopic folds that formed in a shear zone may be treated as examples of discfolds (Hansen, 1971; Wheeler, 1978) and used in analysis of the shear zone. The range of orientations of the fold axes allows estimates to be made of the orientation and sense of the shear zone (slip plane), using the separation angle method. The separation angle (Figure 60) is the arc which divides the two fields of down-plunge fold asymmetries. Slip planes (Figure 60) are determined graphically, and they represent the planar shear zone.

C. Fault Data and Analysis

1. Determination of Principal Axes of the Deformation Ellipsoid

Arthaud's (1969) method was applied to 12 high-angle, third order, conjugate reverse faults in the second order sheared zone at C37-38 (Figure 61). Subhorizontal compression at a high angle to steeply northwest dipping bedding caused the beds to be extended along the faults. Two m pole distributions give great circles approximately normal to the X and Z axes and at right angles to one another (Figure 61). The m pole cluster also implies a horizontal intermediate

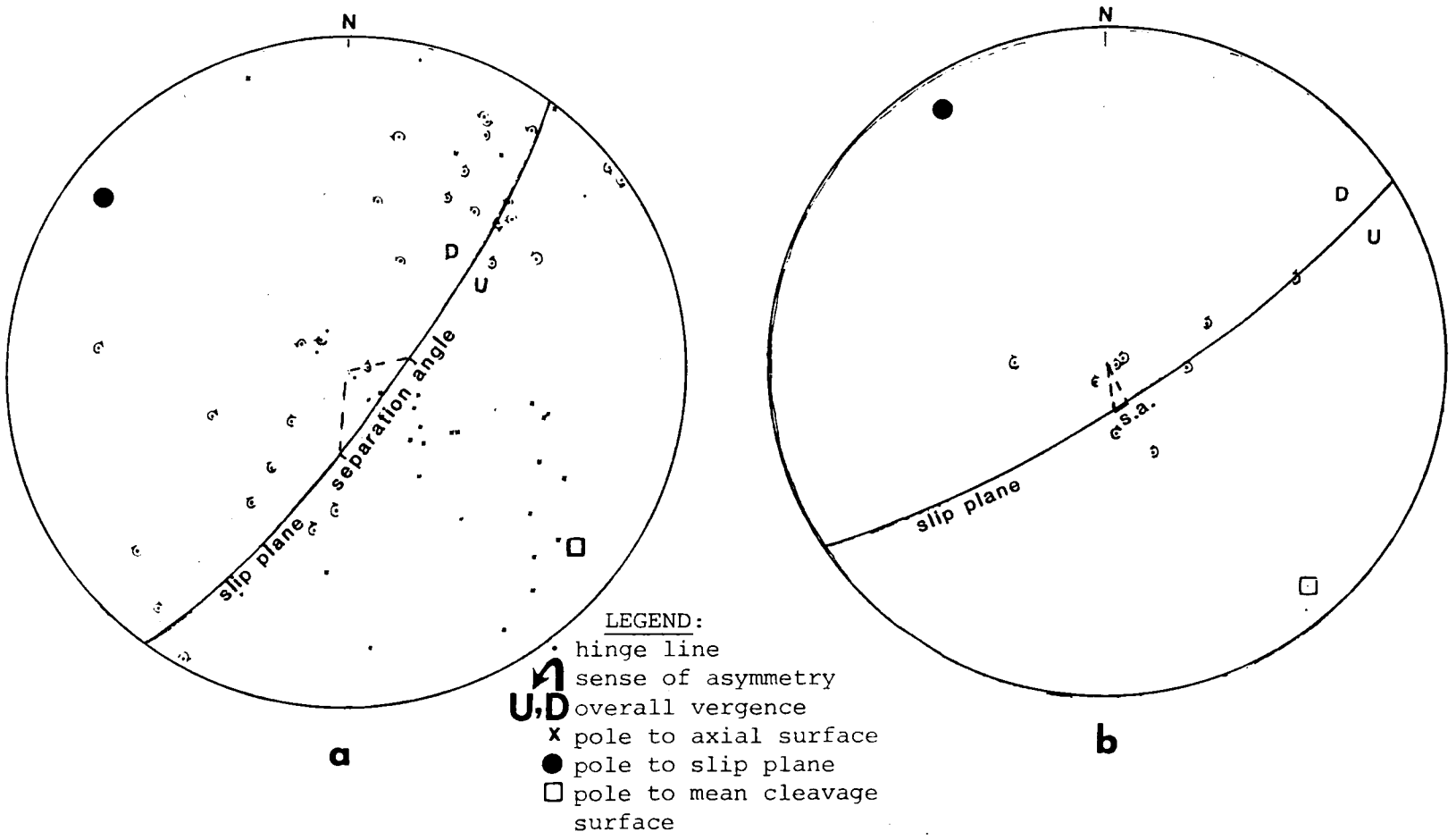

Figure 60. Discfold analysis of Douglas décollement zone. (a) Measured fold data obtained from Blockhouse formation at base of Section A. (b) Data obtained from transitional upper Whitesburg formation/Blockhouse formation at Dandridge Municipal Park.

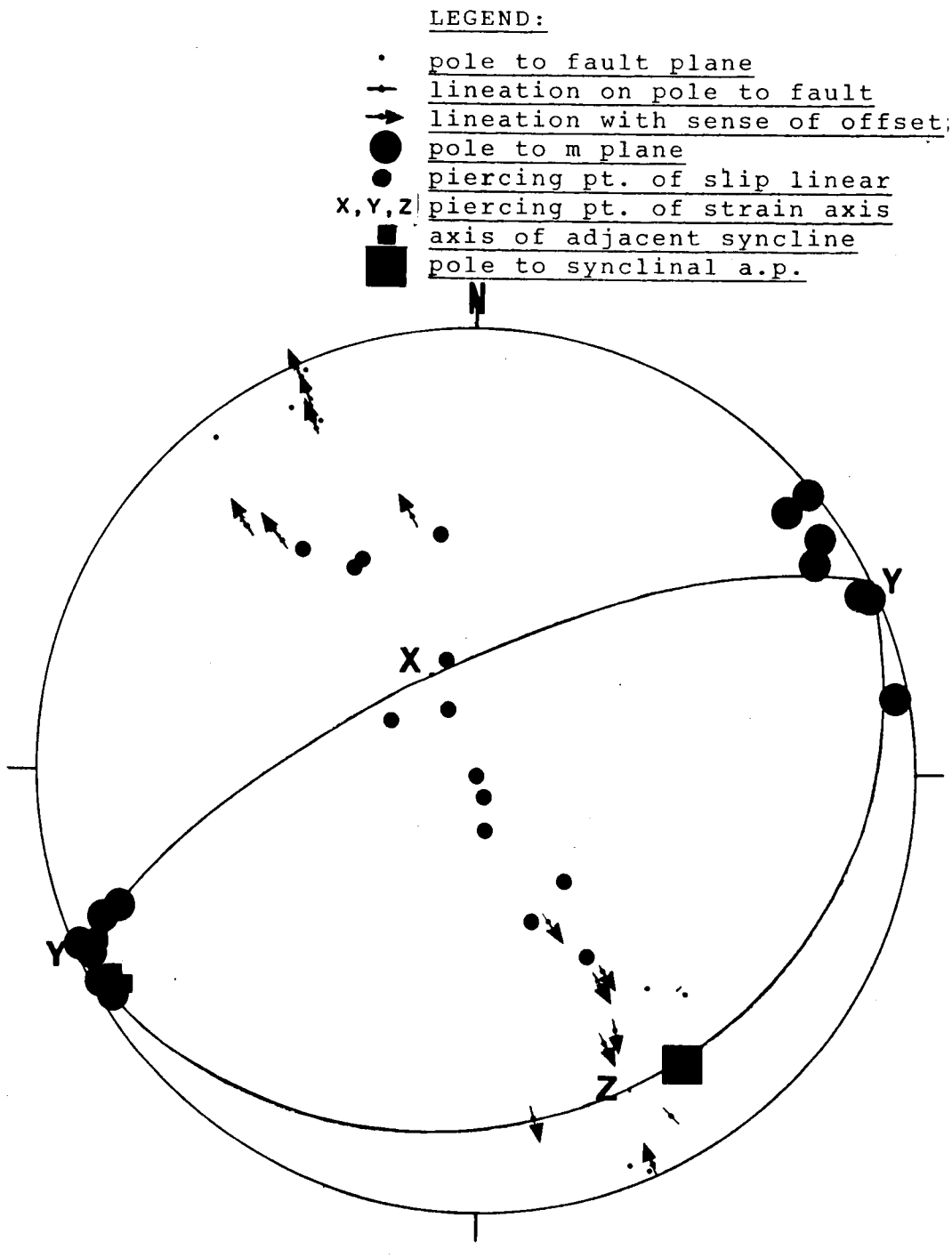

Figure 61. Deformation axes at C36-38 shear zone. Slip linears and senses of offset are plotted on poles to fault surfaces. X: elongation axis; Y: intermediate axis of deformation; Z: shortening axis.

principal direction (Y), at right angles to both the X and Z axes. The measured axis of the adjacent syncline at C36.9 (Plate 3) nearly coincides with the graphically determined Y-axis of deformation. The pole to the axial plane of the same syncline nearly coincides with the Z axis. Similarly, the trace of the axial plane of the syncline in profile coincides with the dip of the X axis. In conclusion, these conjugate fault sets are coaxial with the folding, and fold/fault relations indicate that the faulting occurred either late in folding or shortly after folding. The conventional theory of brittle failure (supported by experimental results; Ramsay, 1967), stating that the shear surfaces occur at less than or equal to 45 degrees from the Z axis (depending on the presence or absence of significant internal friction) is not supported by using Arthaud's method of analysis of the field evidence in this case. The obtuse angle between the shear surfaces is bisected by the maximum principal direction of shortening. This deviation of the methods from both theory and experimental results may in part be explained by flattening (tightening) of the obtuse dihedral angle (which is bisected by the X axis) between the conjugate surfaces (Figure 62). Such flattening would be homotactic with the extreme flattening of the adjacent syncline.

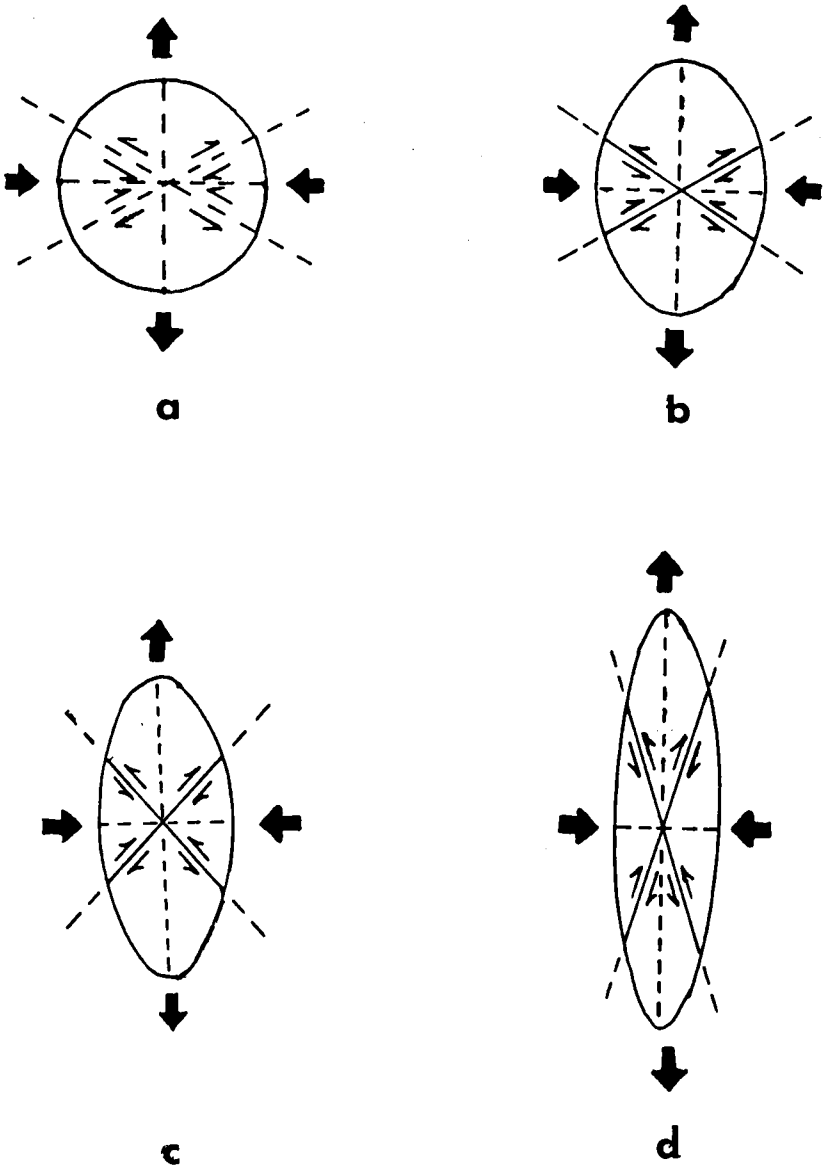

Figure 62. Flattening of dihedral angle between conjugate shear surfaces by pure shear plane strain. (a) represents initial undeformed state. (b), (c), and (d) represent progressively more intense strain as shortening direction becomes bisector of obtuse angle between the shear surfaces.

Analysis of deformation axes in Blockhouse and lower Sevier for both conjugate wrench fault and conjugate thrust fault surfaces implies a reversal of X and Y (Figures 63, 64). The horizontal X axis determined for the conjugate wrench faults (Figure 64a) is approximately parallel to the Y axis determined for the conjugate reverse faults (Figure 64). The X axis for the reverse faults (Figure 64) is similar in orientation, but plunges about 20 degrees steeper than the Y axis for the wrench faults. The Z axis for the reverse faults plunges about 20 degrees shallower than that of the wrench faults (Figure 64). The 20 degree divergence of principal axes in the profile plane may indicate a nonsynchronous relationship between the contrasting fault types. Bedding is not mechanically important as a stress guide in these massively bedded mudstones, but an anisotropy developed by cleavage appears to have constrained orientations implying the more steeply dipping Z axis determined for the wrench faults. The right lateral wrench set, in particular, is approximately parallel to cleavage, and it may have been influenced by the presence of cleavage. The flip of X and Y axes between the two fault types may indicate a change in the sedimentary or tectonic overburden, among numerous other possibilities. One explanation is that ramping in the Saltville fault at depth preceded wrench faulting and followed most thrusting and cleavage development above the Douglas décollement.

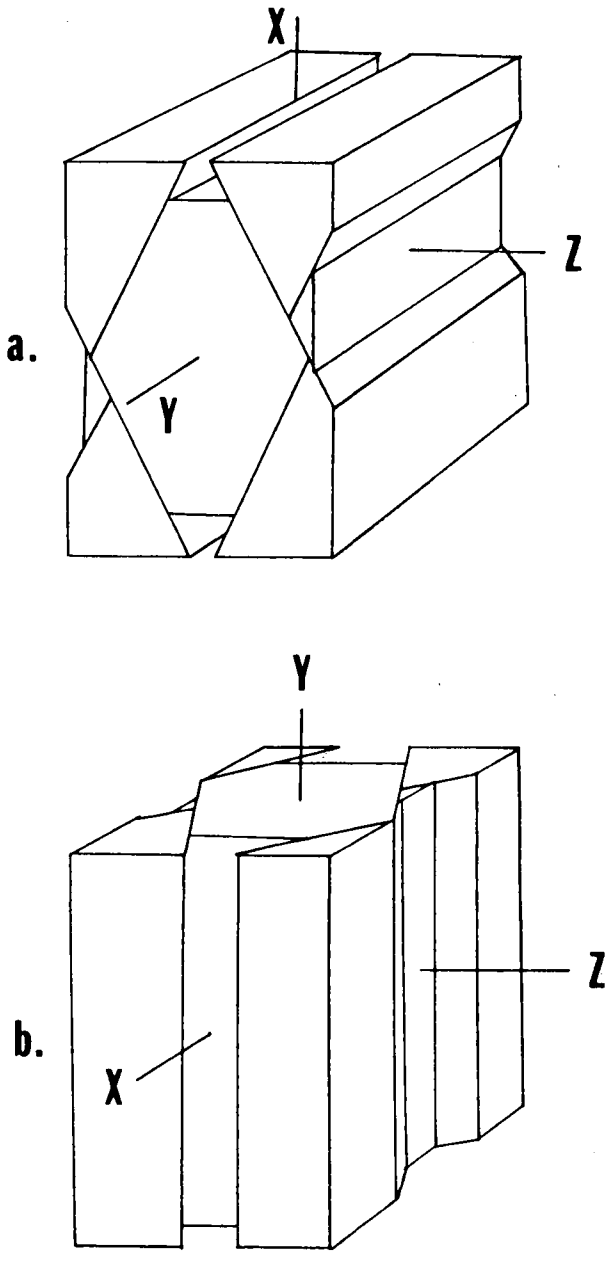

Figure 63. Reversal of X and Y axes between stages of thrusting and wrench faulting. (a) Thrusting; principal axis of extension is vertical. (b) Wrench faulting; principal axis of extension is horizontal and perpendicular to principal axis of shortening.

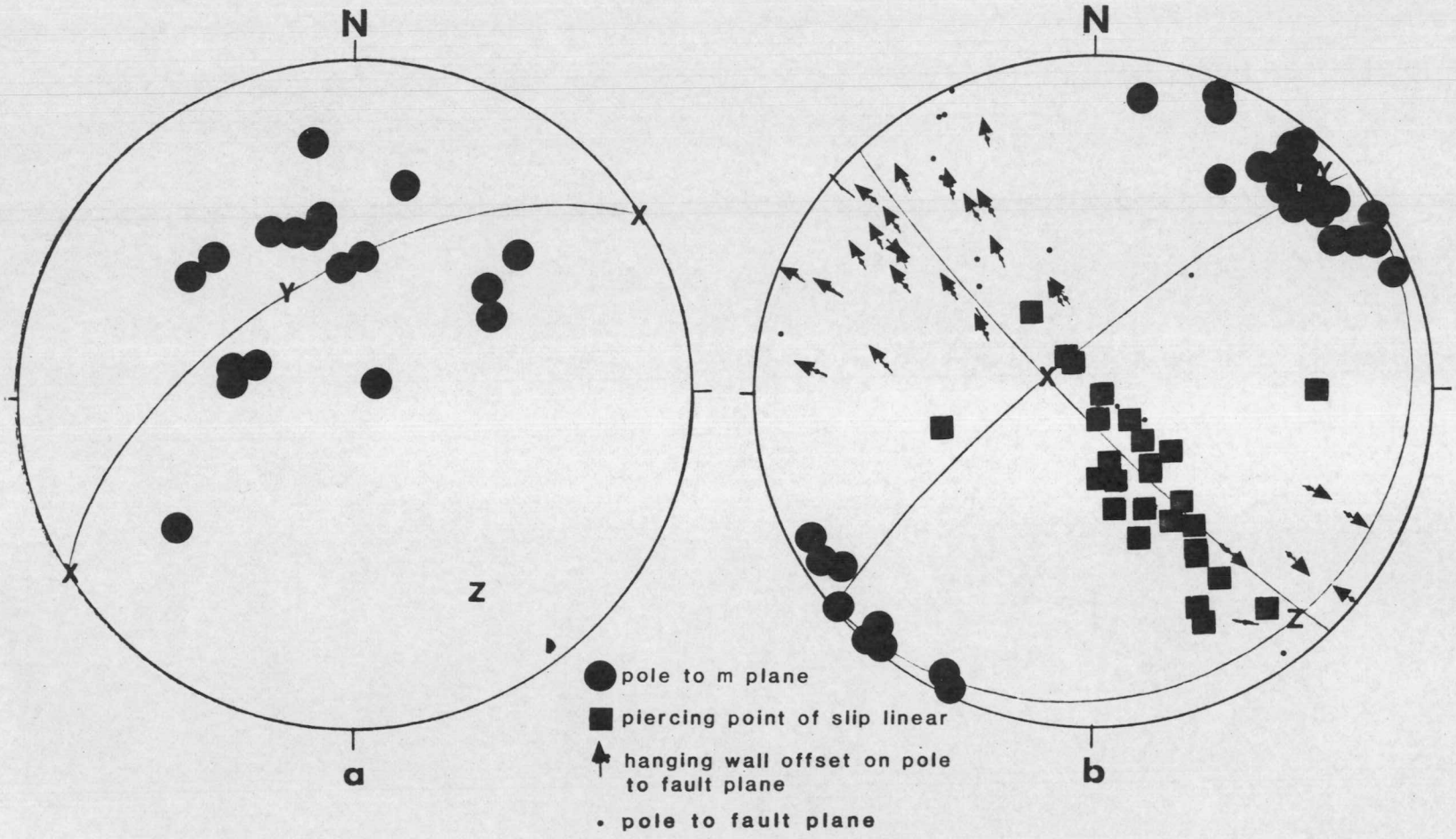

Figure 64. Deformation axes for thrust and wrench faults in hanging wall of Douglas décollement. X: elongation axis; Y: intermediate axis of deformation; Z: shortening axis. (a) Wrench faults. (b) Thrust faults.

2. Discfold Analysis at Douglas Fault Zone, Section A

Small asymmetrical folds in fissile Blockhouse shale (Figure 18b, p. 77) at the Douglas fault zone (Figure 18a, p. 77) are treated as examples of discfolds (Hansen, 1971; Wheeler, 1978), and they are used in analysis of the shear zone. The folds are disharmonic and isoclinal and they are assumed to have formed within a planar zone undergoing shear between the underlying competent carbonates and the significantly less competent upper Blockhouse and Sevier above. The folds occur in a wide range of orientations from which an estimation was made of the orientation and sense of the shear zone using the separation angle method. Slip planes (shown as great circles, Figure 60, p. 95) graphically represent the planar shear zones and the slip plane in Figure 60b roughly coincides with the slickenlined surface at the top of the footwall (Whitesburg). The 38 degree strike of the slip plane transects bedding in Figure 60a. Assuming that use of the method is valid here, this indicates inhomogeneous strain at the fault zone. This inhomogeneity may correspond with an observed, local southwestward thickening of the zone of sheared rock.

3. Cleavage-Contraction Fault Relationship in Transected Folds

Antithetic contraction faults at A18-19 (Plate 1) are at low angles to bedding on the northwest limb and displace the

fold core and offset cleavage. In general, contraction faults that are secondary to second order folds are planar across fold hinges, displace the fold cores and may offset cleavage. This implies that the faults were formed late in fold tightening and that final fault movement was at least, later than the initiation of cleavage development (Figure 65).

In strongly transected folds, the cleavage is subvertical while the axial plane is inclined in the direction of transport on the associated dominant set of contraction faults (i.e., Plate 1: A19, A64; Plate 4: D131.5). One transected fold core (Figure 66), having a positive d transection, is associated with a southeast dipping thrust cutting the fold. This case is consistent with a pattern (Figure 11, p. 47) of dependency of d transection sense on the transport direction of the associated thrust. Most cases of cleavage transection in the Sevier were apparently caused by second and third order contraction faulting, rather than directly by the Douglas décollement or other major faults.

Mechanisms for producing folds transected by cleavage generally involve faulting and may include one or a combination of the following (Figure 58, p. 166):

1. Cleavage is superimposed on irregular folds late in folding; the folds probably developed during early movement on a décollement.

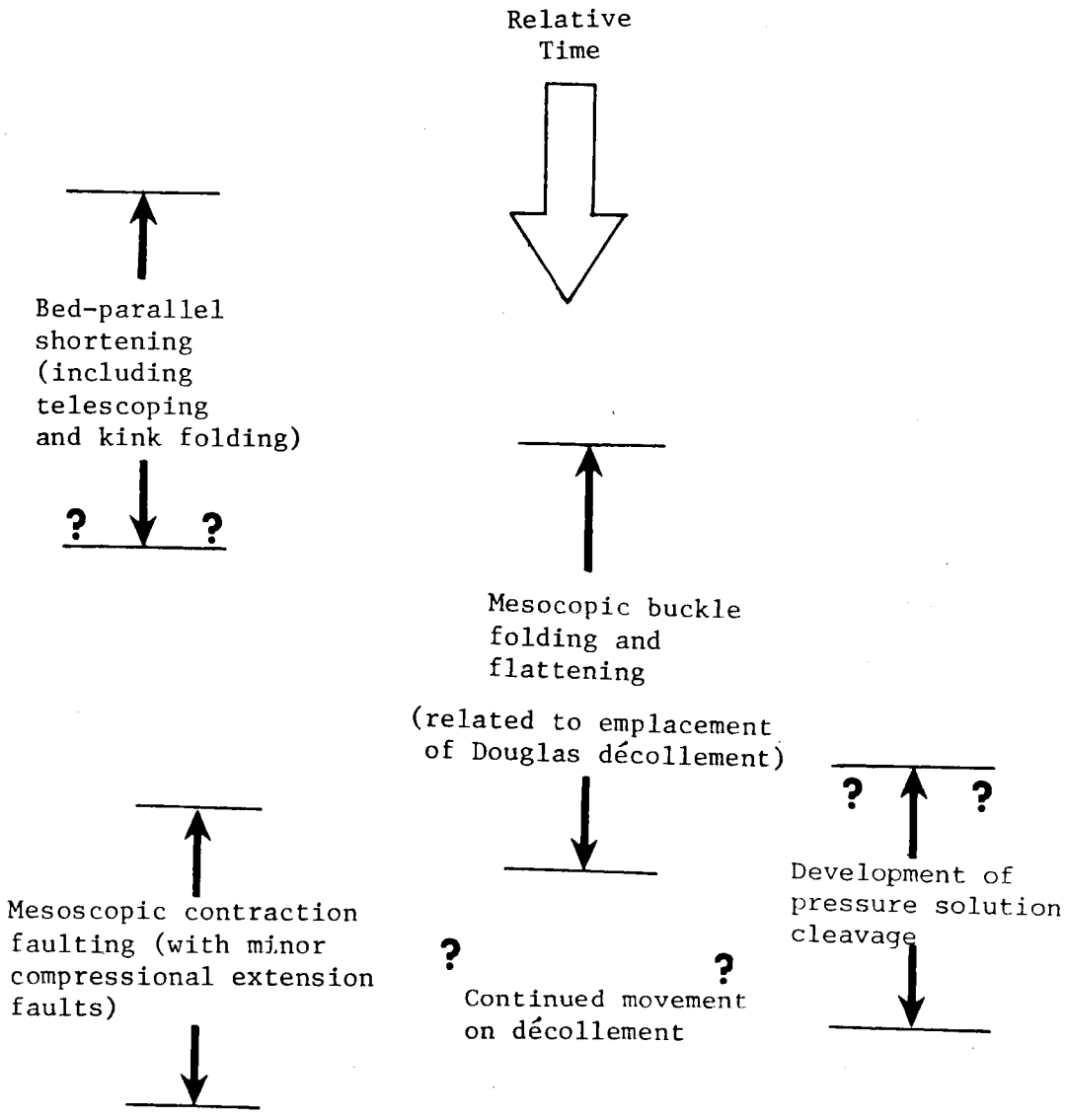

Figure 65. Mesoscopic deformation chronology.

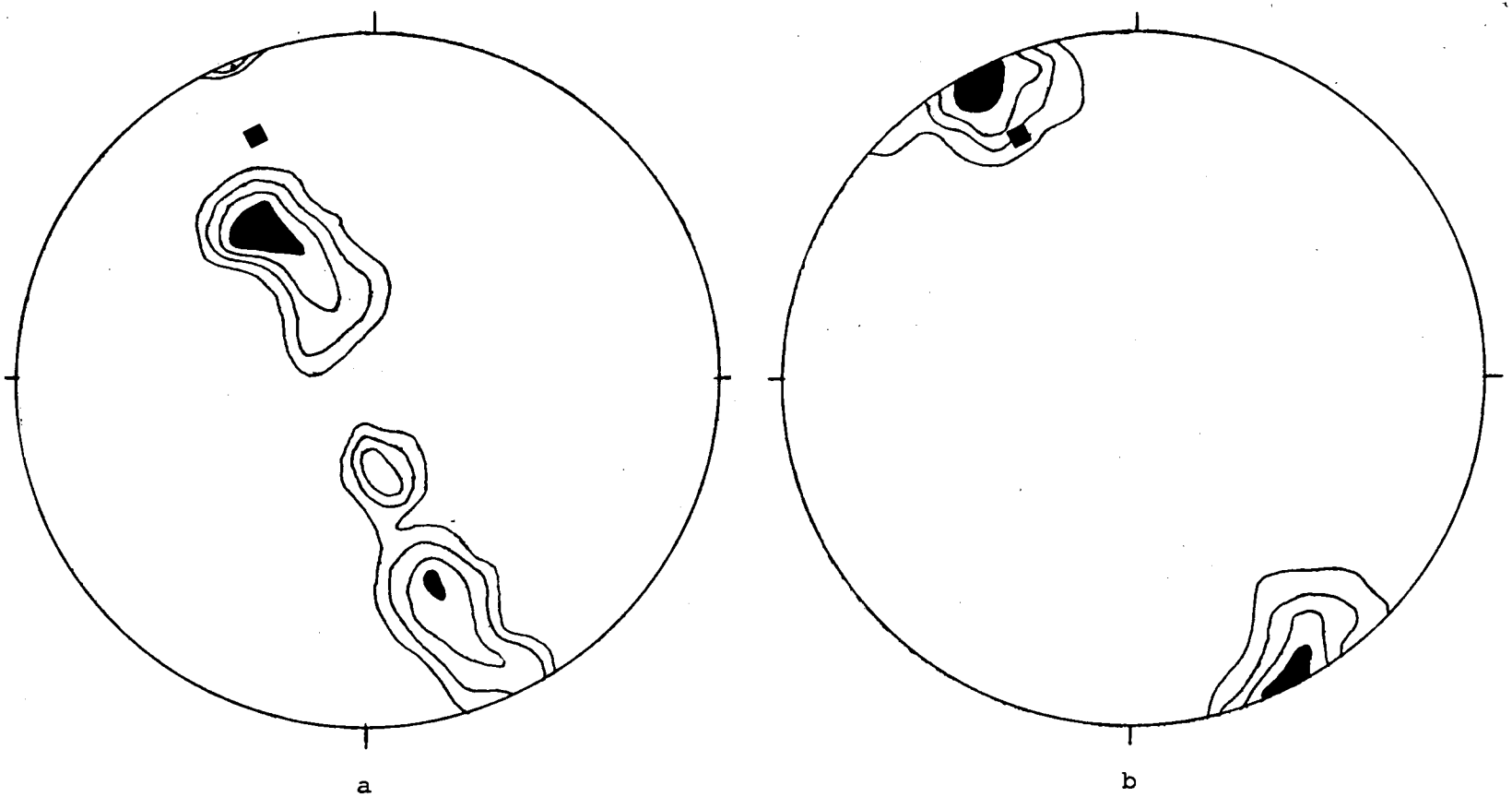

Figure 66. Mesofabric data from transected fold core (A64). Squares represent pole to axial plane. (a) 20 poles to bedding (contours at 2, 5, 10, and 20 percent per 1 percent area). (b) 20 poles to cleavage (contours at 2, 10, 20, and 40 percent per 1 percent area).

2. Faulting of a fold produces a secondary anisotropy, which allows a rotation of the λ_1 and λ_3 axes to orientations compatible with noncoaxial strain represented by transecting cleavage.
3. Drag along a contraction fault may cause reorientation of an axial surface of a preexisting fold, causing a relative rotation of the strain axes with respect to the fold axial surface prior to cleavage development.

4. Analysis of Bed-Parallel Contraction

The controlling factor in telescoping (brittle, bed-parallel contraction) is the presence of a significant competence contrast (Figures 67a,b, 7c, p. 33). Telescoping in Figure 68b cannot be explained as being due to a competence contrast, because it occurs in thick-bedded calcareous mudstone of relatively homogeneous competence. The synthetic telescopes (apparently confined to a single bed) in Figure 68b clearly precede cleavage development.

5. Analysis of Superimposed Strain

Beds which have undergone rotation to vertical may display the effects of bed-parallel extension (boundinage and jointing) superimposed on bed-parallel contraction as in Figures 18 (p. 77), 67c. Beds were extended approximately in the direction of the least principal compressive stress direction after folding and bed-parallel contraction. In the

Figure 67. Bed-parallel extension superimposed on bed-parallel contraction. Shale interbedded with thin limestones at B66. Counterclockwise from top: (a) Boudins and joints clearly postdate telescoping; extension fractures can be traced uninterrupted across telescoped limestone beds (dime scale). (b) Enlargement of center portion of a (dime scale). (c) Extension fractures are superimposed on telescoped calcareous siltstone beds (6 inch scale).

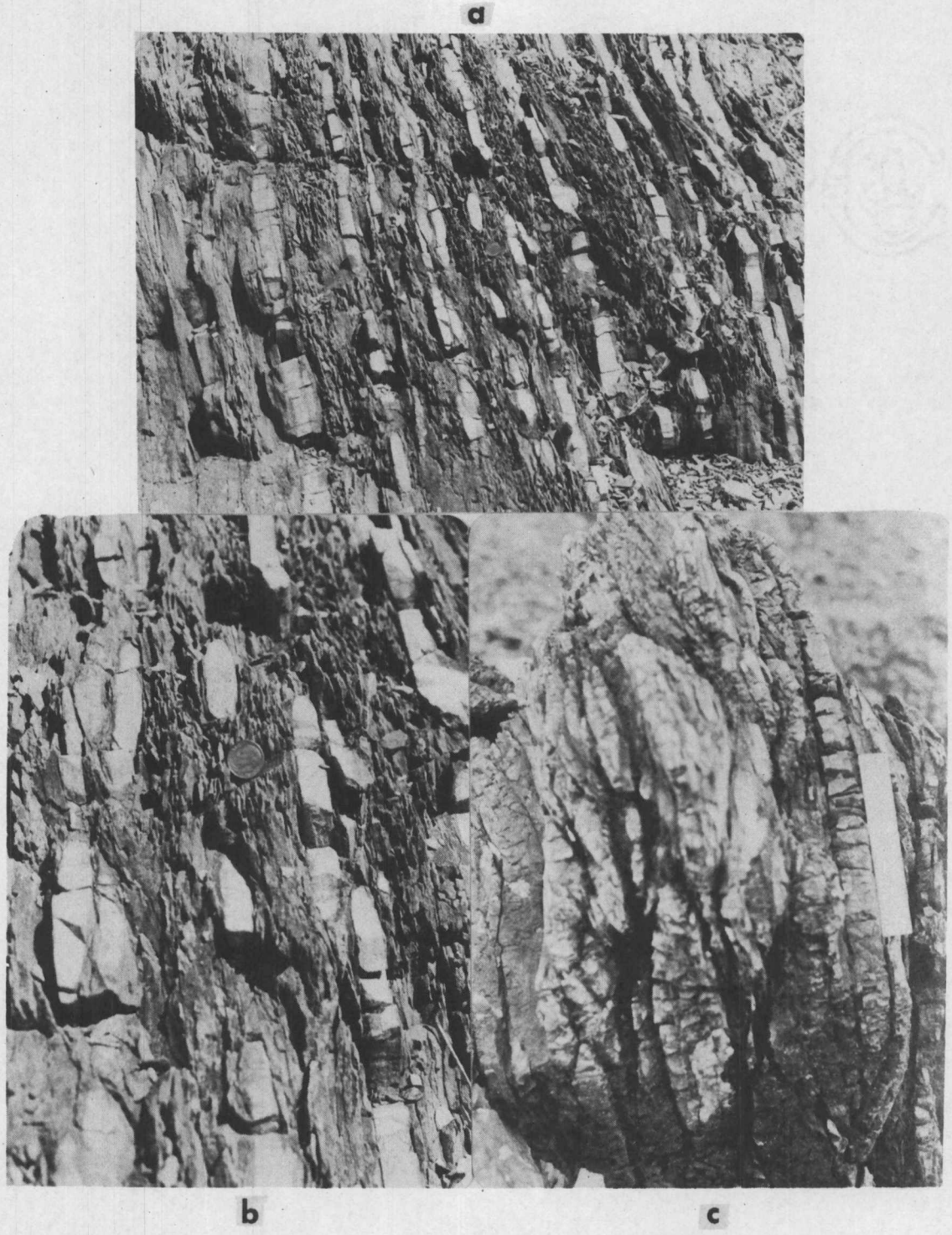

Figure 67

Figure 68. Telescoping in Sevier (A73.2, A06.4). Southeast is at right. Top to bottom: (a) Telescoped, vertical, rare limestone bed, between incompetent clayey shales (outside field of view). Slickenlines imply wedges are tectonic. Present orientation of beds implies that telescoping occurred during early bed-parallel contraction (knife for scale). (b) Telescoped, thick mudstone beds in lower Sevier. Cleavage passes across telescopes unrefracted, implying that telescoping preceded development of cleavage (2 meter scale).

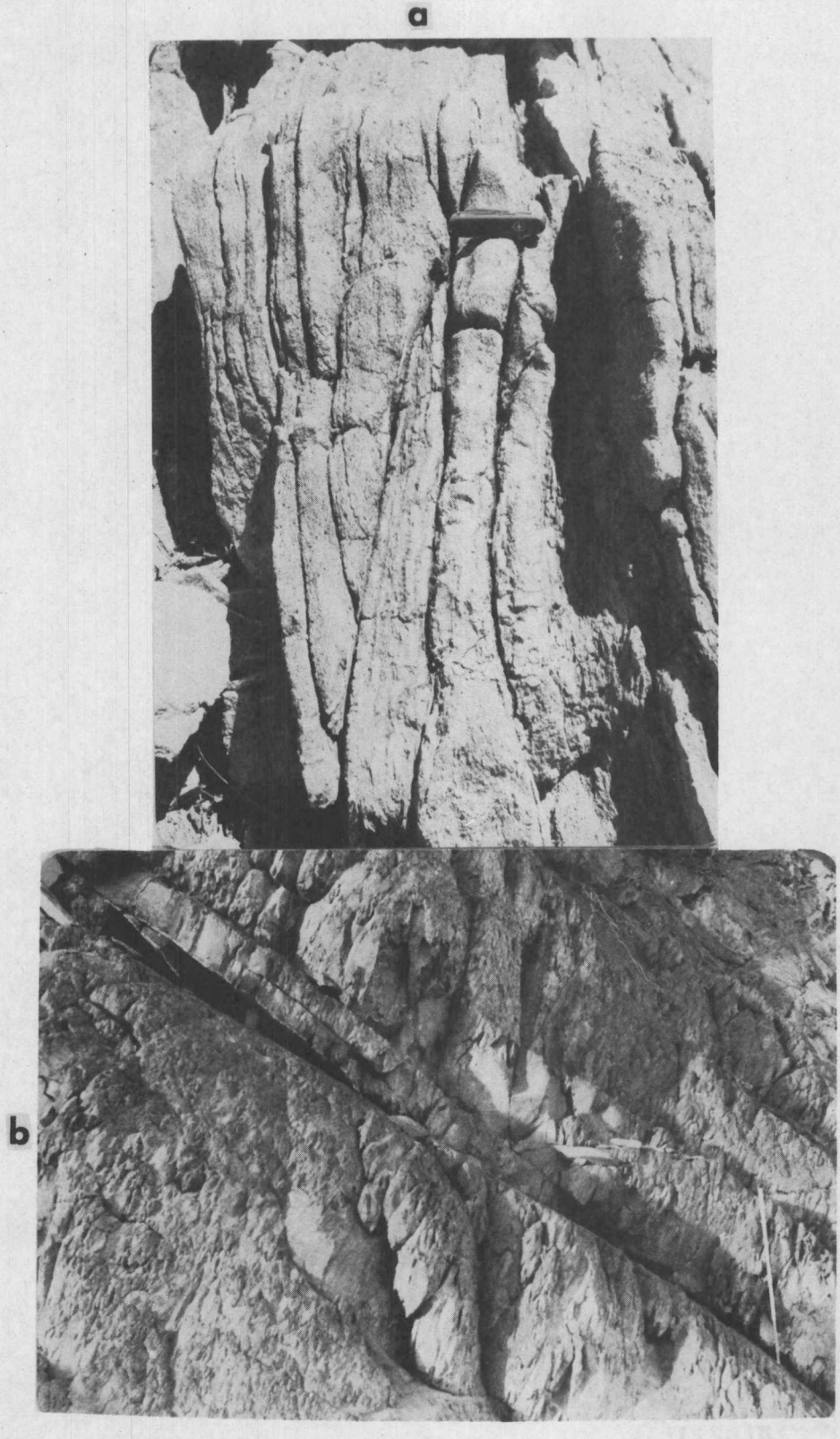

Figure 68

case of Figure 67a,b the beds were rotated to nearly vertical, and extension of bedding overprinted the contractional telescopes.

D. Megascopic Structure

The Tellico-Sevier belt at Douglas Lake is bounded by major faults (Figure 1, p. 3; Plate 6) to both the northwest (Douglas décollement) and southeast (Great Smoky fault). Only a narrow exposure of the Lower Ordovician Knox carbonates near the northeast end of the doubly plunging Fair Garden anticline interrupts the otherwise continuous 12 kilometer wide belt of Blockhouse, Sevier, and Tellico. The Great Smoky fault (fault g, Plate 6) has an estimated slip of 140 kilometers (Witherspoon, 1981), while the Douglas décollement (fault a, Plate 6), combined with splays from this fault, has an estimated slip of up to 20 kilometers. While faults g and a both ride on a footwall consisting of lower Middle Ordovician shales, fault a has no apparent stratigraphic displacement at the surface. Fault g thrusts Cambrian and Precambrian on top of the shales and the underlying Knox (grouped with overlying Lenoir and Whitesburg carbonates).

The local cross-section (Plate 6) fits into Witherspoon's (1981) regional cross-section (Figure 8, p. 39), between fault a and fault g. His section is located between 3 (in

the southeast) and 15 (in the northwest) kilometers to the southwest along strike from the section in Plate 6. The range in distance between the two sections is due to the fact that Witherspoon's section is oblique to a normal to strike and converges towards the author's section in the southeast. Depth to the relatively uninvolved Knox "basement" beneath the shale belt (1,500 meters) is taken from Witherspoon (1981) and Tegland (1978). The dip of the Douglas fault and the corresponding dip of the Lower/Middle Ordovician contact at the surface are considerably steeper (55°SE) than in Witherspoon's section to the southwest (30°SE).

Faults b, c, d, e, and f (Plate 6) thrust shales on shales at the surface. Faults e and f are interpreted as faulting Knox and Cambrian Conasauga at depth on the northwest flank of the Fair Garden anticline. Faults e and f are projected from the southwest along strike (Hardeman, 1966; Witherspoon, 1981) and are traced across the poorly exposed southeastern half of the study area. Faults b, c, and d are interpreted as soling out at fault a at depth. The minimum slip on fault b needed to return the Blockhouse to its original position is 5 kilometers.

Movement on fault g (Great Smoky fault) precedes most of the development of the Fair Garden anticline, although fold discordance in its footwall to the southeast (Figure 8, p. 39) implies that some folding may have preceded movement on fault g.

A megascopic deformation chronology (Figure 69) is primarily derived from Figure 8 (p. 39). Interpretations from the regional cross-section indicate that fault g (Great Smoky fault) moved first in the area. Next, fault a (Douglas décollement) emplacement was initiated, possibly after partial locking of fault g. Fault g discordantly cuts folds which developed above splays off of fault a at depth (Witherspoon, 1981), indicating continuing movement of fault g after the initiation of fault a. Development of the Fair Garden anticline may begin in this stage, above a ramp of fault a.

A polyphase folded fault structure developed as fault a broke away from the basal décollement at a more northwestern position, resulting in: (1) doming of the Newport anticline, (2) folding and probably locking of fault g, and (3) the location of Ordovician Windows (through crystalline Blue Ridge rocks) at the Newport anticline along strike (Figure 8; Witherspoon, 1981).

Ramping of the Saltville thrust at depth (beneath fault f) probably caused further folding of the Fair Garden anticline. Additional ramping of the Saltville at depth beneath the northwest boundary of the shale belt resulted in folding of fault a. Faults e and f cut the northwest limb of the Fair Garden anticline.

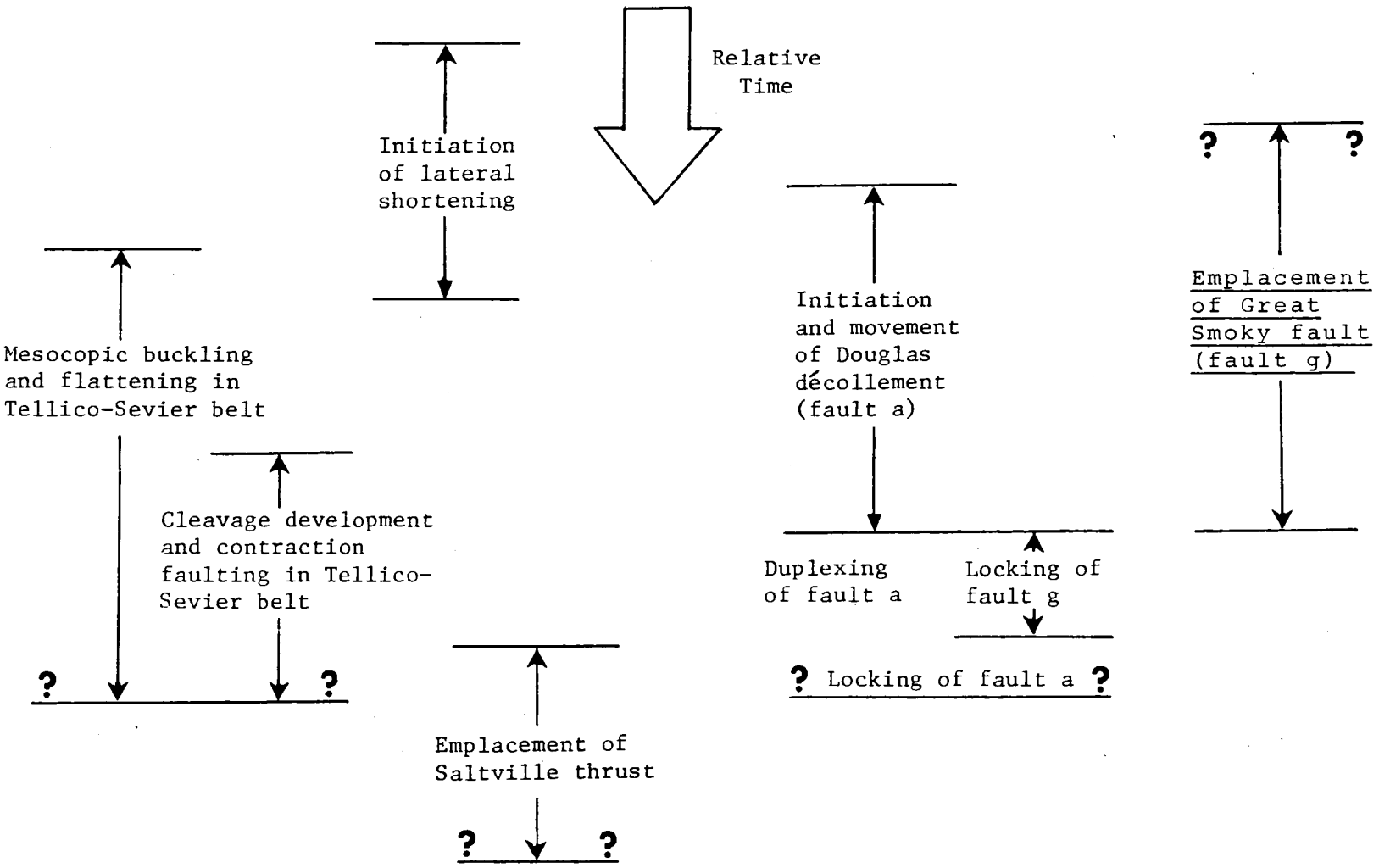

Figure 69. Megascopic deformation chronology.

In one of the above stages, faults b, c, and d were active. These faults strictly involved the Middle Ordovician shales above uninvolved Knox group carbonates (unless fault d rises from a décollement beneath Cambrian upper Conasauga group and ramps through Knox as illustrated in Plate 6). Fault c is a system of splays rising from polyphase folded fault b. Thus, fault c probably occurred after locking of the shallower level of (folded) fault b.

E. Conclusions

Analyses of brittle deformation axes from fault fabric data imply, in most cases, that conjugate contraction fault sets are approximately homotactic with mesoscopic folds. This is apparent, despite the fact that most second order and small-scale faulting occurs in late stages of folding. Evidence of a reversal of X and Y deformation axes between stages of thrust faulting and wrench faulting occurs in the Blockhouse and lower Sevier comprising the hanging wall of the Douglas décollement.

Deviation from theory which states that the shortening deformation axis for conjugate fault sets must bisect the acute dihedral angle ($\leq$ 45 degrees) may be explained by flattening of the obtuse dihedral angle. An alternative explanation is that shortening reactivates early bedding wedges. Extreme flattening is indicated by the presence of

an adjacent strongly flattened syncline that is homotactic to the conjugate faulting.

Discfold analysis of the Douglas shear zone using the separation angle method allowed graphical determination of the slip plane orientation (representing the planar shear zone). The slip plane and slip line orientations roughly coincide with the orientations measured from a slickenlined surface at the top of the footwall (uppermost bedding plane of Whitesburg beneath the fault zone). This indicates that the method may also be valid in analysis of shear zones in which discfolds occur but in which no discrete fault surface is exposed.

Brittle bed-parallel shortening is represented by minor telescoping. Telescoping is usually observed in relatively high competence layers interbedded with less competent layers. Telescoping precedes cleavage and significant buckle folding. Telescoping is best observed in the interbedded limestone and shale unit of upper Whitesburg. In two large second order fault zones, bed-parallel extension (jointing and boundinage) is superimposed on bed-parallel contraction (telescoping). This superposition of strain indicates significant rotation of the rocks with respect to the stress field.

In strongly transected (by cleavage) faulted folds, the cleavage is subvertical while the axial plane is inclined in

the direction of transport on the associated dominant set of contraction faults. This results in a dependency of the sign of the d transection parameter on the transport direction of the associated thrust. Second and third order contraction faults usually accompany the presence of transecting cleavage in fold cores. Three mechanisms for producing transecting cleavage are indicated by field relations. These involve: (a) superposition of uniform cleavage on irregular folds, (b) a local reorientation of strain axes in the vicinity of a fault, and (c) reorientation of a fold axial plane due to drag on a fault (which cuts the fold core) prior to the development of a noncoaxial cleavage.

The Tellico-Sevier belt is bounded by major thrusts on either side (Douglas décollement and Great Smoky thrust). Significant slip has also occurred on imbricate faults within the shale belt which may sole out at the Douglas at depth. Interpretations of seismic lines along strike by previous workers indicate that the depth to the base of the shales (and the extrapolated Douglas décollement) is about 5,000 feet (1,500 meters).

Extended periods of décollement faulting probably occurred on both the Douglas décollement and the Great Smoky fault, according to interpretation of the regional cross-section of Witherspoon (1981). The Great Smoky thrust is significantly folded, indicating that it was emplaced prior

to movement on underlying thrusts. On the other hand, the Great Smoky is fold discordant in its footwall (Witherspoon, 1981), implying significant emplacement following movement on lower thrusts (above which the folds developed). The hypothesized presence of polyphase folded faults requires northwestward progradation of thrust ramps above the basal décollement. Monoclinal warping of the Knox at the northwest boundary of the shale belt suggests a subsurface ramp, possibly in the Saltville fault. Aside from early bed-parallel shortening, most deformation within the shale belt probably occurred during emplacement of the Douglas décollement. Some contraction faulting may have occurred after partial locking of the décollement.

CHAPTER 5

SUMMARY AND CONCLUSIONS

An analysis of mesoscopic structural fabric was performed within a portion of the Middle Ordovician Tellico-Sevier shale belt located on the southeastern portion of the Saltville thrust sheet in Jefferson County, Tennessee. Fabric elements reflect compression perpendicular to strike. The relative intensity of deformation (based on fold interlimb angles and the density and extent of faults) increases southeastward toward the overlying Great Smoky thrust.

Spaced cleavage, mesoscopic folding, contraction faulting, and early bed-parallel shortening probably developed during a single, partially noncoaxial deformation during thrust sheet emplacement. Buckle folding and associated contraction faulting are the predominant means of lateral shortening. Irregular, modified concentric, precleavage folds developed above a first order décollement dominantly by flexural slip, modified by strain at the hinges and flattening. Further modification of fold shape was caused by removal of material by pressure solution during development of cleavage. Symmetry, in general, ranges from orthorhombic for predominantly unfaulted folds to monoclinic

for faulted folds. Fold axial surfaces dip more shallowly in the up-plunge direction, implying lower structural position. Small-scale kink folds are homotactic with buckle folding, and some of the kinks are transected by cleavage. Conjugate sets of kinks show approximately bed-parallel contraction. Second order and small-scale contraction faults are secondary to and generally homotactic with folding. They are localized along high strain zones associated with mesoscopic folding and strong cleavage. Cleavage is best developed in calcareous rocks with a significant fraction of clay-sized material. Variations in cleavage intensity (for consistent lithologies) indicate that the greatest strain occurred in fold hinges and adjacent to contraction faults. The spaced cleavage often transects folds, in which case it has a consistent geometric relationship (in profile) with the orientations of contraction faults that cut fold cores. In strongly transected, faulted folds, the cleavage is subvertical while the axial plane is inclined in the direction of transport on the associated dominant set of contraction faults. Faulted, transected fold cores trend laterally downplunge into unfaulted folds with axial planar cleavage. Thus, cleavage probably was fault-controlled. Adjacent to strongly transected fold hinges, cleavage may approximately coincide with bedding, resulting in a well developed fissility parallel to bedding. Unfaulted fold cores generally have low cleavage/fold axial surface

transection angles (d); d ranges from 0 degrees (axial planar) to more than 45 degrees with random scatter. Low cleavage fan angles for slightly flattened folds, and a lack of influence of interlimb angle on both cleavage fan angle and d suggest that cleavage was superimposed on preexisting folds. The timing of cleavage development was closely related to the timing of second order and small-scale contraction fault emplacement, which occurred in late stages of folding. Mechanisms for producing transecting (noncoaxial) cleavage may include: overprinting of irregular folds by cleavage, a fault-controlled local reorientation of strain axes prior to cleavage development, and drag-induced rotation of a fold core on a fault prior to cleavage development. The presence of high pore fluid pressures may have delayed cleavage development by causing dilation allowing early folding by intergranular flow (Borradaile, 1978).

Bed-parallel extension is represented by shallowly dipping joints found in nearly vertical beds. The presence of kink folds, discfolds (Hansen, 1971), and telescoped beds on which these joints (and sometimes boundinage) are superimposed implies that bed-parallel extension followed bed-parallel contraction and subsequent folding (Figure 13, p. 53). This superposition of strain indicates significant rotation of the rocks with respect to the stress field.

The shortening axis varies from southeast dipping in the northwest (above a postulated ramp in the Saltville fault; Roeder et al., 1978), through horizontal to northwest dipping and even steeply northwest dipping in the vicinity of nearly recumbent folding in the central and southeastern portions of the shale belt. A minimum of 23 percent buckle shortening (increasing toward the southeast) was calculated for the northwestern half of the Tellico-Sevier belt.

The Douglas décollement fault underlies the deformed Middle Ordovician shales, and it is a primary structural control. This fault is exposed at the northwest boundary of the shale belt, and it is localized at a zone of major ductility contrast at the contact between Blockhouse shale and underlying carbonates. Location of the fault coincides with the position of Witherspoon's (1981) hypothetical décollement which has 20 kilometers of slip. Ubiquitous wrench faults in the hanging wall shales postdate cleavage formation and imply a reversal of X and Y deformation axes after movement on dip-slip faults. Relatively high angle splay faults (fault b system) cause repetition of the lower mudstones and siltstones, and these faults probably sole out at the décollement at depth. An unmapped, low angle thrust (fault d) may underlie a large, second order, nearly recumbent anticline. The lack of major fold-discordant faulting may suggest the mechanical importance of layer

anisotropy, and deformation at low temperature and confining pressure (Roeder et al., 1978a).

Complex relationships exist between the timing of emplacement of the Douglas décollement (underlying the shale belt) and the Great Smoky thrust (another primary structural control) which bounds the shale belt to the southeast. The Great Smoky fault is significantly folded, indicating that it was emplaced prior to movement on underlying thrusts. Conversely, the Great Smoky is fold discordant in its footwall, implying significant emplacement following movement on lower thrusts. Aside from early bed-parallel shortening, most deformation within the shale belt occurred during emplacement of the Douglas décollement. Monoclinal warping of the Knox at the northwest boundary of the shale belt suggests a subsurface ramp, possibly in the Saltville fault.

LIST OF REFERENCES

LIST OF REFERENCES

Anderson, E. M., 1951. The dynamics of faulting: Oliver and Boyd, Edinburg, 206 p.

Arthaud, F., 1969. A graphic method of determination of the shortening, elongation, and intermediate directions from a population of faults: Extraut du Bulletin de la Societe geologique de France, 7e Serie, t XI, p. 720-737.

Bayly, B. M., Borradaile, G. J., and Powell, C. McA. (Editors), 1977. Atlas of rock cleavage--Provisional edition: Univ. Tasmania, Hobart, 110 plates + 26 pages.

Benedict, G., and Walker, K. R., 1978. Paleobathymetric analysis in Paleozoic sequences and its geodynamic significance: Amer. Jour. of Sci., v. 278, p. 579-607.

Borradaile, G. J., 1978. Transected folds: A study illustrated with examples from Canada and Scotland: Geol. Soc. Amer. Bull., v. 89, p. 481-493.

Bridge, J., 1955. Disconformity between Lower and Middle Ordovician Series at Douglas Lake, Tennessee: Geol. Soc. Amer. Bull., v. 66, p. 725-730.

Carey, S. W., 1954. The rheid concept in geotectonics: Geol. Soc. Australia Jour., v. 1, p. 67-117.

Chapple, W. M., 1969. Fold shape and rheology: The folding of an isolated viscous plastic layer: Tectonophysics, v. 7, p. 97-116.

Cloos, E., 1947. Oolite deformation in South Mountain fold, Maryland: Geol. Soc. Amer. Bull., v. 58, p. 843-918.

Currie, J. B., Patnode, H. W., and Trump, R. P., 1962. Development of folds in sedimentary rocks: Geol. Soc. Amer. Bull., v. 73, p. 655-673.

Dennis, J. G., 1972. Structural Geology: Ronald, New York, N.Y., 532 p.

Dewey, J. F., 1965. Nature and origin of kink bands: Tectonophysics, v. 1, no. 6, p. 459-494.

Dieterich, J. H., and Carter, N. L., 1969. Stress history of folding: Amer. Jour. of Sci., v. 267, p. 129-154.

Dieterich, J. H., 1970. Computer experiments on mechanics of finite amplitude folds: Canadian Jour. of Earth Sci., v. 7, p. 467-476.

Donath, F. A., and Parker, R. B., 1964. Folds and folding: Geol. Soc. Amer. Bull., v. 75, p. 45-62.

Epstein, A. G., Epstein, J. B., and Harris, D., 1977. Conodont color alteration--an index to organic metamorphism: U.S. Geol. Survey Prof. Paper 995, 27 p.

Feder, G., ms 1963. Geology of the Oak Grove area, Jefferson County, Tennessee: Unpublished Master's thesis, The University of Tennessee, Knoxville, 30 p.

Fleuty, M. J., 1964. The description of folds: Geologist's Assoc. Proc., v. 75, pt. 4, p. 461-492.

Flinn, D., 1962. On folding during three-D progressive deformation: Quart. J. Geol. Soc. London, v. 118, p. 385-433.

Ghosh, S. K., 1966. Experimental tests of buckling folds in relation to the strain ellipsoid in simple shear deformations: Tectonophysics, v. 3, no. 3, p. 169-185.

Goguel, J., 1942. Introduction a letude mecanique des deformations de l'escorce terrestre: Mem. Expl. Carte. Geol. det. France, 2e edit., 544 p.

Gray, D. R., 1977. Some parameters which affect the morphology of crenulation cleavages: J. Geol., v. 85, p. 763-780.

Gray, D. R., and Durney, D. W., 1979. Investigations of the mechanical significance of crenulation cleavage: Tectonophysics, v. 58, p. 35-79.

Gray, D. R., 1981a. Cleavage-fold relationships and their implications for transected folds: an example from southwest Virginia, U.S.A.: Jour. of Structural Geol., v. 3, no. 3, p. 265-277.

Gray, D. R., 1981b. Compound tectonic fabrics in singly folded rocks from southwest Virginia, U.S.A.: Tectonophysics, v. 78, p. 229-248.

Greene, R. C., ms 1959. Geology of English Mountain and vicinity, Cocke, Jefferson and Sevier Counties: Unpublished Master's thesis, The University of Tennessee, Knoxville, 46 p.

Groshong, R. H., 1975. "Slip" cleavage caused by pressure solution in a buckle fold: Geology, v. 3, p. 411-413.

Hamilton, W. B., 1961. Geology of the Richardson Cove and Jones Cove quadrangles, Tennessee: U.S. Geol. Survey Prof. Paper 349-A, 55 p.

Hansen,E., 1971. Strain Facies: Springer-Verlag, New York, N.Y., 207 p.

Hardeman, W. D., Swingle, G. D., and Miller, R. A., eds., 1966. Geologic map of Tennessee: Tennessee Division of Geology, Nashville, Tennessee.

Harris, L. D., and Milici, R. C., 1977. Characteristics of thin skinned style of deformation in the southern Appalachians and potential hydrocarbon traps: U.S. Geol. Survey Prof. Paper 1018, 40 p.

Harris, L. D., Harris, A. G., de Witt, W., Jr., and Bayer, K. C., 1981. Evaluation of southern eastern overthrust belt beneath Blue Ridge-Piedmont thrust: Amer. Assoc. Pet. Geol. Bull., v. 65, no. 12, p. 2,497-2,505.

Hudleston, P. J., 1973. Fold morphology and some geometrical implications of theories of fold development: Tectonophysics, v. 16, p. 1-46.

Ingram, R. R., 1954. Terminology for the thickness of stratification and parting units in sedimentary rocks: Geol. Soc. Amer. Bull., v. 65, p. 937-938.

Keith, A., 1895. Description of the Knoxville Quadrangle, Tennessee-North Carolina: U.S. Geol. Survey Geol. Atlas, Folio 25.

Kellberg, J. M., and Grant, L. F., 1956. Coarse conglomerates of the Middle Ordovician in the southern Appalachian Valley: Geol. Soc. Amer. Bull., v. 67, p. 697-716.

Keller, F. B., 1980. Suprafan turbidities in the Tellico formation, Indian Creek Embayment, Tennessee, in Walker et al., 1980. Middle Orodivician carbonate shelf to deep water basin deposition in the southern Appalachians: Studies in Geology no. 4, The University of Tennessee, Knoxville, 120 p.

Marie, J. R., ms 1963. Stratigraphy and structure of the Millican Creek area, Sevier County, Tennessee: Unpublished Master's thesis, The University of Tennessee, Knoxville, 37 p.

Newman, R. B., 1955. Middle Ordovician rocks of the Tellico-Sevier belt of eastern Tennessee: U.S. Geol. Surv. Prof. Paper, 274-F, p. 141-178.

Paterson, M. S., and Weiss, L. E., 1966. Experimental deformation and folding in phyllite: Geol. Soc. Amer. Bull., v. 77, p. 343-374.

Powell, C. McA., 1979. A morphological classification of rock cleavage: Tectonophysics, v. 58, p. 21-34.

Price, N. J., 1966. The initiation and development of asymmetrical buckle folds in nonmetamorphosed competent sediments: Tectonophysics, v. 4, no. 2, p. 173-201.

Ramsay, J. G., 1962. The geometry and mechanics of formation of "similar" type folds: J. Geol., v. 70, p. 309-327.

Ramsay, J. G., 1967. Folding and Fracturing of Rock: McGraw-Hill, Inc., New York, N.Y., 568 p.

Rodgers, J., 1953. Geologic map of east Tennessee with explanatory text: Tennessee Division of Geol. Bull., 58, pt. II, 168 p.

Roeder, D., Yust, W. W., and Little, R. L., 1978a. Folding in the Valley and Ridge Province of Tennessee: Amer. Jour. of Sci., v. 278, p. 477-496.

Roeder, D., Gilbert, O. E., and Witherspoon, W. D., 1978b. Evolution and macroscopic structure of Valley and Ridge thrust belt, Tennessee and Virginia: Studies in Geology, no. 2, The University of Tennessee, Knoxville, 25 p.

Safford, J. M., 1869. Geology of Tennessee: State of Tennessee, Nashville, Tennessee, 500 p.

Shanmugam, G., ms 1978. The stratigraphy, sedimentalogy, and tectonics of the Middle Ordovician Sevier shale basin in east Tennessee: Unpublished Ph.D. dissertation, The University of Tennessee, Knoxville.

Shanmugam, G., and Walker, K. R., 1978. Tectonic significance of distal turbidites in the Middle Ordovician Blockhouse and lower Sevier formation in east Tennessee: Am. Jour. Sci., v. 278, p. 551-578.

Shanmugam, G., 1980. Rhythms in deep sea, fine-grained turbidite and debris-flow sequences, Middle Ordovician, eastern Tennessee: Sedimentology, v. 27, no. 4, p. 419-432.

Simon, R. I., ms 1981. Mesoscopic structure and strain in part of the Narrows Thrust-Sheet, Giles County, Virginia: Unpublished Master's thesis, Virginia Polytechnic Institute and State University.

Spencer, E. W., 1977. Introduction to the Structure of the Earth: McGraw-Hill, Inc., New York, 640 p.

Stephannson, O., 1976. Finite element analysis of folds: Phil. Trans. R. Soc. Lond., v. 283, p. 153-161.

Stringer, P., 1975. Acadian slaty cleavage noncoplanar with fold axial surfaces in the northern Appalachians: Can. J. Earth Sci., v. 12, p. 949-961.

Tegland, E. R., 1978. Seismic investigations in eastern Tennessee: Tennessee Department of Conservation, Division of Geology Bull., Bull. 78, 68 p.

Treagus, S. H., 1980. A theory of stress and strain variations in viscous layers, and its geological implications: Tectonophysics, v. 72, p. 75-103.

Troensegaard, K. W., ms 1965. Development of cleavage in a portion of the Bays Mountain synclinorium, Greene, Cocke, Hamblen, and Jefferson Counties, Tennessee: Unpublished Master's thesis, The University of Tennessee, Knoxville, 39 p.

Turner, F. J., and Weiss, L. E., 1963. Structural Analysis of Metamorphic Tectonites, McGraw-Hill, Inc., New York, 545 p.

Walker, K. R., Broadhead, T. W., Keller, F. B., 1980. Middle Ordovician carbonate shelf to deep water basin deposition in the southern Appalachians: Studies in Geology, no. 4, The University of Tennessee, Knoxville, 120 p.

Wedow, H., Jr., and Laurence, R., 1943. In "Geology of the Douglas Dam and Reservoir": Open file Tennessee Valley Authority report.

Wheeler, R. L., 1978. Slip planes from Devonian Millboro Shale, Appalachian Plateau Province: Statistical extensions of discfold analysis: Amer. Jour. of Sci., v. 278, p. 497-517.

Wise, T., ms 1980. Significance of solution cleavage in the Chapman Ridge anticline, east Tennessee: Unpublished Master's thesis, The University of Tennessee, Knoxville, 101 p.

Witherspoon, W. D., ms 1981. Structure of Blue Ridge thrust front, Tennessee, southern Appalachians: Unpublished Ph.D. dissertation, The University of Tennessee, Knoxville, 165 p.

Yust, W. W., ms 1976. A mesoscopic fabric analysis of a portion of the Tellico-Sevier belt of east Tennessee: Unpublished Master's thesis, The University of Tennessee, Knoxville, 106 p.

APPENDICES

APPENDIX A

GLOSSARY OF TERMINOLOGY USED

Antithetic shear: Conjugate shear whose sense of shearing stress is opposed to the sense of external rotation.

Axial-planar: Parallel to, or symmetrical about the fold axial surface.

Axial surface: Surface connecting successive positions of fold hinge.

Brittle: Behavior of rock which deforms essentially as an elastic substance; competent.

Cleavage: Set of closely spaced secondary, planar, parallel or subparallel fabric elements that impart mechanical anisotropy to the rock without apparent displacement parallel to the surfaces (in most cases).

Coaxial: State of strain implied by homotactic fabrics; used here mostly to refer only to λ_1, and λ_3 axes (assuming plane strain).

Competent unit: Bed that is able to withstand the pressure of folding without appreciable internal flowage or change in original thickness (Spencer, 1977, p. 38).

Continuous cleavage: Cleavage resulting from continuous parallelism of platy minerals throughout the rock (Dennis, 1972, p. 179), or from cleavage with domains spaced closer than 0.01 mm (Powell, 1979).

Cozonal: Lines of intersection of planar surfaces are parallel.

Crenulation cleavage: Cleavage planes, that are separated by rock displaying crenulated foliation; the foliation is either mechanically anisotropic sedimentary layering or a preexisting tectonic foliation.

Disjunctive cleavage: Spaced cleavage independent of preexisting foliation.

Ductile: Behavior of rock which undergoes permanent deformation before rupture; incompetent.

Fabric: Sum of all structural elements (mostly surfaces and linears and their attitudes), regardless of size.

Heterotactic: Fabric in which subfabrics do not reflect the same symmetry.

Homotactic: Fabric in which the subfabrics reflect the same symmetry.

Joints: Surfaces of visible discontinuity without displacement; some evidence of extension is usually displayed normal to the surfaces.

Limb thrust: Contractional fault which cuts upsection toward an anticlinal hinge and/or away from a synclinal hinge.

Monoclinic symmetry: Symmetry defined by one mirror plane in $\lambda_1\lambda_3$.

Orthorhombic symmetry: Symmetry defined by two mirror planes, one in $\lambda_1\lambda_3$ and one in $\lambda_1\lambda_2$, and a twofold symmetry axis in λ_1.

Paired fold: Asymmetrical double fold in which an adjacent anticline and syncline are separated by a short limb.

Rough cleavage: Nonplanar disjunctive cleavage consisting of short discontinuous cleavage domains that envelop the detrital grains (Gray, 1977).

Shear: Strain resulting from stresses causing adjacent rock masses to slide relative to each other in a direction parallel to their plane of contact.

Smooth cleavage: Planar disjunctive cleavage with continuous domains free from irregularities or unevenness at the scale of observation.

Spaced cleavage: Cleavage spaced at finite intervals, at the scale under consideration (Dennis, in Bayly et al., 1977). The practical lower limit for distinguishing cleavage domains with an optical microscope is 0.01 mm, so that cleavages with domains more closely spaced appear continuous (Powell, 1979). The upper spacing limit is not defined.

Synthetic shear: Conjugate shear whose sense of shearing stress is the same as the sense of external rotation.

Vergence: Sense of fold asymmetry.

APPENDIX B

Tables B-1 and B-2 display parameters, respectively, for 74 folds (B-1) and for 55 folded layers from 11 folds selected for single layer analysis (B-2). Table B-2 lists the section and location of each documented fold, the scale (including fold order and half wavelength), form, bed thickness, lithology, hinge geometry including interlimb angle and angularity parameter, fold class (Ramsay, 1967), cleavage presence and intensity, cleavage fan angle, cleavage transection parameters, fold axis orientation, and axial surface dip. Table B-2 lists the section and location of each folded layer, the form and lithology of the folded layer, as well as interlimb angle, cleavage fan angle, flattening strain ratio, angular deviation of flattening extension direction from the traces of both cleavage and the axial plane, and transections of the axial plane by cleavage in both profile and horizontal view.

TABLE B-1

FOLD PARAMETERS
(Data for 74 folds)

Section/		Fold half-wavelength		Bed		Tightness	Interlimb angle	Hinge	Angularity			Cleavage	Cleavage transection	Cleavage transection	Fold	Axial
D80.4	2°	--	anticline	thin/ medium	calc. siltstone	open	102.5	chevron	30+	hinge:2 limbs:1C	none	none	none	--	--	44,02 NE	70 SE
D106.1	--	--	syncline	thin/ medium	(saprolitic) siltstone	open/close	66.5	chevron	9	hinge:2	none	none	none	--	--	54,11 SW	55 NW
D108.1	2°	--	syncline	thin/ medium	(saprolitic) siltstone	open/close	65	chevron/ box	--	1B/1C	none	none	none	--	--	60,14 SW	45 NW
D109b	2°	36 m	anticline	thick laminated	calc. siltstone	open	88	chevron	31	1B	parallel to axial surface	moderate/ strong	(divergent) -3	+3	+9	55,00	50 NW
D111	2°	36 m	syncline	thin/ medium	silty shale	open	96.5	chevron	9	1B/1C/3	none	none	none	--	--	66,21 SW	52 NW
D111.8	2°	3 m	anticline	thin/ medium	(saprolitic) silty shale	open	102	chevron	15	1B/1C	none	none	none	--	--	64,20 SW	50 NW
D128.9	--	--	anticline	thin	calc. mudstone	close	63	chevron	9	1C	none	none	none	--	--	64,21 SW	42 NW
D131.5	2°	--	anticline	medium	calc. mudstone	open/close	70	chevron	19	hinge:2 limbs:1B/1C	transects axial surface	strong	4	-35	--	65,02 SW	40 NW
D138.1	3°	--	syncline	thin/ medium	interbedded sandstone and shale	open/close	69.5	chevron	--	hinge:1C/2 limbs:1B/1C	none	none	none	--	--	--	75 NW
D128.3	3°	--	anticline	thin/ medium	interbedded sandstone and shale	open	99	chevron	--	hinge:1C/2 limbs:1B/1C	none	none	none	--	--	--	84 NW
D156.7	3°	4 m	anticline	thin/ medium	interbedded sandy sltst. & mudstone	close	59	modified concentric	5	hinge:1C limbs:1B/1C	none	none	none	--	--	66,16 SW	52 SE
D156.9	3°	4 m	syncline	thin/ medium	interbedded sandy sltst. & mudstone	open/close	67.5	chevron	11	hinge:2 limbs:1B/1C	none	none	none	--	--	58,21 SW	54 SE
D157.4	2°	32 m	syncline	thin/ medium	interbedded sandy sltst. & mudstone	open/close	81	chevron	18	hinge:2 limbs:1B/1C	none	none	none	--	--	65,13 SW	46 SE
D158.8	--	2m	paried	thin/ medium	(saprolitic) interbedded ss. and shale	open	88	chevron	--	1B/1C	none	none	none	--	--	47,11 NE	76 NW
D159.6	2°	32 m	anticline	thick	sandstone	close	40.5	chevron	--	--	none	none	none	--	--	--	53 SE
D161.4	3°	--	anticline	thin/ medium	(saprolitic) sandstone	open	112	chevron	7.5	1C/2	parallel to axial surface	strong	12	-7	--	--	80 SE
D161.8	2°	40 m	syncline	thin/ medium	(saprolitic) sandstone	tight	--	--	--	--	--	--	--	--	--	--	48 SE
D164.6	2°	40 m	anticline	thin/ medium	interbedded siltstone & mudstone	gentle	150	chevron	32	1B/1C	none	none	none	--	--	105,02 SW	12 SE
D170.4	2°	--	anticline	medium/ thick	calc. siltstone	close	67	chevron	31	hinge:2 limbs:1B/1C	parallel to axial surface	moderate/	2	-3	--	96,04 SW	46 SE
D174.5	2°	--	syncline	medium	interbedded mudstone & sandstone	open	90	chevron	23	1C	parallel to axial surface	strong	22	+4	--	77,04 SW	56 SE
D178	--	--	anticline	thin/ medium	calc. mudstone	open	109	concentric	≤1.3	1B	none	none	none	--	--	--	--
D181.6	3°	4 m	anticline	--	--	open	78.5	chevron	9	hinge:2 limbs:1C	none	none	none	--	--	--	48 SE
D181.9	3°	4 m	syncline	--	--	open	103	chevron/ modified concentric	3	1C	none	none	none	--	--	--	50 SE
D182.3	2°	--	anticline	thin medium	interbedded mudstone & sandstone	open	97	chevron	--	1B/1C	none	none	none	--	--	93,24 SW	47 SE

TABLE B-2

FOLD PARAMETERS BY LAYER

Section/ Location	Form	Layer	Lithology	Interlimb angle (θ) (degrees)	Cleavage fan angle (γ) (degrees)	Fold flattening strain (R_f) NW limb	Fold flattening strain (R_f) SE limb	Angular deviation of cleavage and X (ϕ_S)	Angular deviation of axial plane and X (ϕ_A)	Profile transection of axial plane by cleavage (d)	Angle between cleavage trace and fold axis (δ)
A15	syncline	1	calcareous mudstone	74	16	--	1.45	+13	0	+13	-9
		2		91	13	∞	2.8	+8	0	+8	-9
		3		93	14	∞	∞	-3	0	-3	-9
		4		98	--	∞	1.44	+7	+10	-3	-9
A19	anticline	1	calcareous mudstone	71	0	1.05	1.6	-22	+20	-42	-4
		2		69	5	--	2.5	-46	--	-46	-4
		3		68	2	∞	1.25	-60	-10	-50	-4
		4		95	1	∞	∞	-39	0	-39	-4
		5		88	-12 (divergent)	1.9	2.1	-46	0	-46	-4
A33.1	syncline	1	calcareous siltstone	83	32	1.18	<1.0	-2.5	0	-2.5	-6
		2		92	35	1.35	<1.0	-1.5	0	-1.5	-6
		3		93	32	2.0	∞	-1	0	-1	-6
		4		93	34	1.65	∞	--	0	--	-6
		5		92	27	1.50	2.8	--	0	--	-6
A64	anticline	1	calcareous siltstone	91	9	>1.0	1.1	+22.5	--	+22.5	-12
		2		92	9	<1.0	1.5	+24.5	--	+24.5	-12
		3		92	1	<1.0	1.2	+25	--	+25	-12
		4		91	--	<1.0	<1.0	--	--	--	-12
		5		89	--	<1.0	>1.0	+10	+10	--	-12
		6		89	7	<1.0	3.0	+17.5	+10	+7.5	-12
		7		86.5	1.5	--	2.7	+8.5	-10	+18	-12
		8		84	0	00	∞	+25	0	+25	-12
		9		69	2	1.27	∞	+37	+10	+37	-12
		10		86	0	1.55	∞	+36	0	+36	-12
B29.8	syncline	1	calcareous siltstone	89	7	∞	2.7	0	0	0	-17
		2		89.5	10.5	1.7	∞	3	0	+3	-17
		3		89	6	2.1	∞	7	+5	+2	-17
		4		91.5	--	3.0	∞	5	+5	--	-17
B30.4	anticline	1	calcareous siltstone	91	2	1.6	∞	11.5	+10	+1.5	-17
		2		89	--	1.3	2.4	11	+5	+6	-17
		3		91	--	∞	1.9	--	0	--	-17
B65	anticline	1	calcareous siltstone	103	62	--	--	--	--	-2.5	--
		2	calcareous mudstone	101	-10 (divergent)	--	--	--	--	+18	--
		3		104.5	16	--	--	--	--	+14	--
		4	calcareous siltstone	107.5	41.5	--	--	--	--	+8.5	--
B91.7	syncline	1	sandy siltstone	78	--	--	1.5	--	--	--	--
		2		76	--	∞	1.58	--	+2	--	--
		3		77	--	1.37	1.72	--	-5	--	--
		4		77	--	∞	2.3	--	0	--	--
		5		74.5	--	∞	2.0	--	0	--	--
C29.3	anticline	1	calcareous siltstone	99	2.5	1.23	<1.0	+13.5	+10	+3.5	+9
		2		112.5	0.5	2.7	1.4	-3	-5	+2	+9
		3		103.5	7	>1.0	∞	+7	+5	+2	+9
		4		107	5	1.15	<1.0	--	--	0	+9
		5		112	3	2.5	--	--	0	--	+9
C36.9	syncline	1	calcareous siltstone	72	24.5	∞	∞	+1	-2.5	+3.5	+3
		2		70	27.5	∞	∞	+10.5	-5	+5.5	+3
		3		68.5	18.5	∞	∞	+0.5	-5.5	+6	+3
D109.6	anticline	1	sandy siltstone	103	0	--	--	--	--	0	+9
		2		102	0	--	--	--	--	+1	+9
		3		89.5	0	--	--	--	--	+3	+9
		4		84.5	0	--	--	+2	0	+2	+9
		5		80	0	--	--	+3.5	+2	+1.5	+9
		6		80.5	0	--	--	+3	+2	+1	+9
		7		82.5	0	--	--	--	--	+1.5	+9

APPENDIX C

GRAPHIC METHOD OF DETERMINATION OF BRITTLE DEFORMATION AXES FROM FAULT ATTITUDES (AFTER ARTHAUD, 1969)

Arthaud's method of describing the geometry of deformation defines the maximum, minimum and intermediate elongation directions for a population of measured fault attitudes. His analogy with experimental fractures (Goguel, 1942), groups the faults into sets of conjugate shear, with each conjugate pair forming a dihedron. The bisectors of the dihedral angles are the maximum and minimum principal axes of deformation. The intersection of the two planes of the dihedron represents the intermediate axis. By analogy with the strain ellipsoid defined for continuous deformation (principal axes: λ_1, λ_2, and λ_3), the principal directions of brittle deformation are as follows (Figure C-1a):

X: direction of principal elongation; length is augmented.
Z: direction of principal shortening (normal to X); length is diminished.
Y: intermediate principal direction (normal to both X and Z);

A detailed outline of steps for using Arthaud's method (with stereonet) follows:

1. Find the plane (m) that is perpendicular to the fault and contains the striation direction (Figure C-1b):

a. Plot the pole of the fault plane and the piercing point of the trace of the striation on the fault plane.
b. The pole of the fault plane and the piercing point of the trace of the striation are rotated to a great circle that is the trace of the m plane from which the m pole is determined.

2. The above operations are repeated for each fault, until a distribution of the m poles is obtained.
3. Plot approximate great circle about which the m poles lie.
4. Locate the pole of one of these great circles (or the intersection of m planes); the pole corresponds to a principal axis of deformation (Figure C-1c). The other two principal axes of deformation for the conjugate faults lie within the plane defined by the same great circle. All of these principal axes are normal to one another.
5. Using the sense of movement indicated by the striations (the arrow on each striation indicates the motion of the upper block), one can determine the relative positions of the directions of principal elongation and shortening as well as the intermediate direction.

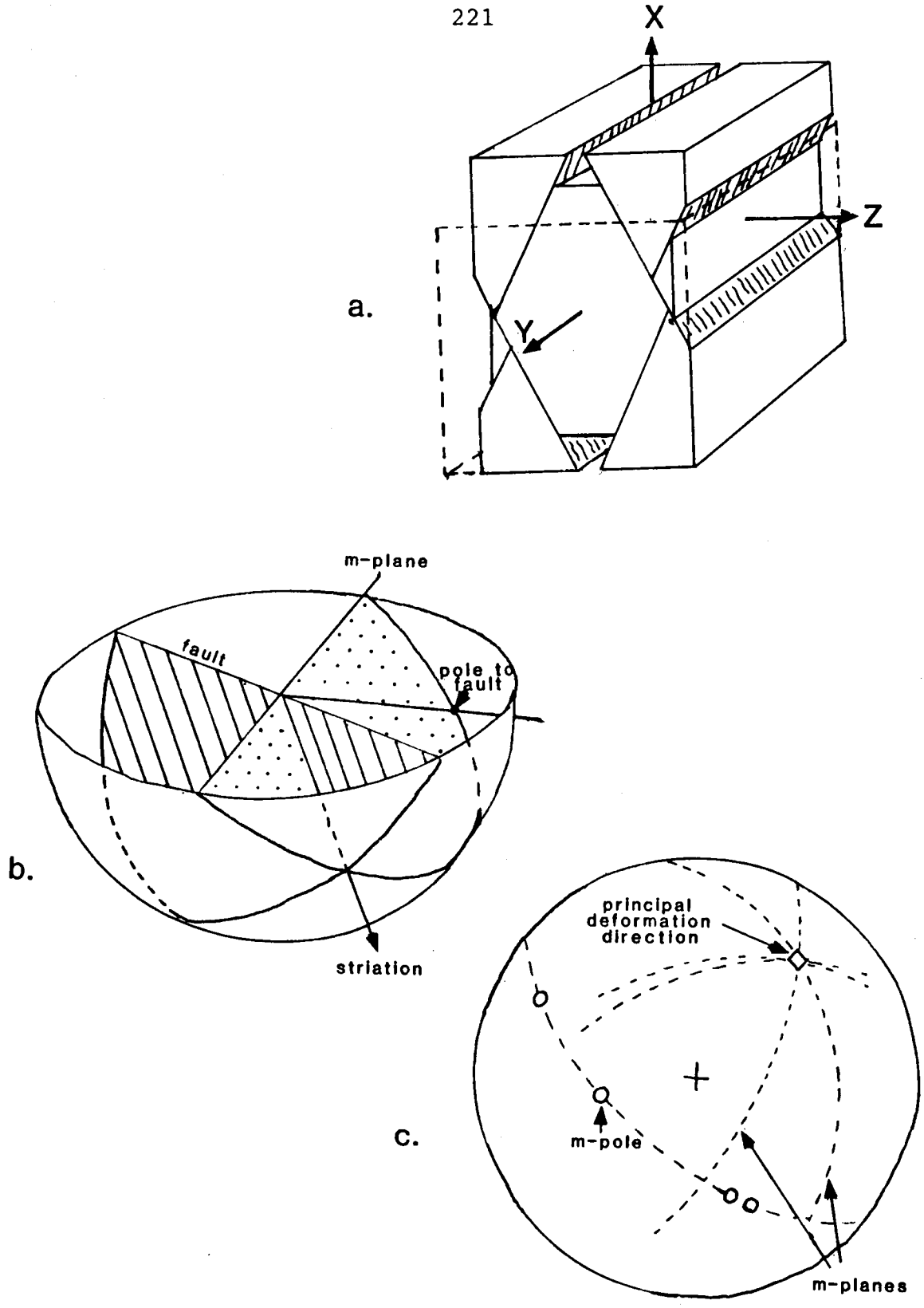

Figure C-1. Arthaud method of determination of brittle deformation axes.

APPENDIX D

ACCURACY OF PHOTOMOSAICS

Parallax causes distortion in each photograph, particularly if the outcrop is not precisely normal to strike. Considerable overlap of successive photographs helped alleviate the problem of parallax by making it possible to use only the middle (least distorted portion) of each photograph. The measuring of the four profile sections (evident as the numbering of 20 meter intervals) is accurate certainly to within 5 percent. Varying distance between the camera and the shoreline exposures results in varying scales on the photomosaics (apparent on Plates 1-4, in back pocket).

APPENDIX E

MAP OF PREVIOUS WORK LOCATIONS

Figure E-1 delineates the field areas of nearby and overlapping M.S. theses and Ph.D. dissertations performed at The University of Tennessee, Knoxville, between 1956 and the present. Stratigraphy and structure were investigated by Bumgarner (1956), Greene (1959), Feder (1963) and Marie (1963). Troensegaard (1965), Hatcher (1965), and Yust (1976) concentrated on structural analysis, while Shanmugam's investigation was primarily sedimentologic. The geographic relations between these previous studies and the present investigation are apparent from the map (Figure E-1).

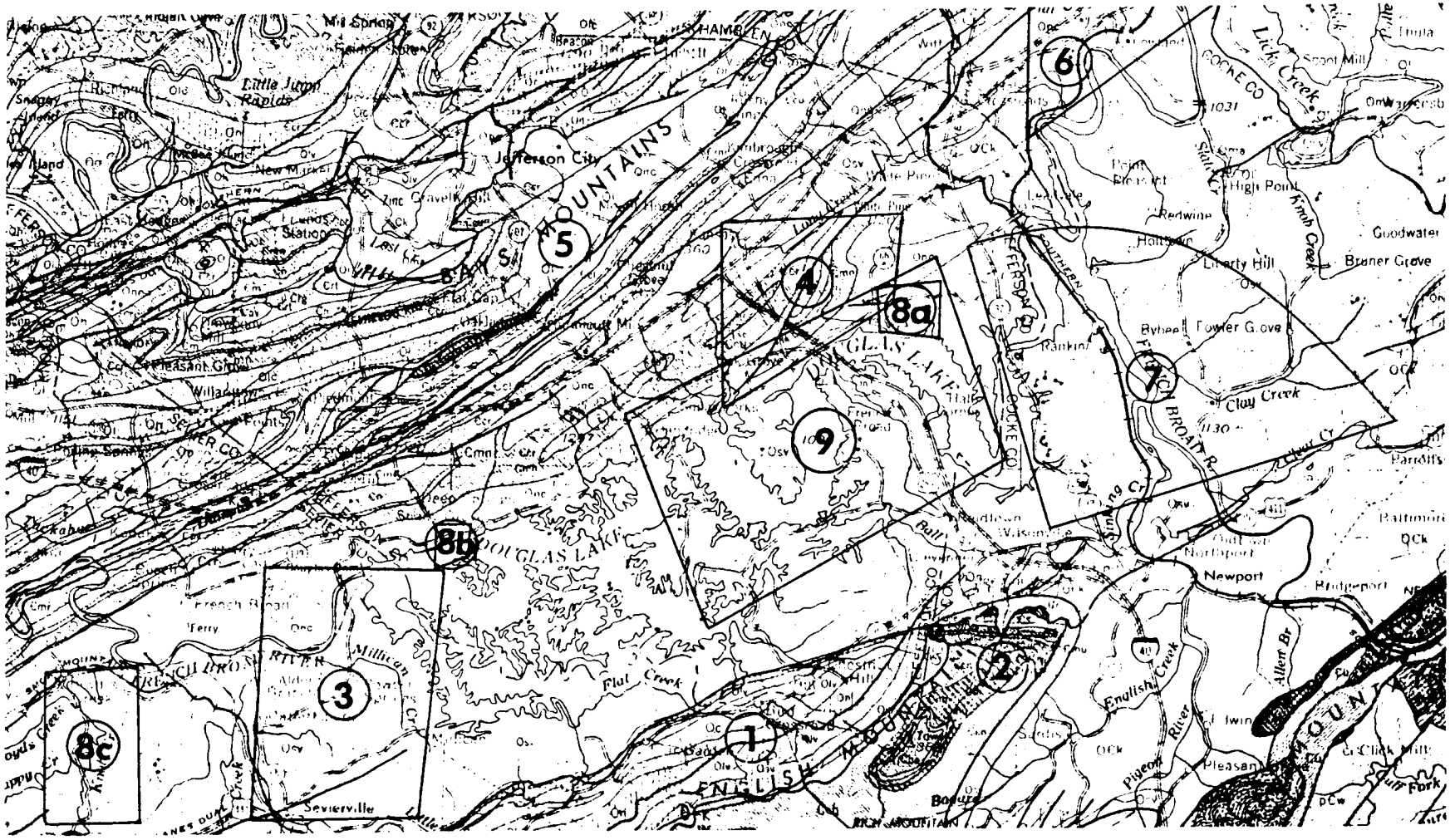

Figure E-1. Map of previous work locations. (1) Bumgarner (1959, M.S.); (2) Greene (1959, M.S.); (3) Marie (1963, M.S.); (4) Feder (1963, M.S.); (5) Hatcher (1965, Ph.D.); (6) Troensegaard (1965, M.S.); (7) Yust (1976, M.S.); (8a, 8b, 8c) Shanmugam (1978, Ph.D.); (9) area of present study.

APPENDIX F

ADJACENT STRATIGRAPHIC SECTION (SHANMUGAM, 1978)

A detailed stratigraphic section, adjacent to Section A of this report, was measured and described by Shanmugam (1978). It is located in an embayment of Douglas Lake 1.3 km northeast of Section A at the base (northwest end) of the section. In the southeast it converges toward and merges with Section A on the main channel of the French Broad River (Douglas Lake). Shanmugam's section begins at the base of the lowest Middle Ordovician formation, the Lenoir limestone. The section measures a total of 390 meters of carbonates (Lenoir and Whitesburg) and clastics (Blockhouse and Sevier), before being terminated due to small-scale faulting to the southeast. Shanmugam's units 6, 7, 8, and 9 correspond, respectively, to units A-1 (Blockhouse), A-2, A-3, and A-4 (each of Sevier) of Section A.

Shanmugam's (1978) Section

Unit No.	Unit Thick. (m)	Cum. Thick. (m)	Descriptions
			LENOIR FORMATION
1	21.03	21.03	Alternating sequence of medium to very thick bedded, medium gray to medium light gray dolostones and micritic limestones. Vertical and horizontal

Unit No.	Unit Thick. (m)	Cum. Thick. (m)	Descriptions
			burrows rare in dolostones. In dolostones, 1-3 cm thick and several cm long contorted limestone layers suggest soft sediment deformation. In the lower part of this unit, limestone beds have stylolites (5-10 mm thick pressure-solution surfaces) parallel and perpendicular to bedding. Rare dolostone lenses with limestone beds. Birdseye structures are common in limestones, and their abundance increases upward within the unit. Based on presence of birdseyes, this unit may be classified as Mosheim Member. Dark gray chert nodules are rare. Dark gray chert layers 2-3 cm thick occasionally intervenes dolostone and limestone beds.
2	20.26	41.29	Mosheim Member: Very thick bedded, medium light gray, micritic limestones. Birdseye structures are very abundant in the upper 12 meters of this unit. Characteristic fluted appearance due to weathering. Rare stylolites parallel to bedding. Rare argillaceous layers several cm thick. Weathering of argillaceous layers provides nodular appearance in the middle part of this unit. Rare gastropods.
3	7.00	48.29	Main body: Sharp basal contact. Nodular medium to thick bedded, medium dark gray, fine to coarse grained limestones. Lower part of this unit is composed of argillaceous limestones, and calcarenite beds constitute the upper part. Brachiopods, gastropods, trilobites, algae Allosaccus common. Characteristic alternation of argillaceous layers and limestone (calcarenite) beds in the upper 2 meters of this unit; contorted limestone layers due to soft sediment deformation.

Unit No.	Unit Thick. (m)	Cum. Thick. (m)	Descriptions
			WHITESBURG FORMATION
4	2.85	51.14	Sharp basal contact. Thick bedded, medium dark gray, coarse grained cephalopod rich pelmatazoan calcarenite with intervening shale layers of a few cm thick.
5	26.40	77.54	Characteristic alternation of dark gray, flaggy, pebbly-limestone and light gray, calcareous, clayey shale. Commonly, the limestones contain dark projected clasts on bedding surfaces. Upward increase in size and amount of these clasts within a bed are common, and thus inversely graded. Floating of clasts in a muddy matrix, and planar fabric common. Well preserved graptolites in three dimensions on bedding surfaces. Thickness of individual limestone beds diminishes upward within the unit, while the intervening shale thickness increases. Shales are rich in graptolites. Rare lingulid brachiopods.
			BLOCKHOUSE FORMATION
6	36.00	113.54	Gradational to sharp basal contact. Thinly laminated, fissile, calcareous, clayey shale. Weathers to pale yellowish orange, thin, 0.5 to 1 cm long chips. Abundant graptolites. Rare brachiopod debris.
			SEVIER FORMATION
7	144.0	257.54	Sharp basal contact. Thin bedded, olive gray, calcareous, silty shale. Weathers to yellowish gray 2-3 cm long chips. Minor increase in bed thickness towards the top of this unit.

Unit No.	Unit Thick. (m)	Cum. Thick. (m)	Descriptions
8	25.20	282.74	Cyclic alternation of resistant, calcareous, light gray, silty shale (siltstones) and nonresistant, calcareous, clayey shale. Siltstone beds of 5-10 cm thick, are uniform and laterally continuous. Bouma C, D, E divisions in siltstone beds. This sequence resembles more of a shaly flysch in outcrops.
9	108.00	390.74	Very thin to medium bedded, medium dark gray, calcareous silty shale. Multiple thinning upward cycles common. Fragments of trilobites, graptolites, brachiopods are common. Rare uncertain sole marks and horizontal burrows, Planolites.

APPENDIX G

INDEPENDENT FOLD PARAMETERS

The following appendix is a collection of graphs of fold parameter data, which are not included in Chapter 3. The reason for the exclusion of these plots from the text is the lack of apparent dependent relationships between the parameters being compared. Figures G-1 and G-2 compare noncleavage fold parameters lacking dependent relationships. The succeeding 7 graphs (Figures G-3 through G-9) are referred to in the text of Chapter 3. Figures G-3 through G-8 compare cleavage with other fold parameters. The lack of dependent relationships in some of these cases may suggest folding/flattening/ cleavage timing relationships and mechanisms. Figures G-1, G-2, and G-9 do not appear to similarly suggest anything about relative timing of strain increments during deformation.

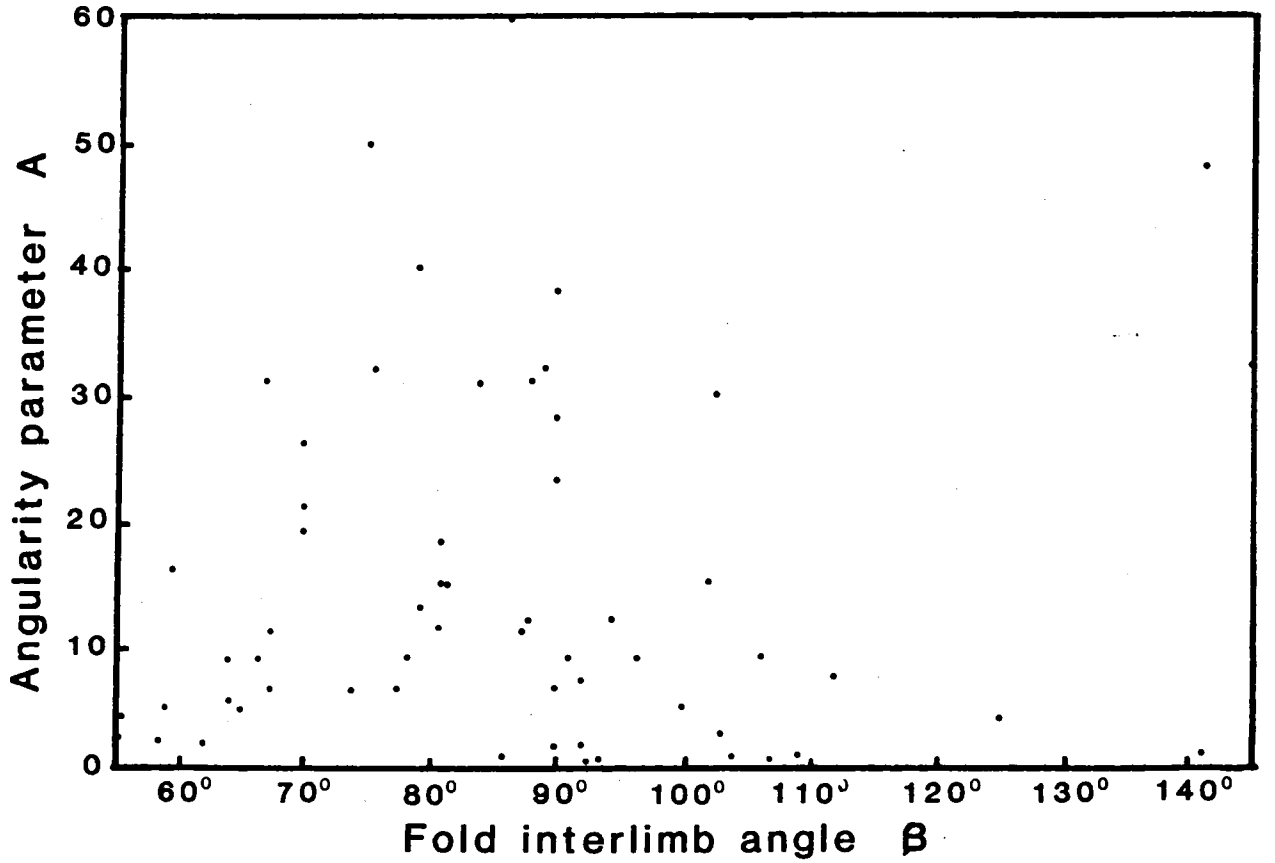

Figure G-1. Angularity parameter A versus fold interlimb angle β. Hinge angularity (A) is determined to be independent of fold tightness (β) for 61 measured folds in the Sevier formation.

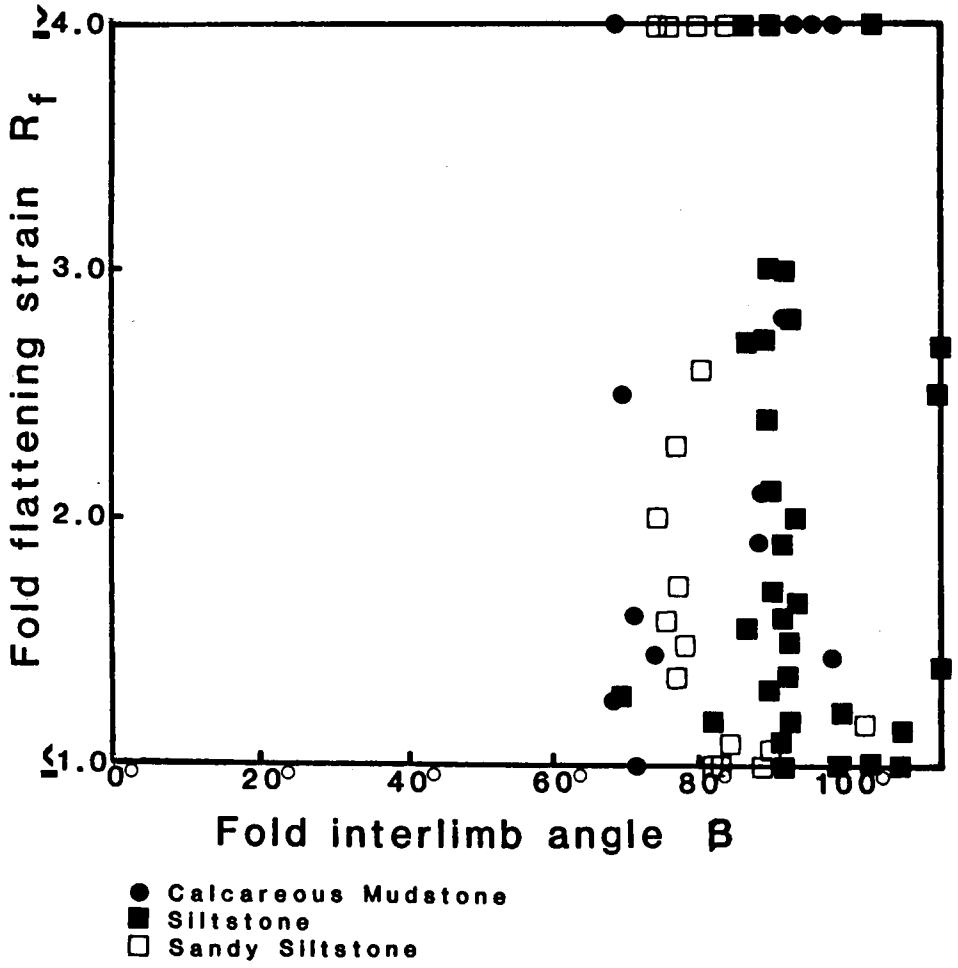

Figure G-2. Fold flattening strain ratio R_f versus fold interlimb angle β. Graph implies that fold tightness is not influenced by fold flattening. This may be because only very minimal flattening has affected most folds. The increased tightness (smaller β) of folds in the coarse sandy siltstone lithology is due to the fact that this lithology occurs only towards the middle of the shale belt where folds are tighter than in the northwest. Data for 63 folded layers (10 folds).

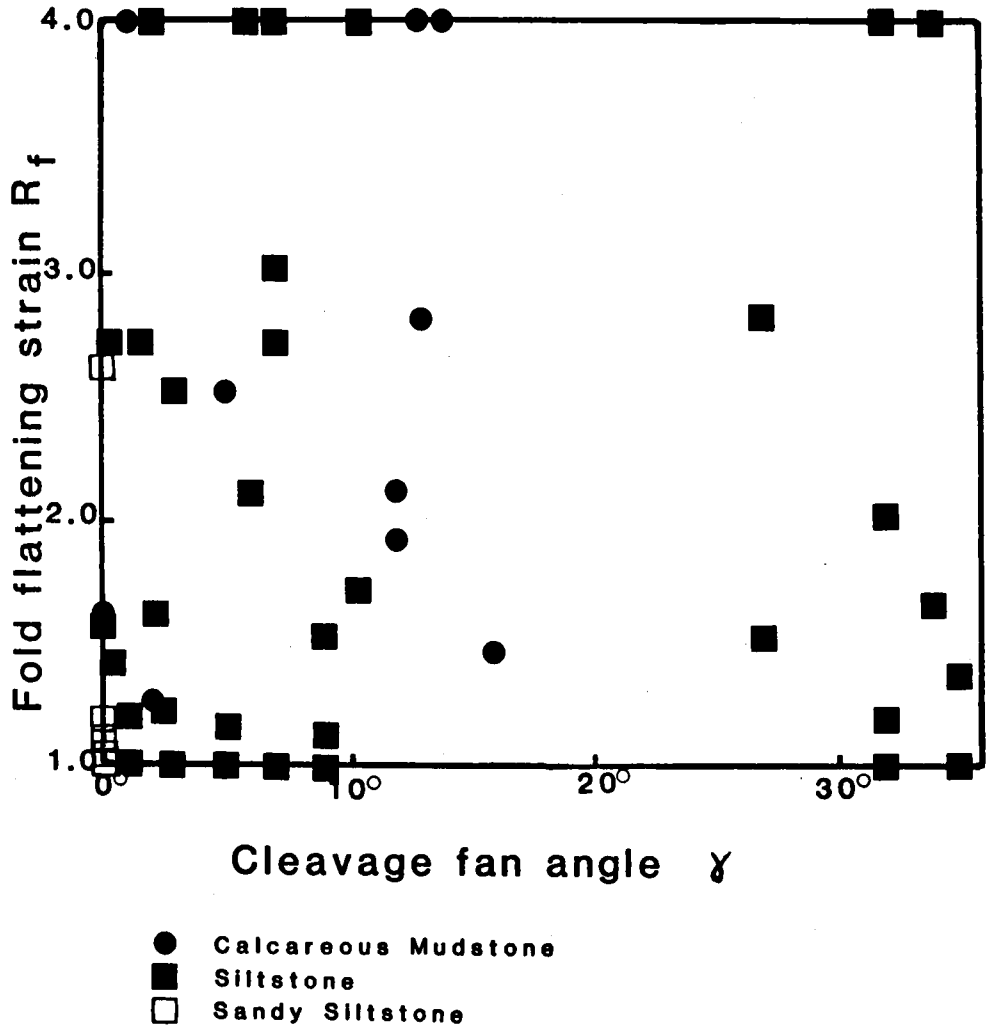

Figure G-3. Fold flattening strain R_f versus cleavage fan angle γ. Fan angle is not influenced by flattening strain, implying either that flattening has been minimal (and its effects on fan angle are not detectable) or that cleavage development postdates flattening strain. Fan angles are larger in the siltstone lithology, suggesting possibly more refraction than in the less competent, fine-grained mudstone. Only one cleaved fold was observed in sandy siltstone, and this is not considered to be a representative sample for this lithology. Data for 50 folded layers (10 folds).

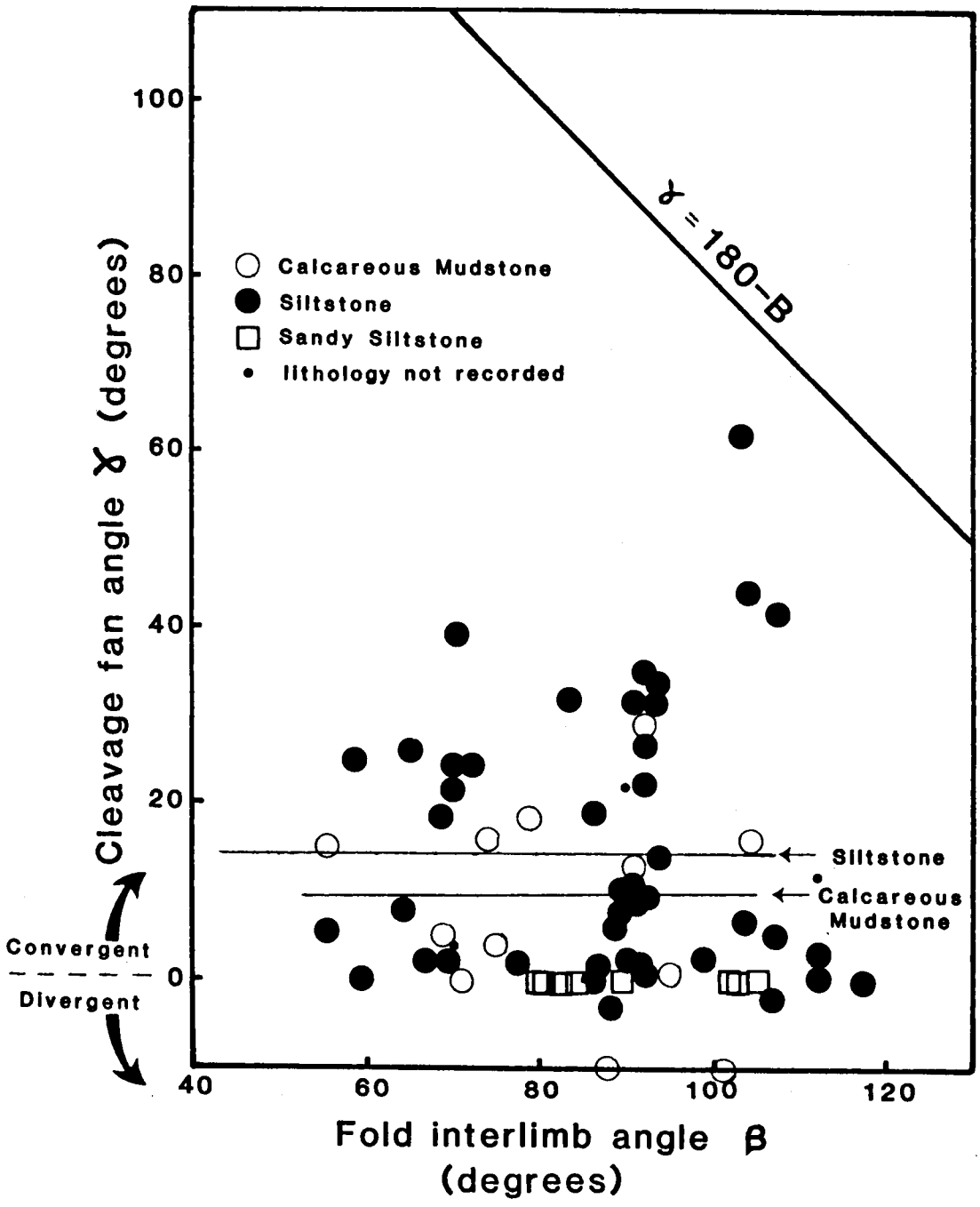

Figure G-4. Cleavage fan angle γ versus fold interlimb angle β. Fan angle is independent of fold tightness. A slightly larger mean fan angle is present for folds in siltstone (γ = 15 degrees) than for those in mudstone (γ = 10 degrees), suggesting greater cleavage refraction in more competent lithologies. Data for 66 folds.

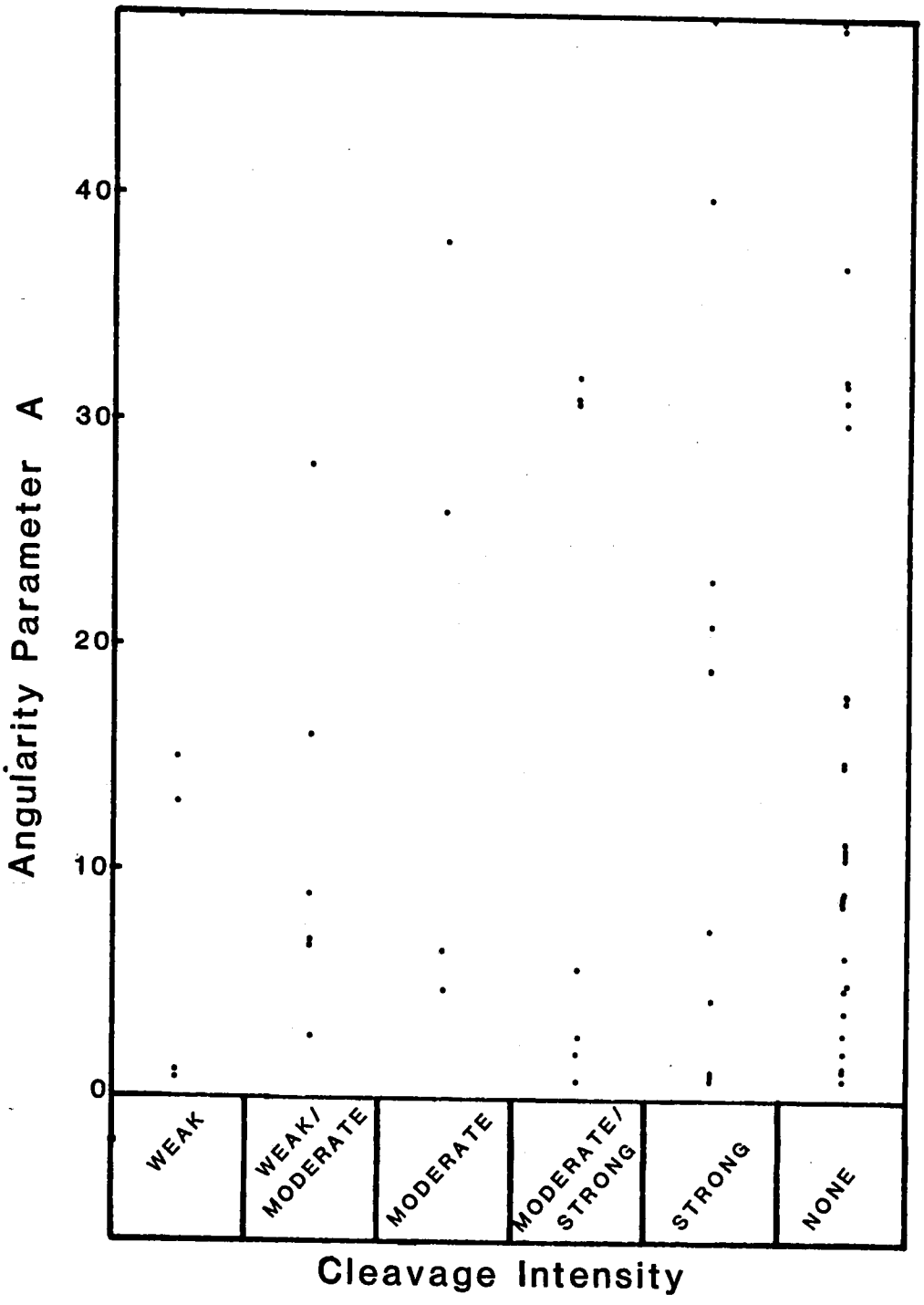

Figure G-5. Angularity parameter A versus cleavage intensity. Hinge angularity and cleavage intensity are independent parameters. Data for 59 folds.

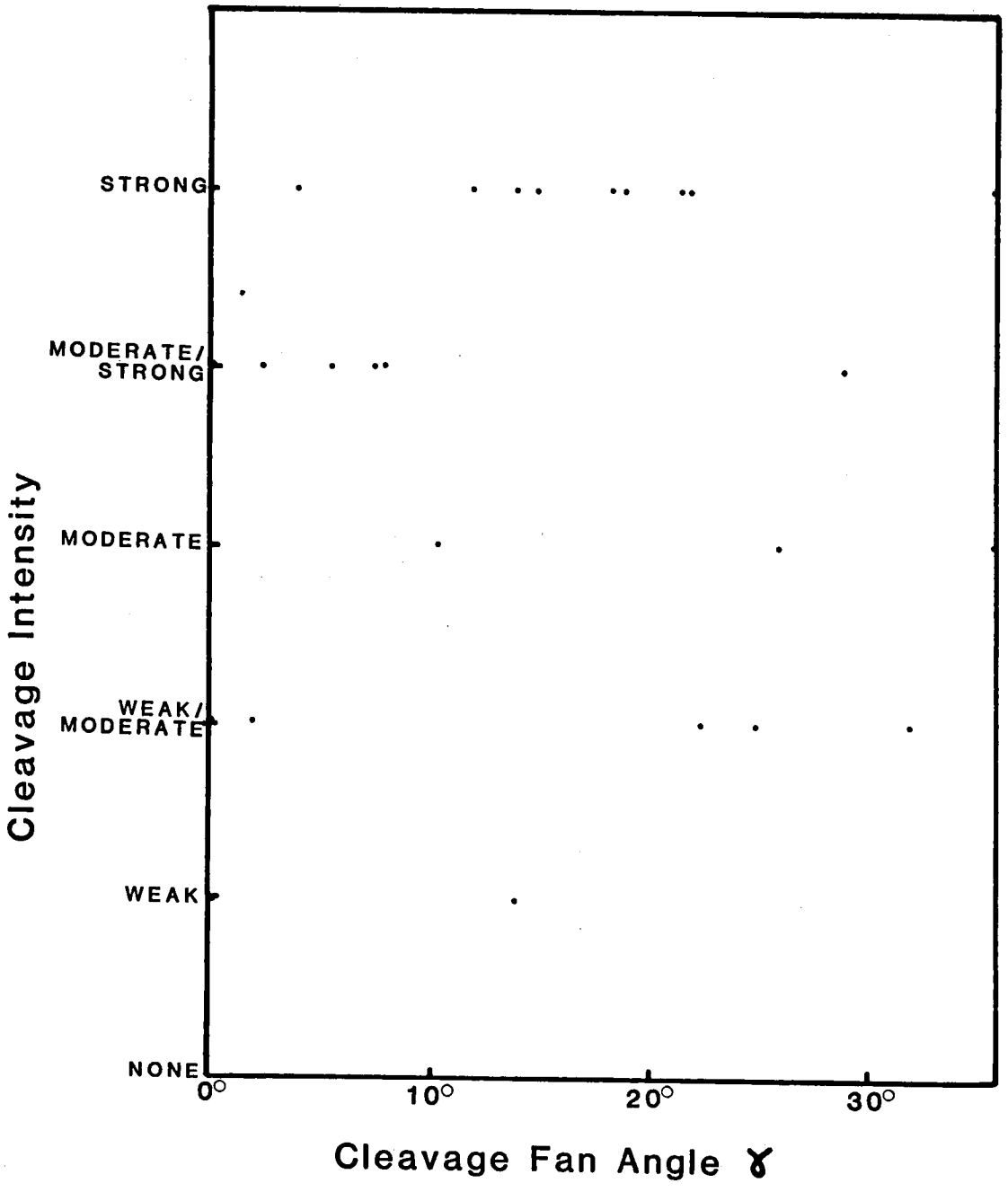

Figure G-6. Cleavage intensity versus cleavage fan angle γ. Cleavage intensity and fan angle are independent parameters. Data for 28 folds.

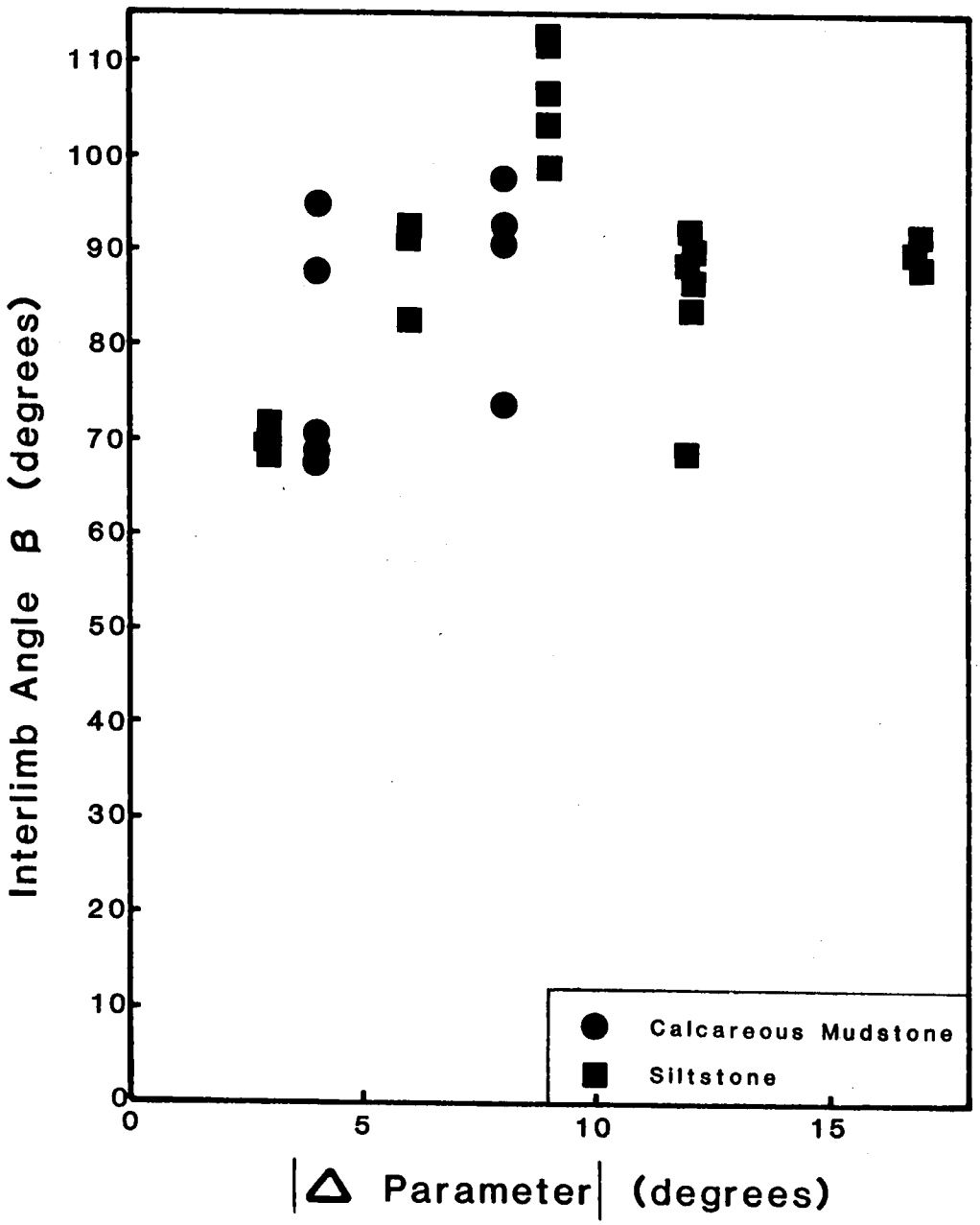

Figure G-7. Interlimb angle β versus transection parameter Δ. The magnitude of Δ is either independent of fold tightness, or it decreases very slightly with tighter folding (smaller β). Larger Δ values in siltstones may suggest refraction of cleavage strike in more competent lithologies. Data for 30 folds.

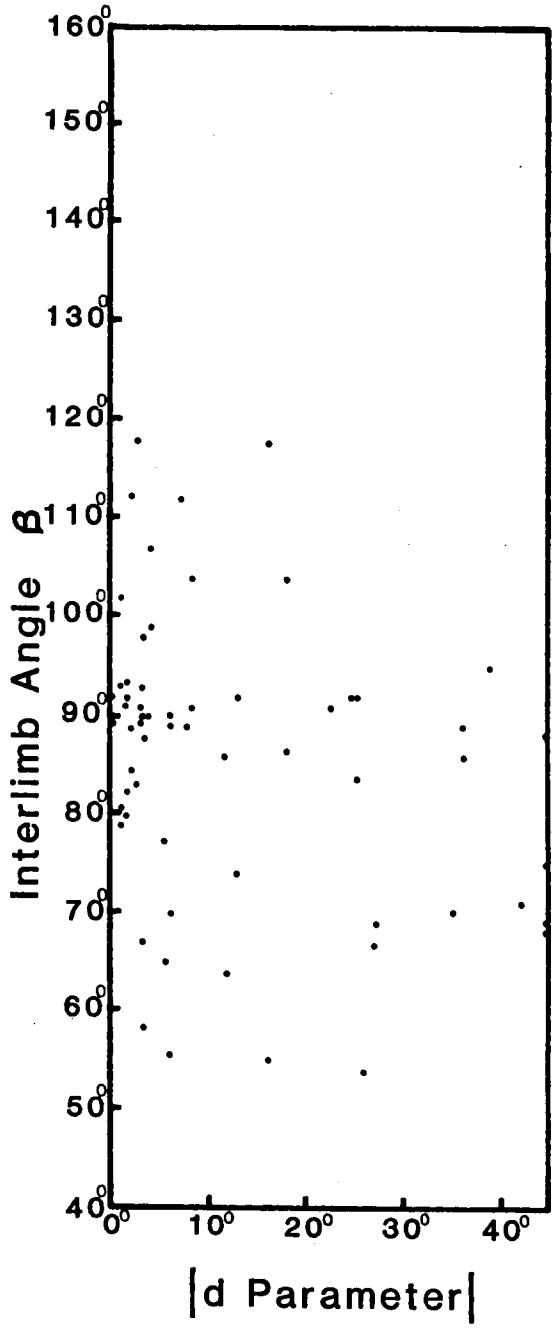

Figure G-8. Interlimb angle β versus transection parameter d. The magnitude of d is not influenced by fold tightness. This implies that cleavage transection develops either as a late synfolding or postfolding episode. Data for 29 folds.

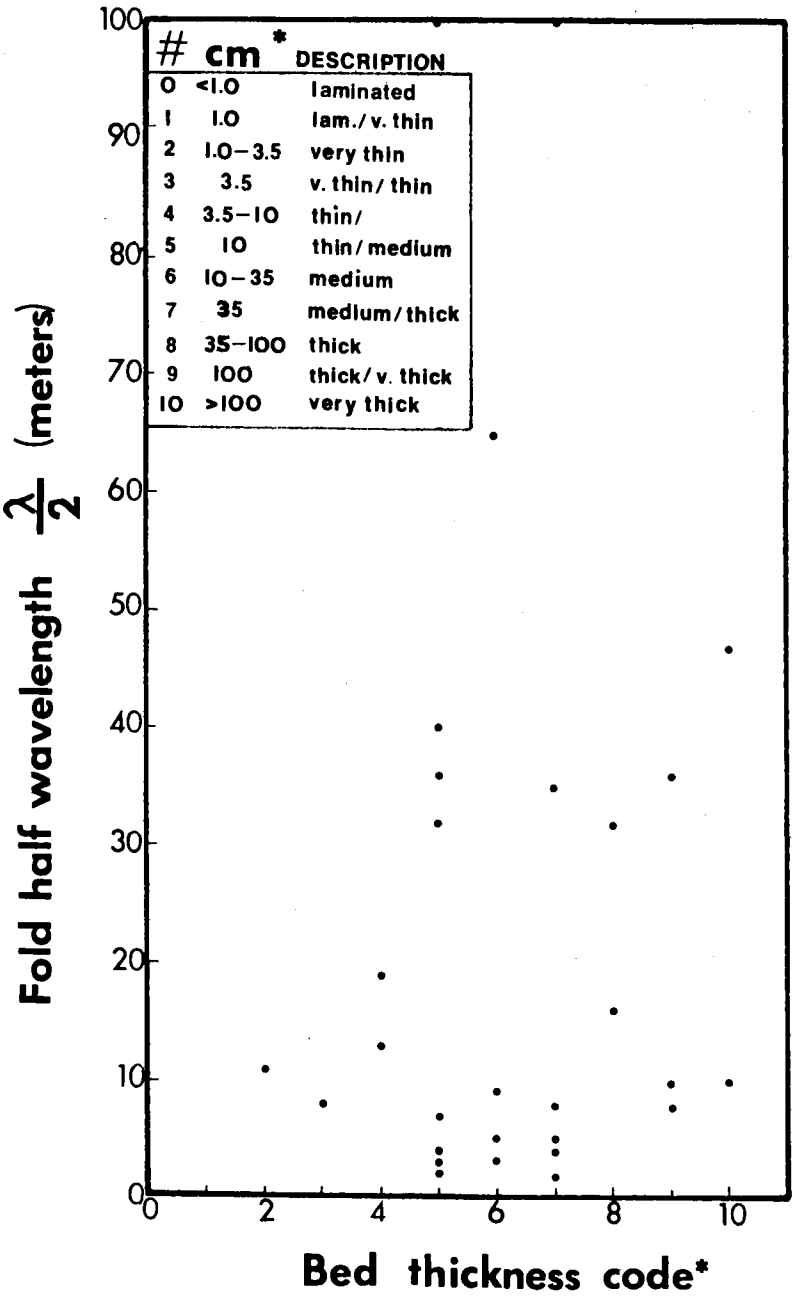

Figure G-9. Fold half-wavelength $\lambda/2$ versus bed thickness. Bed thickness does not influence fold half-wavelength. Data for 29 folds.

VITA

John Hills Weitz, Jr., was born in Cleveland, Ohio on May 12, 1957. He attended elementary school, junior high school and two years of high school in Rocky River, Ohio and was graduated from Western Reserve Academy in June 1975. The following September he entered Bucknell University in Lewisburg, Pennsylvania, and in May 1979 he received a Bachelor of Science degree in Geology. In the fall of 1979 he entered the Graduate School of The University of Tennessee, Knoxville and began study toward a Master of Science degree. This degree was awarded in March 1983.

The author is a member of Sigma Gamma Epsilon, the Geological Society of America, and the American Association of Petroleum Geologists. He coauthored and presented an abstract at the 95th Annual Meeting of the Geological Society of America in New Orleans in October, 1982 (Conway, C. D., and Weitz, J. H., Jr., 1982, Mesoscopic analysis of the Middle Ordovician Tellico-Sevier shale belts in east Tennessee, Saltville and Pulaski thrust sheets: Geological Society of America Abstracts with Programs, v. 14, no. 7, p. 466, August 1982). Mr. Weitz resides in New Orleans, Louisiana, and he is employed with the Geological Department of the Onshore Division of Texaco, U.S.A.

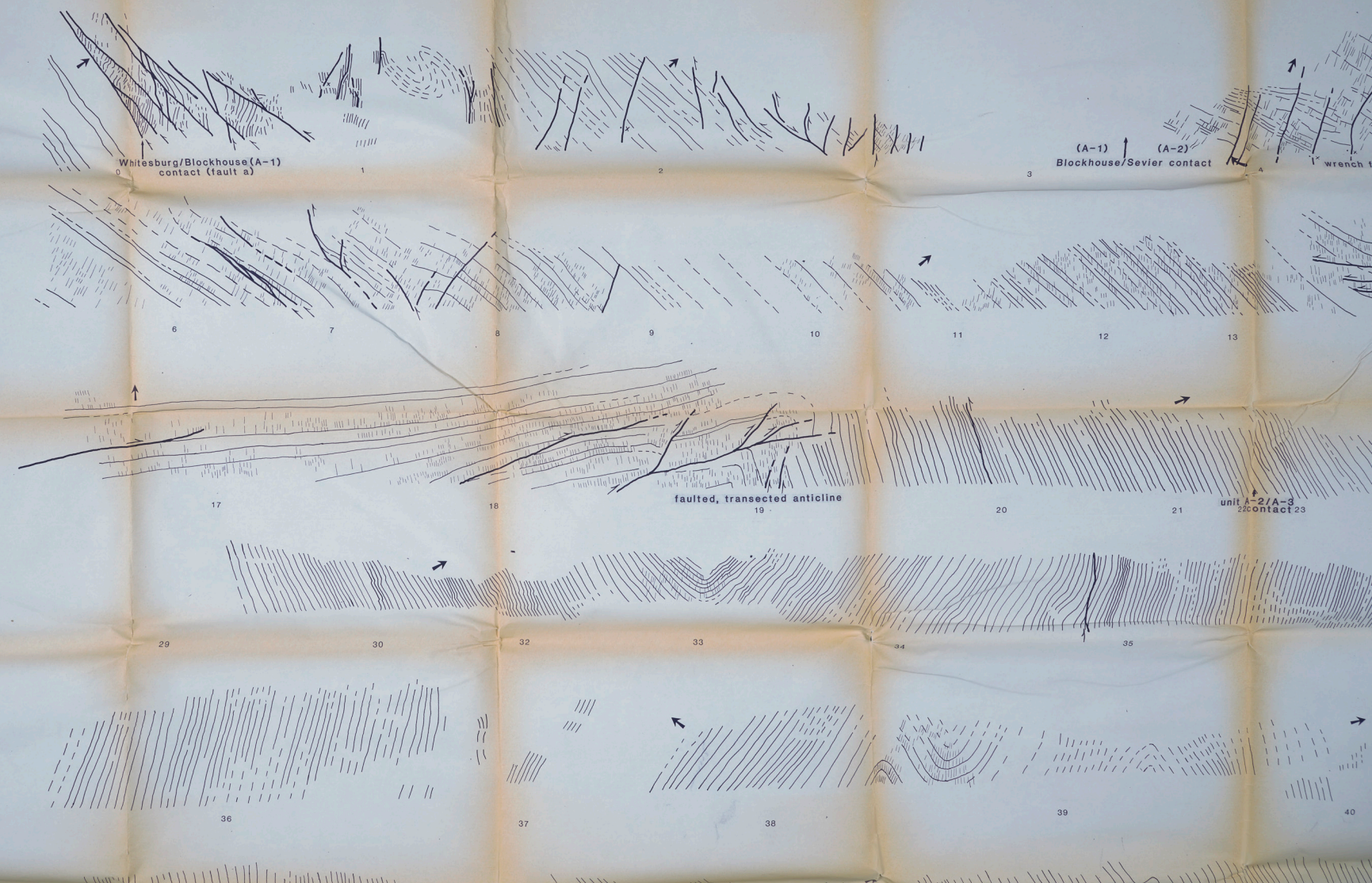
NW
Whitesburg/Blockhouse (A-1) contact (fault a)
(A-1)
(A-2)
Blockhouse/Sevier contact
wrench f
faulted, transected anticline
unit A-2/A-3 contact

PLATE 1

SECTION A

SE

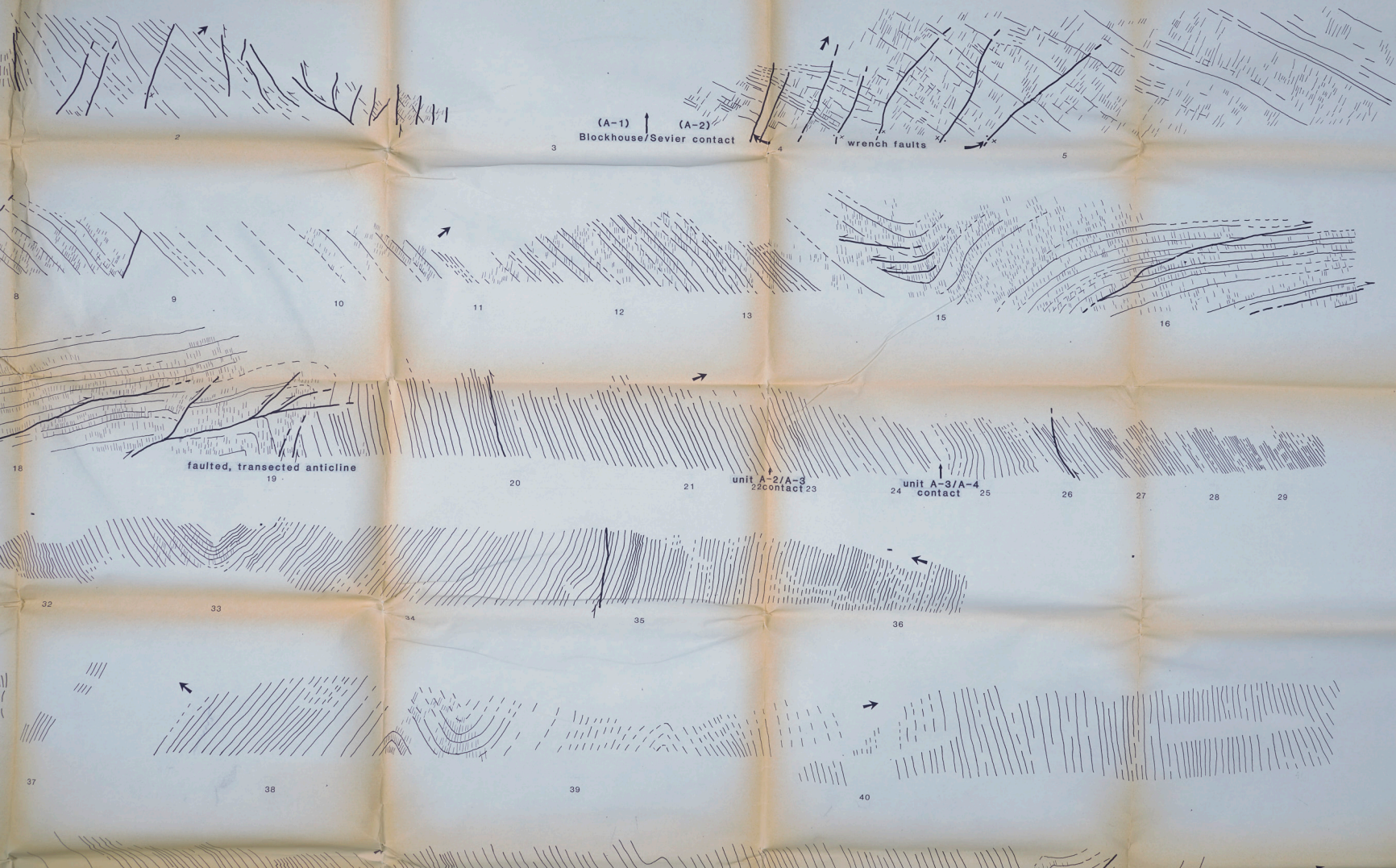


29
30
34
35
36
37
38
39
40
41
42
43
44
45
46
47
50
51
52
top of exposed
unit A-4
53
64
transecting cleavage
is offset by fault
65
66
69
70
unit A-7/A-8
71 contact
74
75
76
77

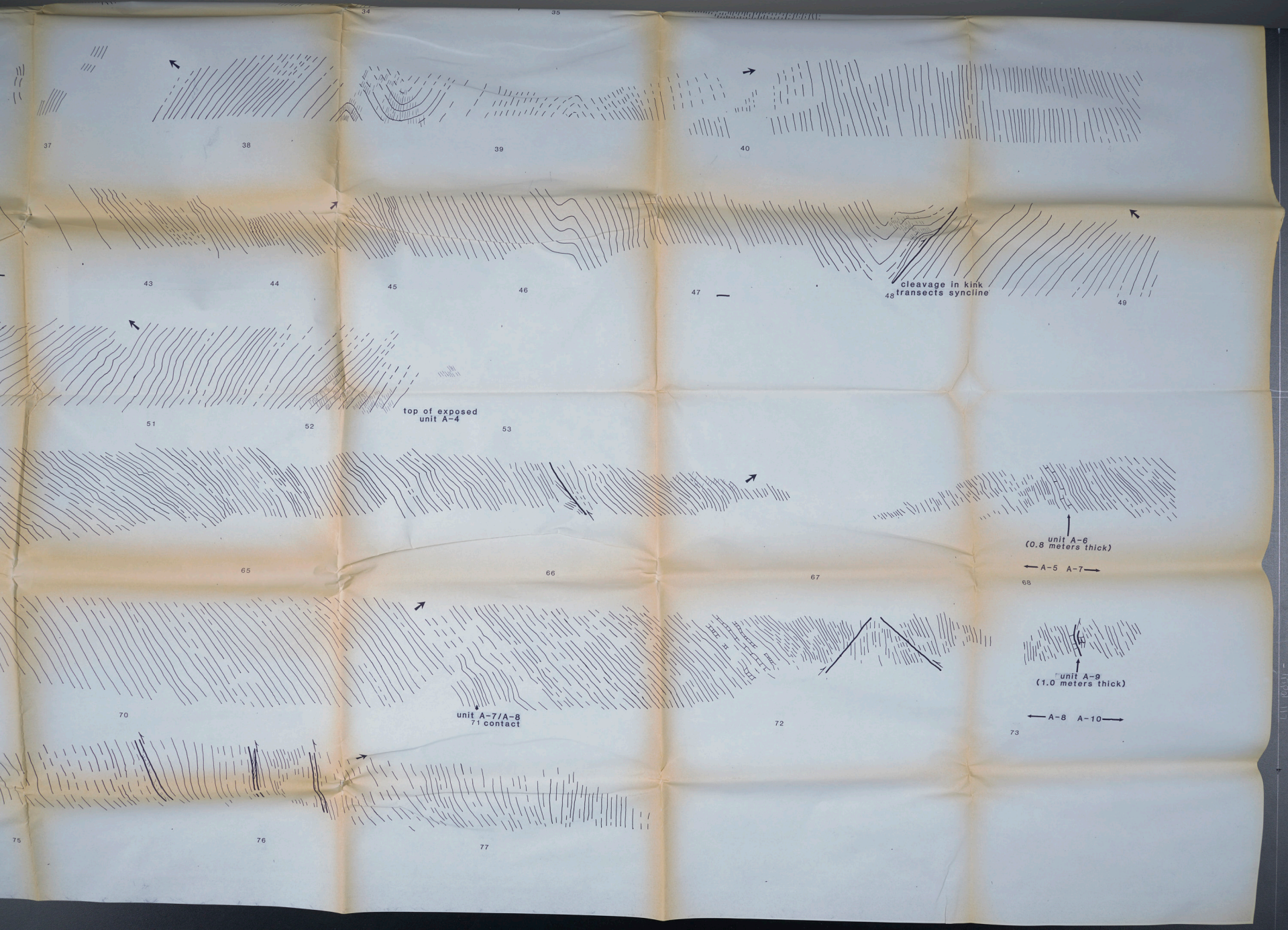
34
35
37
38
39
40
43
44
45
46
47
48
49
cleavage in kink
transects syncline
51
52
top of exposed
unit A-4
53
65
66
67
unit A-6
(0.8 meters thick)
A-5
A-7
68
70
unit A-7/A-8
71 contact
72
unit A-9
(1.0 meters thick)
A-8
A-10
73
75
76
77

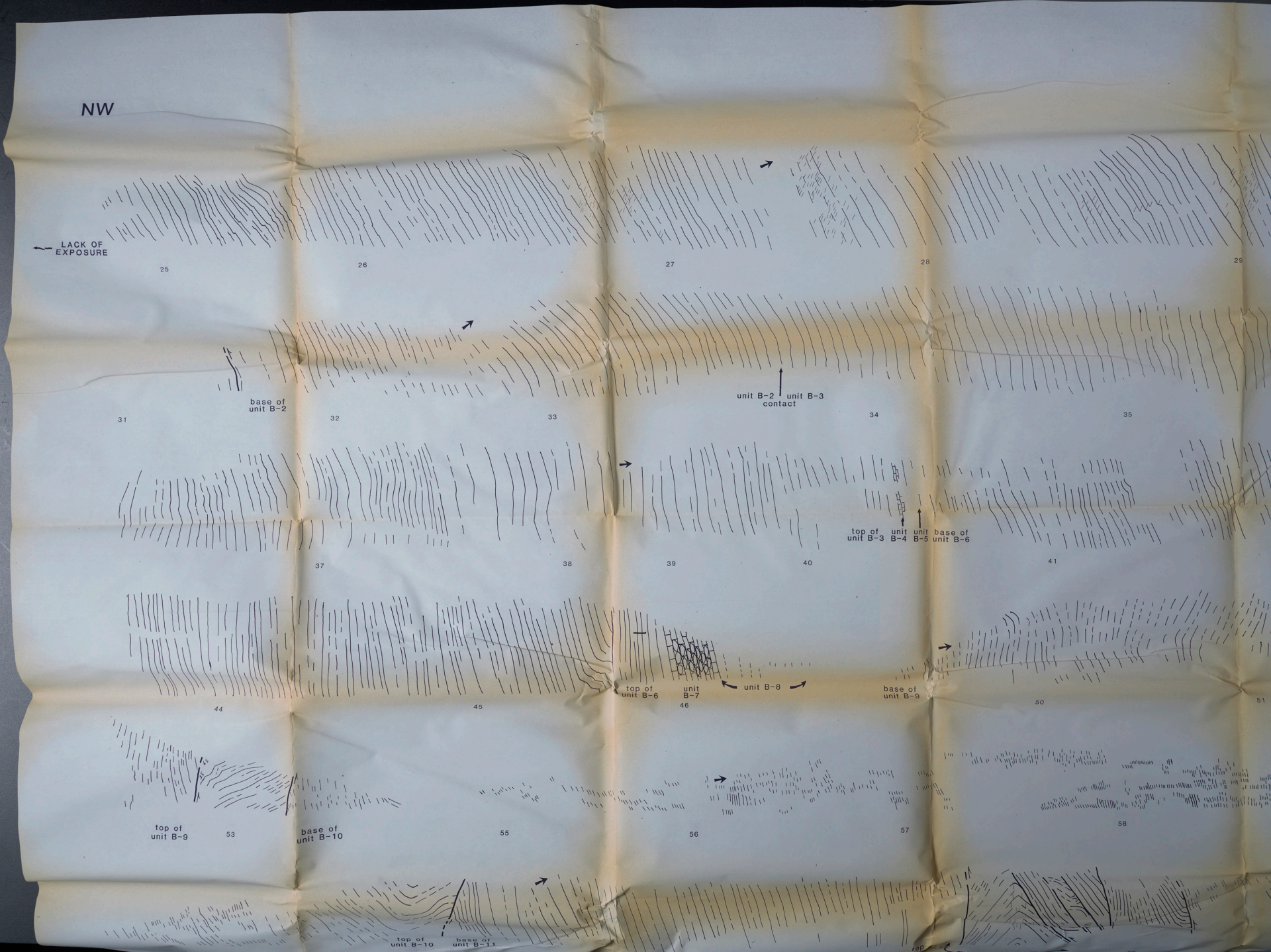
NW
LACK OF EXPOSURE
25
26
27
28
29
base of unit B-2
31
32
33
unit B-2 unit B-3 contact
34
35
37
38
39
40
top of unit B-3
unit B-4
unit B-5
base of unit B-6
41
44
45
top of unit B-6
unit B-7
46
unit B-8
base of unit B-9
50
51
top of unit B-9
53
base of unit B-10
55
56
57
58
top of unit B-10
base of unit B-11

PLATE 2

SECTION B

SE

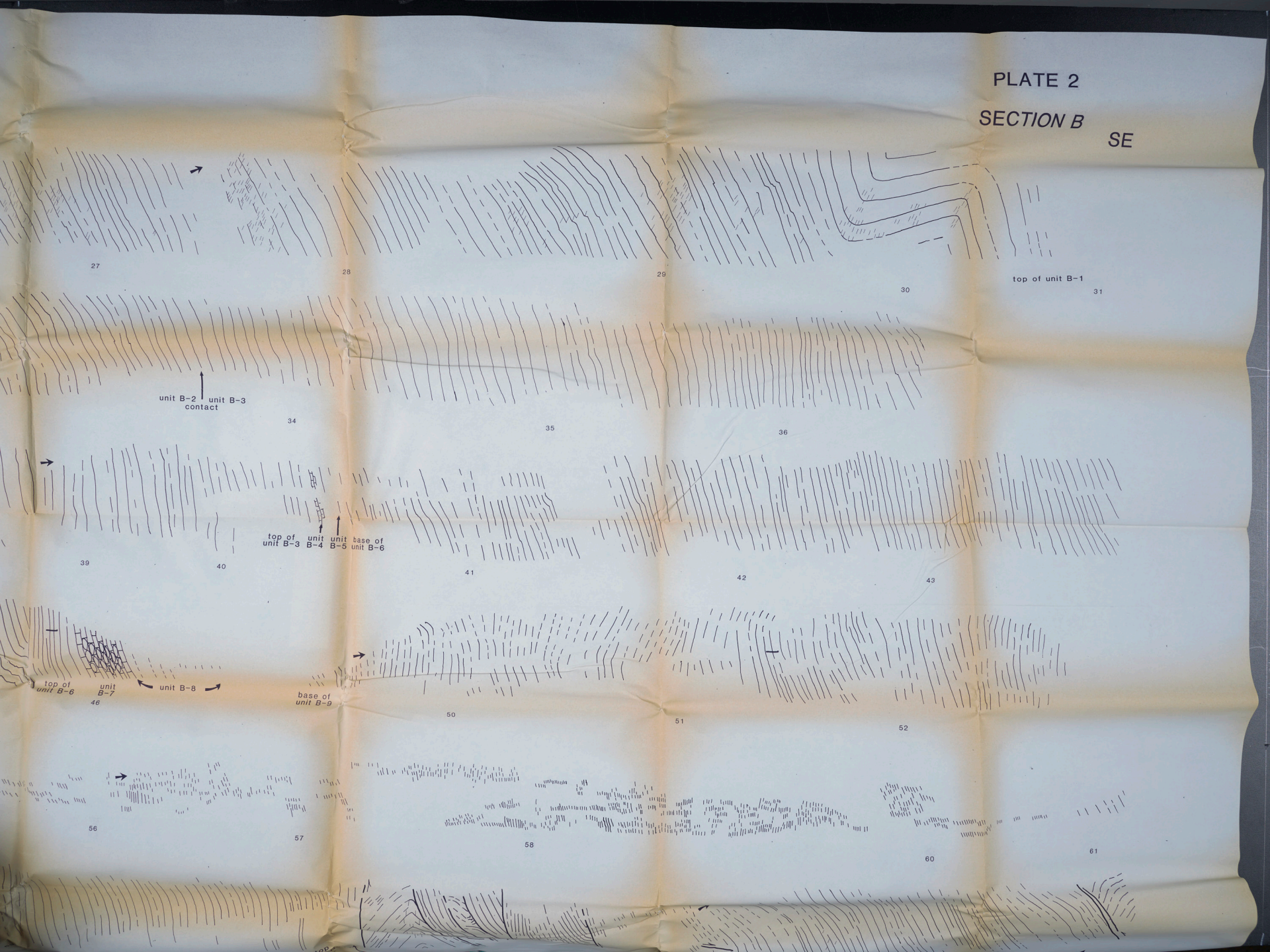

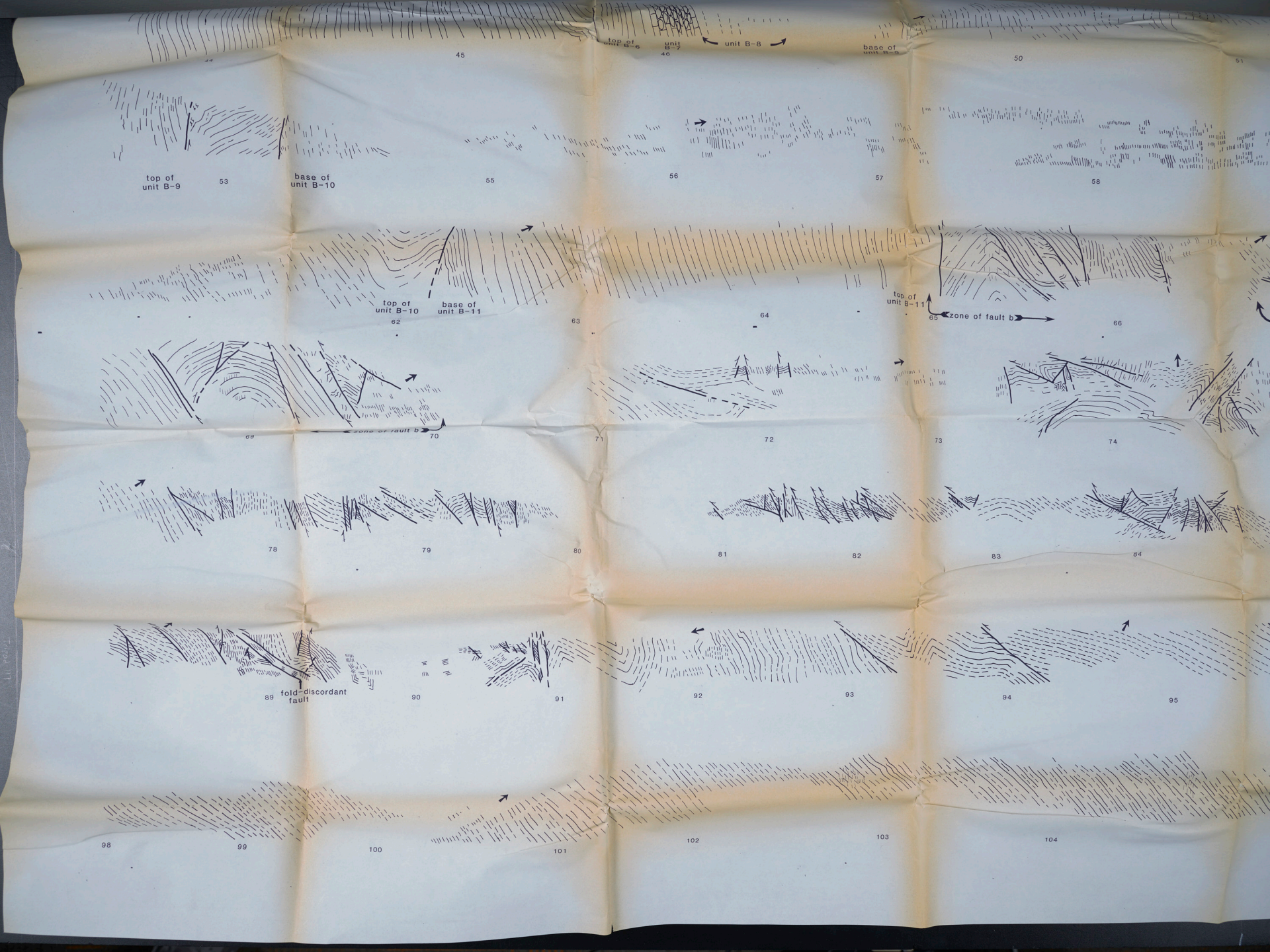
top of unit B-6
unit B-7
unit B-8
base of unit B-8
45
46
50
51
top of unit B-9
53
base of unit B-10
55
56
57
58
top of unit B-10
base of unit B-11
62
63
64
top of unit B-11
65
zone of fault b
66
69
zone of fault b
70
71
72
73
74
78
79
80
81
82
83
84
fold-discordant fault
89
90
91
92
93
94
95
98
99
100
101
102
103
104

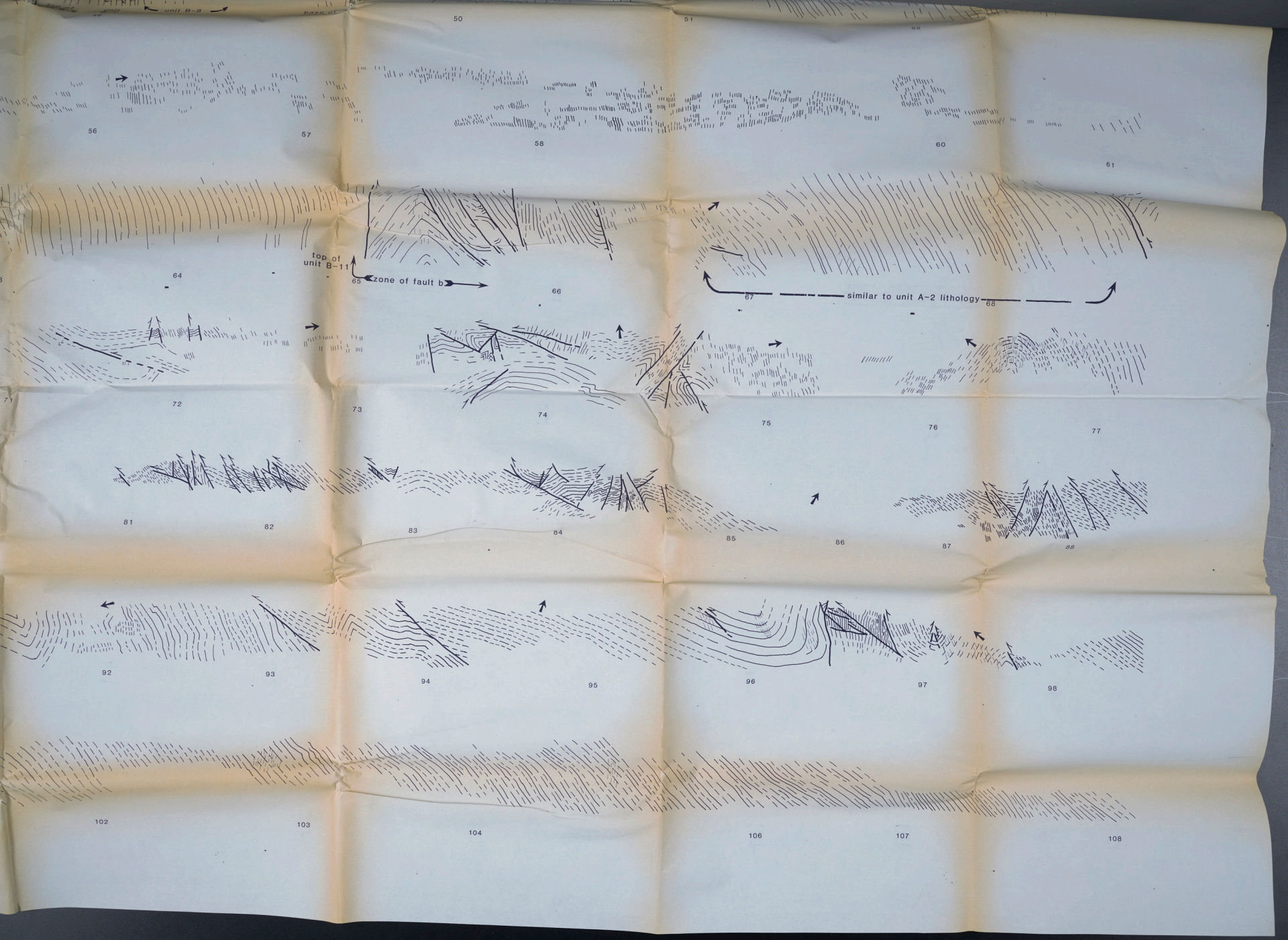
unit B-8
base of
50
51
52
56
57
58
60
61
top of
unit B-11
zone of fault b
64
65
66
67
similar to unit A-2 lithology
68
72
73
74
75
76
77
81
82
83
84
85
86
87
88
92
93
94
95
96
97
98
102
103
104
106
107
108

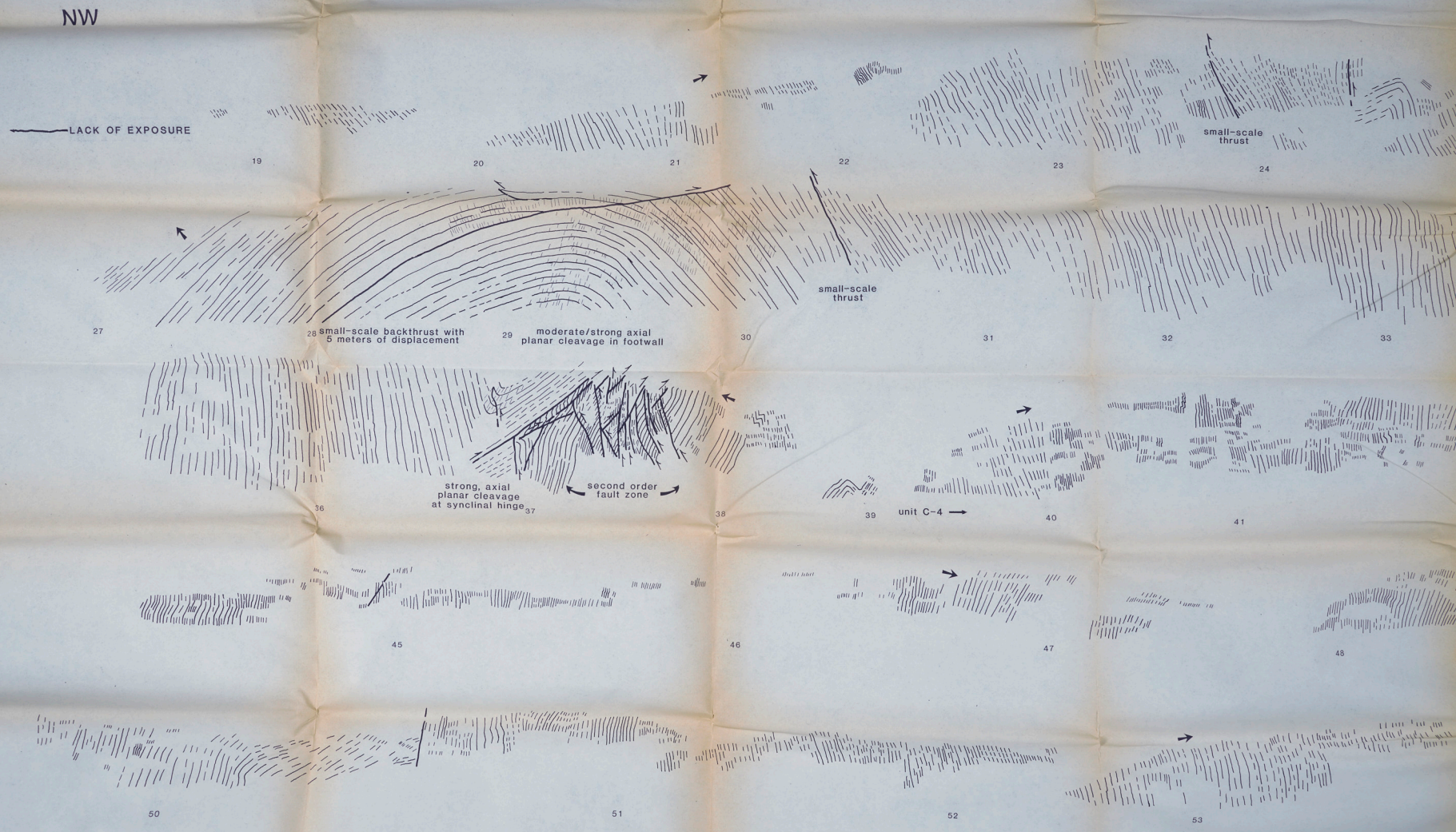
NW
LACK OF EXPOSURE
19
20
21
22
23
small-scale thrust
24
27
28
small-scale backthrust with 5 meters of displacement
29
moderate/strong axial planar cleavage in footwall
30
small-scale thrust
31
32
33
36
strong, axial planar cleavage at synclinal hinge
37
second order fault zone
38
39
unit C-4
40
41
45
46
47
48
50
51
52
53

PLATE 3

SECTION C

SE



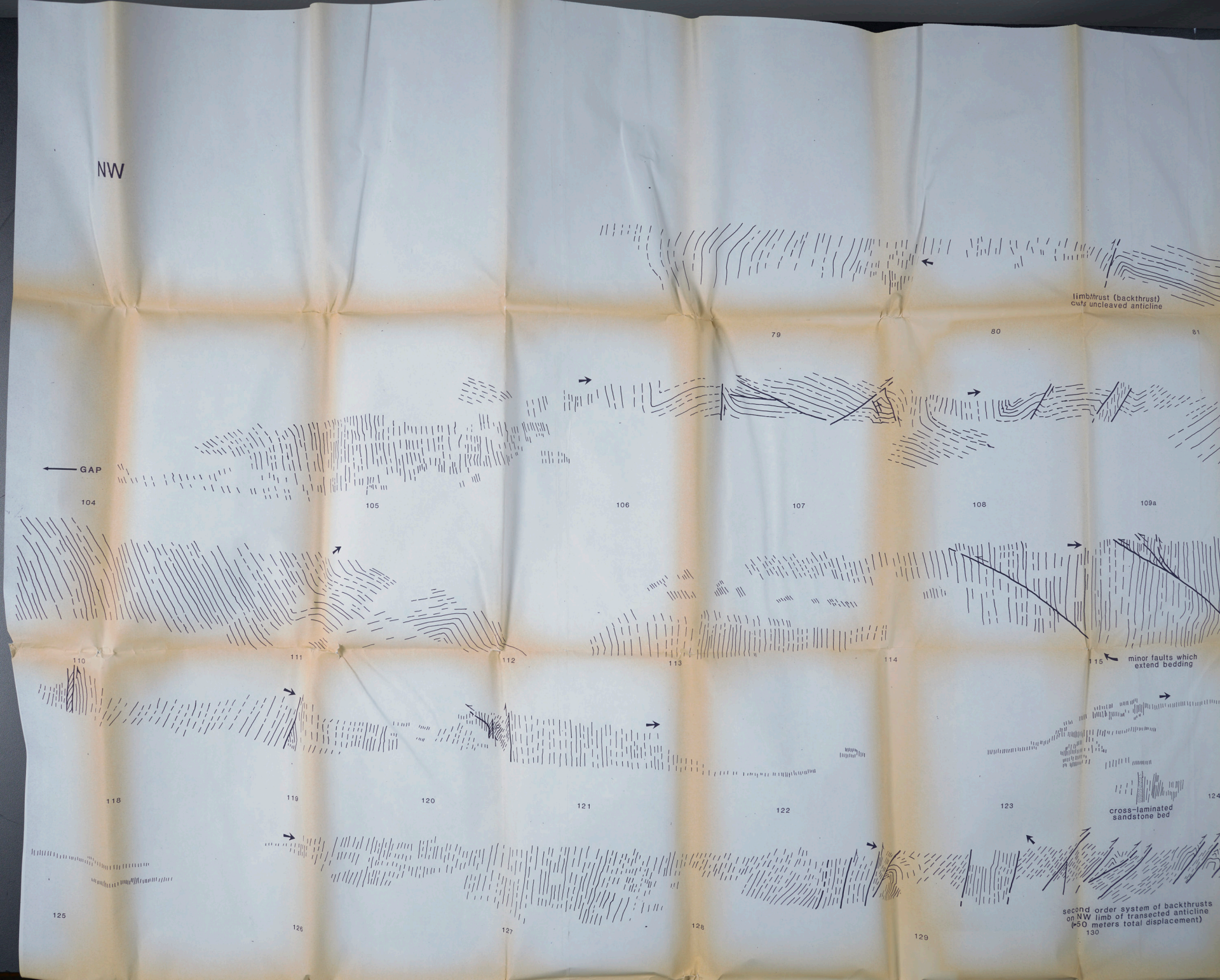
NW
limb thrust (backthrust) cuts uncleaved anticline
79
80
81
GAP
104
105
106
107
108
109a
110
111
112
113
114
115
minor faults which extend bedding
118
119
120
121
122
123
124
cross-laminated sandstone bed
125
126
127
128
129
130
second order system of backthrusts on NW limb of transected anticline (>50 meters total displacement)

PLATE 4

SECTION D

SE

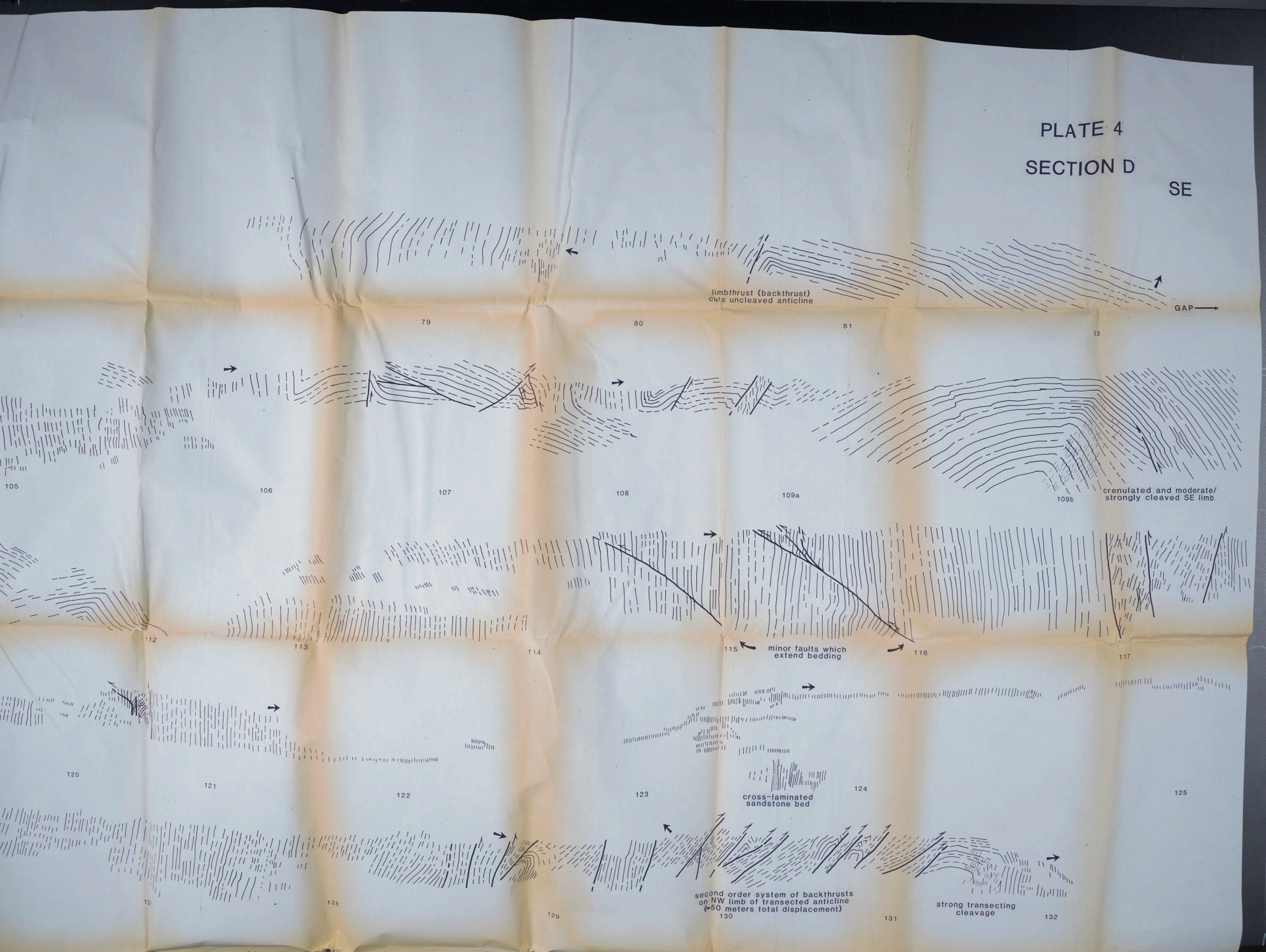


cross-laminated sandstone bed
second order system of backthrusts on NW limb of transected anticline (≤50 meters total displacement)
telescoped sandstones and crumpled interbedded siltstones
fault c
≥300 meters displacement
inferred syncline
inferred anticline
159 telescoping of sandstones
≥40 meters displacement
conjugate contraction faults cut core of syncline with transecting cleavage
inferred anticline
telescoped thick sandstone beds interbedded with shale
faulted syncline
strong/moderate axial planar cleavage
cleavage: strong in mudstones, we
refracted in interbedded sandy si


cross-laminated sandstone bed
second order system of backthrusts on NW limb of transected anticline (~50 meters total displacement)
strong transecting cleavage
telescoped sandstones and crumpled interbedded siltstones
fault c ≥300 meters displacement
inferred syncline
inferred anticline
disharmonic folding and second order faulting
conjugate contraction faults cut core of syncline with transecting cleavage
inferred anticline
faulted syncline
strong/moderate axial planar cleavage
cleavage: strong in mudstones, weak and refracted in interbedded sandy siltstones
sporadic, strong, nearly axial planar cleavage


134
135
136
137
telescoped sandstones and crumpled interbedded siltstones
138
fault c
≥300 meters displacement
139
141
142
143
144
145
6
147
inferred syncline
inferred anticline
150
151
152
153
154
155
156
inferred anticline
159 telescoping of sandstones
≥40 meters displacement
160
conjugate contraction faults cut core of syncline with transecting cleavage
161
162
63
164
telescoped thick sandstone beds interbedded with shale
167
168
faulted syncline
169
170
strong/moderate axial planar cleavage
171
cleavage: strong in mudstones, refracted in interbedded sandy
172
17
(same syncline as above right)
174
175
strong cleavage
176
177
disharmonic, small-scale anticline at core of second order syncline (saprolitic)
178
bed-parallel fault, discfolds and abundant calcite veins are evidence of intense shearing
179
moderate/weak cleavage
abundant graptolites in mudstones interbedded with thin sandstones
180
181

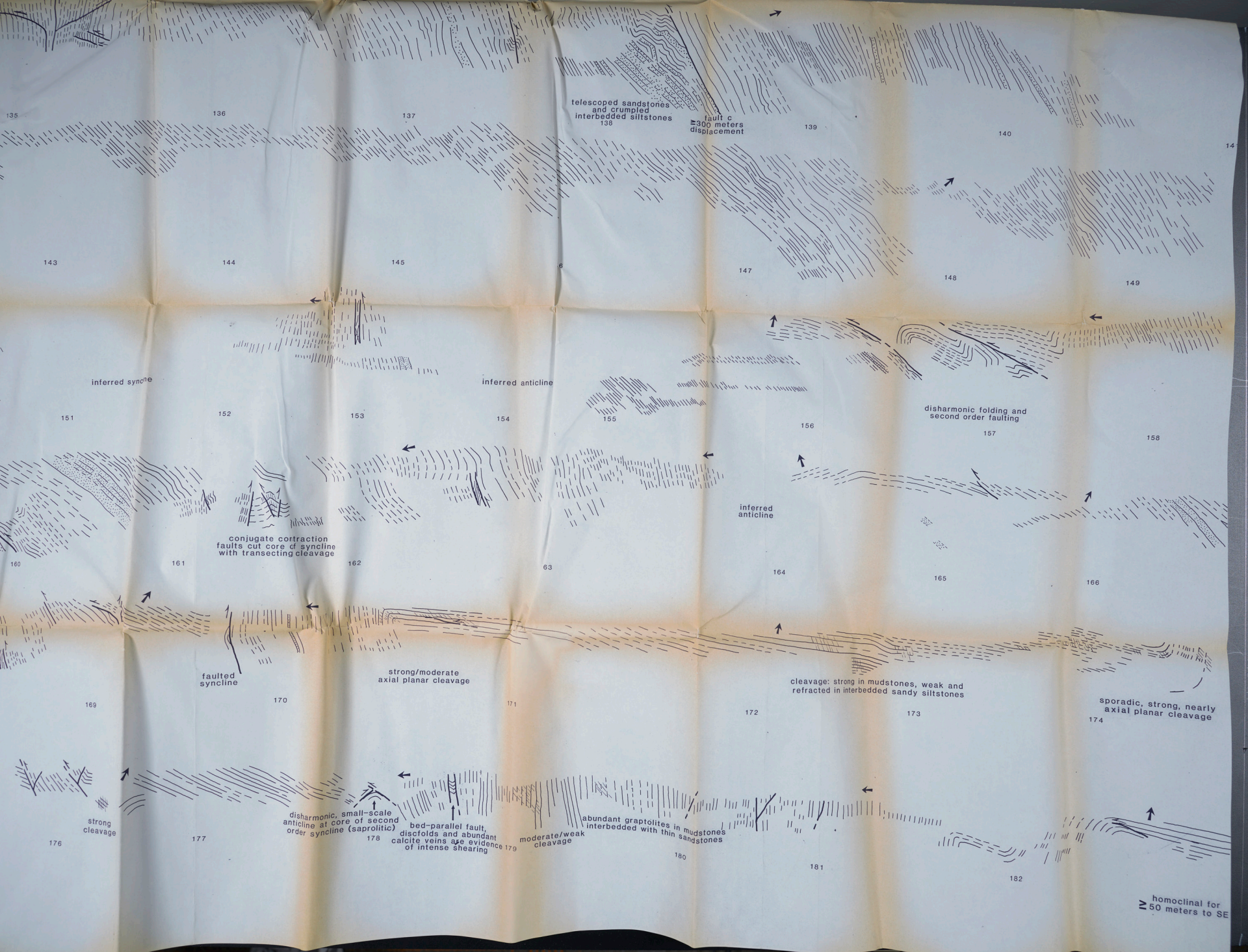
telescoped sandstones and crumpled interbedded siltstones
fault c
≥300 meters displacement
inferred syncline
inferred anticline
disharmonic folding and second order faulting
conjugate contraction faults cut core of syncline with transecting cleavage
inferred anticline
faulted syncline
strong/moderate axial planar cleavage
cleavage: strong in mudstones, weak and refracted in interbedded sandy siltstones
sporadic, strong, nearly axial planar cleavage
strong cleavage
disharmonic, small-scale anticline at core of second order syncline (saprolitic)
bed-parallel fault, discfolds and abundant calcite veins are evidence of intense shearing
moderate/weak cleavage
abundant graptolites in mudstones interbedded with thin sandstones
homoclinal for ≥50 meters to SE

PLATE 5
GEOLOGIC MAP



PLATE 5 GEOLOGIC MAP

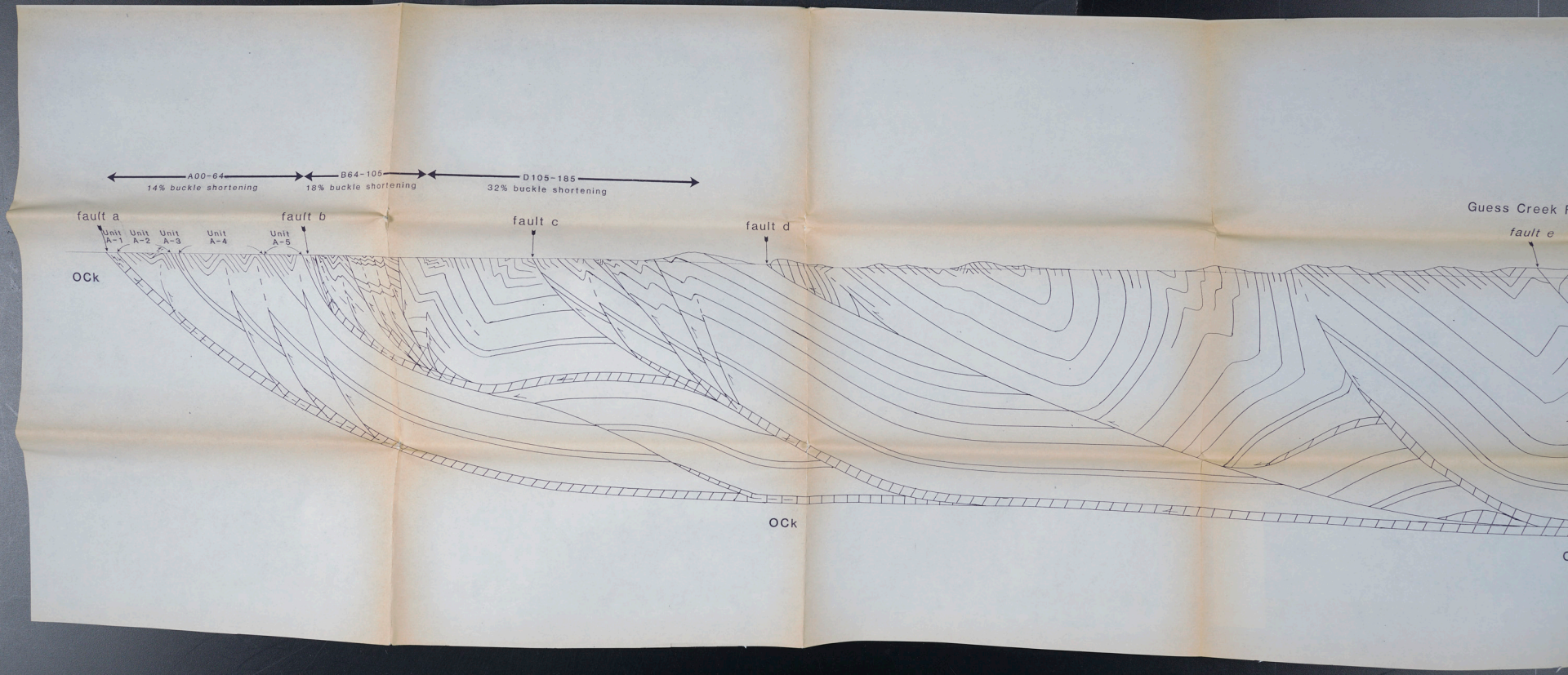
A00-64
14% buckle shortening
B64-105
18% buckle shortening
D105-185
32% buckle shortening
fault a
fault b
fault c
fault d
fault e
Guess Creek F
Unit A-1
Unit A-2
Unit A-3
Unit A-4
Unit A-5
OCk
OCk

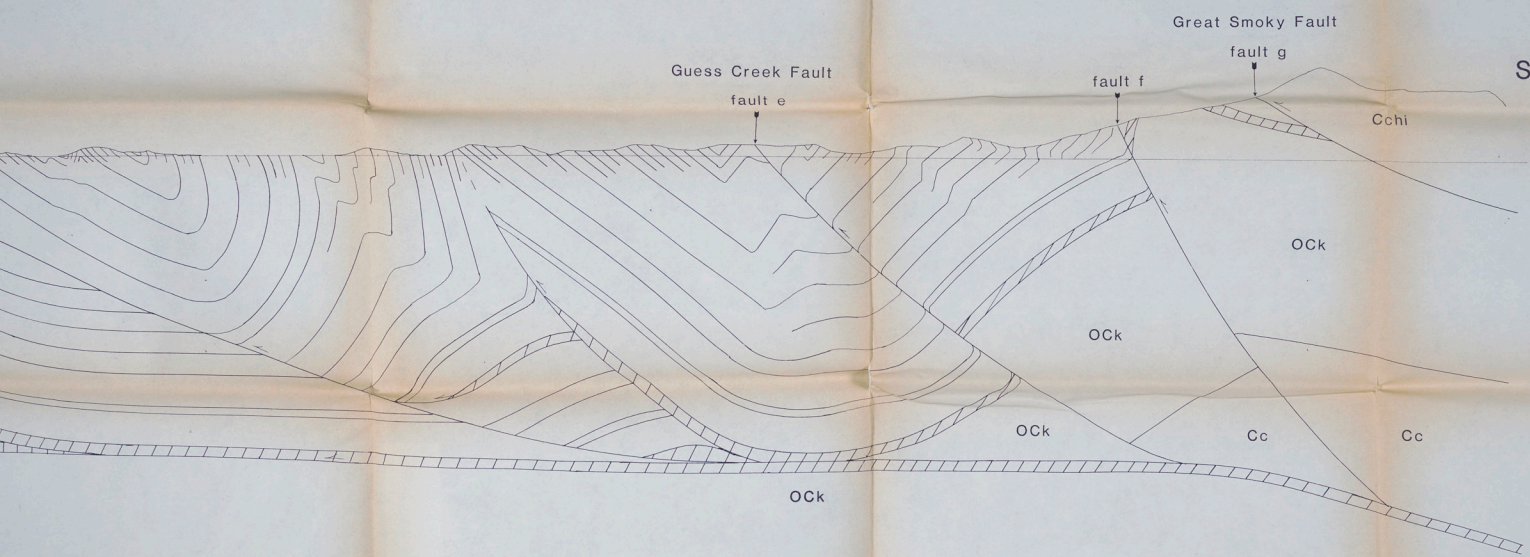

PLATE 6

STRUCTURE SECTION

EXPLANATION

Cchi: Chilhowee Group
Cc: Conasauga Group
OCk: Knox Group
▨: Blockhouse Fm.
unmarked: Sevier Fm.

0 1000 2000
FEET

0 0.5 1
KM.

Scale 1:12,000